8-2018

Utilization Of Variable Valve Actuation To Improve Fuel Efficiency And Aftertreatment Thermal Management In Diesel Engines

Aswin Karthik Ramesh
Purdue University

UTILIZATION OF VARIABLE VALVE ACTUATION TO IMPROVE FUEL EFFICIENCY AND AFTERTREATMENT THERMAL MANAGEMENT IN DIESEL ENGINES

A Dissertation

Submitted to the Faculty

of

Purdue University

by

Aswin Karthik Ramesh

In Partial Fulfillment of the

Requirements for the Degree

of

Doctor of Philosophy

August 2018

Purdue University

West Lafayette, Indiana

THE PURDUE UNIVERSITY GRADUATE SCHOOL
STATEMENT OF DISSERTATION APPROVAL

Dr. Gregory M. Shaver, Chair

School of Mechanical Engineering

Dr. Peter H. Meckl

School of Mechanical Engineering

Dr. John H. Lumkes

School of Agricultural and Biological Engineering

Dr. Oleg Wasynczuk

School of Electrical and Computer Engineering

Approved by:

Dr. Jay P. Gore

Head of the School Graduate Program

To the first engineers in my life: Dr. Nagalakshmi and Venugopal Ramesh.

ACKNOWLEDGMENTS

Looking back through time, I walked into the engine test cell at Herrick Labs as an undergrad in 2012 and I didn't have a clue what was going on. It has been quite a journey and a wonderful experience seeing myself, my colleagues and friends grow in the course of my PhD. Firstly, I want to thank my parents and my brother for being constant source of support and encouragement throughout my life. I would like to thank my advisor Prof. Gregory Shaver, for all his awesome guidance and encouragement through out the years. It was truly a blessing to have him as a leader in my life. Since the first time I met him during my summer internship in my junior year of college, his passion for diesel engines has been embedded in me in a positive manner. It was a pleasure being part of his awesome research team. I want to thank my PhD committee members Prof. Peter Meckl, Prof. Oleg Wasynczuk and Prof. John Lumkes for their valuable input during my prelim and defense. I want to especially thank Prof. Meckl for his mentorship during my short teaching stint as a Lambert Fellow in 2017. Teaching truly is an art, I learnt more while teaching than while studying. I would also want to thank Eric Holloway, for his excellent management and guidance on all the projects throughout my PhD. I learned a great deal on various soft skills including time management from his style of leadership. Furthermore, I would like to thank David Meyer for his great help in the test cell and in keeping me and my colleagues sane when the VVA broke down. His infinite patience and chill attitude was a blessing during hard times in the lab. I would also like to thank the shop staff Bob Brown, Ron Evans and Ryan Thayer for their great help in keeping the experimental setup running safe and sound. I also would like to thank Julia Colby for her assistance during the tail end of my PhD. I also want to thank Donna Cackley and Cindy Cory for their excellent support thoroughout my PhD, and for making the transitions in and out of graduate school easy. I also want to extend

my gratitude towards Cummins and Eaton for their valuable inputs every month over the last five years. I want to thank Tim Lutz for his excellent mentorship during my intership at Cummins during the late stages of my PhD. My time at Herrick Labs would never be as awesome as it was without the amazing colleagues I got a chance to work with in the group. I also would like to thank David Fain who was my first mentor during the initial stages of my PhD, and who taught me everything I needed to know about engine testing. I would like to thank Dheeraj Gosala, Cody Allen for all the time we spent debating crazy ideas while running the engine. I will definitely miss the debates after I graduate. I have not met another person who is as hard working and as friendly as Dheeraj. I also would like to appreciate his better half, Vaidehi Hoshing for being an amazing friend and support. Further I want to thank my collegues, Kalen Vos, Mrunal Joshi, Troy Odstricil, Jonathoan Ore, Ife Ibitayo, Sylvia Lu, Miles Droege, Matt Van Voorhis and wish them the best for thier future endevors. I want to thank Soumya Nayyar for being a great engine run buddy and an even greater friend. I also want to thank Alexander Taylor for being a free spirit renegade, learnt a lot about industry, life, research from his various trivia. I also would like to thank Lucius Wang, Bradley Pietrzak, Riccky Cao for all the fun hangouts early on in my PhD. I also want to thank my friends Adithyan Raja, Harish Thadandala, Anirudh Roshan Sriram, Shamiek Mangipudi, Ishant Khurana, Kelsi Lynde, Saurabh Mishra, Jessica Chen, Siddarth Mehra, Akash Agarwal for keeping great company outside the lab. I would also like to extend my gratitude towards Annelies Richmond who taught me the yogic way of life and meditation. I feel blessed to have shared friendships with Akshay Ponda, Shipping Kuo, Andrew Nunberg for being mentors on my journey towards mindfullness. I also want to thank my friends from latin and ballroom dance community, Joanna Xin, Sheik Dawood, Debroah Kull, Yuerwhen Yih and Daniel Dilley. Alas, I also would like to thank my better half, Sarah Savage, for being a constant source of support and enccouragement during the later stage of my PhD. I can say with confidence that the experiences I gained and friends I have met during the last five years, are a great blessing, I wouldn't change a thing.

TABLE OF CONTENTS

Page

Page

LIST OF TABLES

LIST OF FIGURES

Figure Page

Figure Page

Figure Page

Figure Page

Figure Page

Figure Page

ABBREVIATIONS

AC	Alternating Current
AFR	Air Fuel Ratio
AFT	After-Treatment
BMEP	Brake Mean Effective Pressure
BSFC	Break Specific Fuel Consumption
BTE	Break Thermal Efficiency
CAD	Crank Angle Degrees
CAC	Charge Air Cooler
CCE	Closed Cycle Efficiency
CDA	Cylinder Deactivation
CI	Compression Ignition
CR	Compression Ratio
CPL	Cummins Power Lab
DEF	Diesel Exhaust Fluid
DOC	Diesel Oxidation Catalyst
DOE	Design of experiments
DPF	Diesel Particulate Filter
ECM	Electronic Control Module
EEVO	Early Exhaust Valve Opening
EGR	Exhaust Gas Recirculation
EIVC	Early Intake Valve Closing
EM	Exhaust Manifold
ERB	Exhaust Rebreathing
EVC	Exhaust Valve Closing
EVL	Exhaust Valve Lift

EVO	Exhaust Valve Opening
EPA	Environment Protection Agency
Fig	Figure
ft-lbs	Foot-pounds (unit of Torque)
FSN	Filtered Smoke Number
FTP	Federal Testing Procedure
GHG	Green House Gases
HC	Hydrocarbons
HDFTP	Heavy Duty Federal Test Procedure
HRR	Heat Release Rate
ICE	Internal Combustion Engine
iEGR	Internal Exhaust Gas Recirculation
IM	Intake Manifold
IRB	Intake Rebreathing
IVO	Intake Valve Opening
IVL	Intake Valve Lift
IVC	Intake Valve Closing
LFE	Laminar Flow Element
LIVC	Late Intake Valve Closing
LVDT	Linearly Variable Differential Transformer
ME	Mechanical Efficiency
NFRB	Non fired Reverse Breathing
NHSTA	National Highway safety administration
NOx	Nitrogen Oxides
NVO	Negative Valve Overlap
OCE	Open Cycle Efficiency
PM	Particulate Matter
RPM,rpm	Revolutions Per Minute
RVB	Reverse Breathing

SOI	Start of Injection
SCR	Selective Catalytic Reduction
SI	Spark Ignited
TOT	Turbine Outlet Temperature
TOP	Turbine Outlet Power
VGT	Variable Geometry Turbocharger
VVA	Variable Valve Actuation

GLOSSARY

AVL QC34C	A type of In-cylinder pressure transducer
dSPACE	Micro-controller used to control the engine and VVA system
GT Power	Engine simulation software produced by Gamma Technologies
ISB	Mid-range on-road Cummins engine
ISX	Heavy-duty on-road Cummins engine
Minitab	Statistical software
Autonomie	Vehicle modeling software
Open VGT	Opening the variable geometry turbine turbocharger's inlet guide vanes

ABSTRACT

Ramesh, Aswin Karthik Ph.D., Purdue University, August 2018. Utilization of Variable Valve Actuation to Improve Fuel Efficiency and Aftertreatment Thermal Management in Diesel Engines. Major Professor: Gregory M. Shaver, School of Mechanical Engineering.

Fuel consumption in heavy-duty vehicles is expected to double by the year 2050 [1]. The majority of heavy duty vehicles incorporate diesel engines which emit air pollutants including particulate matter (PM), unburnt hydrocarbons (uHC) and oxides of nitrogen (NOx). Increasing demand for heavy duty transportation coupled with strict emission regulations by the Environmental Protection Agency (EPA) and California Air Regulations Board (CARB) to improve air quality drive innovation of advanced engines and auxiliary systems. Complex exhaust aftertreatment (AFT) systems are required to meet stringent tailpipe-out emission regulations. The effectiveness of AFT systems, affected by emission conversion efficiency, is limited when turbine outlet temperatures (TOTs) are low (usually $<250°C$). This is a problem for extended low-load operation, such as idling and during cold start conditions. AFT thermal management, required to ensure efficient reduction of engine-out emissions, includes temperature increase, and temperature maintenance, of the AFT system components via control of engine exhaust flow and temperature. Conventional strategies used for AFT thermal management such as late fuel injection and over-closed variable geometry turbine (VGT) turbocharger are effective but fuel expensive. Variable valve actuation (VVA) is a potential fuel-efficient solution for improving the AFT thermal management characteristics to reduce tailpipe emissions in diesel engines. This dissertation focuses on promising VVA strategies such as cylinder deactivation (CDA) and intake valve closure (IVC) modulation as ways to improve AFT performance in a fuel efficient manner. This dissertation shows that CDA and IVC modulation can be

used to reduce the fuel consumption by 5 to 30% depending on the engine load, increase the rate of warm-up of AFT, maintain higher AFT temperatures, and achieve active diesel particulate filter regeneration without requiring HC dosing of the diesel oxidation catalyst. At cruise operating condition (1200 rpm/300 ft-lbs), Late IVC (LIVC) strategy does not show any fuel economy penalty when compared to conventional operation of the valves, but shows a TOT increase of about 150-200°C, thereby enabling warmer AFT temperatures. This dissertation also introduces several novel engine breathing modes, viz. fired/non-fired reverse breathing and intake/exhaust rebreathing. Reverse breathing is a novel method where exhaust gases are recirculated, as needed, from exhaust manifold to intake manifold via one or more cylinders. Rebreathing is an innovative method, where the gas exchange takes place only in either the intake or exhaust manifold for a certain number of cylinders. These strategies provide in-cylinder oxygen dilution and reduction in airflow leading to lower pumping work at low-load engine operation.

Approximately 40% of typical heavy-duty vehicle operation occurs at loaded curb idle, during which the conventional diesel engines are unable to maintain sufficient AFT component temperatures while retaining fuel economy. Fuel economy and thermal management at loaded curb condition can be improved via reverse breathing due to reduced airflow. Several strategies for implementation of reverse breathing are described in detail and compared to CDA and internal EGR operation. Experimental data demonstrates 26% fuel consumption savings, when compared to conventional stay-warm operation; 60°C improvement in TOT, and 28% reduction in exhaust flow compared to conventional best fuel consumption operation at the curb idle condition (800RPM, 1.3 bar BMEP). Similarly, intake rebreathing in three of the six cylinders yields 50°C improvement in TOT and 20% reduction in exhaust flow while maintaining NOx levels without using EGR. The incorporation of non-fired reverse breathing, in order to efficiently maintain desired AFT temperatures during curb idle conditions, is experimentally demonstrated to result in fuel savings of 2% over the HDFTP drive-cycle relative to conventional operation.

1. INTRODUCTION

1.1 Motivation

Transportation is a significant source of global air pollution, contributing to about 14% of greenhouse gas (GHG) emissions [2]. Air pollution has direct impact on the natural environment, contributes to climate change, reduces crop yields and pollutes oceans. Cleaner air will create a better environment for everyone to live, work and thrive in. As the world population grows, the demand for clean and efficient transportation is increasingly paramount. Almost all (95%) of the world's transportation energy comes from petroleum-based fuels, largely gasoline and diesel [2]. The diesel engine, invented in the late 19th century by Dr. Rudolf Diesel, is one of the most fuel efficient among all type of internal combustion engines known today. Other diesel features that have not been matched by competing energy conversion machines include durability, reliability, and fuel safety. Hence, the majority of heavy-duty vehicles incorporate diesel engines, which also emit air pollutants including particulate matter (PM), unburnt hydrocarbons (uHC), oxides of nitrogen (NOx) along with carbon dioxide (CO_2) which is a major GHG. Climate change is linked to the climbing levels of (CO_2) and other GHG in our atmosphere. Furthermore, NOx and PM pose severe health risks for human beings especially in high population density regions around the world. NOx is a group of gases that are predominantly formed during the combustion of fossil fuels. PM is a mixture of solid particles and liquid droplets found in the air. Figures 1.1 and 1.2 show that road transportation is a major source of NOx/PM, and significantly affecting human health [3].

The Environmental Protection Agency (EPA) and the National Highway Traffic Safety Administration (NHTSA) are taking coordinated steps to enable the produc-

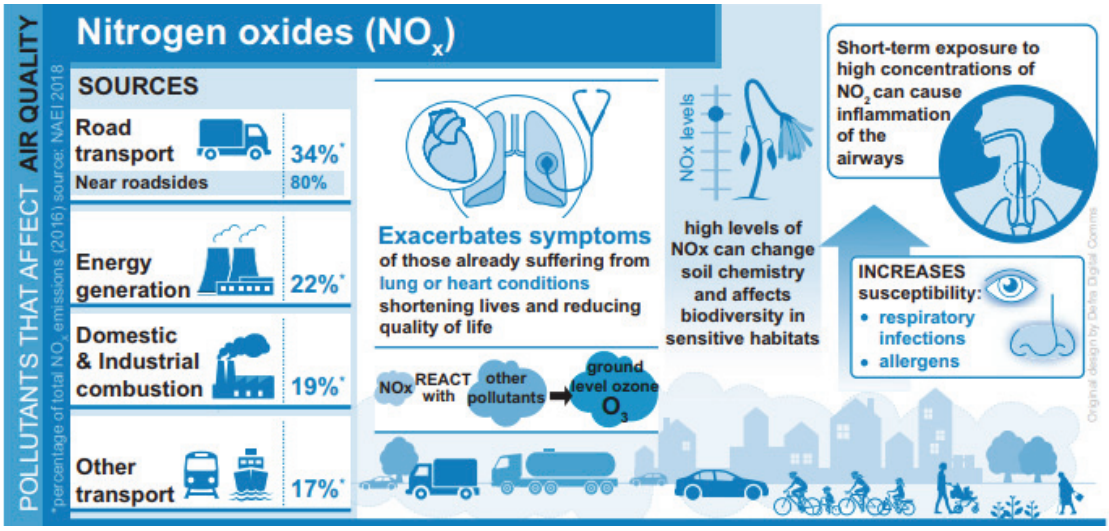

Figure 1.1. Major sources of NOx and its impact on human health. Short term exposure to concentrations of NO_2 can cause inflammation of the airways and increase susceptibility to respiratory infections and to allergens. It exacerbates the symptoms of those who are already suffering from lung or heart conditions, shortening their lives [3].

tion of a new generation of clean vehicles, by reducing GHG emissions and improving fuel use from on-road vehicles and engines, from the smallest cars to the largest trucks.

Over 80% of all U.S. freight tonnage is transported by diesel power and over 75% is transported by trucks [4]. The EPA estimates a 23% increase in fuel consumption for the U.S. heavy-duty truck segment between 2009 and 2020. In order to meet this growing demand in a fuel efficient manner, the EPA has set regulations for CO_2 (as seen in Figure 1.3). The EPA also mandates limits on other pollutant emissions such as NOx, PM and uHC, which are getting stricter as shown in Figure 1.4.

Hence the truck manufacturing and supporting industries are faced with numerous challenges to reduce fuel consumption and GHG while meeting stringent emissions regulations. A key part of the strategy to meet these requirements is an improvement of the efficiency of the internal combustion engine powering the truck. Variable valve actuation (VVA) can increase the fuel efficiency, reduce tailpipe-out emissions and improve the efficiency of the aftertreatment (AFT) systems.

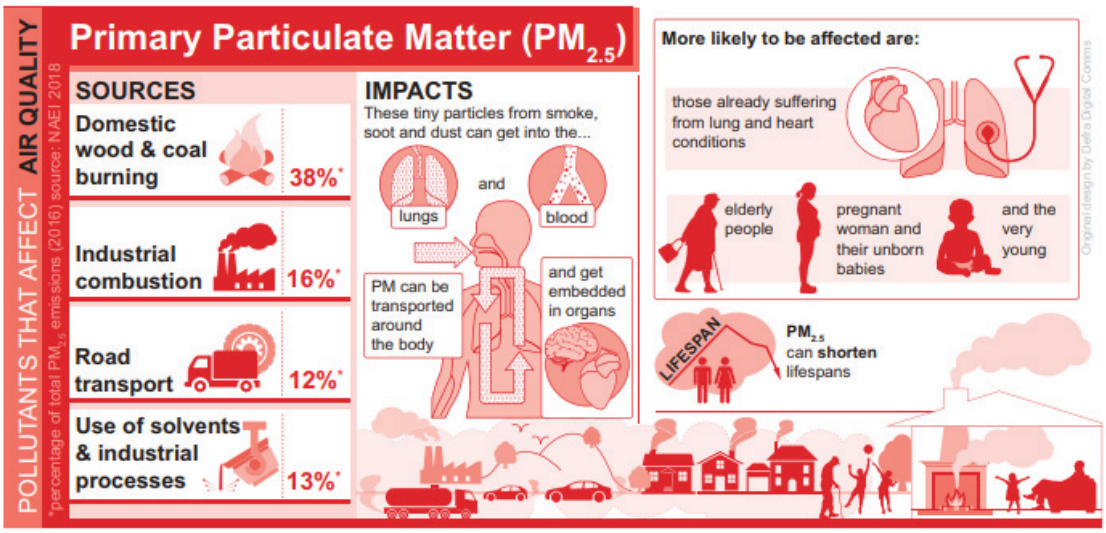

Figure 1.2. Major sources of PM and its impact on human health. PM can have short-term health impacts over a single day when concentrations are elevated, and long-term impacts from lower level exposure over the life course. Effects are amplified in vulnerable groups including young children, the elderly, and those suffering from breathing problems like asthma [3].

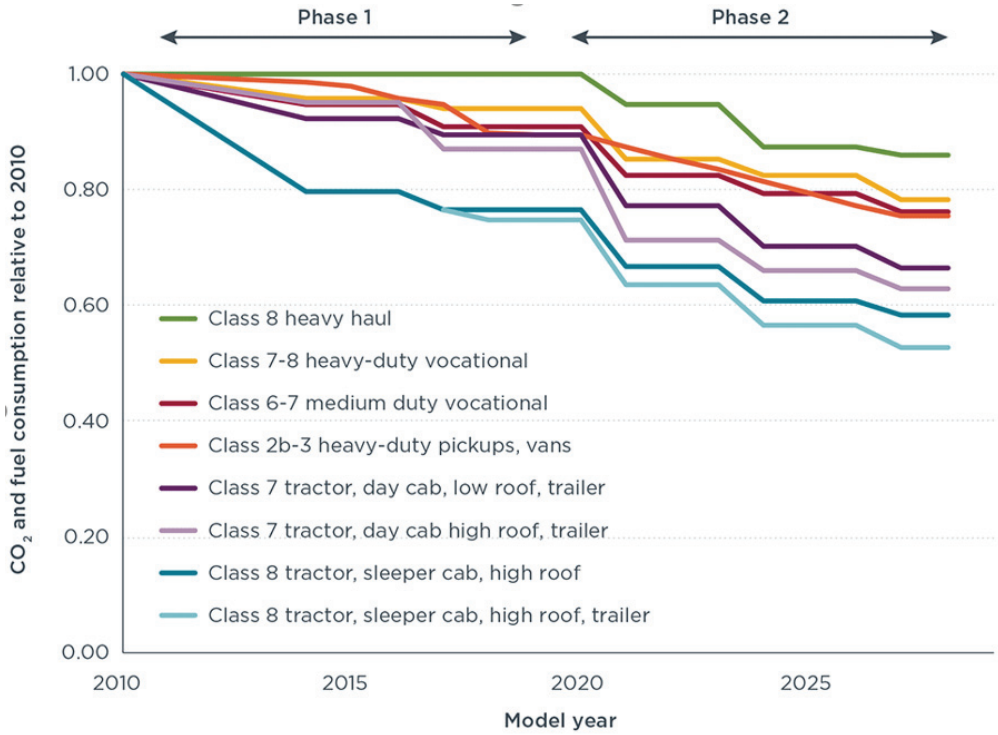

Figure 1.3. Summary of CO_2 and fuel consumption reduction from adopted Phase 1 and proposed Phase 2 heavy-duty vehicle standards for selected vehicle categories [1].

US EPA & California Emission Standards for Heavy-Duty CI Engines, g/bhp·hr

Year	CO	HC[a]	HC[a]+NOx	NO_x	PM	
					General	Urban Bus
1974	40	-	16	-	-	
1979	25	1.5	10	-	-	
1985	15.5	1.3	-	10.7	-	
1987	15.5	1.3	-	10.7[d]	0.60[f]	
1988	15.5	1.3[b]	-	10.7[d]	0.60	
1990	15.5	1.3[b]	-	6.0	0.60	
1991	15.5	1.3[c]	-	5.0	0.25	0.25[g]
1993	15.5	1.3[c]	-	5.0	0.25	0.10
1994	15.5	1.3[c]	-	5.0	0.10	0.07
1996	15.5	1.3[c]	-	5.0[e]	0.10	0.05[h]
1998	15.5	1.3	-	4.0	0.10	0.05[h]
2004[j]	15.5	-	2.4[i]	-	0.10	0.05[h]
2007	15.5	0.14[k]	-	0.20[k]	0.01	
2015	15.5	0.14	-	0.02[l]	0.01	

a. NMHC for 2004 and later standards
b. For methanol-fueled engines, the standard is for total hydrocarbon equivalent (THCE).
c. California: NMHC = 1.2 g/bhp·hr, in addition to the THC limit.
d. California: NOx = 6.0 g/bhp·hr
e. California: Urban bus NOx = 4.0 g/bhp·hr
f. California only, no federal PM limit.
g. California standard 0.10 g/bhp·hr
h. In-use PM standard 0.07 g/bhp·hr
i. Alternative standard: NMHC+NOx = 2.5 g/bhp·hr and NMHC = 0.5 g/bhp·hr
j. Under the 1998 Consent Decrees, several manufacturers supplied 2004 compliant engines from October 2002.
k. NOx and NMHC standards were phased-in on a percent-of-sales basis: 50% in 2007-2009 and 100% in 2010. Most manufacturers certified their 2007-2009 engines to a NOx limit of about 1.2 g/bhp·hr, based on a fleet average calculation.
l. Optional. Manufacturers may choose to certify engines to the California Optional Low NOx Standards of 0.10, 0.05 or 0.02 g/bhp·hr

Figure 1.4. US EPA regulations over the years showing the limits for CO, HC, NOx and PM. All values listed in this table are in **g/hp-hr**. The 2015 regulations essentially show a ten fold reduction in tailpipe NOx levels from 0.2 g/hp-hr to 0.02 g/hp-hr [5].

1.2 Literature Review

In order to reduce the production of the harmful engine-out exhaust gases, several on-engine strategies including multiple fuel injections, high fuel injection pressures, late fuel injections, and high-pressure cooled exhaust gas recirculation (EGR) have been incorporated in modern diesel engines [6]. These strategies are unable to meet the regulations at all operating conditions. As a result, complex AFT systems are coupled with the diesel engine in order to meet the tailpipe emission regulation limits.

Typical AFT systems, as illustrated in Figure 1.5, incorporate selective catalytic reduction (SCR) system to reduce NOx emissions, a diesel oxidation catalyst (DOC) to reduce HC and carbon monoxide (CO), and a diesel particulate filter (DPF) to reduce PM emissions.

SCR is effective in reducing NOx to N_2 and H_2O [8], provided the catalyst temperature is between approximately 250°C to 450°C [9–11]. Urea is injected upstream of the SCR system, decomposing into ammonia and CO_2. This process requires SCR inlet temperatures above approximately 200°C to avoid build-up of solid deposits on the catalyst bed [1]. The SCR efficiency is maximized over the interval from 300 to 450°C of SCR catalyst bed temperature. In order to keep the AFT warm in a robust manner, TOT between 350 and 500°C are desirable. The DPF is regularly regenerated in a passive manner by oxidizing the collected PM, provided the TOT are high enough, approximately 250°C to 300°C in the presence of NO_2 [12, 13]. Active regeneration of the DPF requires temperatures in excess of 450°C. The DOC must reach approximately 200°C to perform effective oxidation of CO and HC. Once activated, the DOC oxidizes HC resulting in increased AFT temperatures, while converting NO to NO_2, both of which enable passive reactions in DPF at temperatures above 250 °C [14, 15]. In short, the aforementioned AFT components work effectively in reducing emissions when operated at the correct temperatures. However, during cold-start and low-load engine operation, the exhaust gas temperature is too low to keep the AFT catalysts at effective operating temperatures as shown in Figure 1.6.

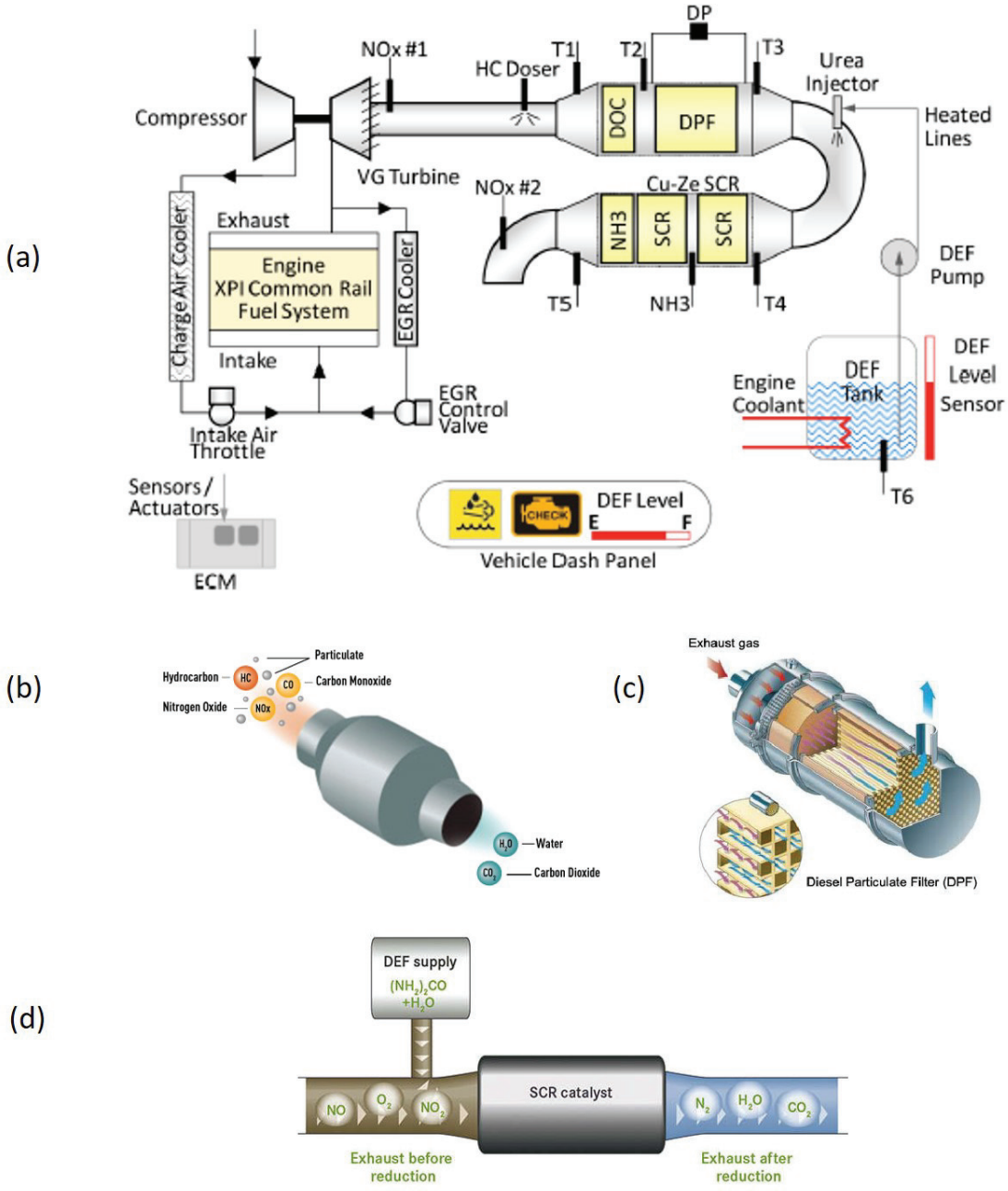

Figure 1.5. (a)Engine and AFT system architecture employed in 2013 on-highway vehicle applications. [1]. (b) Schematic of diesel oxidation catalyst. [7] (c) Schematic of diesel particulate filter. [7] (d) Schematic of selective catalytic reduction system. [7]

A significant portion of the engine operating map (below 5 bar BMEP) has exhaust temperatures below 250°C thereby leading to low SCR conversion efficiency. Engines used in mid-range and heavy-duty vehicles spend a sizable amount of time at low-load conditions, when used in stop and go applications.

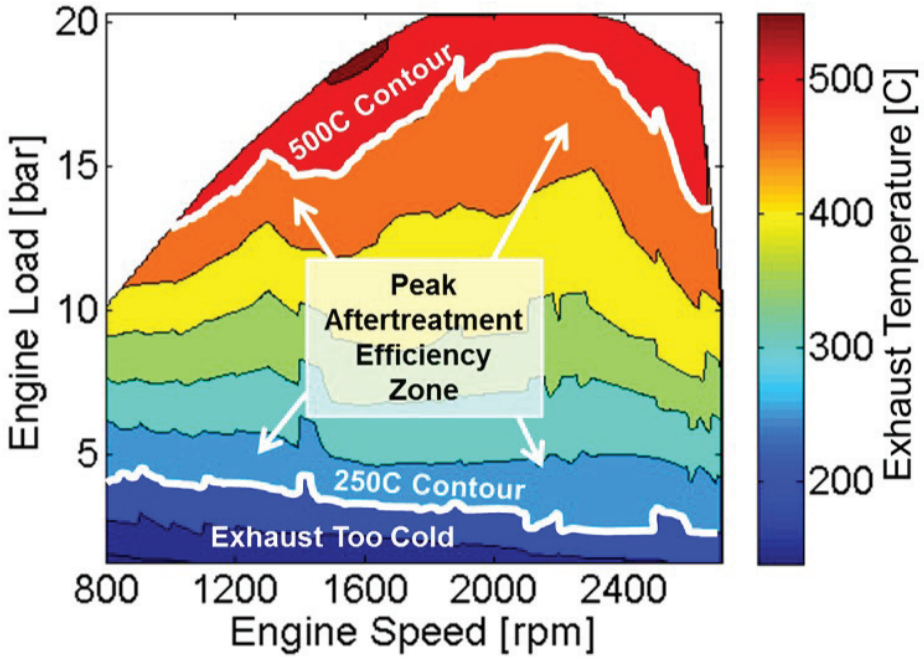

Figure 1.6. Experimental steady state data (Cummins Confidential) showing the exhaust temperatures of the Cummins mid-range diesel engine. The figure shows a significant portion of the torque speed region has lower exhaust temperatures (less than 300°C) thus requiring a need for better thermal management strategies.

Hence thermal management strategies designed to increase AFT component temperatures are needed for efficient AFT operation over a wide range of engine operating conditions [4, 16]. Figure 1.7 shows the evolution of different diesel engine and AFT technologies over the last two decades to meet emission regulations. As the emission regulations become stricter over the next few years, novel and cost effective approaches are needed to solve this problem.

Research continues on methods for improving AFT thermal management by means of increased diesel engine exhaust temperatures [17, 18]. One technology currently

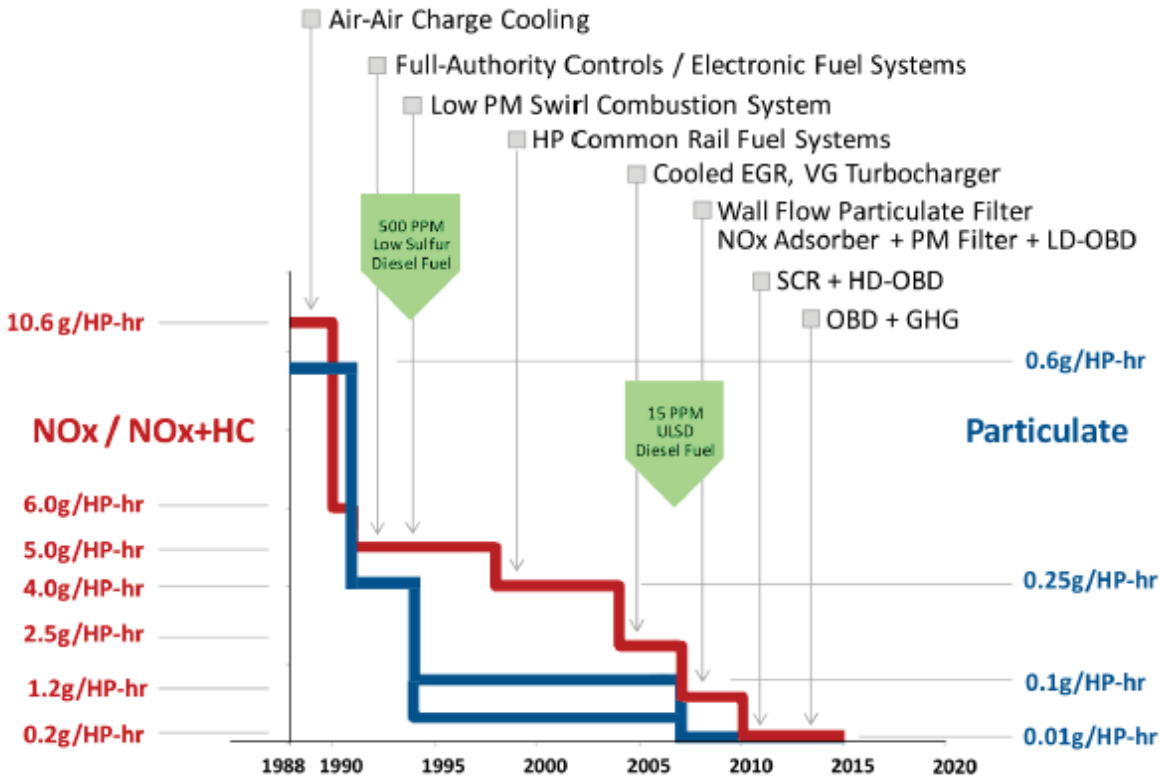

Figure 1.7. Evolution of diesel engine and aftertreatment technologies to meet emissions regulations. [1]

being studied to accomplish this goal is variable valve actuation (VVA) [19–23]. This includes technologies such as cylinder deactivation (CDA), intake valve closure (IVC) modulation and alternate breathing strategies such as intake rebreathing and reverse breathing.

These variable valve actuation enabled strategies such as CDA, reverse breathing and IVC modulation essentially reduce airflow which reduces the air-fuel ratio (AFR). Figure 1.8 shows that a reduction in AFR is consistent with an increase in TOT. Hence these strategies can be employed to increase the TOT, thereby aiding in thermal management.

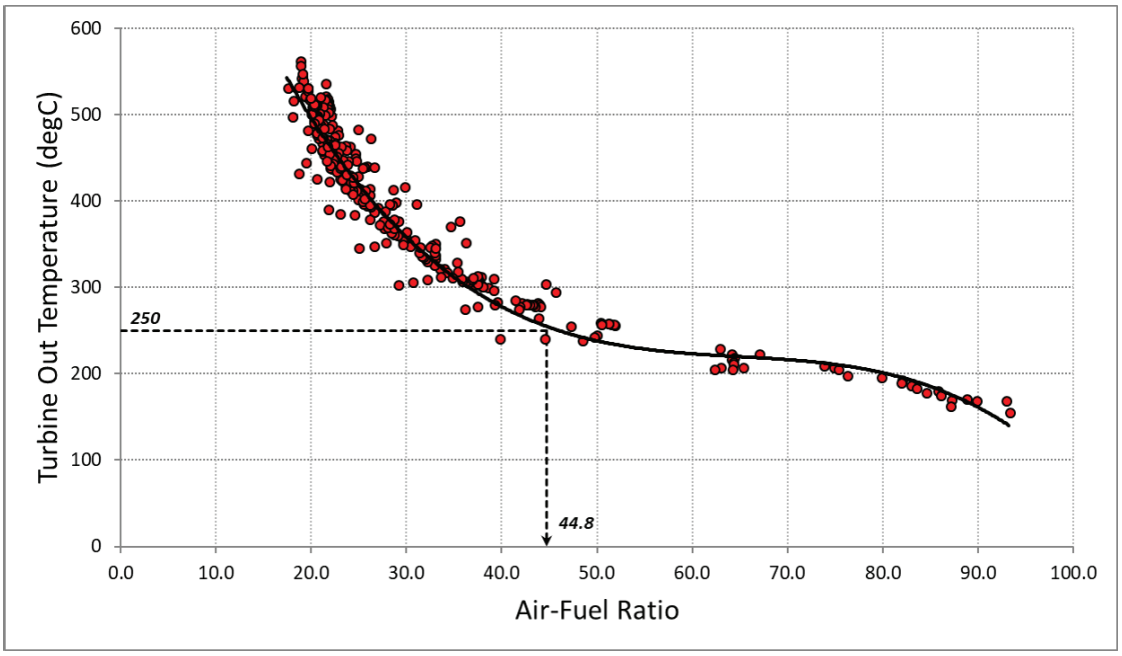

Figure 1.8. TOT vs AFR trend for different speed and load condition in a diesel engine [22].

1.2.1 Cylinder Deactivation

CDA is a method to increase exhaust temperatures by reducing the AFR, and in some cases can also result in improved Brake Thermal Efficiency (BTE). A lean-burn

diesel engine operating with deactivated cylinders must inject more fuel per activated cylinder relative to an engine operating at the same load with all cylinders activated. The displaced volume is reduced by half when half of the cylinders are deactivated, resulting in a reduction in the AFR. CDA has been studied as a method for efficiency improvement in spark ignited (SI) engines and is implemented in several production vehicles equipped with SI engines. In SI engines, CDA reduces the amount of throttling required at low loads to stay at stoichiometric conditions, enabling a reduction in pumping penalty [24]. However, diesel CDA is being extensively studied as a method for improving fuel economy and AFT thermal management [21, 23, 25–27]. *Foster et al* simulated CDA using a GT-Power model of a six-cylinder compression ignition engine equipped with a turbocharger operating at 1800 rpm and a BMEP of 9 bar [28]. The results showed that deactivating three of the six cylinders increased exhaust gas temperatures at the exit of the turbocharger to 290°C. The authors concluded that these increased temperatures could be used to improve NOx absorption, NOx reduction, diesel particulate trap purging, and desulfation of a NOx absorber. Prior efforts by several of the authors have demonstrated that CDA is an effective method for increasing TOT and fuel efficiency during diesel engine idle operation [23, 27], and for enabling active DPF regeneration without requiring DOC fuel dosing during highway cruise condition [21, 26]. The incorporation of CDA to maintain desired AFT temperatures during idle conditions is experimentally demonstrated to result in fuel savings of 3% over the HDFTP drive-cycle [29]. Full engine CDA enables upto 78% reduction in motoring torque at an engine speed of 2100 rpm and thus could serve as a fuel saving strategy when the vehicle is coasting [27, 30].

1.2.2 Intake Valve Closure Modulation

IVC modulation is another method to manage exhaust gas temperatures. Late IVC (LIVC) strategy reduces AFR by pushing some of the inducted charge back into the intake manifold prior to intake valve closure, resulting in an increase in

TOT. LIVC can reduce NOx emissions via a reduction in effective compression ratio. Previous research explored LIVC on diesel engines in one-dimensional and three-dimensional simulations. *Deng et al* showed a 2% to 6% BSFC reduction on a Caterpillar 6.6L heavy-duty diesel engine [31]. *Yang and Keller* used a simulation model to demonstrate a 24% NOx reduction and 1% fuel economy benefit by using LIVC and VGT [32]. *Fessler et al* experimentally demonstrated a 6% BSFC improvement on a 3.0-L diesel engine with optimized cylinder charging [33]. *Gurney et al* tested LIVC on a 2.0-L diesel engine and showed PM reduction through increased charge motion, which was favorable at low speed and load conditions [34]. *Gehrke et al* showed that LIVC enabled exhaust temperature increase at a relatively low fuel consumption on a single-cylinder heavy-duty engine [35]. *Murata et al.* demonstrated the advantage of combining premixed combustion and LIVC for NOx reduction as well as elevated exhaust gas temperature with reduced flow rate on a single-cylinder light-duty engine [36]. Similar to LIVC, Early IVC (EIVC) also reduces the air flow as the intake valve closes before the cylinder is fully charged. *De Ojeda et al* experimentally demonstrated that EIVC reduced fuel consumption and soot emissions on a medium-duty V8 6.4L engine [37]. The results showed that EIVC prolonged ignition delay and increased the amount of fuel burning in the premixed combustion mode, which is beneficial for thermal efficiency. Prior efforts by *Garg et al* have also shown that LIVC can be used to increase TOT [22].

1.2.3 Reactivation of Cylinders from Half-Engine CDA Operation to Full Engine Operation

In modern diesel engines, control of the air handling system is achieved through actuation of a VGT and EGR valves, which together modulate EGR flow and fresh air flow. The proportion of the recirculated exhaust gas and fresh air in the cylinder plays an important role in determining the transient response of an engine [38]. Kitabatake et al. [39] studied the use of CDA on a 6-cylinder 9.8 liter 3-stage turbocharged

diesel engine for efficiency benefit. The camless VVA system was driven by hydraulic pressure. This study showed that deactivation of three or four cylinders produced a fuel economy improvement of 8.9% at light load due to a reduction in heat loss. The researchers also describe that this is only viable at low loads; therefore, there is a need to switch to activating the cylinders during transient operation. Similar conclusions were derived from a prior study conducted at Herrick Labs by *Roberts et al.* [40]. The study concluded that the reduced air flow in CDA that comes from deactivating three cylinders causes higher PM emission when attempting to meet the load transitions required during transient operation.

1.2.4 Reverse Breathing and Alternate Breathing Strategies

Using a fully flexible VVA at Herrick labs, several technologies such as rebreathing and reverse breathing can be realized on the diesel engine. Reverse breathing is a novel method, where exhaust gases are recirculated, as needed, from exhaust to intake manifold via one or more cylinders. Rebreathing is another innovative method, where the gas exchange takes place only in either the intake or exhaust manifold for a certain number of cylinders. These strategies effectively reduce the amount of air flow to the engine, thereby reducing the effective AFR leading to a increase in TOT. Prior GT power simulation work has shown an increase in both TOT and fuel efficiency at 1200 rpm 50 ft-lbs and 100 ft-lbs [41].

1.3 Experimental Setup

The testbed under observation in this study is a camless 6-cylinder 2010 Cummins diesel engine equipped with an electro-hydraulic VVA system, high-pressure cooled EGR, a sliding nozzle-type VGT, an air-to-water charge air cooler and electronically controlled Bosch high-pressure common rail as shown in Figure 1.9. The Cummins ISB engine is a 6.7 liter, 350 horsepower, 6-cylinder direct-injection diesel engine with a 17.3:1 geometric compression ratio. A schematic of the engine architecture is

presented in Fig. 1.10. A summary of nominal engine parameters is shown in Table 1.3. The fresh intake air flows through the laminar flow element into the compressor and is then cooled in the charge air cooler. The intake air is mixed with cooled EGR. The exhaust flows either through the turbine of the VGT to the exhaust pipe or into the EGR system.

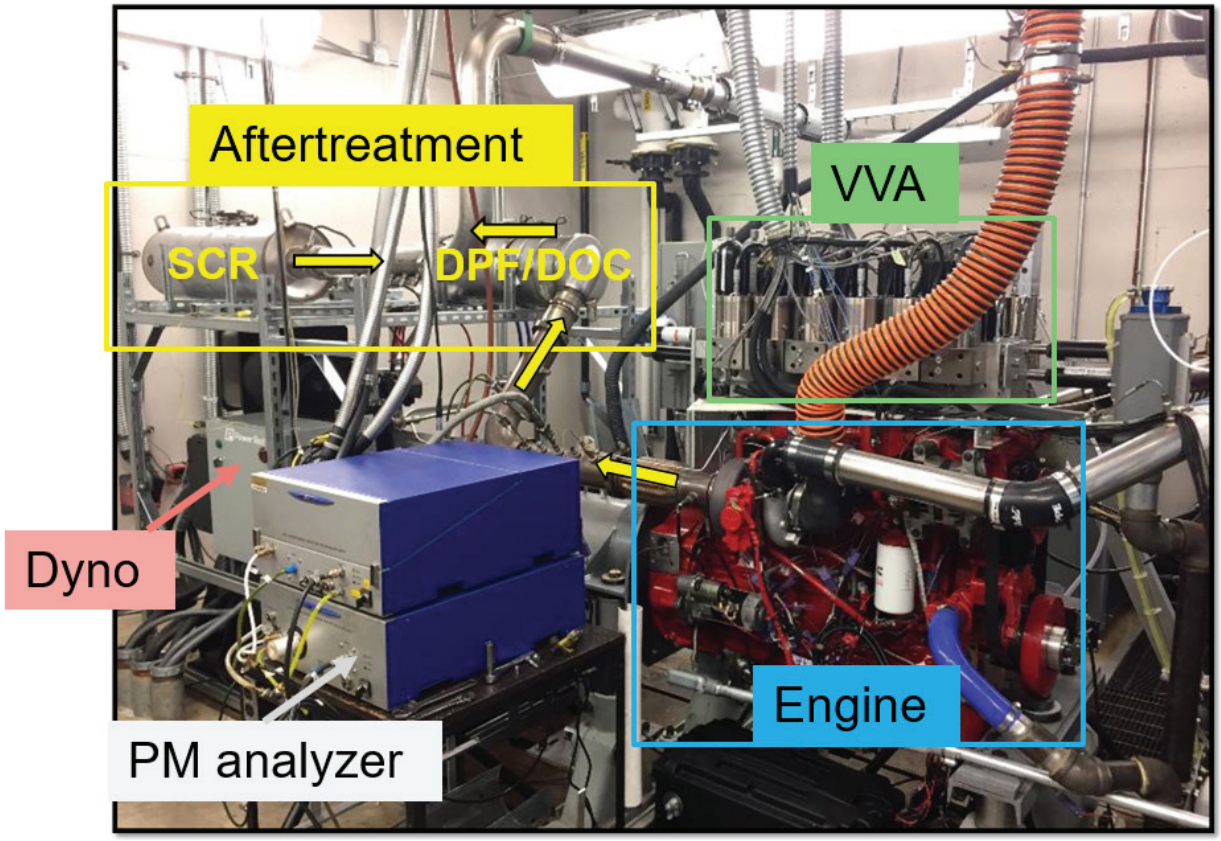

Figure 1.9. Camless Cummins multi-cylinder engine testbed at Purdue University. The engine exhaust is connected to a 2010 Cummins aftertreatment hardware.

The engine is connected to a PowerTest AC dynamometer via a rubberized drive shaft, which controls the speed and applies load to the engine. This dynamometer can be used for transient operations, which helps in emulating drive cycles such as HD-FTP or FTP-72 on the engine.

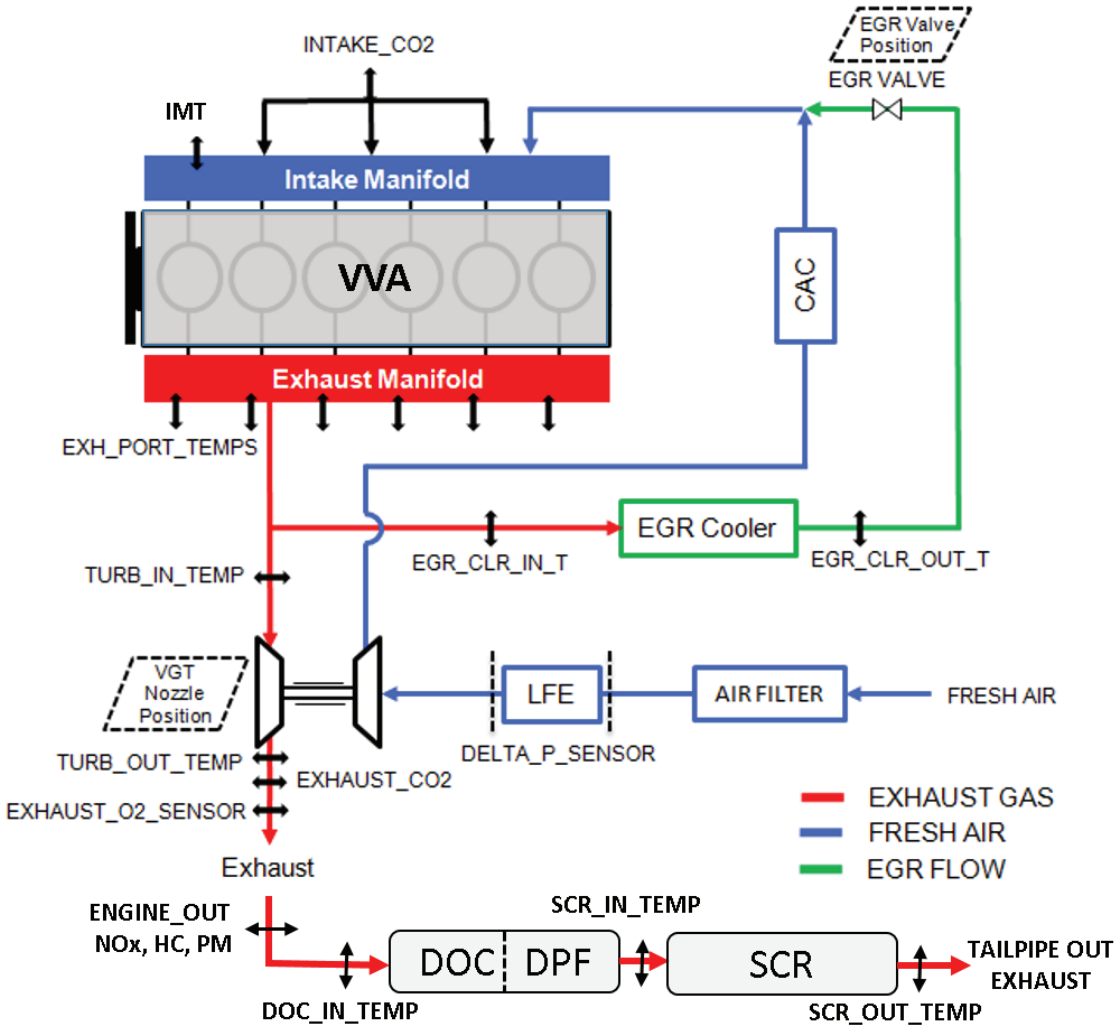

Figure 1.10. Schematic of the Camless Cummins multi-cylinder Engine Testbed at Purdue University.

Table 1.1. Nominal engine parameters and metrics

Parameter	**Value**	**Units**
Number of cylinders	6	–
Number of valves per cylinder	4	–
Bore diameter	107	mm
Stroke length	124	mm
Connecting rod length	192	mm
Geometric Compression ratio	17.3:1	–
Firing Order	1,5,3,6,2,4	–
Intake Valve Open (IVO) timing	340	aTDC
Intake Valve Close (IVC) timing	565	aTDC
Peak Intake Valve Lift (IVL)	8.5	mm
Exhaust Valve Open (EVO) timing	120	aTDC
Exhaust Valve Close (EVC) timing	380	aTDC
Peak Exhaust Valve Lift (EVL)	10	mm
Exhaust Valve diameter	29.4	mm
Intake Valve diameter	29.27	mm
Maximum Injection Pressure	1800	bar

The aforementioned equipment, full access to adjustment of parameters in the engine control module (ECM), and additional temperature and pressure sensors are integrated using a dSPACE system. The dSPACE system simultaneously controls the VVA system, sends and receives data with the ECM, and samples all of the external measurement channels.

1.3.1 Measurements

The exhaust temperature is measured at the outlet of the turbine and is referenced in this document as TOT. Two Kistler 6067 and four AVL QC34C in-cylinder pressure transducers are used in tandem with an AVL 365C crankshaft position encoder together with an AVL 621 Indicom module for high-speed in-cylinder pressure data acquisition. Laboratory-grade fuel flow measurement is used to measure the fuel consumption. A laminar flow element is used to calculate the air flow through the engine. The fuel flow rate is measured gravimetrically using a Cyrius Fuel Subsystem (CFS) sourced from Cybermetrix. CO_2 concentration is measured in both the intake manifold and exhaust stream through the use of Cambustion NDIR500 analyzers. These analyzers are fast-responding and suitable for transient operation. NOx is measured in the exhaust stream using a Cambustion fNOx400 analyzer. NOx and uHC concentrations are also measured using a California Analytical Instruments (CAI) heated chemiluminescent detector (HCLD) and heated flame ionization detector (HFID) analyzer, respectively. PM in the exhaust stream is measured using an AVL483 photo-acoustic transient analyzer. Unless otherwise specified, all emissions measurements in the exhaust stream are located upstream of the AFT system.

1.3.2 Variable Valve Actuation System

Figure 1.11 presents a schematic of the VVA system. The valve profiles are generated in Simulink/MATLAB and the dSPACE hardware is used to transmit voltage feedback to the servo valves via the controller and amplifier. The servo valves shuttle high-pressure hydraulic oil to one side of the valve actuators. These actuators push on the valve pairs through a valve bridge to open them. The return force from the valve springs closes the valves as the actuators retract. The valve position of the valve actuator is measured using a LVDT which then sends a voltage to the controller for closed-loop feedback control of the valves in a cycle-cycle and cylinder-independent

basis. Both the intake and exhaust valve pairs for each of the six cylinders are actuated by the VVA system such that it has a total of twelve actuators.

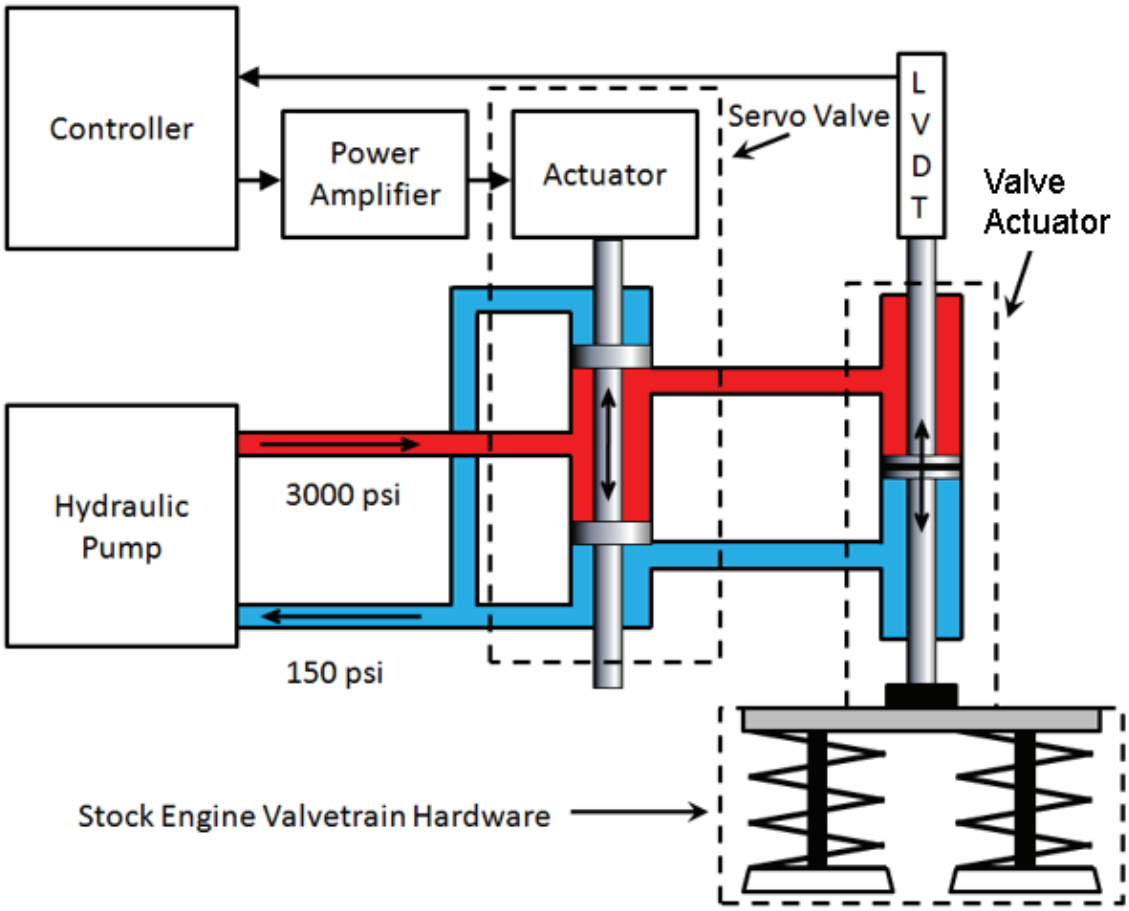

Figure 1.11. Schematic of Purdue Variable Valve Actuation System.

The valve profiles have six key features that describe the valve lift shape (as illustrated in Figure 1.12):

1. Intake Valve Opening, IVO
2. Peak Intake Valve Lift, IVL
3. Intake Valve Closing, IVC

4. Exhaust Valve Opening, EVO

5. Peak Exhaust Valve Lift, EVL

6. Exhaust Valve Closing, EVC

Using these inputs as shown in Figure 1.12, valve strategies such as IVC modulation (Early IVC or Late IVC) can be realized on the engine. Late and early IVC valve strategy can be achieved by delaying or advancing the IVC timing from the nominal position. CDA is achieved by deactivating the valve motions and fuel injections for either 2, 3 or 4 cylinders.

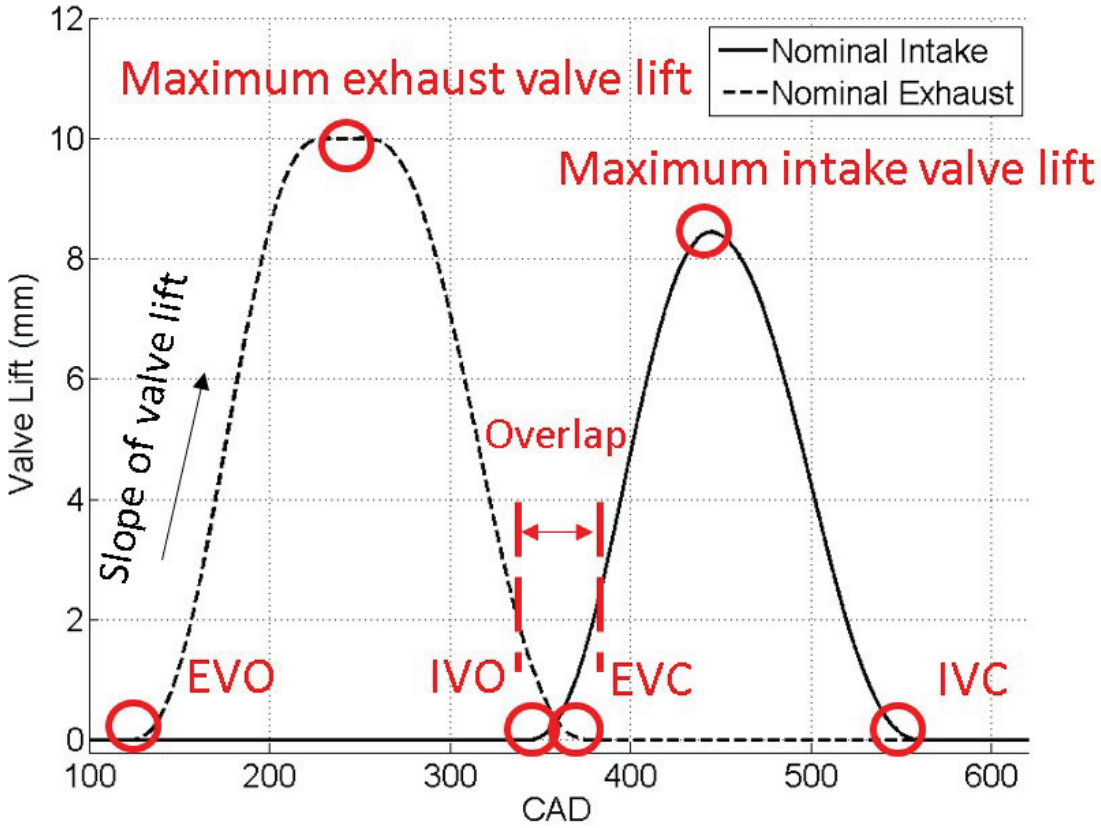

Figure 1.12. Valve profiles for conventional operation illustrating the opening, lift and closing for intake and exhaust valve profiles.

1.3.3 Aftertreatment System

A Cummins AFT system, equipped with a DOC, DPF and SCR, is connected to the outlet of the engine, as shown in Figure 1.9. The AFT is used in passive mode, i.e., the exhaust gas is passed through the system without active urea injection, for measurement of catalyst bed temperatures. Thermocouples and thermistors are installed at the inlet and outlet of DOC, DPF and SCR to measure the temperature of gas entering and exiting each AFT component. A differential pressure sensor is installed in the DPF to identify if the DPF is excessively clogged, so that an active regeneration may be performed. Primarily two specific modes are studied for this system:

1. warm-up operation: wherein the AFT is warmed up quickly to its most efficient operating temperature as fast as possible.

2. stay-warm operation: wherein the system temperature is maintained in a most fuel efficient manner as possible.

1.3.4 Boundary Conditions

Intake and exhaust boundary conditions such as pressures and temperatures on the engine are to be maintained to ensure testing repeatability. Fuel supply temperature is maintained via the fuel metering system at 41°C. Fresh air maintained at 50% relative humidity and 25°C is supplied to the engine through a combustion air supply system. Additionally, the temperature of the water-side supply of the CAC heat exchanger is controlled via an active heat exchanger at a constant 25°C. Repeatable conditions at the intake manifold are important due to the sensitivity of engine performance, particularly NOx production which is dependent on intake manifold temperature and relative humidity. The supply pressure is maintained at atmospheric pressure via a weighted damper system that vents excess supply air to the test cell. This prevents an artificial supercharging effect of the turbocharger compressor.

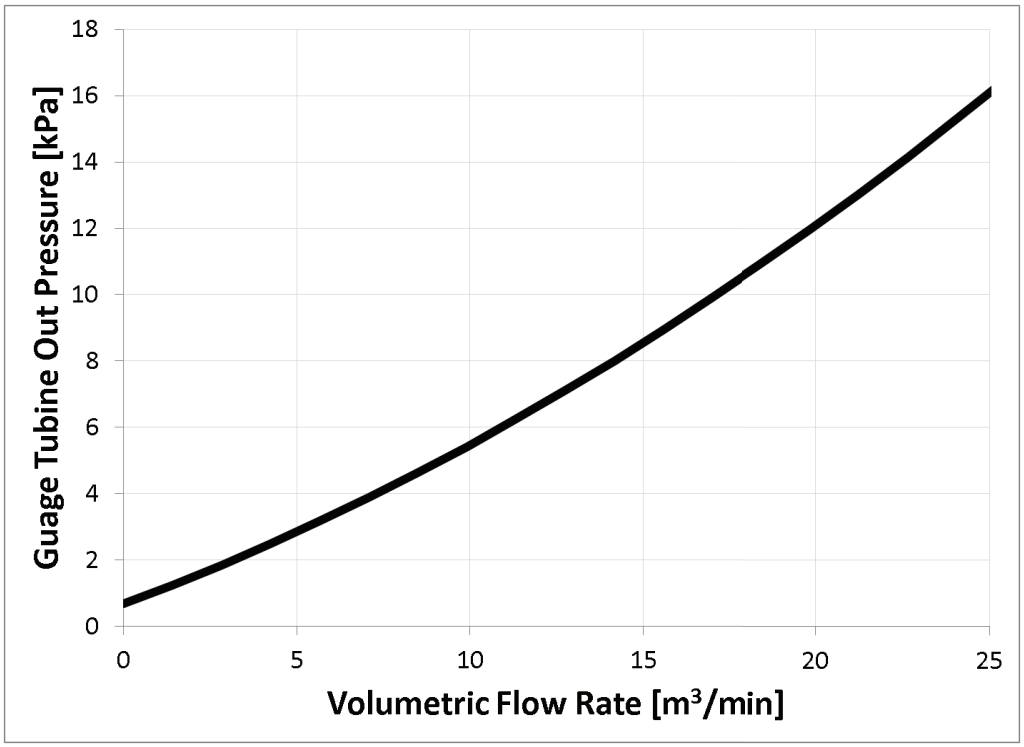

Figure 1.13. Turbine outlet pressure vs volumetric flow rate relationship simulating AFT back pressure for a heavy-duty diesel engine.

The exhaust pressure boundary condition is maintained via one of two methods with the goal of representing the downstream pressure of an on-vehicle engine. If the AFT system is attached during testing, this system provides the necessary downstream pressure because the setup represents an on-vehicle system. However, for steady-state testing, the AFT system is often bypassed. In order to simulate the downstream pressure applied by the AFT system in this scenario, a butterfly valve is used in the exhaust by-pass pipe to simulate the back pressure for steady-state experiments. At each operating condition the butterfly valve is adjusted to match the desired turbine outlet pressure based on the volumetric flow rate per Figure 1.13.

1.4 Contributions

1.4.1 Intake/Exhaust Rebreathing and Fired/Non-Fired Reverse breathing

The author led the efforts to implement non-fired reverse breathing (NFRB) and intake rebreathing (IRB), two unique AFT stay-warm strategies, for the first time on a modern diesel engine. The author also co-led the study with Soumya Nayyar, a former MSME student, to develop and test valve controller code in simulink, to run alternate breathing strategies such as exhaust rebreathing (ERB) and fired reverse breathing (FRB) on the testbed at Herrick labs. Preliminary experimental screening work was then carried out to implement single and two cylinder FRB at 1200 rpm/50 ft-lbs. Screening work was also carried out for single and two cylinder ERB at 750 rpm/11 ft-lbs. The preliminary results showed both fuel economy and AFT thermal management benefits. The author then led the study on characterizing the benefits of implementing *FRB*, *NFRB*, *ERB* and *IRB* at loaded idle (800rpm/50 ft-lbs) condition. The author also carried out extensive study to implement various reverse breathing modes experimentally on the engine. The author also led work on optimizing these strategies at idle for stay-warm AFT performance. It was demonstrated using experimental data that *NFRB* enabled 26% fuel consumption savings when compared to conventional stay-warm operation, 60°C improvement in TOT and 28% reduction in exhaust flow compared to conventional best fuel consumption operation. *2-cylinder NFRB* was also run at idle portions during HDFTP drive-cycle and showed 2% fuel consumption benefit when compared to conventional thermal management calibration. Further details of this work are discussed in chapters 5 and 6.

1.4.2 CDA and IVC Modulation at High Speed Low Load Operation

The author led the work to study the impact of low air flow strategies such as *open VGT* and *CDA* at high speed (2200 RPM) operating conditions. Approximately 30%

of the fuel consumed during typical heavy-duty vehicle operation occurs at these elevated speeds with low-to-moderate loads. The experimental screening work was carried out between 1.3 and 6.4 bar BMEP engine load, while constraining for emissions and other physical engine constraints. The fuel economy and AFT thermal management of the engine at these conditions can be improved using conventional means as well as *CDA* and *IVC modulation*. Airflow reductions result in higher exhaust gas temperatures, which are beneficial for AFT thermal management, and reduced pumping work, which improves fuel efficiency. Airflow reductions can be achieved through a reduction of displaced cylinder volume by using *CDA* and through reduction of volumetric efficiency by using *IVC modulation*. This work showed that, depending on load, *CDA* and *IVC modulation* can be used to reduce the fuel consumption between 5% and 25%, increase the rate of warm-up of AFT, maintain higher temperatures, or achieve active DPF regeneration without requiring dosing of the DOC [42]. Further details of this work is discussed in Chapter 2.

1.4.3 LIVC Optimization at 1200 rpm/7.6 bar BMEP

The author led GT power simulation and experimental study to optimize the engine operation at highway cruise operation (1200 rpm/ 7.6 bar BMEP) using late *LIVC* modulation. This work was part of Cummins SuperTruck 1 project which aimed at improving the brake thermal efficiency of the engine to greater than 50%. To begin simulations, the GT-power engine simulation model was calibrated using the engine experimental data. This provided a platform to study the gas exchange process during *LIVC* in detail before experimental testing. The design of experiments was developed and simulations were run on a calibrated model in GT power to develop data regression models. Using the regression models, constrained optimization was carried out to:

1. Minimize fuel consumption

2. Maximize TOT

3. Maximize turbine outlet power

The optimized inputs (EGR fraction, VGT position, fuel injection timing, fuel rail pressure) were used to experimentally validate the results on the engine testbed. *LIVC* enables about 150-200°C at low NOx levels although it does not enable any fuel saving at cruise operation. Further details of this work is discussed in Chapter 3.

1.4.4 Transient CDA Characterization

The author led the work to study the transient launching capability of *CDA* to normal *6-cylinder* operation at 1200 RPM. This work was based on prior efforts from Leighton Roberts, a former MSME student, on identifying the challenges of transient *CDA* operation. Assistance was also given to Dheeraj Gosala, a direct PhD student, for experimental testing and valve controller code development to test the launching capacity of *CDA* at different instances during the HDFTP. The main goal of this work was to verify if *CDA* can meet the torque profile while having similar or lower emission levels as normal *6-cylinder* operation. The work demonstrated that it is possible to operate a diesel engine at low loads in *CDA*, without compromising its transient torque performance, a key finding in enabling the practical implementation of *CDA* in diesel engines [43]. Further details of this work is discussed in Chapter 4.

1.4.5 Idle Optimization Using Flexible Valve-train

The author co-authored an experimental published study along with Chuan Ding, a former PhD student, to improve fuel efficiency and AFT thermal management during unloaded idle (800RPM, 11 ft-lbs) and loaded idle (800RPM, 100 ft-lbs) operating conditions, for a modern diesel engine equipped with VGT. Various novel VVA strategies such as *CDA*, *variable valve lift* and *internal EGR* were studied and compared with conventional thermal management strategies such as late fuel injections and throttling via over-closed VGT [23]. *CDA* was found to increase TOT above 300°C at loaded idle condition without a fuel penalty. At unloaded idle condition, *CDA*

along with flexible valve-train increased TOT above 200°C without a fuel penalty compared with stock *6-cylinder* operation. All the strategies were constrained for emissions (NOx, PM, uHC) and other physical engine limits.

1.4.6 CDA at Cruise Condition (1200 rpm/300 ft-lbs)

The author co-led experimental published study along with Xueting Lu, a former MSME student, to improving fuel efficiency and AFT thermal management characteristics at highway cruise condition using *half engine CDA* and *two-third engine CDA* [21]. CDA can be used to generate the 500 to 600°C DPF-inlet temperatures required for particulate matter regeneration with oxygen without the need for a fuel doser, DOC or HC burner at cruise condition. This is primarily a result of a reduction in AFR realized by reducing the displaced cylinder volume through *CDA*.

1.4.7 Using EEVO and iEGR for Get Hot Operation During HDFTP

The author co-led an experimental published study with Dheeraj Gosala, a direct PhD student, to improve the AFT warm up operation of the engine during a HDFTP. Several technologies such as *CDA*, *EEVO* and *internal EGR* were screened for steady state operation at different speed and load conditions with the focus mainly on idle (800 rpm /50 ft-lbs) condition. The semi-optimized conditions were then used over the HDFTP to estimate the AFT warm-up potential of these strategies. This work showed that strategies such as *EEVO* and *internal EGR* could significantly improve the thermal management characteristics of the AFT but has a slight fuel penalty. The results demonstrate that implementing *EEVO with iEGR* during steady-state loaded idle conditions enables TOT above 400°C, and when implemented over the HD-FTP, is expected to result in a 7.9% reduction in tailpipe-out NOx, but with a 7% fuel penalty.

1.4.8 Cylinder Cutout Comparison with CDA

The author co-led published study with Kalen Vos, a direct PhD student, to understand the differences between *cylinder cutout* and *CDA*. *CDA* includes both fuel and valve deactivation whereas cylinder cutout only has fuel injection deactivation. This study focuses on AFT thermal management improvements possible via *CDA* and *cylinder cutout* at a curb idle condition of 800 RPM and 1.3 bar BMEP. It is experimentally demonstrated that both *CDA* and *cylinder cutout* enable a similar improved thermal management performance by preserving efficient AFT operation over a conventional thermal calibration with late injections and a shut VGT. In addition, *cylinder cutout* demonstrates a 17% fuel savings, while *CDA* demonstrates a 40% fuel savings, over the conventional 6-cylinder thermal calibration. However, the performance of *cylinder cutout* is subject to the geometry of the split exhaust manifold. Specifically, the location of the exhaust gas recirculation (EGR) loop on this split manifold directly impacted the composition of the EGR gas. Effectively, for the same thermal management performance/improvement, the hardware required to implement *CDA* is worth an additional 23% fuel savings over *cylinder cutout*, which only requires fuel-deactivation for implementation.

1.4.9 Torsional Characteristics of CDA

The author led the work to identify and characterize the torsional vibrations, using a hall effect sensor, during CDA and conventional operation. Load sweeps were conducted at constant speed of 1200 RPM for *6-cylinder* and *3-cylinder CDA* operation (keeping all other parameters constant) as shown in Figures 1.14 (a) and (b). For *6-cylinder* case, the load was swept from 100 to 500 ft-lbs. The firing frequency is 60 Hz and the difference in resultant torsional characteristics are captured in the amplitude and frequency of the fast fourier transform (FFT). As load is increased, the amplitude increases with the load proportionally due to more fuel being burnt per cylinder, which increases the in-cylinder pressure forces acting on the piston. This

then translates to increased forces on the crankshaft leading to increased torsion. The trend is also consistent for *3-cylinder CDA*. For *3-cylinder CDA*, the main firing frequency is 30 Hz. The maximum load that could be attained at this speed was 300 ft-lbs without reaching very low AFR. *3-cylinder CDA* has higher amplitude due to increased per-cylinder fueling.

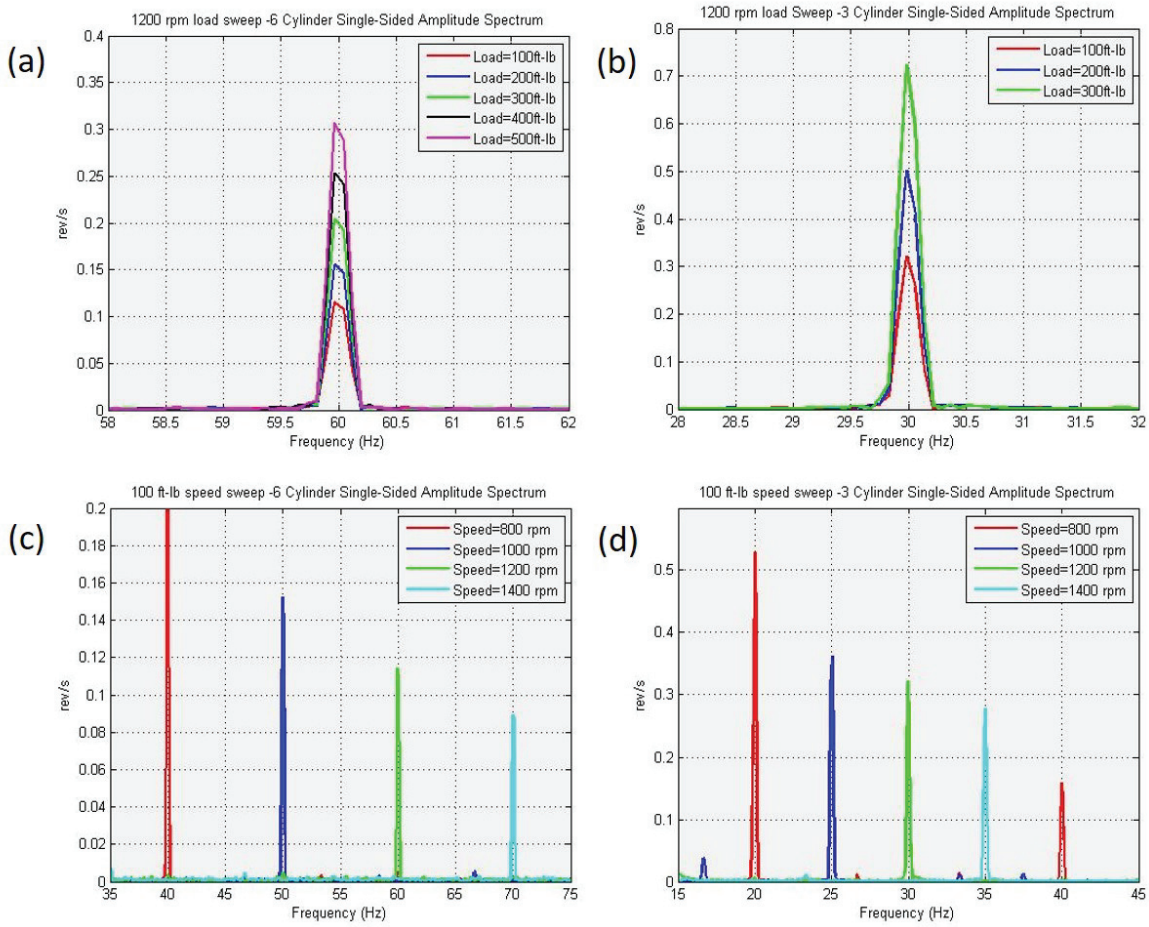

Figure 1.14. Experimental results showing the FFT of angular acceleration of (a) *6-cylinder* operation at 1200 RPM with varying loads, (b) *3-cylinder CDA* operation at 1200RPM with varying loads, (c) 6-*cylinder operation* with varying engine speeds, (d) *3-cylinder CDA* operation with varying engine speeds.

Speed sweeps were conducted at 100 ft-lbs and the torsional response for *6-cylinder* operation and *3-cylinder CDA* operation mode was compared as shown in Figures 1.14 (c) and (d). As the speed increases, the firing frequency increases and shifts away from the natural frequency of the system (<20 Hz), thus the torsional amplitude response decreases. This is consistent even in *3-cylinder CDA* operation. However for *3-cylinder CDA*, the torsional response is higher when compared to *6-cylinder* cases which is the expected due to improper balancing.

Differences in torsional characteristics when variables such as rail pressure, start of injection and boost pressures were varied, were also identified. No significant difference in torsional response for SOI, rail pressure sweeps were observed. As boost pressure is increased, the amplitude of the FFT increased due to higher fueling which leads to higher forces on the piston. The main goal of these experiments was to identify if any of the CDA mode operation activates any frequencies closer to the resonance frequency of the engine-driveshaft-dyno system and ensure safe operation of the system. In order to do this, the inertias of all the components and torsional stiffness of the driveshaft were used to estimate the resonance frequency of the system. Using this information and the data from the above-mentioned experiments, safe CDA combinations were identified for the current driveshaft system. Also recommendations for a new driveshaft for the new test facility were made using this information.

1.4.10 Early Exhaust Valve Opening to Improve Transient Performance

The author led the study to identify the benefits of using early exhaust valve opening (EEVO) during the initial few cycles during transient load increase at an engine speed 2200 RPM. The valve controller code in simulink was modified to allow transient load increase at a constant speed. Also, the code was modified to enable *EEVO* mode for a few cycles during the transient load increase. This work was motivated to identify solutions to capitalize on the fuel economy benefits shown in the previous subsection. The stock calibration at this high engine speed is set up

in such a way that the VGT is squeezed in order to prepare the air flow path for a transient fueling event. At an engine speed of 2200 RPM, a load ramp of 0 to 550 ft-lbs at 300 ft-lbs/sec ramp rate is considered. In Figure 1.15, three cases of open VGT with *EEVO* are compared with fully ECM controlled case where the VGT is squeezed. The shaded region represents when *EEVO* occurs for the *open VGT* cases. For this experiment, the number of engine cycles where the EEVO mode is active is set to 20 cycles. For the three *open VGT* cases shown in the figure, the *EEVO* during transients is set to 120 CAD (nominal), 60 CAD and 30 CAD, respectively. The VGT is initialized to 50% open until the 1 second mark for the *open VGT* cases and then the ECM takes control of the VGT during the engine load increase. The ECM controls all other conventional actuators (SOI, rail pressure, fueling quantity, fueling timing) throughout the experiment. When compared to the ECM baseline, all the *open VGT* cases lag in terms of transient torque response. The torque response for the most aggressive *EEVO* case eventually catches up with the *ECM controlled* case, as seen in the zoomed in plot. The main reason why the torque starts to catch up for the aggressive *EEVO* case with the ECM controlled case is due to additional turbocharger speed gained during *EEVO*, which allows more air flow through the engine and hence more fueling later on in the transient event (less fuel limiting action). Hence, by using *EEVO* during the initial few cycles, the majority of the fuel energy is transferred to the exhaust, which then increases the enthalpy transfer to the turbocharger thereby reducing the turbocharger lag. The work showed that *EEVO* gives mild performance benefits for reducing the turbo lag and hence is a potential solution.

1.4.11 Oil Accumulation Estimation during CDA

Assistance was given to Mayura Halbe and Brad Peitrzak, former MSME students, for experimental testing and data analysis for estimating the amount of oil accumulated in the deactivated cylinders. Unique valve controller code in simulink was developed and tested, to synchronize valve events with fuel injection events dur-

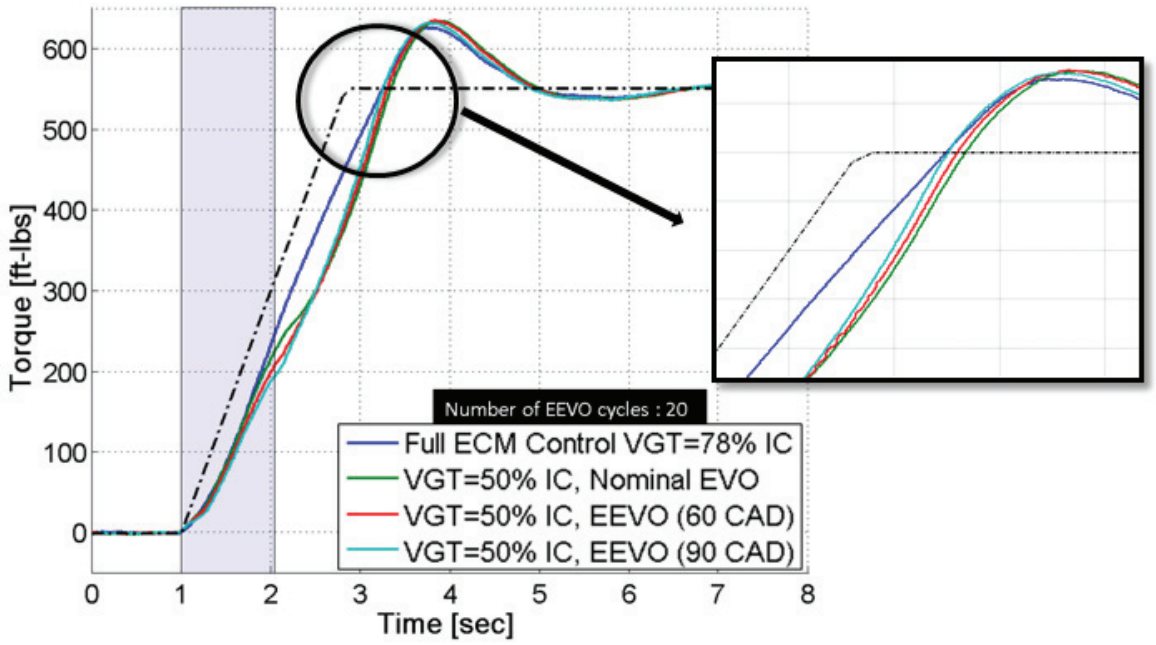

Figure 1.15. Comparison of torque response for cases with open VGT and EEVO with the full ECM controlled case. For the open VGT cases, the VGT position is 50% open untill the 1 second mark and then ECM takes over control of the VGT. The zoomed in plot shows the response near the 550 ft-lb reference torque value.

ing reactivation of cylinders, in order to conduct these experiments. In the first engine cycle after reactivation, it was verified that all cylinders receive the correct amount of fuel per the engine firing order. This work led to development of suggestions regarding the duration of time the engine could be operated in *CDA* mode without significant oil accumulation, and other methods to minimize oil accumulation during *CDA* [44].

1.4.12 CDA Cylinder Combination Code Development

Valve controller code in simulink was developed and tested to enable any cylinder combination of deactivation during *CDA* and added the functionality to change the number of cycles for recharging the deactivated cylinders via the intake or the exhaust valves. This work served as foundation for several future *CDA* experiments carried out at engine testcell in Herrick labs.

1.4.13 Optical In-cylinder Imaging of a Multi-cylinder Diesel Engine

Assistance was given to Conor Martin, Emerson Houck and Yuhui Zhu for developing instrumentation for optical imaging of in-cylinder conditions of a multi-cylinder diesel engine. The main goal of this work is to develop and test optical imaging hardware, similar to a typical in-cylinder pressure transducer, so that the new hardware can be used for studying the in-cylinder combustion characteristics of a multi-cylinder diesel engine.

1.4.14 SuperTruck II Vehicle Modeling and Simulation

The author co-led efforts to develop a heavy-duty vehicle simulation tool to study real-world drive cycles and estimate key vehicle metrics as part of the Supertruck II program. SuperTruck II is a DOE-funded program, to continue to improve upon the SuperTruck I program. Following were the objectives of this work:

1. To develop a common vehicle/power-train simulation tool for all industry partners

2. To replicate the 2017 baseline vehicle field test results.

3. To evaluate value propositions put forth by the partners.

4. To use a common simulation tool for various SuperTruck II analysis tasks

Autonomie was selected as the tool of choice by the industry partners. The model architecture used for class 8 truck simulations is shown in Figure 1.16. The archi-

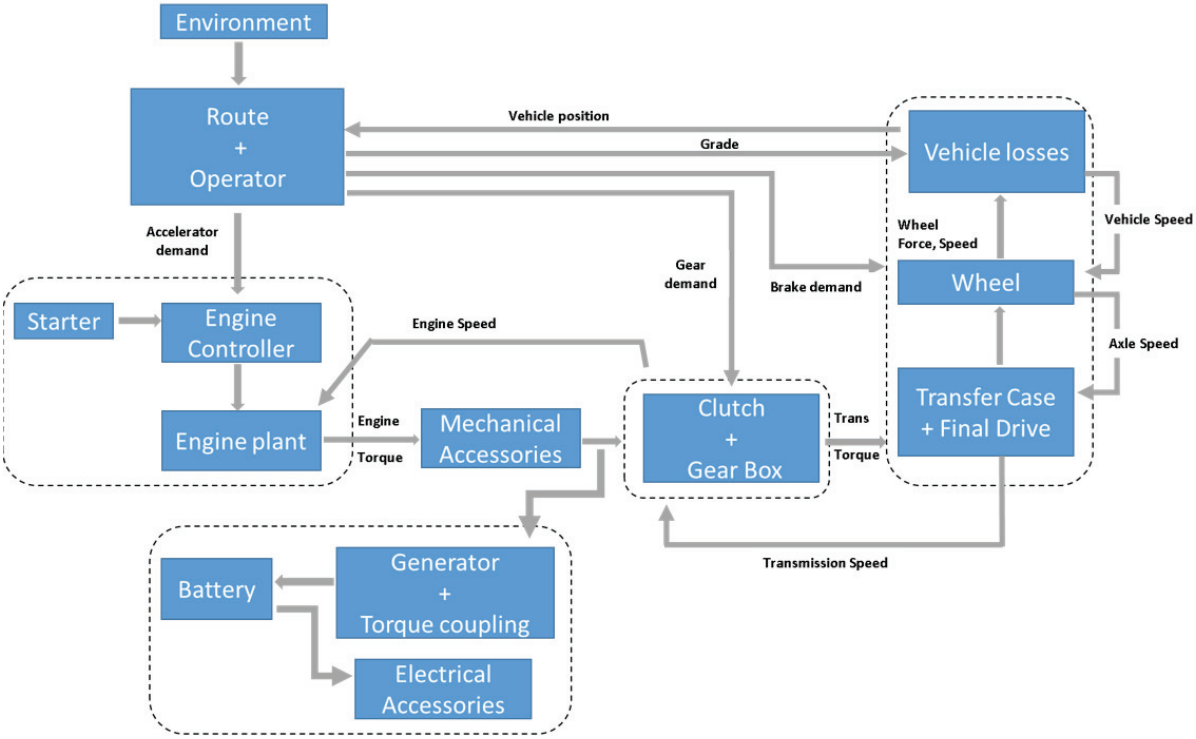

Figure 1.16. Model architecture used for SuperTruck 2 built using Autonomie. The model shown is for a class 8 line-haul 4WD architecture.

tecture was adapted from a default architecture available in the Autonomie software, and modified accordingly per the information provided by the industry partners.

The model is forward looking and at present does not include any electrification or advanced technologies. The route sub-model generates a vehicle speed target for each vehicle position. The operator sub-model generates throttle, brake and clutch commands in order to achieve the desired vehicle speeds. The engine responds to the throttle response and produces the corresponding torque. After accounting for the drivetrain losses, and the vehicle resistive forces (aero, rolling resistance and grade), the net force on the vehicle propels the vehicle.The model is built on a MATLAB/Simulink interface. The ode4 (Runge-Kutta) solver is used with a step size of 0.01 sec (fixed step). The model was developed successfully and simulations were run to validate the model using experimental field data from SuperTruck I program. The calibrated model was also compared with Cummins in-house tool and then handed over to the industry sponsors.

1.4.15 Modeling Fuel Economy Impact of Full Engine CDA

The author co-led the study with Kalen Vos, a direct PhD student to model the impact of different types of *CDA* on real-world vehicle routes for a Class 8 heavy-duty vehicle. The model described in the previous subsection was used in this study. Using the steady-state results at different operating conditions, a fuel savings model was developed as shown in Figure 1.17.

This model was then used to estimate the fuel savings due to *CDA* during HDFTP drive cycle and real-world driving route from SuperTruck I program. *CDA* was estimated to provide about 4.84% benefit over the HDFTP when compared to conventional six-cylinder operation.

1.4.16 Modeling Diesel Decel Compressor Surge

Assistance was given to Alex Taylor, a PhD student, and Troy Odstricil, a MSME student, with the experimental published study to model and avoid compressor surge

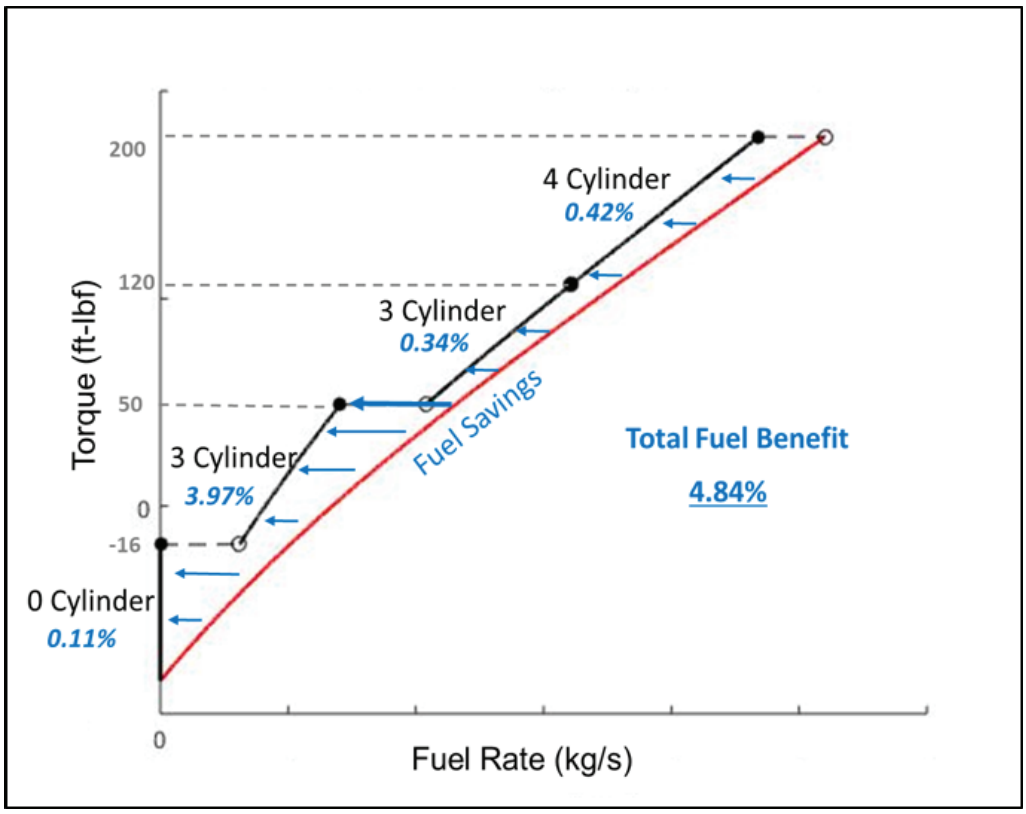

Figure 1.17. Fuel savings model predicting amount of fuel benefit with different modes of *CDA* including *full engine CDA* where all the cylinders are deactivated.

in diesel engine during CDA transitions. This study proposes and validates an algorithm which:

1. predicts the intake manifold pressure increase instigated while transitioning into cylinder deactivation during motoring,

2. estimates future mass air flow,

3. avoids compressor surge by implementing staged CDA during the onset of engine motoring operation.

1.4.17 Impact of Compression Ratio on Closed Cycle Efficiency

The author led efforts to evaluate the effect of increased compression ratio (CR) on a Cummins 15L diesel engine. Constrained optimization process was carried out for each piston to maximize closed-cycle efficiency (CCE). Two pistons with different CR was tested on a Cummins heavy-duty engine to evaluate the impact of CR on CCE of the engine. An optimization process was carried out for each piston to maximize CCE. Increasing CR leads to an increased EER and increasing charge-fuel-ratio helps achieve lower in-cylinder heat loss. Maximum CCE is achieved by maximizing effective expansion ratio and lowering in-cylinder heat transfer. The CCE for the higher CR piston is about 4% higher than that for the lower CR piston.

1.5 Outline

The previous section introduces in brief, the personal contributions of the author to the activities of Professor Shaver s research group. Each contribution demonstrates a case in which the author was able to significantly contribute to the effort, as evidenced by either lead or second/third authorship on the accompanying archival journal write-ups. The remainder of this thesis focuses on the specific academic contributions in which the author was the lead investigator, as outlined below:

Chapter 2: CDA and IVC Modulation at High-Speed Low-Load Operation outlines the work done by the author, to study the fuel economy and AFT thermal management benefits of *CDA* and *IVC modulation* at 2200 RPM/1.3-6.4 bar BMEP. The fuel savings of *CDA*, *open VGT* and *IVC modulation* are between 5% to 25% depending on the load. The stay-warm characteristics of these strategies were also identified and compared with the stock six-cylinder operation. The warm-up characteristics of these strategies was studied using analytical model of heat transfer rate developed prior in the research group. Based on the steady-state results, *half engine CDA* was also implemented over the HDFTP drive-cycle at all loads below 3 bar BMEP to evaluate the fuel economy benefits.

Chapter 3: LIVC Optimization at 1200 rpm/7.6 bar BMEP outlines the GT-POWER simulation work carried out to study and optimize the performance (BSFC, TOT, TOP) characteristics vs emissions (BSNOx) trade-offs at 1200 RPM/7.6 bar BMEP (highway cruise condition). Regression models were developed in Minitab software using the data from GT-POWER simulation package. Using the models developed, several optimized parameter values were derived for different trade-offs and the trade-offs were experimentally verified on the engine.

Chapter 4: Transient CDA Characterization details the experimental work done by the author to study and characterize the transient *CDA* to normal operation transition. This work served as the basis for the published work on dynamic engine operation using *CDA* [43].

Chapter 5: Alternate Breathing Strategies details the work led by the author to implement and study the fuel economy and AFT thermal management benefits of novel alternate breathing strategies such as reverse breathing and rebreathing, for the first time in a modern diesel engine. This chapter also describes in detail certain challenges implementing these strategies and offers solutions to enable the benefits achieved from these strategies.

Chapter 6: Low-Load AFT Stay-Warm Strategies details the work led by author to implement and compare the fuel economy and AFT thermal management benefits of reverse breathing and *IRB* strategies with other VVA strategies such as *CDA*, *internal EGR*, *IVC modulation* at 800 RPM/1.3 bar BMEP. Similar comparisons were made at 1200 RPM/1.3 and 2.6 bar BMEP. *NFRB* was implemented at all stay-warm idle portions during HDFTP and enabled 2% fuel benefit compared to conventional thermal management 6-cylinder strategy.

Chapter 7: Summary and Recommendations recaps the work done on *CDA*, *IVC modulation* and alternate breathing strategies, such as reverse breathing to improve fuel efficiency and AFT thermal management and recommends future work to be implemented on the engine testbed.

2. CDA AND IVC MODULATION AT 2200 RPM

2.1 Introduction

In order to study the impact of advanced engine system strategies on AFT thermal management, it is helpful to compare strategies during operation of standardized test procedures provided by the EPA. The HDFTP is used for regulatory emission testing of heavy-duty on-road engines in the United States. This test was developed by taking actual operating data over a variety of heavy-duty truck and bus driving patterns on roads and expressways [1]. Figure 2.1 shows the speed and normalized BMEP profile through time for the HDFTP. Figure 2.2 shows the fuel consumption over a HDFTP mapped around 8 steady-state engine operating regions. The number displayed next to a bubble signifies the percentage of fuel consumed at these operating conditions. In this study, the benefits of using VVA for improving fuel efficiency and AFT thermal management is studied for the cross-hatched bubbles at an engine speed of 2200 RPM, for two reasons:

(i) more than 30% of the fuel used during the HD-FTP is consumed in these operating regions, and

(ii) as will be shown, there is an opportunity to increase fuel efficiency and exhaust temperatures at these conditions by reducing airflow via both conventional engine actuators and variable valve actuation.

During these high-speed low-load conditions, the AFR is elevated given the reduced fueling required at low loads, and in order to prepare for a sudden increase in fueling resulting from a commanded increase in desired torque and power. There are several possible strategies for improving the engine torque response to acceptable levels when AFR is reduced during high-speed, low-load operating conditions such as:

(i) early exhaust valve opening (EEVO) [38]

(ii) internal exhaust gas recirculation (iEGR) via combustion gas trapping or re-induction

(iii) turbocharger electrification [45]

(iv) supercharging [46, 47]

(v) powertrain hybridization [48, 49] and

(vi) availability of look-ahead information [50], through vehicle data connectivity with other vehicles or the cloud, to allow anticipation of an upcoming transient event.

These methods are not the subject matter discussed in detail in this chapter. Instead, this chapter outlines, in detail, the strategies for achieving, and benefits of, low AFR operation at high-speed, low-load conditions. AFR reduction strategies considered in this chapter include:

(i) "opening up" the variable geometry turbine turbocharger (VGT),

(ii) reducing the displaced volume through *CDA*,

(iii) reducing volumetric efficiency via *LIVC*, and

(iv) some combination of these strategies.

Implementation of EIVC and LIVC was observed to produce a notable increase in the exhaust gas temperature [51, 52]. Prior efforts have also shown that LIVC can be used to increase exhaust temperature [22].

The first results section of this chapter focuses on evaluating the fuel economy benefits of the above specified strategies at elevated speed (2200 RPM), low-load operating conditions (1.3 to 6.3 bar BMEP). The second results section focuses on which strategy works best, when the main goal is to maintain elevated AFT system

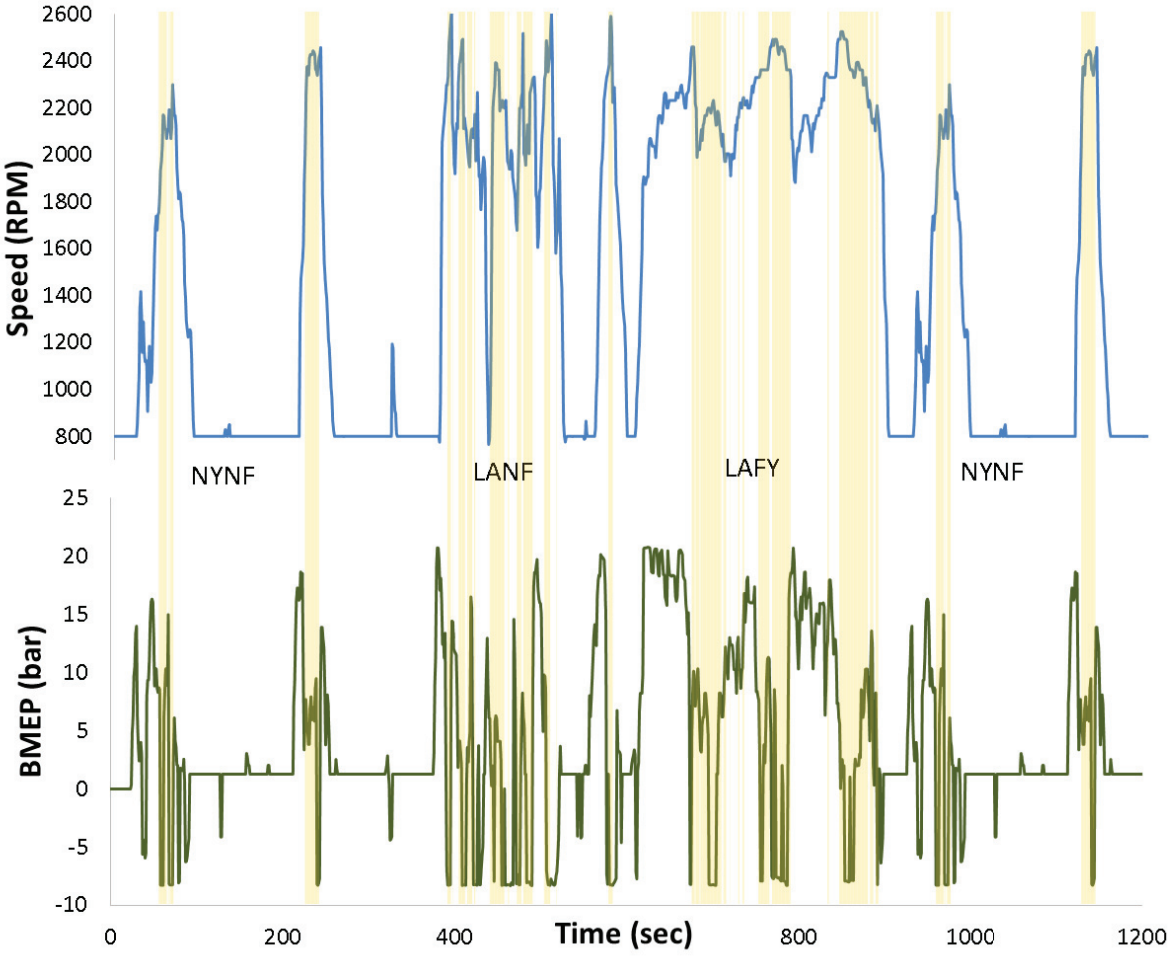

Figure 2.1. Engine speed and BMEP vs time profile for the HDFTP. The highlighted sections shows the high engine speeds, low load conditions as crosshatched in Figure 2.2.

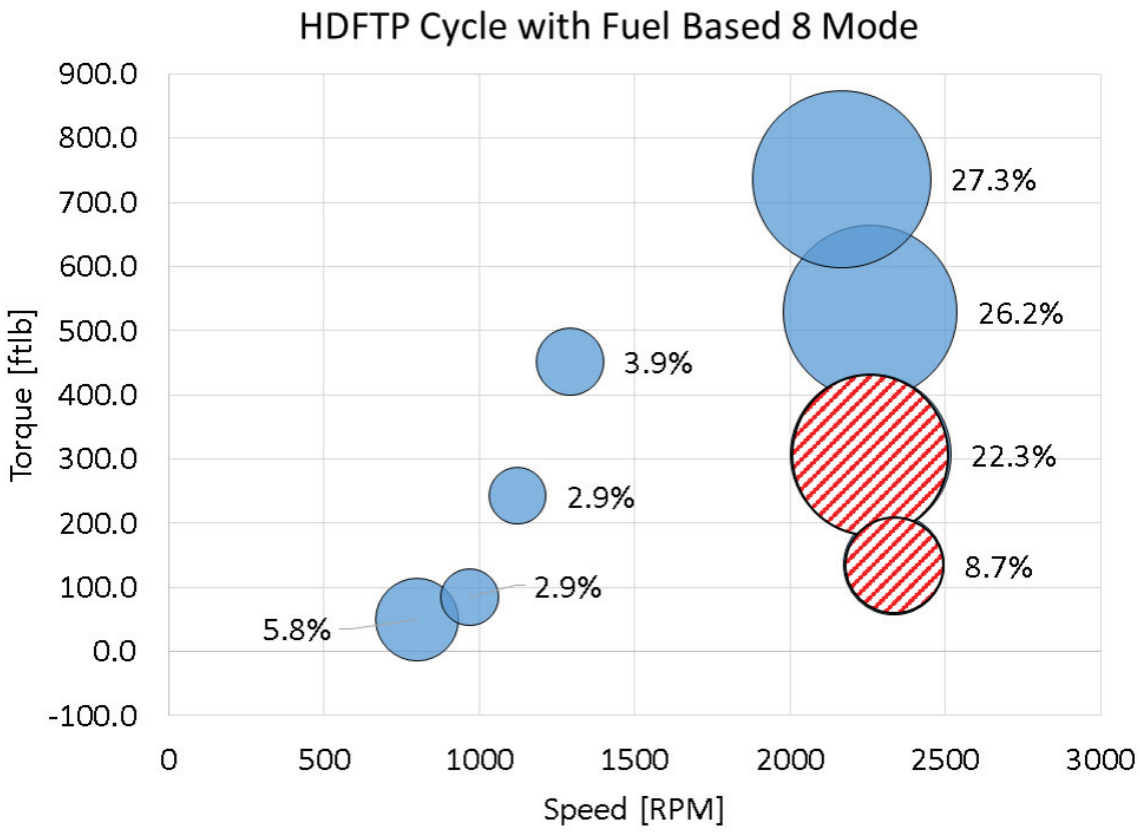

Figure 2.2. Fuel consumption distribution over a HDFTP mapped around 8 operating conditions. The cross-hatched bubbles are the two operating regimes under consideration. About 30 % of the fuel being consumed is in these regions thus necessitating a need to optimize for fuel economy at these conditions.

temperatures. The third results section focuses on which strategies allow the fastest warm-up of the AFT system. And finally, the fourth results section focuses on which strategy is preferable for enabling active DPF regeneration.

2.2 Methodology and Nomenclature

A total of five loads (1.3, 2.6, 3.8, 5.1 and 6.4 bar BMEP) were selected to study the fuel economy and AFT thermal management benefits of reduced air flow conditions at 2200 RPM. All experimental data shown, and discussed in the following sections, were subject to strict emissions and mechanical constraints. The mechanical constraints are shown in Table 2.1.

Table 2.1. Mechanical constraints for the High Speed study

Turbine Inlet Temperature	<760 C
Compressor Outlet Temperature	<230 C
Turbocharger Speed	<126 kRPM
Peak Cylinder Pressure	<172 bar
Exhaust Manifold Pressure	<1.4 bar
Pressure Rise Rate	<100 bar sec

The VGT position, EGR valve position and fuel injection timing for VVA strategies was semi-optimized via detailed screening for maximum fuel efficiency. Further optimization would enable to realize more benefits for VVA strategies. The PM, NOx, and UHC limits for each operating load are the same as the engine achieves with stock calibration and conventional valve motions.

2.2.1 Strategy Description

This section outlines the different VVA strategies compared with 6-cylinder operation in this study. Following are the descriptions of all the strategies:

6-Cylinder

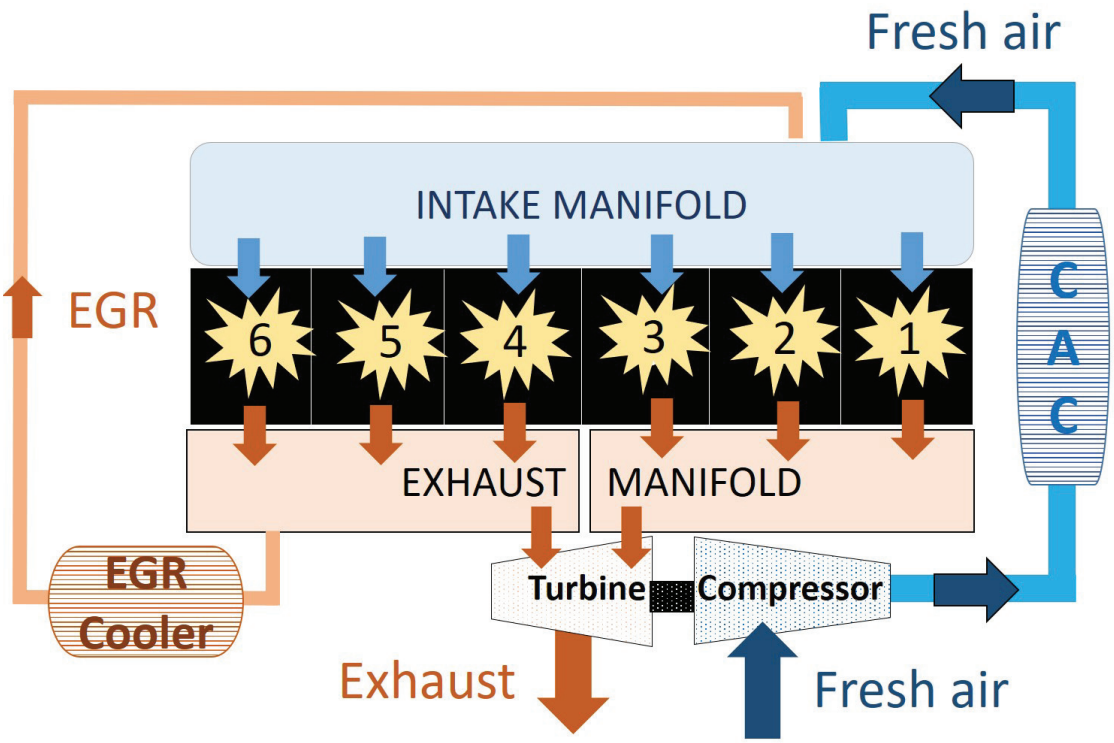

Figure 2.3. Conventional 6-cylinder Operation.

Figure 2.3 illustrates the gas exchange during conventional 6-Cylinder operation. The strategy defined as *6-cylinder stock calibration* is conventional six-cylinder operation tuned for minimum fuel consumption and is used as a fuel consumption baseline for all the operating conditions. The *6-cylinder Open VGT* is a strategy where the VGT nozzle position is opened up to reduce the pumping work and airflow. This

strategy would serve as a fair six-cylinder baseline for fuel economy comparison. The *6-cylinder open VGT + IVC modulation* is a strategy where IVC modulation is used along with opening up VGT to reduce the airflow.

3-Cylinder (half engine) Operation

Figure 2.4 illustrates the gas exchange during three-cylinder operation wherein both valve motion and fuel injection is deactivated for cylinders 4, 5 and 6. There is fuel combustion occurring only in cylinders 1, 2 and 3. This CDA firing strategy is

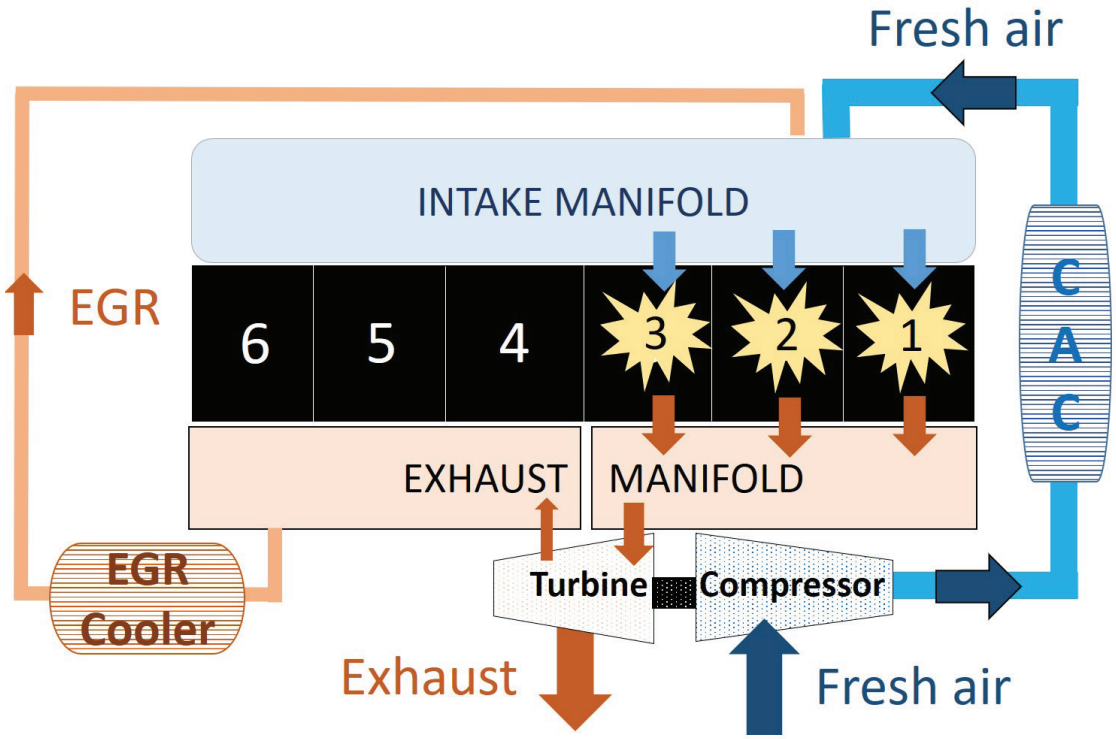

Figure 2.4. 3-cylinder (half-engine) firing operation showing the gas exchange in the engine wherein both valve motion and fuel injection is deactivated for cylinders 4, 5 and 6.

referred to as *3-cylinder* in this study and is compared with 6-Cylinder baseline at various operating conditions.

4-Cylinder (two-third engine) Operation

Figure 2.5 illustrates the gas exchange during four-cylinder operation wherein both valve motion and fuel injection is deactivated for cylinders 1 and 6. There is fuel combustion occurring only in cylinders 2, 3, 4 and 5. This CDA firing strategy is referred to as *4-cylinder* in this study and is compared with 6-cylinder baseline at various operating conditions. The valve profiles during CDA and IVC modulation

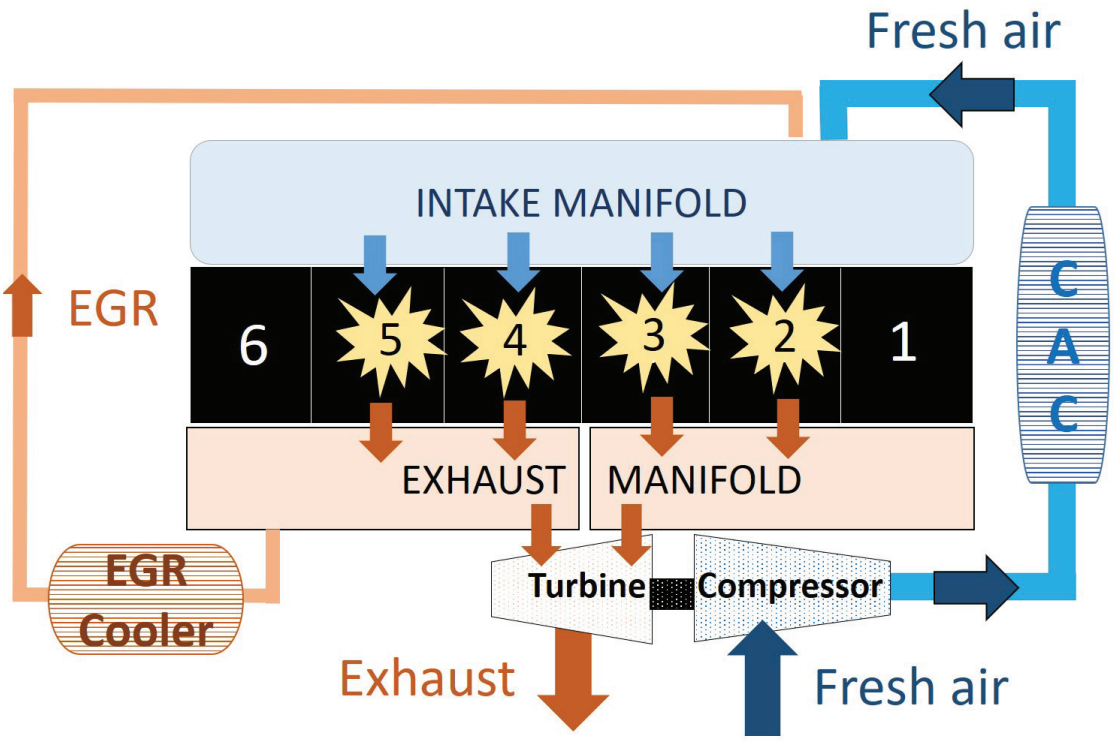

Figure 2.5. 4-cylinder (two-third engine) firing operation showing the gas exchange wherein both valve motion and fuel injection is deactivated for cylinders 1 and 6.

operation is shown in Figure 2.6. Early/late IVC modulation is achieved using either advancing or delaying the IVC timing as shown in Figure 2.6 (b) and (d), respectively. CDA is achieved by deactivating the intake and exhaust valves as shown in Figure 2.6 (c).

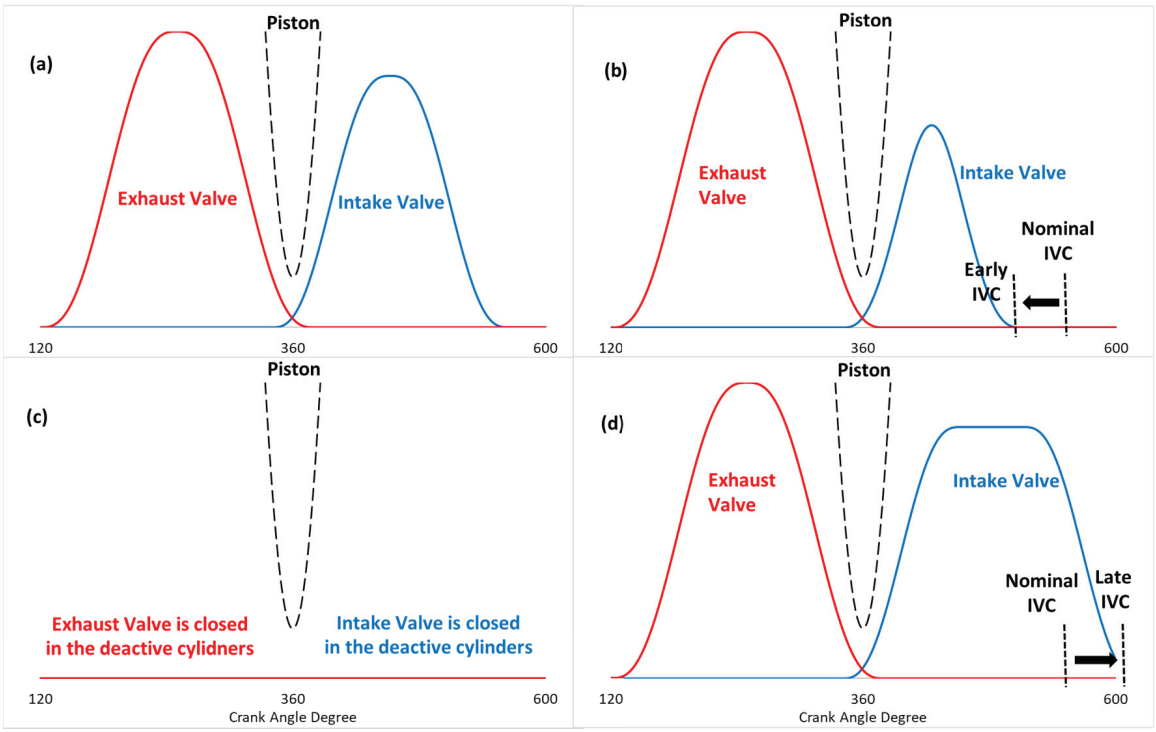

Figure 2.6. Valve profiles during (a) conventional 6-cylinder operation, (b) early IVC modulation, (c) CDA operation and (d) late IVC modulation operation.

For the *open VGT* and *open VGT + IVC modulation* strategies, SOI and rail pressure were modulated to screen for operating strategies to achieve improved efficiency and/or thermal management responses. During *CDA*, VGT position, SOI and rail pressure were modulated to achieve improved efficiency and/or thermal management. Engine cycle efficiency analysis is carried out in order to understand the fuel efficiency benefits as described in the following section.

2.2.2 Cycle Efficiencies

The fuel efficiency of a diesel engine is typically described as the brake thermal efficiency (BTE), which includes contributions from the closed cycle efficiency (CCE),

open cycle efficiency (OCE), and mechanical efficiency (ME) (per Eqn.2.1). The calculations of mean effective pressure (MEP) including gross indicated MEP (GIMEP), net indicated MEP (NIMEP), pumping MEP (PMEP), frictional MEP (FMEP) and brake MEP (BMEP) are based on in-cylinder pressure measurements. MEP is defined as the total work divided by the displaced volume, for instance GIMEP is defined as the gross indicated work divided by the displaced volume.

$$\text{BTE} = \eta_{\text{closed cycle}} \times \eta_{\text{open cycle}} \times \eta_{\text{mechanical}} \tag{2.1}$$

$$\eta_{\text{closed cycle}} = \frac{\text{GIMEP}}{\text{Fuel Equivalent Work}} \tag{2.2}$$

The closed cycle is defined as the portion of time where the intake and exhaust valves are closed, as shown in Figure 2.7. This encompasses the compression, combustion, and expansion processes. CCE per Equation 2.2 is affected by combustion completeness, piston expansion work, and in-cylinder heat transfer [1].

$$\eta_{\text{open cycle}} = \frac{\text{GIMEP+PMEP}}{\text{GIMEP}} = \frac{\text{NIMEP}}{\text{GIMEP}} \tag{2.3}$$

The open cycle is defined as the period of time the intake or exhaust valves are open, as shown in Figure 2.7. OCE, per Equation 2.3, quantifies the effectiveness of the gas exchange and is affected by turbine and compressor efficiency, and pressure differences between the intake and exhaust manifolds [1].

The ME is a measure of the efficiency of the engine to transmit the work generated by the expanding gases in the cylinder to the output shaft [1]. The losses associated with this work transfer are due to mechanical friction and accessory loads (work to drive the water pump, lubrication pump, etc.). It is typical to only include accessories needed to operate the engine. The ME per Equation 2.4 captures losses from friction and parasitic loads. The load to drive the intake and exhaust valves via hydraulic actuation is not accounted for during these calculations.

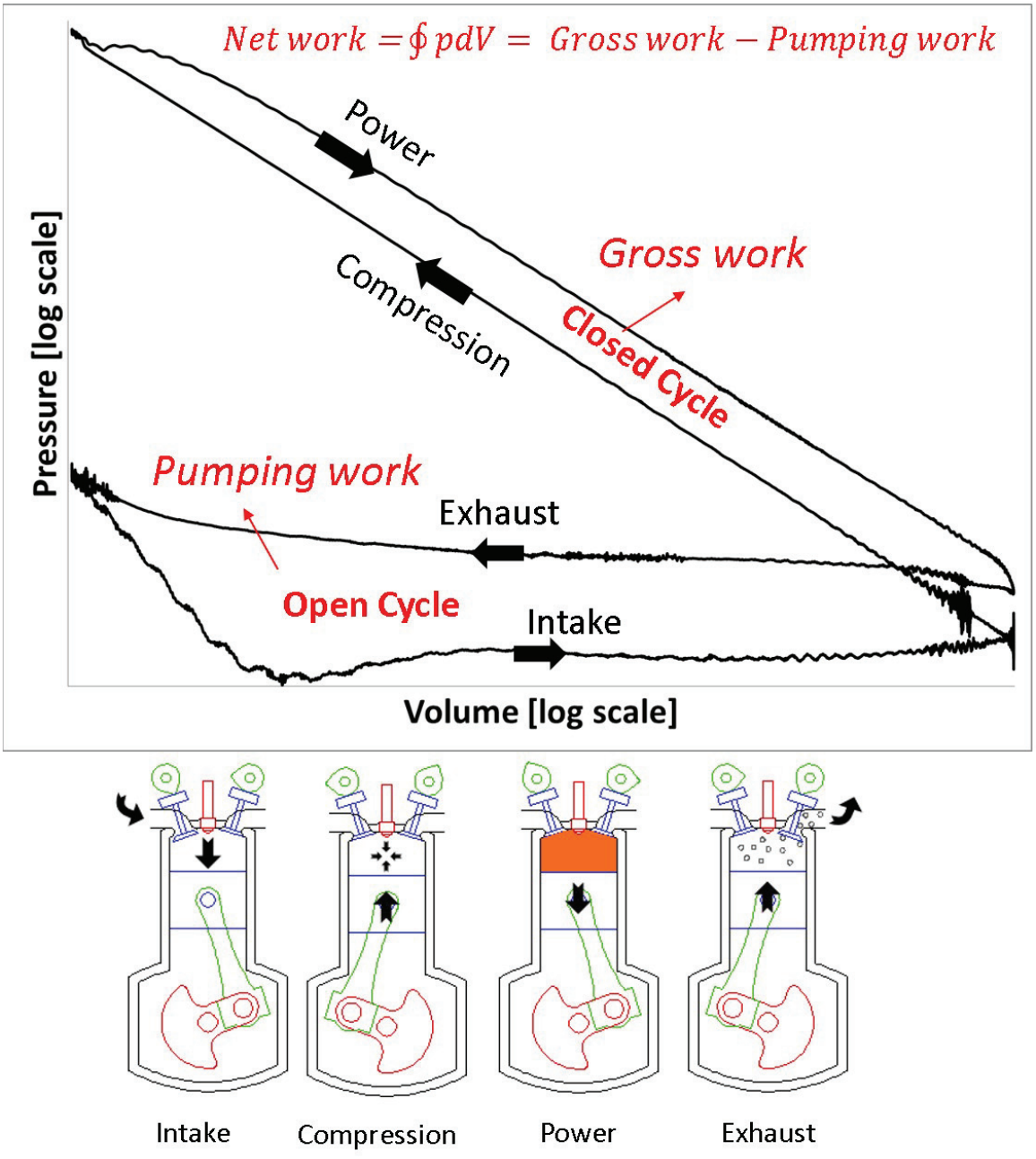

Figure 2.7. Pressure volume diagram illustrating the closed loop and open loop during the diesel 4-stroke (intake, compression, power/expansion, exhaust) operation.

In summary, the fuel upon combustion releases heat energy which gets converted to the brake work as illustrated in Figure 2.8. The combustion efficiency for a diesel engine is close to 100%, and hence it is not applied in Equation 2.1.

$$\eta_{\text{mechanical}} = \frac{\text{BMEP}}{\text{BMEP+FMEP}} = \frac{\text{BMEP}}{\text{NIMEP}} \tag{2.4}$$

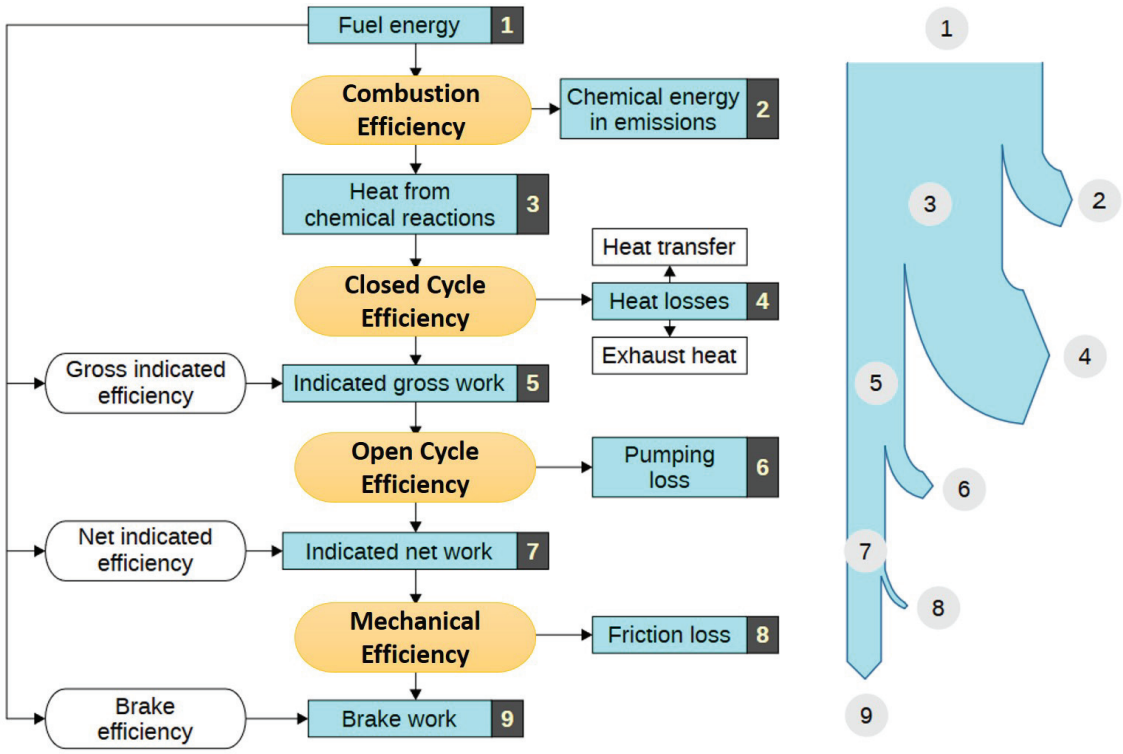

Figure 2.8. Fuel energy distribution illustrating cycle efficiency calculations. The combustion efficiency for a diesel engine is almost 100%.

As shown, BTE is the product of the closed cycle, open cycle, and mechanical efficiencies. A more detailed explanation of the cycle efficiency analysis strategy is explained by *Stanton et al.* [1].

2.3 Experimental Results

The benefits of the low air flow strategies described in the following four sections include:

(i) fuel efficiency increases enabled through increased OCE via reduced pumping work,

(ii) maintaining elevated AFT component temperatures through elevated engine exhaust temperature as a result of reduced airflow operation,

(iii) increasing the rate of warm-up of the AFT components through elevated engine exhaust gas temperatures, and

(iv) enabling active DPF regeneration through elevated engine exhaust gas temperatures.

A summary of the experimental screening results is shown in Table 2.2 .

2.3.1 Fuel Efficiency

Figure 2.9 summarizes the fuel efficiency benefits through the BMEP range of using *CDA*, *IVC modulation*, or *opening up the VGT*. The results are normalized with respect to the stock calibration, and show that fuel savings between 5% and 30% are possible depending on load (e.g., BMEP). *CDA* leads to a significant (25%) fuel consumption reduction at loads less than 2.5 bar. This is primarily a result of a 35% increase in the OCE, per Figure 2.10, achieved through a reduction in pumping work. Pumping work is lower because airflow is lower, as shown in Figure 2.11. Airflow is lower as a result of a reduction in displaced volume via *CDA*. At 2.5 bar, the increase in OCE for *CDA* compared to *open VGT* operation is negated by a decrease in closed cycle efficiency (CCE) during CDA per Figure 2.12. As a result, the BSFC is almost the same for the *CDA* and *open VGT* strategies.

Table 2.2. Summary of the experimental results illustrating the ideal operating modes for fuel efficiency, AFT warm up, AFT stay warm and Active DPF regeneration. The numbers in the fuel efficiency row represent the percentage fuel savings when compared to stock calibration. The numbers in the AFT stay warm and active DPF regeneration row represent the TOT for the strategy.

Operating Load (bar)	**1.3**	**2.5**	**3.8**	**5.1**	**6.3**
Fuel Efficiency	3 Cylinder (25.1%)	IVC mod (28.7%)	IVC mod (17.7%)	VGT (12%)	VGT (5.6%)
AFT Warm up(T<100 ° C)	Stock Cal	Stock Cal	Stock Cal	4 Cylinder	EIVC
AFT Warm up(T>100 ° C)	3 Cylinder	3 Cylinder	4 Cylinder	4 Cylinder	EIVC
AFT Stay Warm	3 Cylinder (314°C)	4 Cylinder (371°C)	IVC mod (377°C)	VGT (397°C)	VGT (417°C)
Active DPF regen	3 Cylinder (314°C)	3 Cylinder (473°C)	4 Cylinder (484°C)	4 Cylinder (537°C)	VGT (314°C)

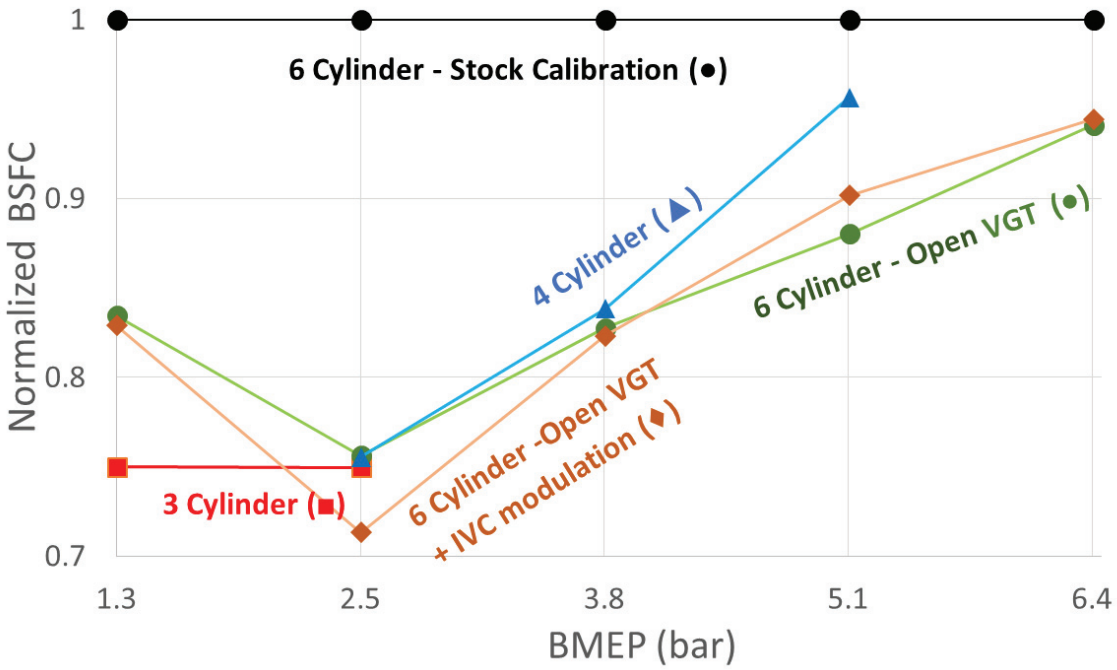

Figure 2.9. Comparison of BSFC vs BMEP trends at 2200 RPM. Low airflow strategies show a lower BSFC due to increased OCE.

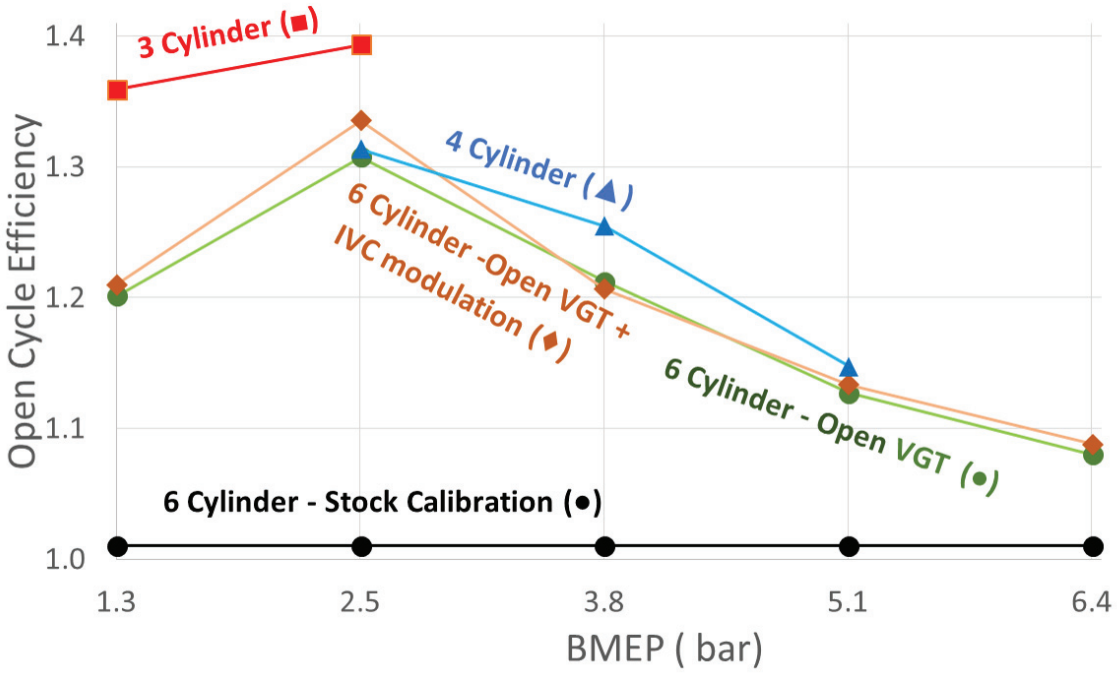

Figure 2.10. Comparison of OCE vs BMEP trends at 2200 RPM. All the strategies have a higher OCE than stock calibration due to reduced engine pumping work. 3-Cylinder strategy has about 35 to 40% increase in OCE.

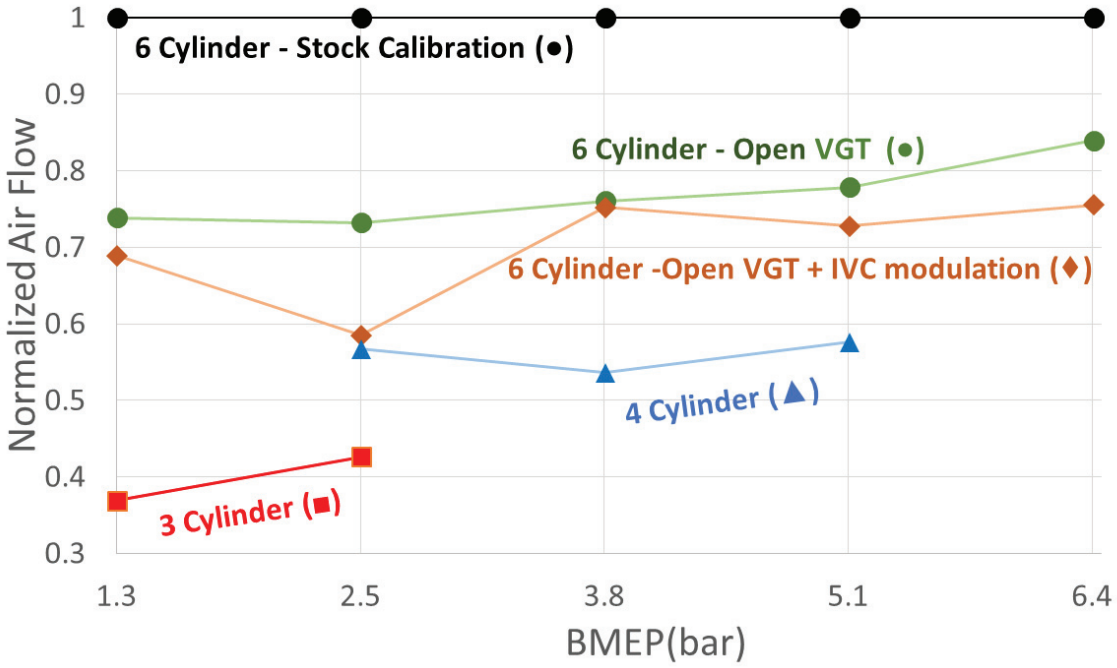

Figure 2.11. Comparison of normalized air flow vs load trends at 2200 RPM. There is a significant decrease in air flow when cylinders are deactivated or when the VGT is opened. There is a minor decrease in air flow when IVC modulation is used. The decrease in air flow is due to the lowering of boost pressure as the VGT is opened up.

At loads greater than, and equal to 2.5 bar, *CDA* has a slightly higher fuel consumption than *open VGT* operation because of a decrease in CCE efficiency as a result of:

(i) higher in-cylinder heat transfer as shown in Figure 2.13 and longer heat release caused by higher per-cylinder fueling in active cylinders, as shown in Figures 2.14 and 2.15, and

(ii) later injection timings required to maintain engine-out NOx levels per Figure 2.14.

At loads above 6.3 bar BMEP, *CDA* was not implemented as there is not enough oxygen available in *CDA* mode to keep PM within constraints.

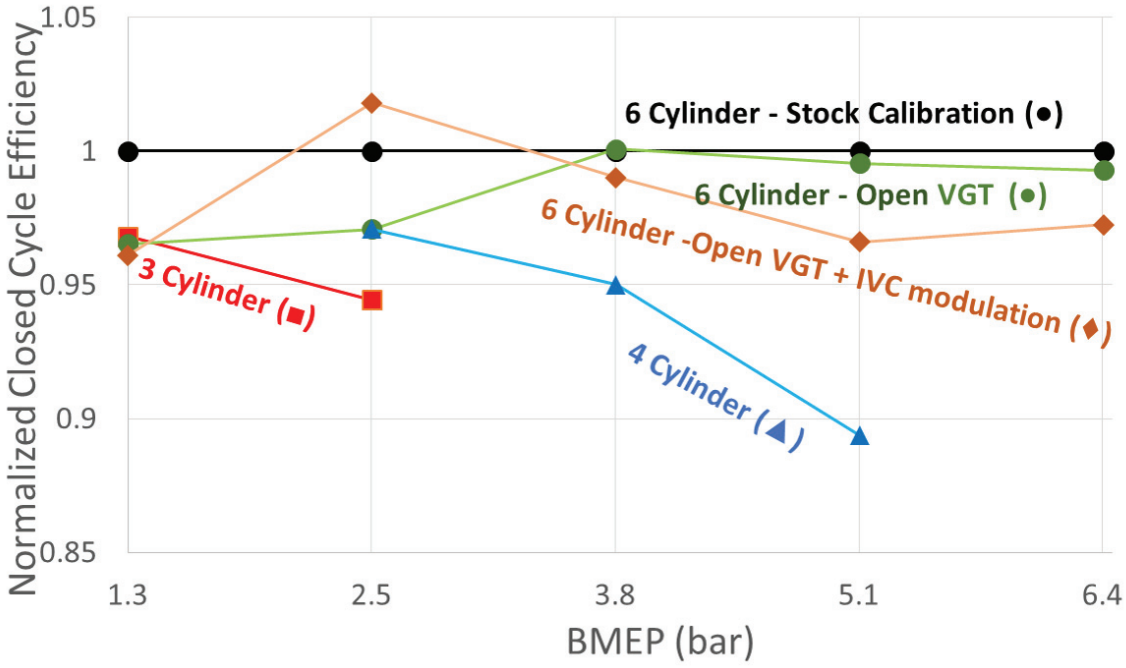

Figure 2.12. Comparison of CCE vs BMEP trends at 2200 RPM.

The *open VGT + IVC modulation* strategy has a slightly lower fuel consumption than *open VGT* due to better OCE and CCE at 2.5 bar BMEP. The OCE increases

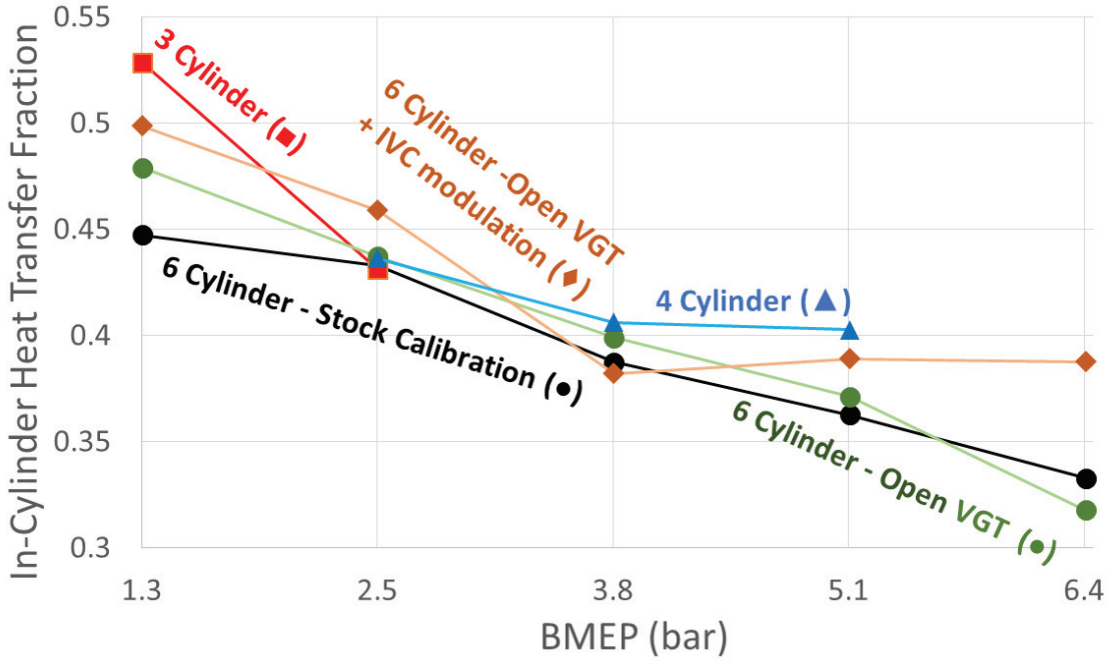

Figure 2.13. Comparison of in-cylinder heat rejection of an active cylinder in *CDA* and *6-cylinder open VGT* strategy at 2200 RPM/2.5 bar BMEP.

for the *open VGT + IVC modulation* strategy, as the air flow is reduced and pumping work is reduced which leads to an increase in OCE (as shown in Figures 2.11 and 2.10). The *IVC modulation* also allows for a reduction in effective compression ratios which reduces NOx through reductions in in-cylinder charge temperatures prior to, during, and following combustion. This enables earlier injection timing for the *open VGT + IVC* strategy at 2.5 bar, as shown in Figure 2.14, thereby providing a small CCE improvement, as shown in Figure 2.12.

At loads greater than 2.5 bar BMEP, the *open VGT* strategy and *IVC modulation* strategies have similar fuel consumption benefits when compared to the stock calibration, as shown in Figure 2.9.

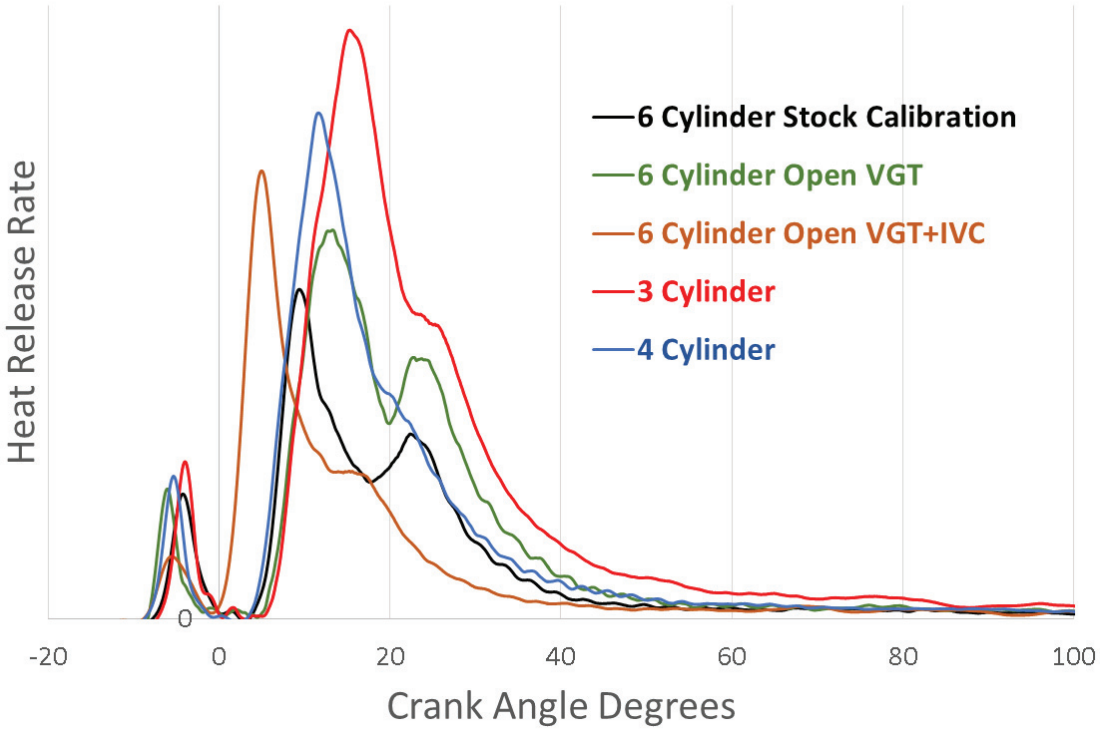

Figure 2.14. Comparison of heat release rate of an active cylinder in *CDA* and *6-cylinder open VGT* strategy at 2200 RPM/2.5 bar BMEP. *CDA* has a larger and more spread-out heat release rate when compared to *6-Cylinder open VGT* strategy.

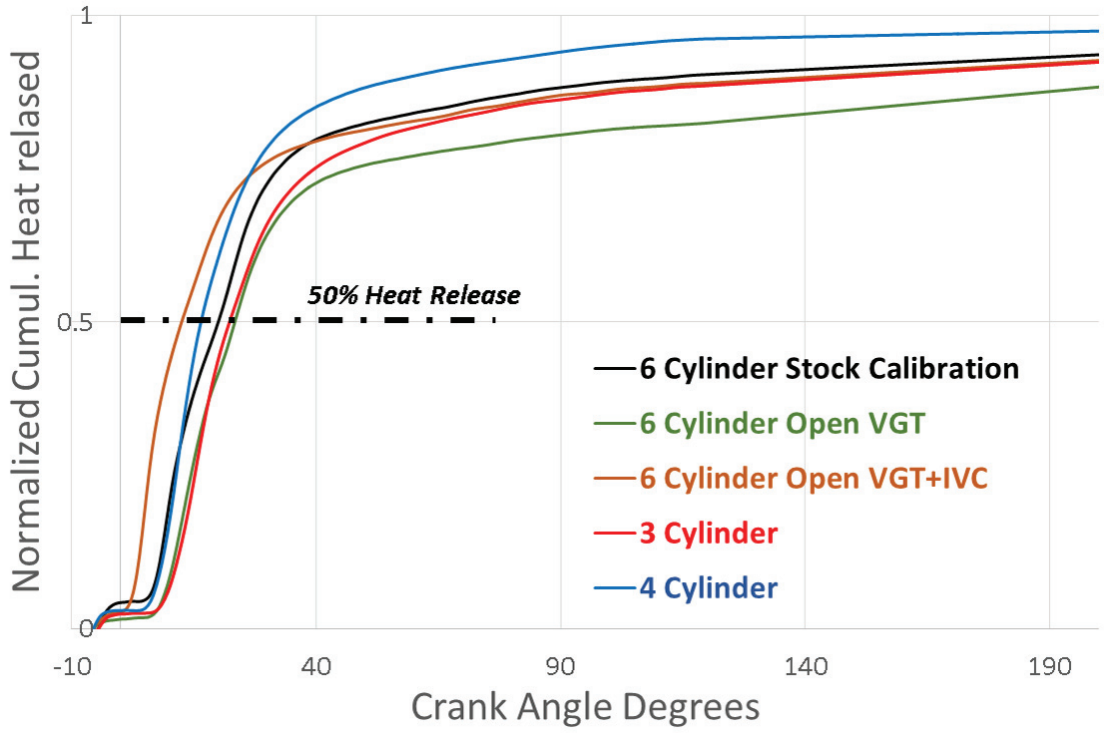

Figure 2.15. Comparison of cumulative heat released of an active cylinder in *CDA* and *6 cylinder open VGT* strategy at 2200 RPM/2.5 bar BMEP. The dash-dotted line signifies completion of 50% combustion.

A shortcoming of these low air flow strategies is that the turbo speed is lower for these strategies when compared to results from the stock calibration (as shown in Figure 2.16). This is because the exhaust flow through the turbine is lower when cylinders are deactivated, *IVC modulation* is used or when the VGT is opened.

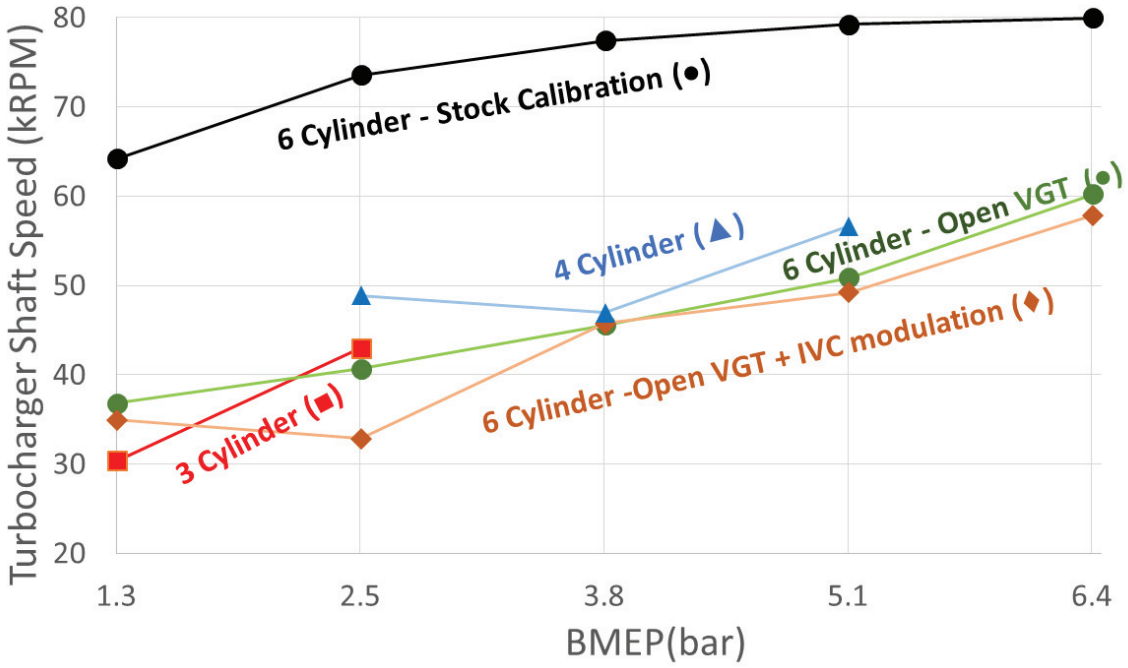

Figure 2.16. Comparison of turbocharger Speed vs BMEP at 2200 RPM for different strategies. All the strategies have a lower turbocharger speed when compared to stock calibration.

Lower pre-acceleration airflows and turbo speeds increase turbo-lag in turbocharged diesel engines during transients. In addition, as shown in Figure 2.17, the pressure differential across the EGR loop is decreased for these strategies when compared to the stock calibration due to the reduction in airflow (as shown in Figure 2.11). Lower pre-acceleration EGR pressure differentials decrease the potential to drive EGR flow, which may lead to undesirable increases in NOx during transients.

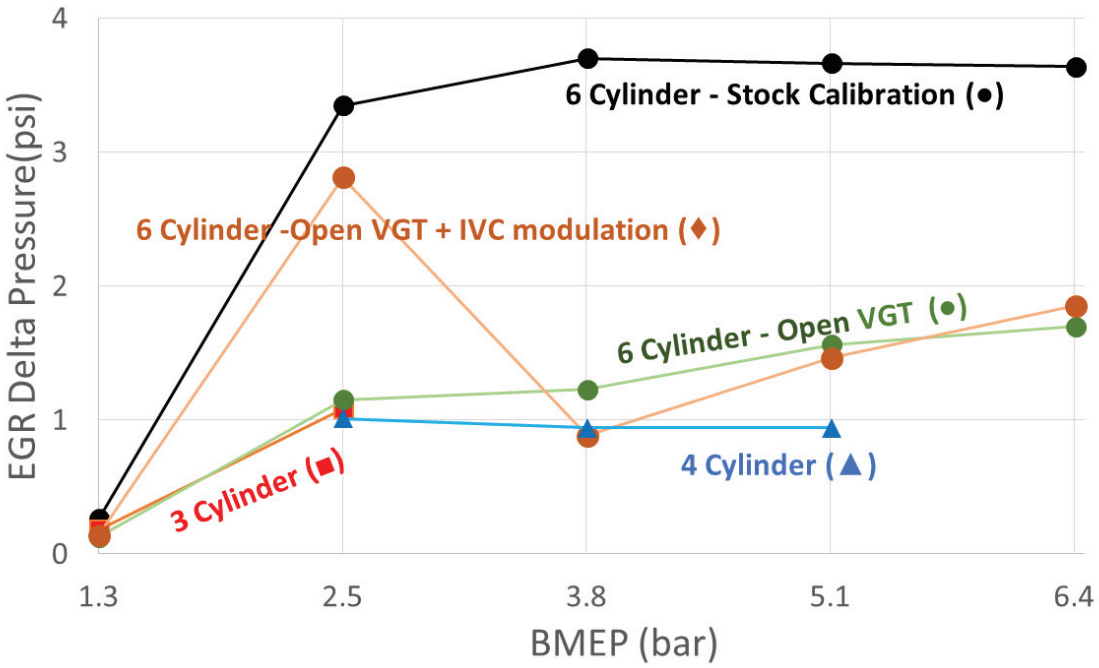

Figure 2.17. Comparison of delta pressure across the EGR vs BMEP at 2200 RPM for different strategies. All the strategies have a lower EGR delta pressure when compared to stock calibration.

The implication of these phenomena on transient performance at these conditions requires further study. As mentioned in the introduction, *EEVO*, *internal EGR*, turbocharger electrification, supercharging, and power-train hybridization are all potential solutions, but are out-of-scope for this study. Availability of look-ahead information, through vehicle data connectivity with other vehicles or the cloud, to allow anticipation of an upcoming transients would also allow the use of one of the strategies outlined in this study when an upcoming transient is not immediately pending.

2.3.2 Maintaining Elevated Aftertreatment System Temperatures

The SCR system operates most efficiently when temperatures are between approximately 300 and 450°C. Once the AFT has reached these temperatures, it is

preferable to maintain TOT at the upper end of this range so that DOC-fuel dosing (which still requires temperatures above 250 °C) is not required to keep the SCR system temperatures elevated.

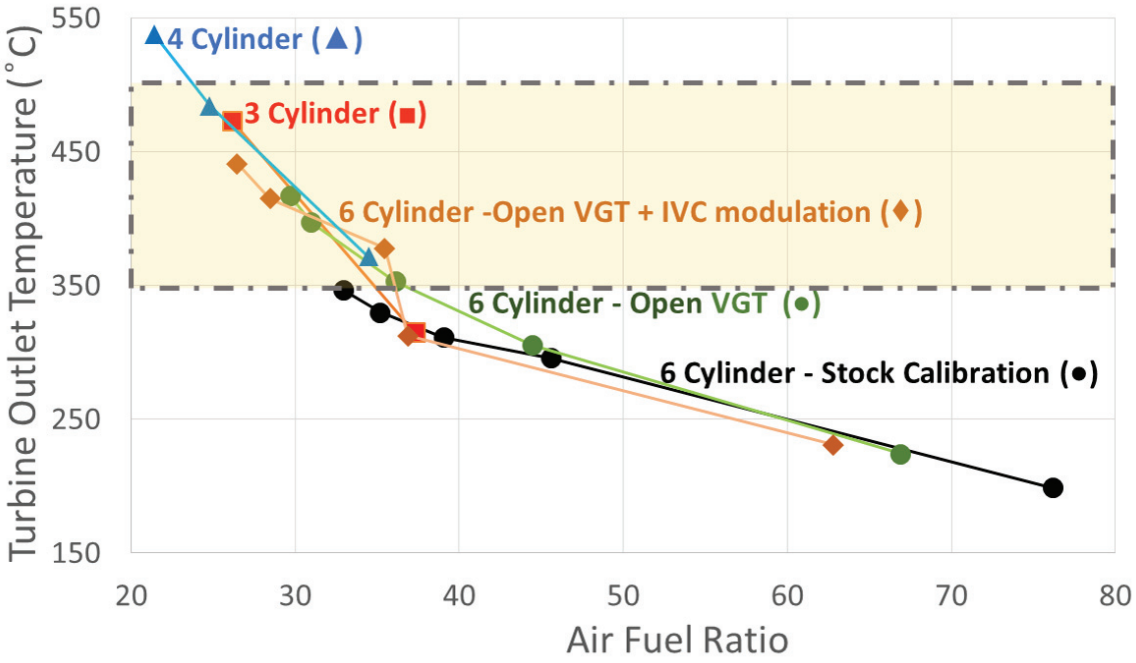

Figure 2.18. Increase in TOT with the reduction of AFR at an engine speed of 2200 RPM for different operating strategies.

Reducing the AFR is the most direct way to increase engine outlet temperatures. Figure 2.18 specifically shows a direct, monotonic relationship between TOT and AFR, regardless of operating strategy or load. As shown, and expected, a reduction in AFR results in an increase in TOT. The most fuel efficient way to reduce AFR is by reducing the airflow (as opposed to increasing the fuel required). As discussed in the previous section, *CDA* and *IVC modulation* are fuel efficient ways to reduce engine airflow, and as such, are also effective strategies for maintaining exhaust AFT component temperatures. More specifically, at a given load, lower AFR is possible

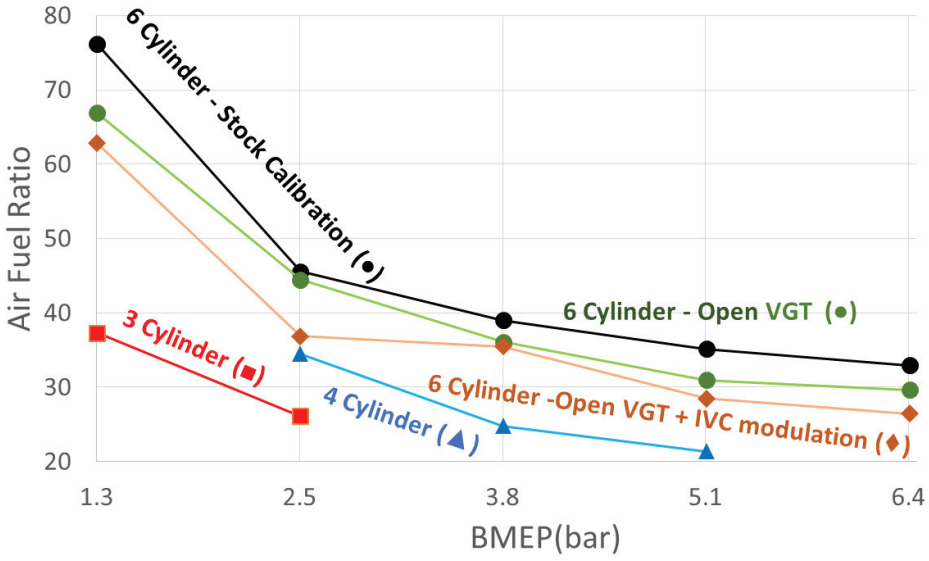

Figure 2.19. Comparison of AFR vs BMEP trends at 2200 RPM.

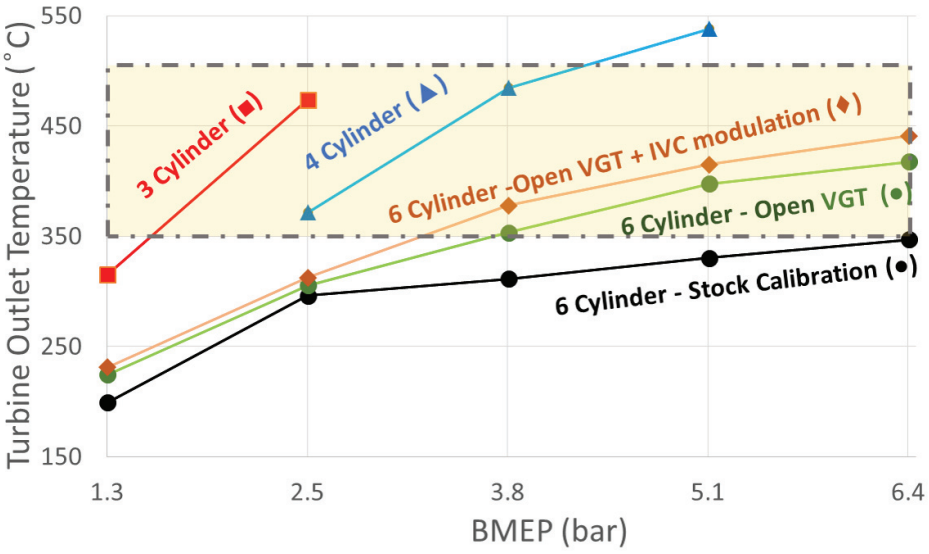

Figure 2.20. Comparison of TOT vs BMEP trends at 2200 RPM. The shaded region indicates the engine-out temperature range consistent with maintaining SCR temperature between 350 and 500 °C.

via *CDA* and *IVC modulation*, as shown in Figure 2.19, resulting in higher TOT, per Figure 2.20. Figure 2.20 and Table 2.2 show that:

(i) 3-Cylinder operation is preferred below a load of 2.5 bar,

(ii) 4-Cylinder operation is preferred between a load of 2.5 and 4 bar, and 6-Cylinder operation with an open VGT is preferred for loads above 4 bar.

Also note from Figure 2.20 that below 6.5 bar BMEP the stock engine calibration and valve profiles do not meet desirable TOT for maintaining already-elevated exhaust AFT component temperatures. On the other hand, the combination of opening the VGT and valve-train flexibility (*IVC modulation* or *CDA*) allows desirable temperatures to be reached for loads greater than 1.5 bar.

2.3.3 Reaching Desired Aftertreatment System Temperatures Quickly

As a first approximation, the heat transfer rate between the exhaust gas and an AFT catalyst depends on the TOT, exhaust flow rate, and instantaneous catalyst bed temperature. As an approximation, consider the heat transfer rate between an incoming gas and the wall within a round pipe from [23], as given in Equation 6.3, wherein $\dot{m}$ is the mass flow rate of the exhaust gas going through the catalyst, $T_{Catalyst}$ is the temperature of the catalyst, and C is a constant that depends on the geometry and material of the catalyst.

$$q = C \times \dot{m}^{4/5} \times (TOT - T_{Catalyst}) \tag{2.5}$$

As expected, Equation 2.5 will predict heat transfer from the gas to the catalyst when the TOT is larger than the instantaneous catalyst bed temperatures, and the rate of that heat transfer increases with increasing mass flow rate or temperature difference between the gas and catalyst. A higher heat transfer rate is preferred during the catalyst warm-up phase and is achieved using the optimal combination of exhaust flow and TOT for a particular catalyst bed temperature.

Figure 2.21 illustrates the catalyst warm up characteristics of the *stock calibration*, *open VGT*, *open VGT + IVC modulation* and *CDA* strategies at 1.3 bar BMEP. The figure shows the heat transfer rate of each mode normalized w.r.t *6-cylinder stock calibration*'s heat transfer rate when the catalyst bed temperature is 0°C. A positive heat transfer rate corresponds to catalyst warm up as heat is transferred from the exhaust gas to the catalyst. Negative heat transfer rate corresponds to catalyst cooling down as the heat is transferred from the catalyst to the exhaust gas. As

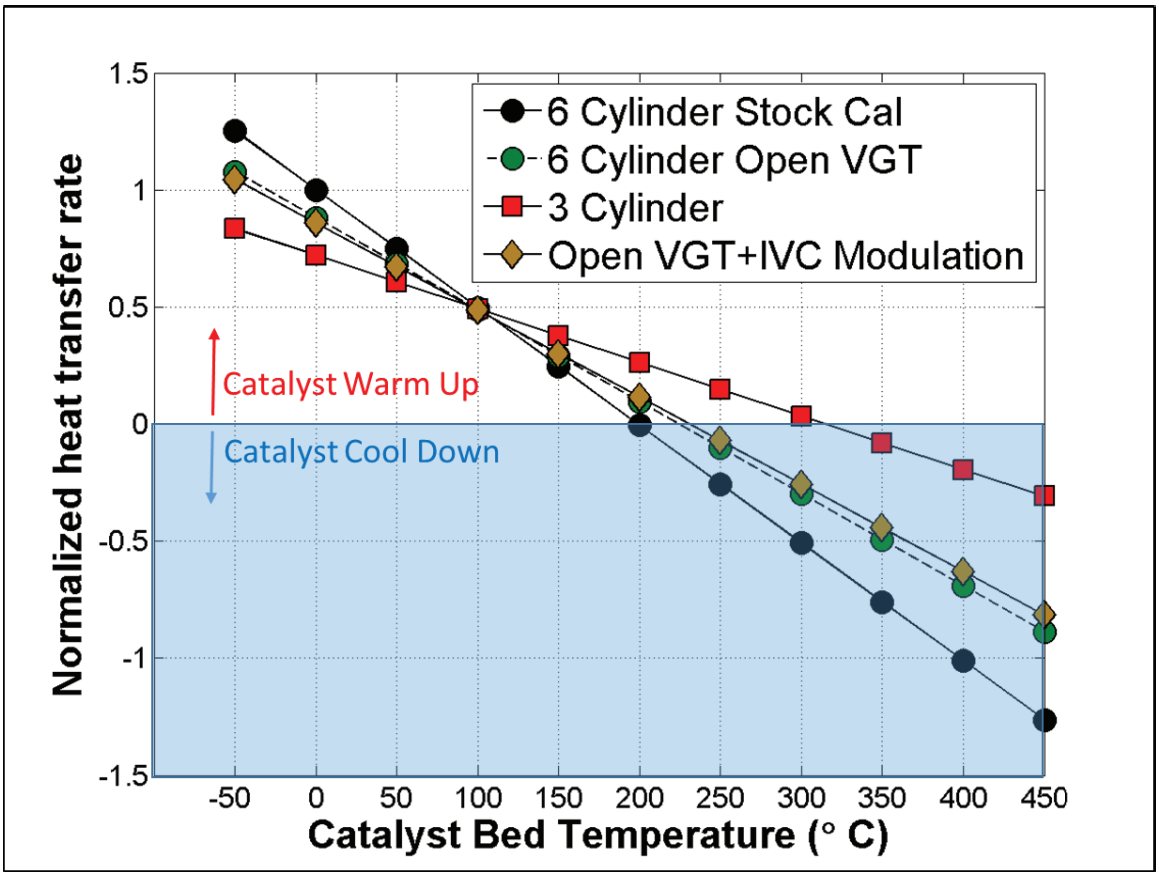

Figure 2.21. AFT catalyst warm-up characteristics of different strategies at 2200 RPM, 1.3 bar BMEP. At temperatures above 100 ° C, *3-cylinder* mode has a higher heat transfer rate than the other two case as the exhaust temperature begins to play a more influential role in heat transfer. At lower temperatures stock calibration would be preferred warm-up strategy.

shown in Figure 2.21, when the catalyst bed temperature is lower than 100°C the *6-Cylinder stock calibration* mode has highest heat transfer rate. This is because the positive impact of elevated exhaust mass flow is more important than elevated TOT at lower catalyst bed temperatures.

At temperatures above 100°C, *3-cylinder* mode has a higher heat transfer rate than all of the other cases as the exhaust temperature begins to play a more influential role in heat transfer. The catalyst can only reach temperatures of 200°C while operating in *6-cylinder stock calibration* mode, whereas *3-cylinder* mode enables catalyst temperatures up to 300°C.

Figure 2.22 illustrates the catalyst warm-up characteristics of the *stock calibration*, *open VGT*, *CDA* and *open VGT+IVC modulation* at 2.5 bar BMEP. As shown in the figure, for catalyst bed temperatures below 100°C, operating in normal *6-cylinder stock calibration* will result in higher heat transfer rates to the catalyst. Once the catalyst reaches a temperature of 100°C *3-cylinder* strategy becomes the preferred method for accelerated warm-up, for the same reason as was the case for the 1.3 bar BMEP load. Of additional significance, the *3-cylinder* strategy can heat the catalyst to temperatures in excess of 470°C.

Figure 2.23 shows the catalyst warm-up characteristics of the *stock calibration*, *open VGT*, *open VGT+ IVC modulation* and *4-cylinder* strategies at 3.8 bar BMEP. Again, until the catalyst bed temperature reaches 100°C, the *6-cylinder stock calibration* has the highest heat transfer rate. As the catalyst temperature increases above 100°C the *4-cylinder* strategy has higher heat transfer rates than the other three cases. This is because the *4-cylinder* mode has a TOT which is about 200° C higher than the other two modes as shown in Figure 2.20. The *6-cylinder stock calibration* strategy is only capable of warming up the catalyst to a catalyst bed temperature of 350°C whereas the *4-cylinder* strategies enables a TOT in excess of 400° C.

Figure 2.24 illustrates the warm up thermal characteristics of *stock calibration*, *open VGT*, *open VGT + IVC modulation* and the *4-cylinder* strategy at 5.1 bar BMEP torque. The *4-cylinder* strategy has a higher heat transfer rate compared

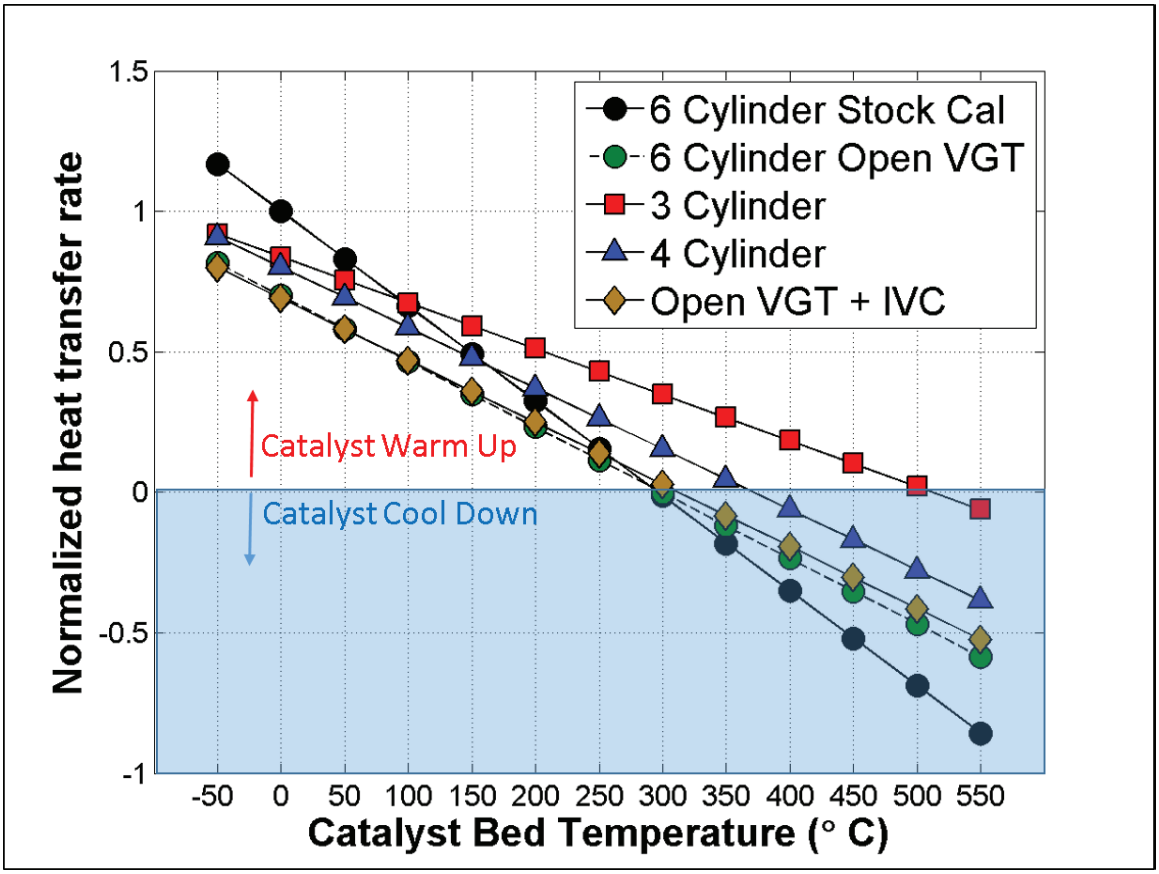

Figure 2.22. AFT catalyst warm-up characteristics of different strategies at 2200 RPM, 2.5 bar BMEP. At temperatures above 100 ° C, 3-cylinder mode has a higher heat transfer rate than the other two case as the exhaust temperature begins to play a more influential role in heat transfer. At lower temperatures stock calibration would be preferred warm-up strategy.

with the other three cases at all catalyst bed temperatures, and, as such, should be implemented at this load for any time catalyst warm-up is required, regardless of the instantaneous catalyst temperature. This is due to the combination of significantly higher TOT and marginally lower exhaust flow for the *4-cylinder* mode, when compared to the six cylinder modes (as shown in Figure 2.25). The *4-cylinder* mode at this load can also heat a catalyst up to temperatures in excess of 520°C.

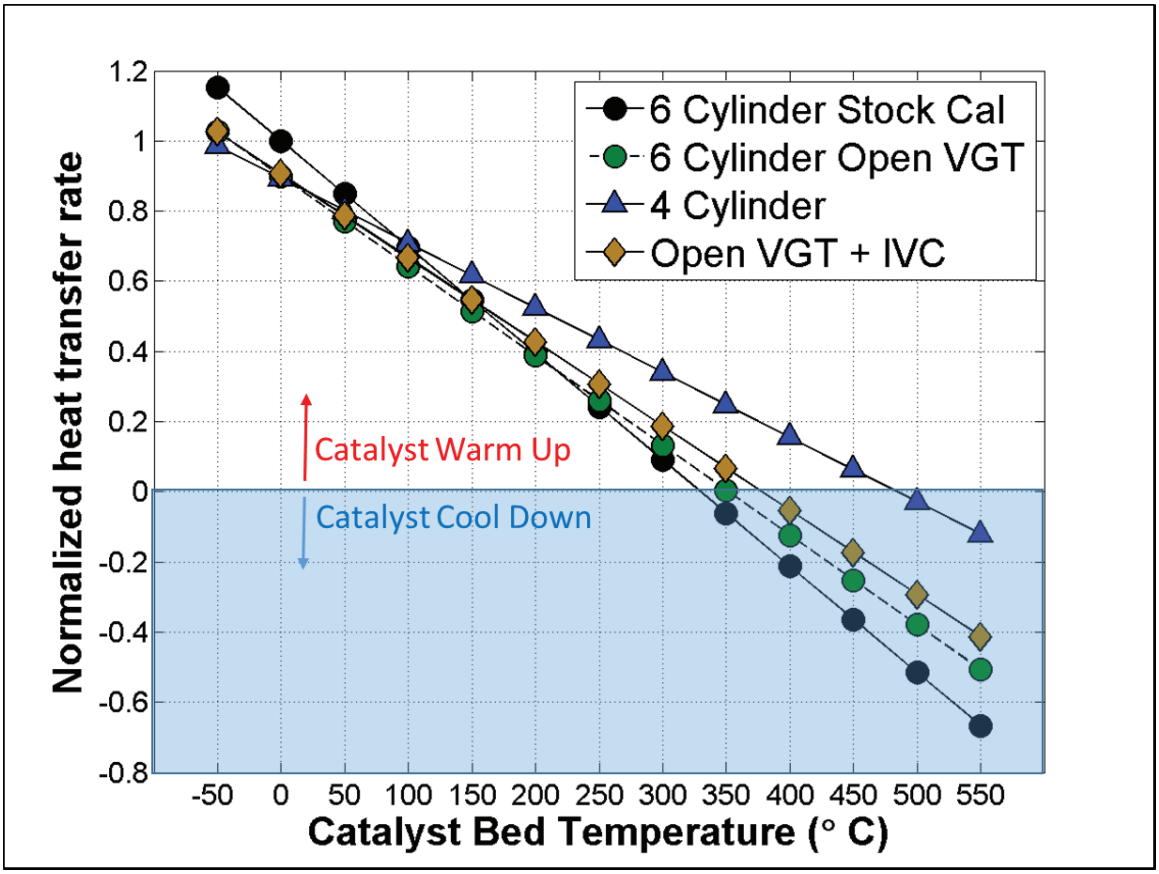

Figure 2.23. AFT catalyst warm-up characteristics of different strategies at 2200 RPM, 3.8 bar BMEP. At temperatures above 100 ° C, 4-cylinder mode has a higher heat transfer rate than the other two case as the exhaust temperature begins to play a more influential role in heat transfer. At lower temperatures stock calibration would be preferred warm-up strategy.

Figure 2.26 illustrates the warm-up thermal characteristics of the *stock calibration*, *open VGT* and *open VGT + IVC modulation* strategy at 6.3 bar BMEP. The *open VGT + EIVC* strategy has the highest heat transfer rate, and can heat a catalyst to temperatures in excess of 450 ° C.

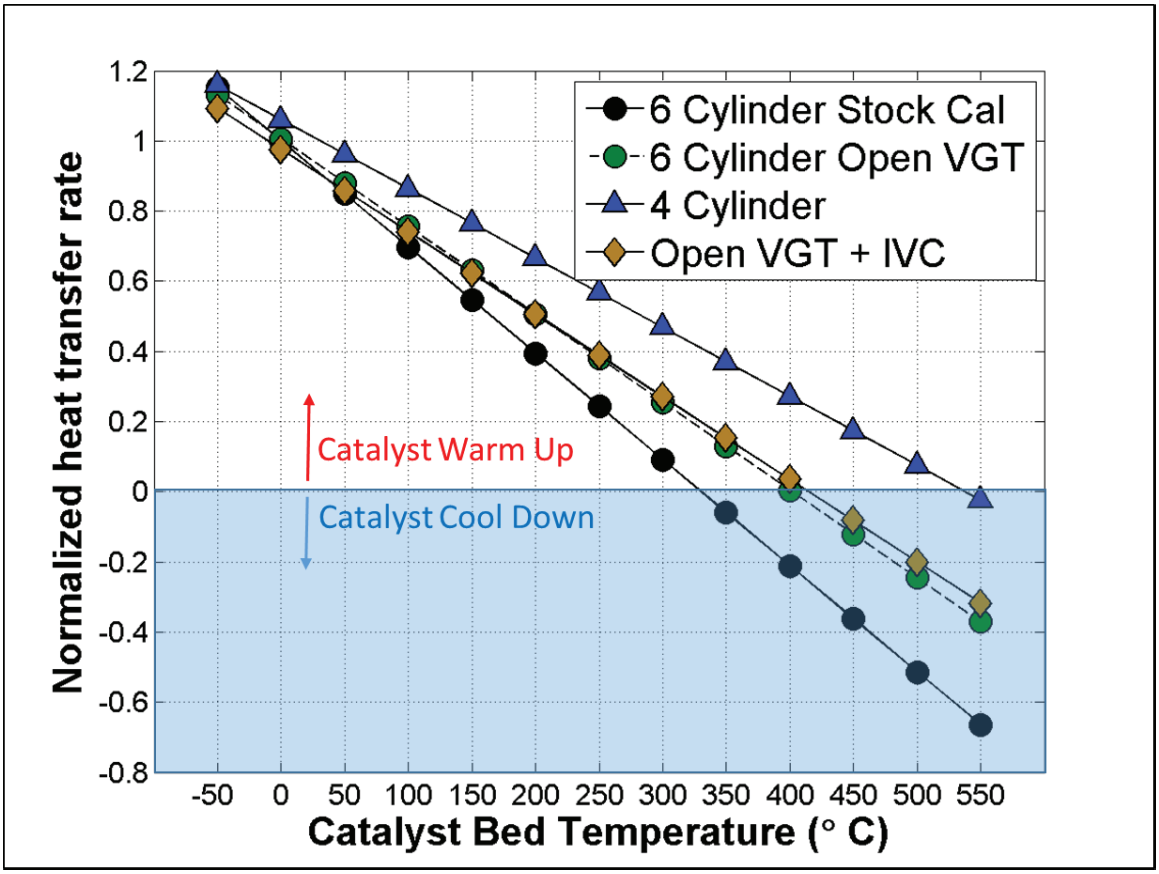

Figure 2.24. AFT catalyst warm-up characteristics of different strategies at 2200 RPM, 5.1 bar BMEP. At all temperatures, 4-cylinder mode has a higher heat transfer rate than the other two cases as the exhaust temperature plays a more influential role in heat transfer.

2.3.4 Active DPF regeneration

The engine needs to operate in such a way that the turbine-outlet gas temperature is above 450° C in order to enable an active DPF regeneration without dosing the DOC. At 1.3 bar BMEP, the *3-cylinder CDA* mode yields the highest TOT when compared to stock cal and open VGT strategy. At loads between 2.5-5.1 bar BMEP, *CDA* enables TOT to reach 450°C, which is enough to realize active regeneration in DPF without dosing the DOC. For 6.31 bar BMEP, *3-cylinder or 4-cylinder CDA* is not possible as the air flow gets too low to sustain acceptable PM levels. As such, at

h

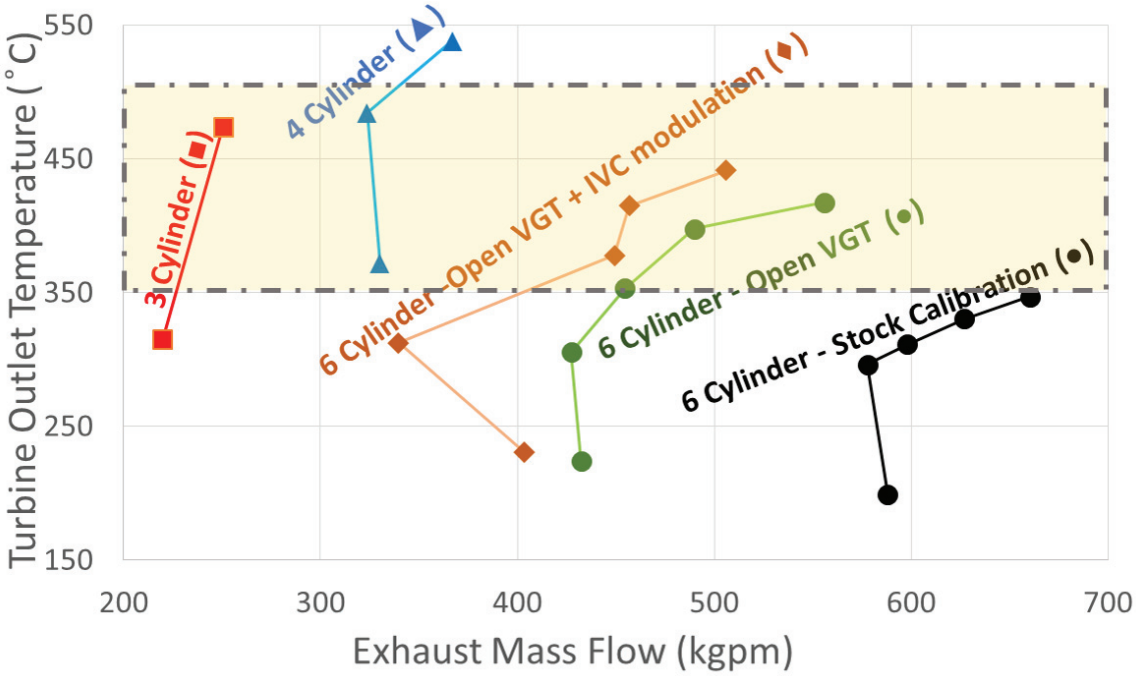

Figure 2.25. Variation of turbine outlet temperature with exhaust flow for different operating loads at an engine speed of 2200 RPM.

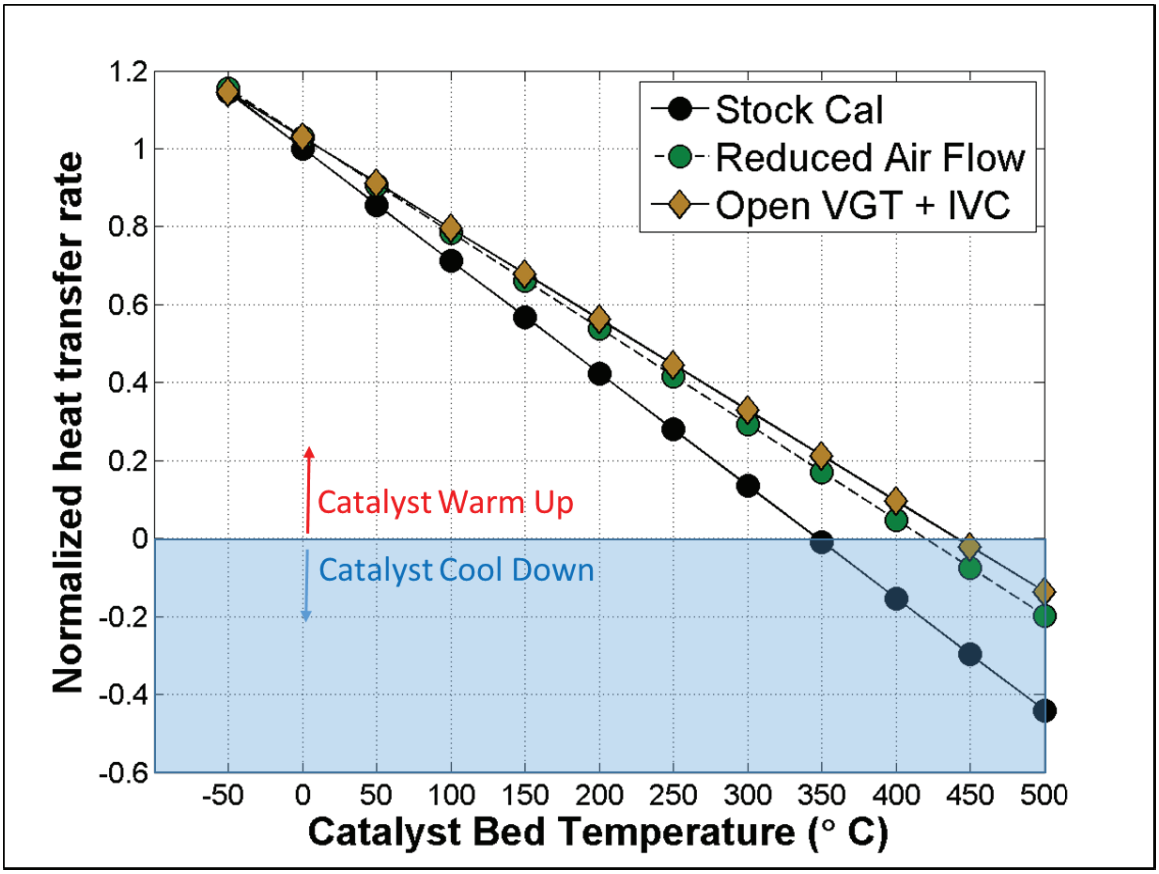

Figure 2.26. AFT catalyst warm-up characteristics of different strategies at 2200 RPM , 6.31 bar BMEP. At all considered temperatures, EIVC strategy would be the preferred mode for AFT warm up.

6.3 bar BMEP, the best way to operate would be to be in *Open VGT+IVC* strategy, as it has a higher TOT as well as a lower fuel consumption when compared to the stock calibration.

2.4 Transient Drive-cycle Results

This subsection compares the fuel consumption and tailpipe NOx reduction of *CDA*-enabled AFT thermal management strategies during the HDFTP. The HDFTP consists of a cold-start drive cycle, followed by an identical hot-start drive cycle with

a soak period of 20 min between the cycles. The speed and torque profiles for the HDFTP drive cycle are shown in Figure 2.1. The AFT system temperature was brought to the same initial conditions prior to starting the cold cycle, by flowing fresh air at 25°C from an external source through the AFT system. The drive cycle was started after the inlet and outlet gas temperatures of all the catalysts stabilized at 25°C. The net drive cycle fuel consumption and NOx emission for the cold-start and hot-start cycles are weighed with factors of 1/7 and 6/7, respectively, as shown by Equations 2.6 and 2.7.

$$FC_{net} = \frac{1}{7}FC_{cold} + \frac{6}{7}FC_{hot} \tag{2.6}$$

$$NOx_{net} = \frac{1}{7}NOx_{cold} + \frac{6}{7}NOx_{hot} \tag{2.7}$$

CDA was run at all loads <3 bar BMEP during the HDFTP to evaluate its impact in comparison to conventional six-cylinder operation. The upper limit on load for CDA was chosen by using the steady-state results from the previous section. Figure 2.27 illustrates the process by which the tailpipe NOx is predicted in this study. The AFT system is connected passively to the engine exhaust and gas temperatures at the inlet and outlet of DOC, DPF and SCR are measured using thermocouples. Measured SCR temperature along with the SCR efficiency, the tailpipe-out NOx is predicted. The instantaneous tailpipe NOx values are integrated to get the cumulative tailpipe NOx values for the drive-cycle. The SCR efficiency curve shows that efficiency reaches its maximum value for catalyst temperatures between 250°C and 450°C.

Four cycles were run and compared:

1. *6-cylinder Fuel Economy (FE) baseline* - The HDFTP drive-cycle run using an engine calibration tuned for best engine fuel efficiency. The turbine outlet temperatures are not enough to maintain efficient aftertreatment thermal management.

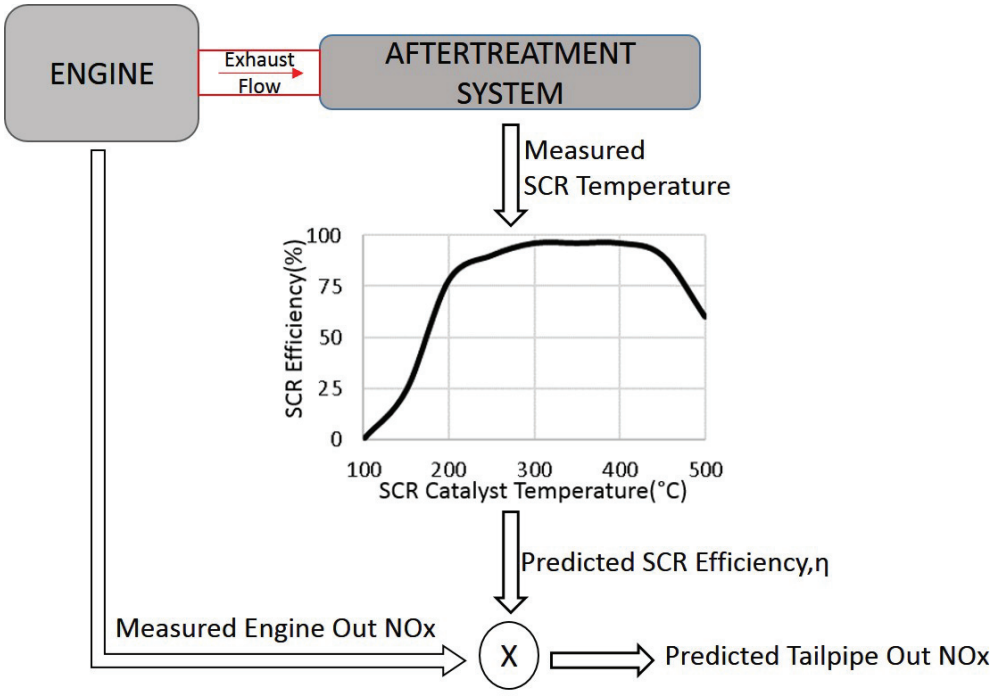

Figure 2.27. Measured SCR temperature from the A/T hardware is used to predict SCR efficiency. The SCR efficiency curve shows that efficiency reaches its maximum value for catalyst temperatures between 250°C and 450°C. Tailpipe out NOx is estimated using this predicted SCR efficiency.

2. *6-cylinder Thermal Management (TM) baseline* - The HDFTP drive-cycle run using an engine calibration tuned for AFT thermal management that meets current on-highway emissions limits. This strategy incorporates delayed fuel injections at all possible operating conditions (including non-idle conditions), and maximally-closed VGT positions at idle, in order to increase TOT and flow rates. At non-idle conditions, the late injections also reduce engine-outlet NOx, which together with faster AFT system warm-up, reduce tailpipe NOx to regulation levels.

3. *3-cylinder CDA at Stay-Warm Idle* - The HDFTP drive-cycle similar to *6-Cylinder TM baseline* with one modification: running *3-cylinder stay-warm* mode instead of the *6-cylinder stay-warm* mode at idle conditions once the

SCR outlet temperature is above 200°C (ie., after 600 seconds). This strategy demonstrates the fuel savings possible through use of CDA during idle for maintaining AFT system temperature.

4. *3-cylinder CDA <3 bar* The HDFTP drive-cycle similar to *3-cylinder CDA stay-warm Idle* with one modification: *3-cylinder CDA* operation at all stay-warm non-idle sections when load <3 bar BMEP. This results in a further 0.4% reduction in fuel consumption, while maintaining tailpipe out NOx emissions levels consistent with emission limits.

Figure 2.28 summarizes the main HDFTP cycle results for each of the above four strategies. As shown, *6-cylinder TM* strategy has 35% reduction in tailpipe NOx with the expense of an approximate 4.5% increase in fuel consumption, when compared to *6-cylinder FE Baseline*. The *3-cylinder CDA Stay-Warm Idle* drive-cycle, wherein *3-cylinder CDA* strategy was implemented during idle conditions, when the SCR system temperature was at least 200°C, results in very similar tailpipe NOx levels, and enables a 3% fuel consumption reduction compared to the *6-cylinder TM* cycle [53]. The *3-cylinder CDA Stay-Warm Idle* drive-cycle, wherein *3-cylinder CDA <3 bar* strategy is implemented at all stay-warm non-idle conditions whose load is less than 3 bar, enables 3.4% fuel savings and 6% lower tail pipe NOx than *6-cylinder TM* cycle, due to better stay warm performance. The fuel consumption results shown in Figure 2.28 were determined via experimental gravimetric fuel consumption measurements. Measured SCR outlet temperatures were used as inputs to an assumed SCR NOx conversion efficiency map (per Figure 2.27) to estimate the instantaneous tailpipe NOx emissions. These were then integrated to generate the results shown in Figure 2.28.

Figure 2.29 shows the TOT, SCR inlet temperature, SCR NOx conversion efficiency, predicted tailpipe out NOx, for each of the four strategies described above. Using CDA enables a higher SCR inlet gas temperature leading to a better SCR NOx conversion efficiency which leads to tailpipe NOx reductions. *3-cylinder CDA <3 bar*

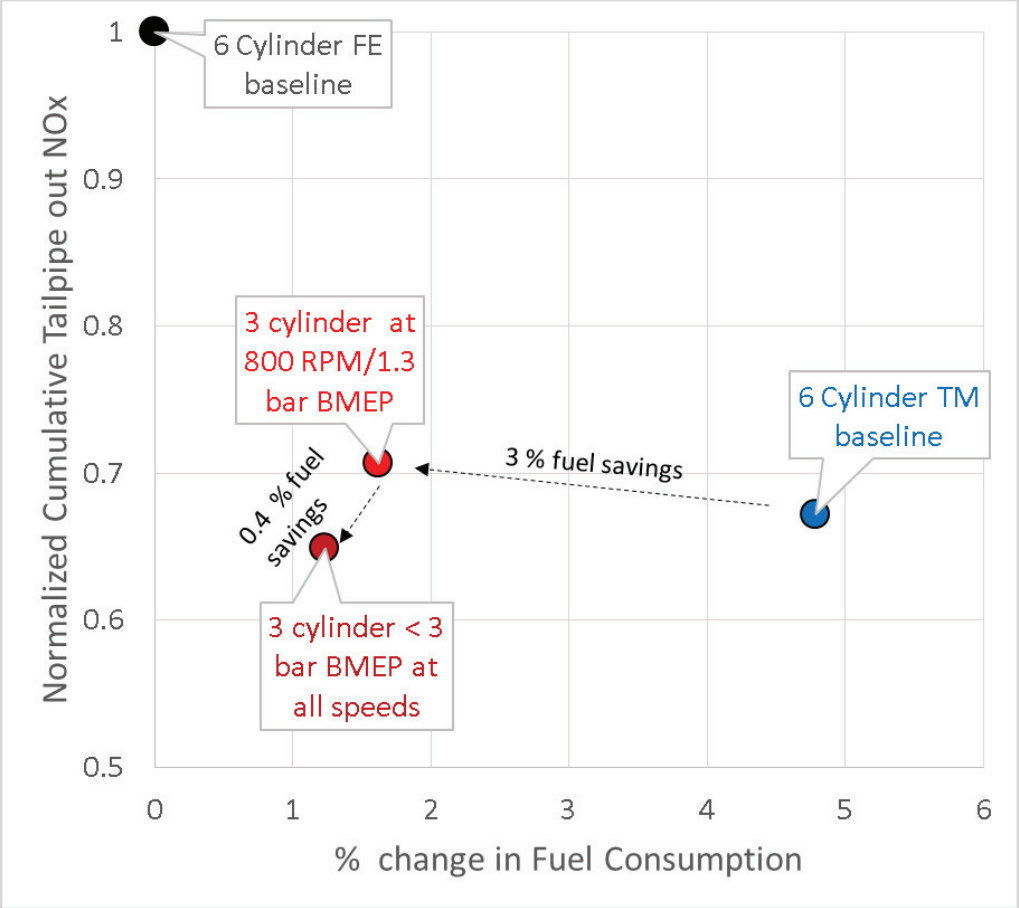

Figure 2.28. HDFTP drive-cycle results showing the NOx vs Fuel consumption trade-offs, showing the added benefits of running 3-cylinder strategy at loads less than 3 bar BMEP. *3-cylinder CDA Stay-Warm Idle* results in a further 0.4% reduction in fuel consumption, while maintaining tailpipe-outlet NOx emissions levels consistent with emission limits.

has higher TOT and SCR temperature leading to a higher SCR conversion efficiency and lower tailpipe NOx.

2.5 Summary

This chapter summarizes the benefits of CDA and other low airflow strategies under high-speed, low-load operation when the goal is to:

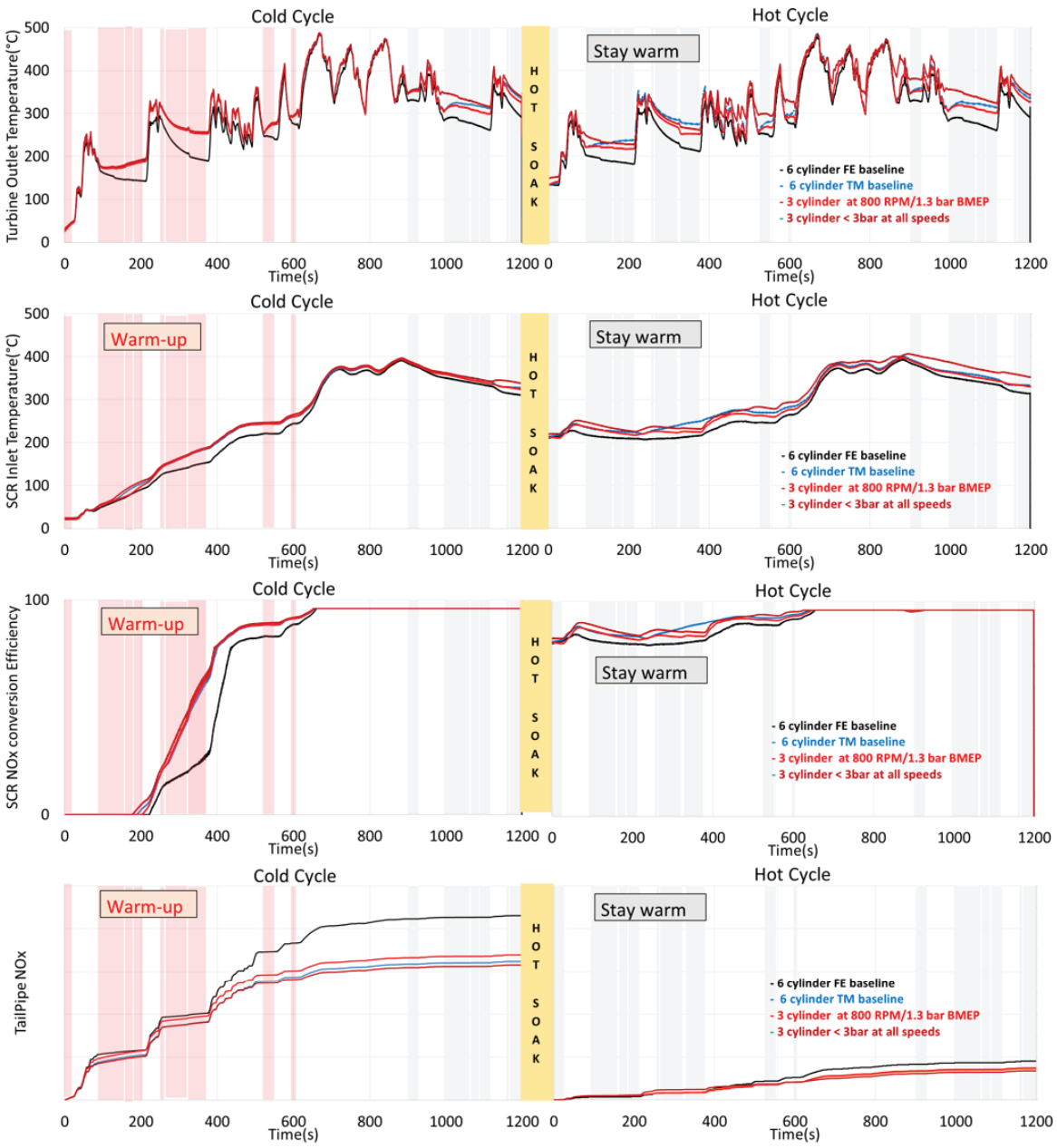

Figure 2.29. Transient HDFTP (cold and hot start) data showing (a) TOT, (b) SCR inlet Temperature, (c) Predicted SCR NOx conversion efficiency and (d) Predicted Tailpipe NOx emissions. Shaded areas highlight the idle (800 RPM/1.3 bar) sections. Using CDA enables a higher SCR inlet gas temperature leading to a better SCR NOx conversion efficiency which leads to tailpipe NOx reductions. *3-cylinder CDA <3 bar* has higher TOT and SCR temperature leading to a higher SCR conversion efficiency and lower tailpipe NOx.

(i) reduce fuel consumption,

(ii) warm-up the AFT system,

(iii) maintain elevated AFT system temperatures, or

(iv) enable active DPF regeneration without doing the DOC.

The key conclusions are:

(1) The fuel savings of *CDA*, *open VGT and IVC modulation* are between 5% to 25% depending on the load. The fuel savings are primarily due to a reduction in airflow leading to an increased OCE. For loads less than 2.54 bar BMEP, *CDA* has higher fuel efficiency than *open VGT* operation. For loads greater than 2.54 bar BMEP, the *open VGT and IVC modulation* strategy have better fuel economy than *CDA* as there is higher in-cylinder heat loss during *CDA* which causes its overall efficiency to decrease for *CDA* strategy.

(2) The VGT is squeezed under these low-load conditions in order to prepare for a transient event. Opening up the VGT decreases the delta pressure across the engine thereby increasing the fuel efficiency. Although this also might have detrimental effects on transients which needs to be understood.

(3) At catalyst bed temperatures below 100°C, the *stock calibration* warms up the AFT faster for loads between 1.3-3.8 bar BMEP ft-lbs. For loads between 3.8-5.1 bar BMEP ft-lbs, the *4-Cylinder* mode will warm-up the AFT system more quickly.

(4) At 6.31 bar BMEP, there is not enough oxygen available in the cylinder to sustain smoke-free combustion during cylinder deactivation. However, *open-VGT and IVC modulation* can help realize faster warm up at all catalyst bed temperatures.

(5) When the AFT is warm, *CDA* helps keep the engine and AFT system above 250° C for loads below 2.54 bar BMEP. For loads above 2.54 bar BMEP, the *open-VGT and IVC modulation* strategies help keep the system warm in a fuel efficient manner.

(6) *CDA* not only helps to warm up the DPF faster under certain conditions but also enables DPF gas inlet temperatures required for active DPF regeneration without using a DOC doser.

(7) Using *3-Cylinder CDA* at all loads less than 3 bar during HDFTP enables about 3.4% fuel savings and 6% lower tail pipe NOx than *6-Cylinder TM* cycle, due to better stay warm performance. *3-Cylinder CDA <3 bar* has higher TOT and SCR temperature leading to a higher SCR conversion efficiency and lower tailpipe NOx.

(8) Strategies including turbocharger electrification, supercharging, powertrain hybridization and availability of look-ahead information can be used to improve the transient behavior of the engine. Several VVA strategies such as zero valve overlap or EEVO could also prove as viable strategies to improve transients but are out of scope of this thesis.

3. LATE INTAKE VALVE MODULATION AT HIGHWAY CRUISE CONDITION

3.1 Motivation

The analytical and experimental efforts described here focus on fuel economy and exhaust thermal management at 1200 rpm/7.6 bar BMEP, a speed and load consistent with cruise conditions for over the road trucks. This study was carried out in collaboration with Cummins, as part of the Department Of Energy SuperTruck I project which aimed to increase the engine BTE to above 50%. This study only focused on ISX type applications and so a smaller turbocharger consistent with heavy-duty applications, was used to emulate and study the cruise condition. Using conventional valve-train operation, the exhaust temperature at the turbine exit is around 350°C. Higher exhaust temperatures are necessary to more quickly heat up the SCR and periodically regenerate the DPF.

In a prior study which was conducted at Purdue [22], IVC modulation was used as a method for AFT thermal management. LIVC can be used to reduce the air-flow to the engine, which reduces the AFR, leading to an increase in TOT (as illustrated in Figure 1.8). The area of engine operating map was identified where IVC modulation could be used to increase the TOT. It was observed that the target TOT required for optimal AFT performance could be achieved at all engine operating conditions, using a combination of IVC modulation and atmospheric intake manifold pressures. It was found that as TOT increased along the IVC sweeps, turbine out power almost remained constant due to the accompanying reduction in exhaust flow. Thus results developed in that study suggested IVC modulation as a viable strategy for exhaust thermal management. IVC modulation seems like an attractive strategy to keep the AFT performing at its optimal efficiency while moving between high and low load

conditions without compromising on fuel efficiency and increasing engine-out NOx emissions.

So the main goal of this study is to optimize the cruise operating condition at 1200rpm/7.6 bar BMEP, using LIVC for fuel economy and AFT thermal management. On-highway vehicles spend the majority of time at cruising speed conditions. Hence, emissions control and AFT thermal management are very important considerations at these conditions. Any benefit in thermal management as a result of LIVC would be significant. Since experimental optimization is time intensive, GT power was used as a simulation tool to develop regression models and then constrained optimization was carried out to be validated experimentally on the engine testbed.

3.2 Methodology

3.2.1 Optimization at target BSNOx levels

This study focused on three BSNOx targets at 1.5g/hp-h, 3g/hp-h and 4g/hp-h. In order to thoroughly understand the potential benefit of LIVC, trade-offs were investigated through optimization at following aspects:

(i) Minimize BSFC at given NOx levels within constraints using stock hardware,

(ii) Minimize BSFC @ given NOx levels within constraints using LIVC,

(iii) Minimize BSFC @ given NOx levels @ TOT = 250°C using LIVC,

(iv) Maximize TOP @ given NOx levels within constraints using LIVC and

(v) Maximize TOT @ given NOx levels within constraints using LIVC.

The optimization was conducted within emission and mechanical constraints as listed below in Tables 3.1 and 3.2.

Table 3.1. Emission constraints for the optimization

Emission	**Level**
HC	100 ppm
PM (Experimental)- AVL Smoke	1.5 FSN
PM (GT Power)- AVL Smoke	18
NOx (GT Power)	1.5, 3, 4 g/hp-h

Table 3.2. Mechanical constraints for the LIVC optimization study.

Turbine Inlet Temperature	<760°C
Compressor Outlet Temperature	<230°C
Turbocharger Speed	<193 kRPM
Peak Cylinder Pressure	<172 bar
Exhaust Manifold Pressure	<1.4 bar
Pressure Rise Rate	<100 bar sec

3.2.2 DOE and optimization in GT Power

Engine testing is a direct way to evaluate advanced combustion recipes and control techniques. However, optimization via engine testing takes a long time and the results can be affected by many factors such as fuel quality, sensor and actuator accuracy, combustion stability and even test cell environment. Hence, during the beginning of a new technique exploration, simulation tools could be a good choice to expand research without being limited to physical constraints.

In this study a GT-power model calibrated by Cummins, was used to simulate a 2010 ISB Cummins diesel engine. The model predicted BSFC within 5% error, BSNOx within 25% error, Charge flow within 5% error, temperatures and pressures within 3% error. Using this high-fidelity model the optimization process started with a design of experiment (DOE). The independent inputs included valve timing, EGR valve diameter, VGT% closed, start of injection (SOI) and Rail pressure. These inputs were limited in a reasonable and wide range as listed in Table 3.3.

Table 3.3. DOE with the range for the inputs used for the LIVC study.

Input Variable	**Units**	**Min**	**Max**
EGR Valve Diameter	mm	0	40
VGT % Closed	%	0	80
Main SOI	ATDC	-5	5
Rail Pressure	bar	800	1800
IVC Timing	CAD	565	665

The optimization process followed is described using the schematic shown in Figure 3.1. The data for the regression models are first obtained from running the DOE in GT Power simulation software. Using that data, regression models were developed using Minitab software and the required optimization process was done for the

given constraints. The optimized set points were then experimentally validated on the engine. For example, in the BSFC vs BSNOx trade-off, DOE results were used to generate regression models for BSFC, BSNOx and engine constrains separately. Iterations of regression model and re-ranged DOE are performed to obtain accurate regression models. Using generated regression model using Minitab statistical software, a set of inputs were optimized to find the lowest BSFC at fixed BSNOx targets with physical constraints not being violated.

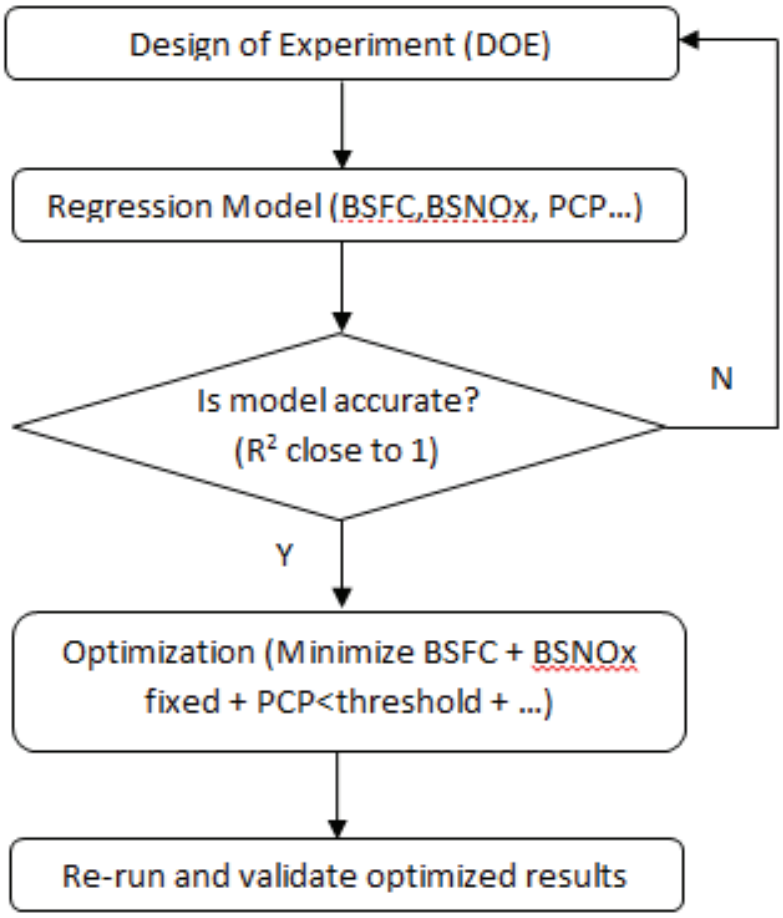

Figure 3.1. Optimization process followed for the LIVC study.

When the optimized results from simulation were validated on the engine, parameters such as IVC, SOI and rail pressure were set exactly the same as it is in the

model. Instead of EGR valve diameter and VGT% closed, EGR fraction and charge flow were set in the experiment as realized during the simulation. Due to the small difference between model and experiment, further adjustment was generally needed in experiment to reach desired BSNOx targets. In this study, rail pressure and EGR fraction were adjusted to get to desired BSNOx target. Fueling was also adjusted to maintain constant torque. In addition, charge flow was maintained close to the optimized results.

3.3 BSFC vs BSNOx Analysis

In order to investigate fuel economy using LIVC, optimizations have been conducted with stock hardware and LIVC. The results show that compared with stock hardware LIVC does not bring BSFC benefit in Figure 3.2(a). The optimized inputs and results were quite similar between these two trade-offs. Thus LIVC does not add any fuel economy benefit at 1200/7.6 bar BMEP speed load condition. The optimized IVCs for best BSFC trade-offs are around 575 CAD (as shown in Figure 3.2(b)) because at that IVC the volumetric efficiency is the maximum, which indicates that the engine is trying to breathe more efficiently when LIVC is used. Since TOT is higher than 250°C in all the data for BSFC vs BSNOx trade-offs, this data also represent the BSFC vs BSNOx trade-offs with temperature constrained above 250°C.

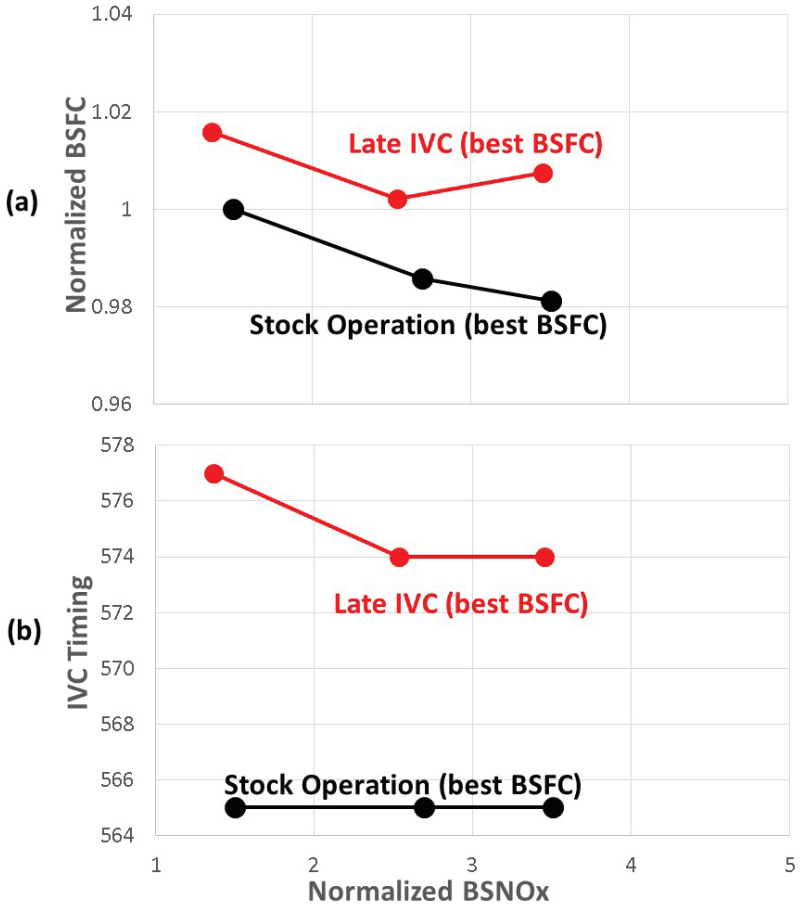

Figure 3.2. Comparison of normalized (a) Brake Specific Fuel Consumption vs BSNOx and (b) IVC timing vs BSNOx at 1200 RPM/7.6 bar BMEP. There is no benefit to using LIVC for achieving better fuel economy. This is because the stock hardware is optimized for maximum fuel economy for the cruise condition. The optimization process yields IVCs closer to 575 CAD in order to maximize the volumetric efficiency of the engine.

3.4 TOT vs BSNOx Analysis

For TOT vs BSNOx trade-offs, stock hardware and LIVC were investigated to explore the maximum TOT achieved in either case. The maximum TOT with stock hardware is 400°C, as shown in Figure 3.3, which is achievable via delayed SOI of 5 CAD ATDC in Figure 3.5.

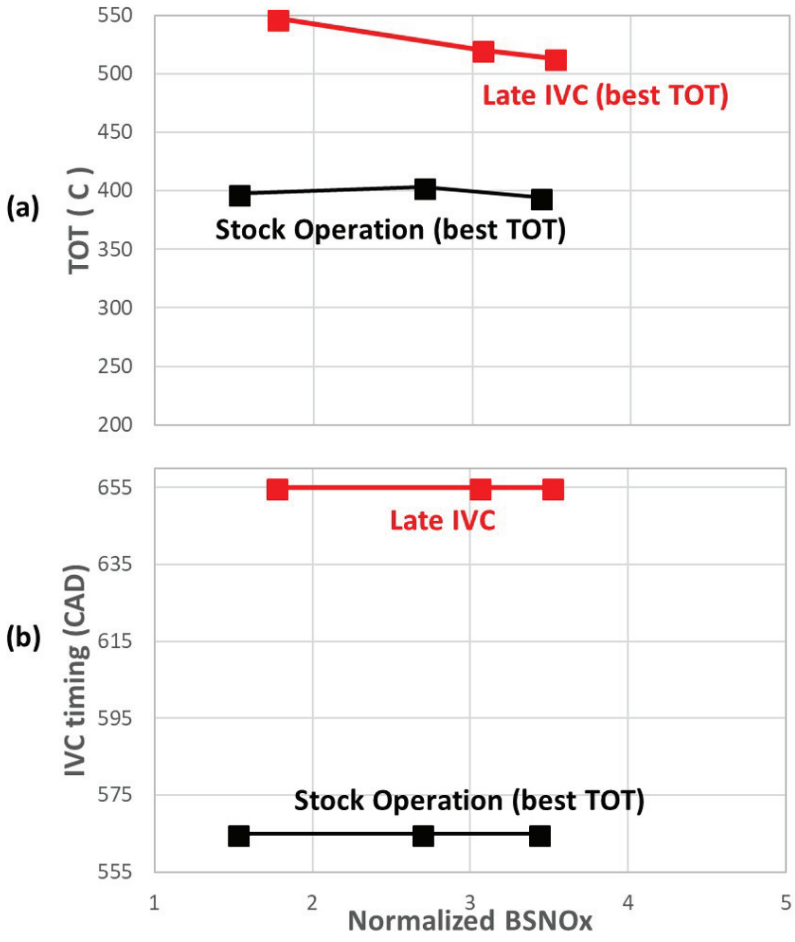

Figure 3.3. Comparison of (a) Turbine Outlet Temperature vs BSNOx and (b) IVC timing vs BSNOx at 1200 RPM/7.6 bar BMEP. LIVC enables higher TOT when compared to the stock hardware. The IVC timings were optimized to very late timings at 655 CAD for increased TOT.

LIVC further increases the maximum TOT by 200°C at the lowest BSNOx level, when compared with baseline (stock hardware best BSFC). This is primarily due to a reduction in AFR for this strategy.

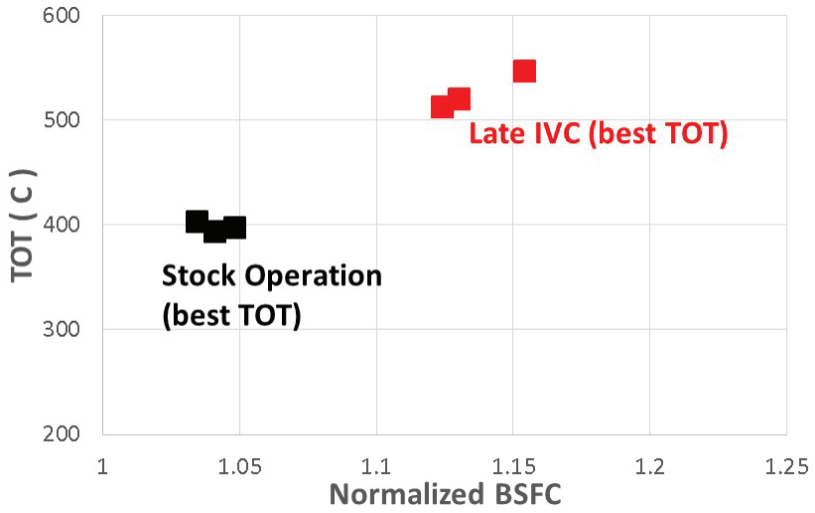

Figure 3.4. Comparison of TOT vs BSFC at 1200 RPM/7.6 bar BMEP. There is a linear trade-off between TOT and BSFC as there is a fuel penalty for an increase in TOT.

As seen in Figure 3.4, there is a fuel penalty paid for achieving higher TOT. This is because, while optimizing for maximum TOT, SOI is delayed at 5 ATDC as shown in Figure 3.5. The IVC timings were optimized to very late timings at 655 CAD (Figure 3.3). This along with delayed injection timing decreases CCE compared with baseline, as the heat release is more delayed for LIVC. The LIVC heat release is not only delayed but also more spread out, which is most likely due to the lower in-cylinder bulk temperatures and reactant concentrations resulting from the reduction in effective compression ratio, brought on by the delay in IVC. The spreading out of the heat release is the likely cause of the additional drop in CCE for the LIVC strategy. Thus, there is a fuel penalty for higher TOT with LIVC as the combustion process becomes less efficient.

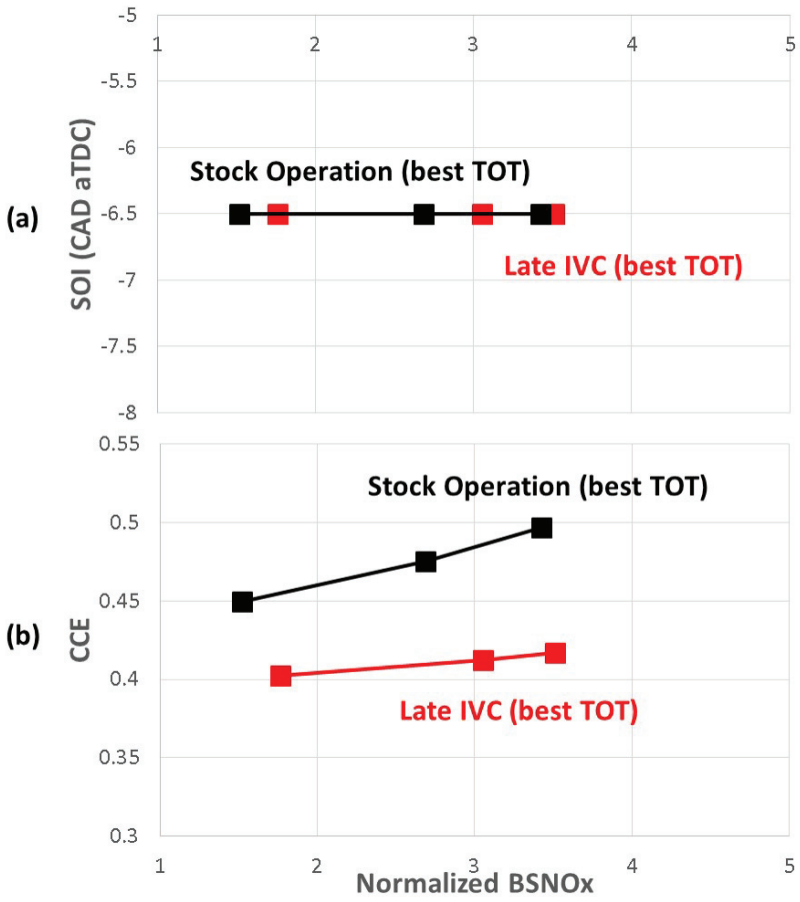

Figure 3.5. Comparison of SOI and its effect on CCE vs BSNOx at 1200 RPM/7.6 bar BMEP. The CCE decrease for the *best TOT* cases is due to the late injections.

Delaying the IVC timing to 655 CAD reduces the volumetric efficiency as more air is being pushed out of the cylinder. This process reduces the AFR which increases the TOT. From Figure 3.6 we find that lower AFR tends to be a major reason for high TOT observed. Hence the IVC timing is optimized to very late timing, to reduce AFR in order to achieve very high TOT.

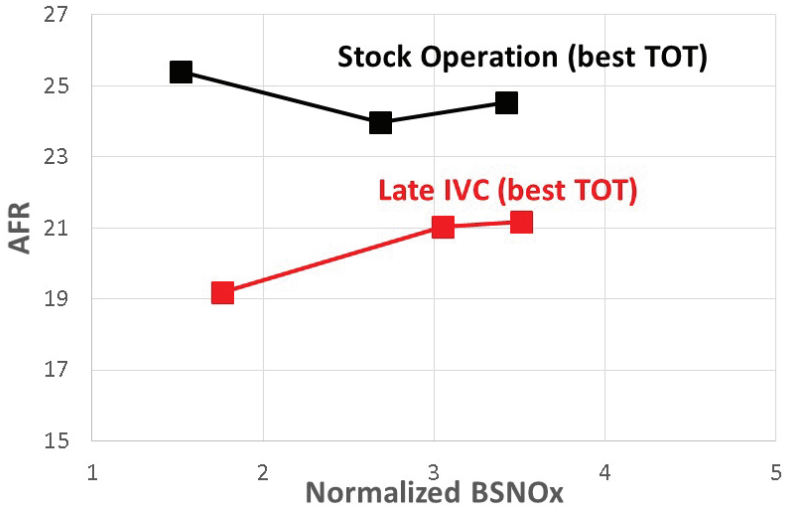

Figure 3.6. Comparison of AFR ratio vs BSNOx at 1200 RPM/7.6 bar BMEP. The reduction in AFR for LIVC is the primary reason for the increase in TOT.

3.5 TOP vs BSNOx Analysis

TOT and exhaust flow are the critical parameters for AFT system warm up. In this study, turbine out power (kW) is optimized using the Equation:

$$TOP = ExhaustMassFlow * Cp * TOT \tag{3.1}$$

The results show that LIVC has higher TOP than stock hardware at low to medium BSNOx levels, as shown in Figure 3.7. At higher BSNOx level, the stock hardware has higher TOP than stock hardware.

While optimizing the parameters using Equation 3.1, it is interesting to note that the exhaust flow parameter is maximized and the temperature is not maximized. There is essentially a trade-off between maximizing TOT or the mass flow parameter. All the IVC timings were optimized at around 575 CAD, which is around the CAD where maximum volumetric efficiency is achieved. Thus it is evident that the mass flow parameter tends to be a more dominant parameter during this optimization.

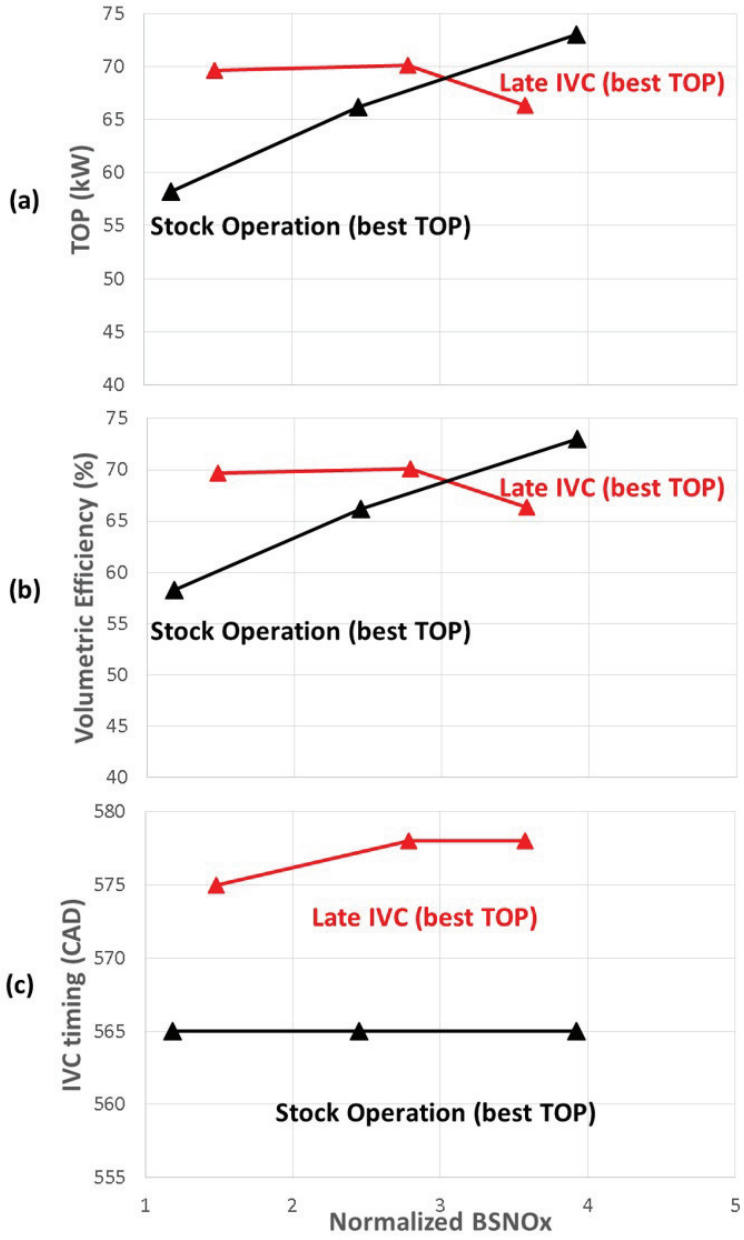

Figure 3.7. Comparison of (a) Turbine outlet power, volumetric efficiency and IVC timing vs BSNOx at 1200 RPM/7.6 bar BMEP. Clearly the volumetric efficiency is maximized for the TOP maximization case. This leads to an increase in exhaust flow which is a prime driver to increase TOP.

There is no merit in delaying IVC, as this decreases the volumetric efficiency and thus reduces the fresh air flow. At low to medium BSNOx levels, TOP is maximized by increasing fresh air flow with stock hardware and LIVC. LIVC performs better as the volumetric efficiency is higher. These cases have very late SOI, which delays the heat release thus reducing the CCE. Essentially, the TOT is increased by delaying the injection timing, which also increases the amount of fuel injected per cylinder. Thus there is a reduction in BTE as the CCE is reduced. Also there is a fuel penalty being paid at these NOx levels, as the VGT is squeezed to allow high charge flows required to achieve these TOP.

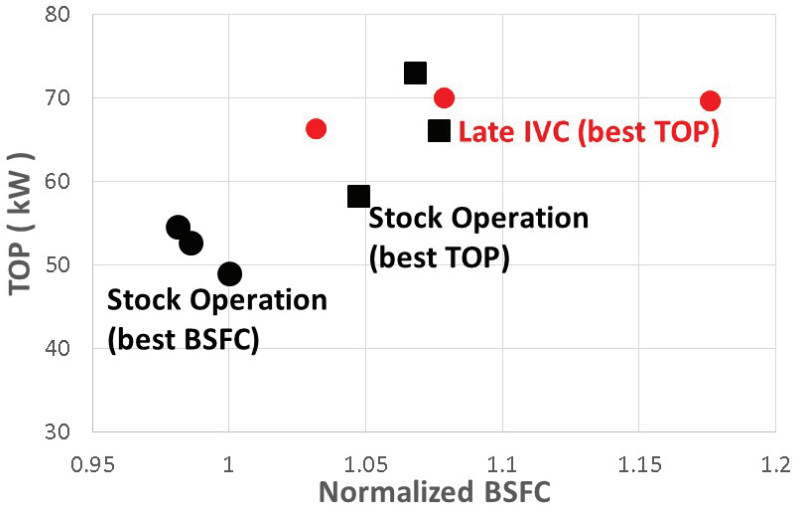

Figure 3.8. Comparison of Turbine outlet power vs BSFC at 1200 RPM/7.6 bar BMEP. SOI is delayed which decreases CCE and VGT is over-squeezed which decreases the OCE.

3.6 TOP (ref 250°C) vs BSNOx Analysis

Another way to evaluate TOP is with reference to TOT at 250°C. This is a good indicator of which mode would serve best to keep the AFT warm, when the AFT is

above 250°C. Thus it is a good measure of the stay-warm capability of these modes. Equation 3.2 shown below illustrates how this TOP is calculated:

$$TOP = \dot{m}_{exhaust} \times C_p \times (TOT - 250^oC) \tag{3.2}$$

Calculating TOP with TOT referenced to 250°C places more weight on TOT in Equation 3.2. LIVC has higher TOP (reference to 250°C) since it has higher TOT than stock hardware. TOP is maximized with higher exhaust flow and lower TOT. As more weight is put on TOT, TOP (ref. 250°C) is higher for cases where TOT was maximized than the cases where TOP was maximized. Note, however, that the optimization in this effort was not done with regard to maximizing TOP, when TOT is referenced to 250°C. This result indicates that LIVC is a better strategy for stay-warm operation of the engine AFT system.

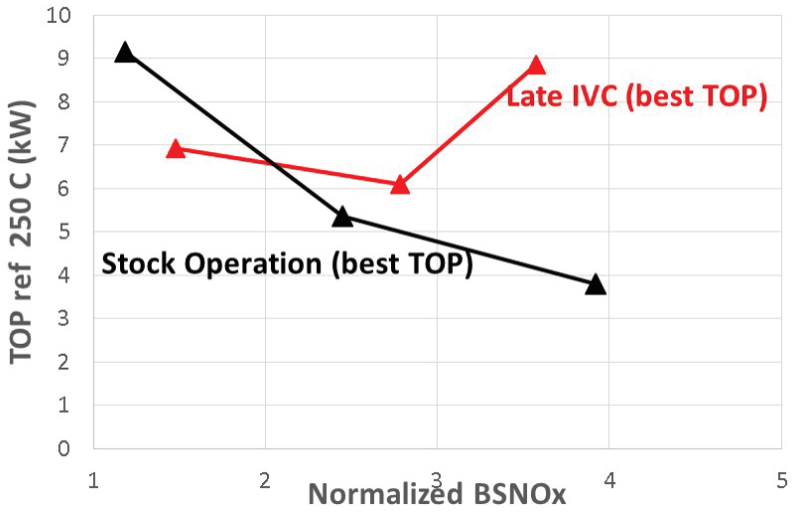

Figure 3.9. Comparison of Turbine outlet power (ref 250°C) vs BSNOx at 1200 RPM/7.6 bar BMEP.

3.7 Emissions

All the cases studied satisfy the PM limit as shown in Figure 3.10. Most of the cases satisfy the HC limit. All the LIVC cases have lower HC levels than stock operation.

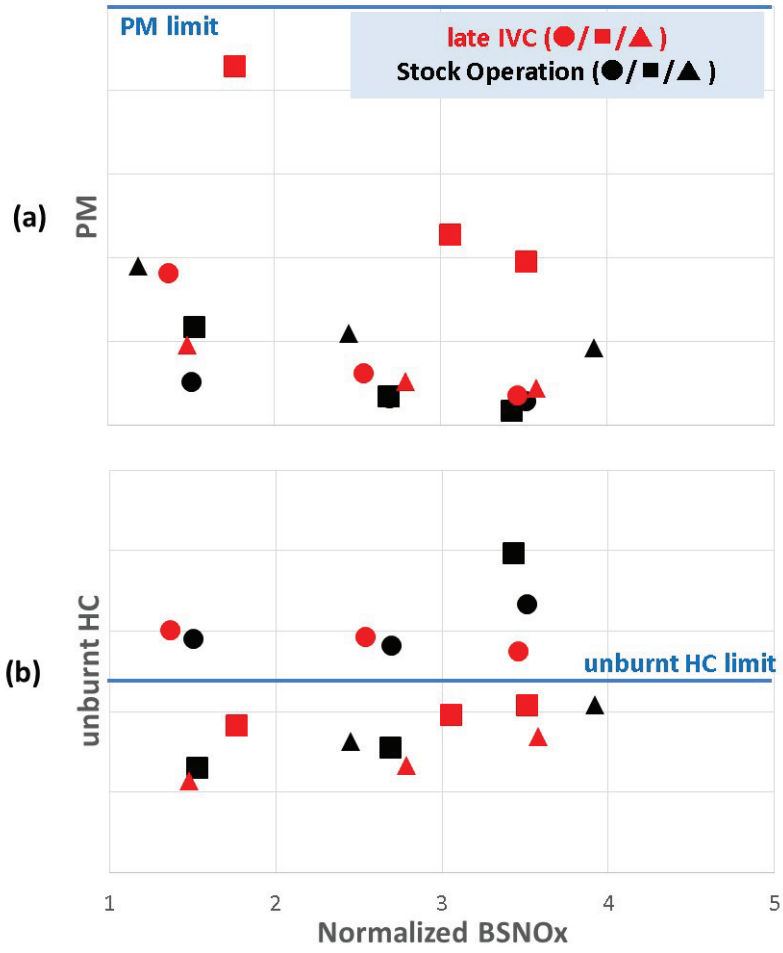

Figure 3.10. Comparison of (a) PM, (b) unburnt HC vs BSNOx at 1200 RPM/7.6 bar BMEP.

3.8 Summary

Constrained optimization was carried out in GT power by developing regression models to minimize fuel consumption, maximize TOT and TOP by using LIVC. Following are the key conclusions from the study:

- LIVC does not bring any fuel economy benefit at 1200/300 when compared to stock hardware as the stock hardware is already optimized for best fuel economy.
- The IVCs for *best TOP LIVC* case is optimized at around 575 CAD, so as to maximize volumetric efficiency, thus making the engine breathe more efficiently. At low to moderate BSNOx levels, there is a TOP increment of 12 KW and 4 KW, respectively, using LIVC. However, there is a BSFC penalty for the cases when TOP is maximized, as later injections and over-squeezed VGT are used. This is because exhaust mass flow is the more dominating parameter than TOT for estimating TOP at this condition.
- A TOT increment of about 150-200°C was observed while trying to maximize TOT using LIVC. This was primarily due to the decrease in airflow due to delayed IVC timings in this optimization.

Thus, LIVC does appeal as a viable function to increase TOT at highway cruise condition and could be a viable strategy for stay-warm engine operation. Further benefits can be realized if LIVC is combined with other VVA technologies, such as CDA, EEVO, internal EGR and Reverse Breathing.

4. CDA TRANSIENTS

4.1 Motivation

The previous chapters on CDA showed numerous fuel economy and AFT thermal management benefits of CDA at light or low-load operation. Similar benefits were also noted on studies at loaded and unloaded idle [23]. Previous research work at Herrick labs showed significant thermal and fuel economy benefits of deactivating cylinders at 1200 RPM [20, 21, 26, 27, 29, 40]. In order to capture these steady-state benefits, the dynamic operation of CDA should be verified. For this purpose, testing of these strategies in a transient drive-cycle is important.

The federal test procedure is a regulatory emissions testing standard designed to replicate various driving cycles in urban and freeway conditions. This procedure is a dynamic drive cycle test, and contains a series of engine load and speed set points over a period of time. On-road vehicles must meet the emissions requirements outlined by this procedure when subjected to this procedure. The load transitions represented in the FTP are also representative of the load response that would be required of an engine. In this study, any cases that does not meet this response while maintaining other emissions limits was determined to be unable to meet the FTP standard. The HDFTP, at one instance, requires an approximately constant-speed load transition from near zero load to about 6.3 bar BMEP within approximately one second. Similar scenarios exist during mid-range FTP, also known as FTP 72.

Leighton Roberts [40] conducted a transient study to characterize the potential challenge for load performance of the engine during CDA operation. The transient response of the engine using the stock calibration in 6-cylinder operation, which is used in production systems, is used as the baseline to compare the response when transitioning out of CDA, as shown by the blue curve in Figure 4.1. The quality

of the transients is defined by the closeness of the load response and emissions to that achieved via stock six-cylinder operation. The study concluded that the reduced airflow that comes from deactivating three cylinders was shown to cause issues when attempting to meet the load transitions required by the FTP. At 1200 rpm, it was concluded that the mid-range FTP cycle cannot be met with any fueling strategy or by relaxing the benefit of CDA at higher loads via higher steady-state AFR (as seen in Figure 4.1.

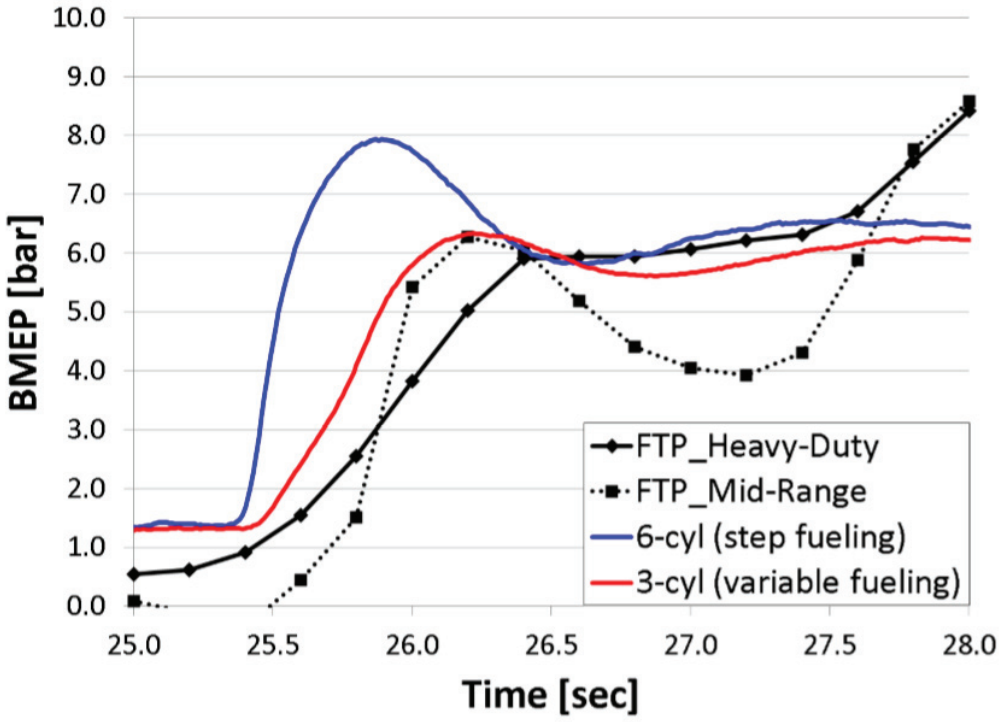

Figure 4.1. BMEP response vs Time of 6-cylinder and 3-cylinder mode compared to FTP-HD and FTP-MR transient load profiles. The 3-cylinder CDA mode cannot achieve the aggressive FTP-MR profile, however it can achieve the FTP-HD transient performance by increasing the AFR. [40]

However, the heavy-duty cycle transient can be met by increasing the steady-state AFR at 6.3 bar BMEP, from 18 to 21, decreasing the TOT by 60°CC. Also, NOx is increased from 3.2 to 10.3 g/hp-hr with a decrease in EGR to raise the airflow. Also the PM response during the load transition in *3-cylinder CDA* mode was the main

drawback in increasing the performance in *3-cylinder CDA* mode. This is again due to limited fresh air flow available during transient operation in CDA.

The main motivation of this study is to potentially solve this issue of limited air flow with one viable strategy, i.e to reactivate the deactivated cylinders when air flow limitation is observed. This would enable the engine to operate in CDA at low and light loads, thereby achieving higher fuel economy and better thermal management at these load conditions during the FTP.

4.2 Methodology

The valve controller code in simulink was modified to allow transition between *3-Cylinder CDA* and *6-cylinder* mode, during transient experiments. In order to study the transient reactivation of cylinders, the experiments are set up in such a way that the engine starts from low load (1.3 bar BMEP) in *3-cylinder CDA* and transitions to *6-cylinder* mode at the beginning of the load increase to high load (6.4 bar BMEP) condition. The constraints for this study are shown in Table 4.1 below.

Table 4.1. Constraints for the CDA transient performance study.

Turbine Inlet Temperature	<760°C
Compressor Outlet Temperature	<230°C
Turbocharger Speed	<126 kRPM
Peak Cylinder Pressure	<2500 psi
Exhaust Manifold Pressure	<120 inHg (gauge), 1.4 bar
Pressure Rise Rate	<100 bar sec
PM	<1.5 FSN
Turbine Inlet Pressure	<65 psi
AFR	<18

The set-points for all inputs at each load were obtained from the steady-state load sweep data obtained from prior experiments [20] at Herrick Labs. The CDA inputs were taken from the data points targeting nominal BSNOx emission level. The start of injection, rail pressure, VGT, and EGR actuators were given a step change command at the time of transition. It is important to observe emissions limits to maintain a fair comparison between *3-cylinder CDA* and 6-cylinder operation, during the FTP transient event. The assumed transient smoke limit for this effort was 1.5 filtered smoke number (FSN). Also, it was assumed that the AFR is to remain above the stoichiometric condition. The following section will discuss the results of experiments at 1200 rpm. The result was compared with the previous transient results from *6-cylinder* and *3-cylinder* transient study, which showed that there is a challenge in meeting a reasonable torque response with CDA operation. The following Table 4.2 shows the test plan in detail for the study. The first two tests (*3-cylinder CDA* and *6-cylinder*) are steady-state points to ensure repeatability and the last one is the *3-cylinder CDA* to *6-cylinder* transition test. The steady-state set points enable best fuel economy during CDA. The control was reverted to the ECM after transitioning to *6-cylinder* operation during the acceleration.

Table 4.2. Test plan for the CDA transient performance study.

Mode	**Load**	**VGT pos**	**EGR pos**	**Fueling**	**SOI**	**Rail Press**
Unit	bar BMEP	% closed	% open	mg/st	CAD ATDC	bar
3-cyl CDA	1.3	65	22	27.5	-0.05	1180
6-cylinder	6.4	25	22	60.25	-5.5	1150
3-cyl to 6-cyl	1.3-6.4	65	22	27.5-60.25	ECM	ECM

4.3 CDA Transients Experimental Results

Figure 4.2 compares engine response of this transition with the MD-FTP, HDFTP as well as the CDA mode transition (*3-cylinder CDA* to *6-cylinder*). The green line, which is the *3-cylinder CDA* to *6-cylinder* mode switch and load increase from 1.3 bar BMEP to 6.4 ft-lbs, is the line of interest.

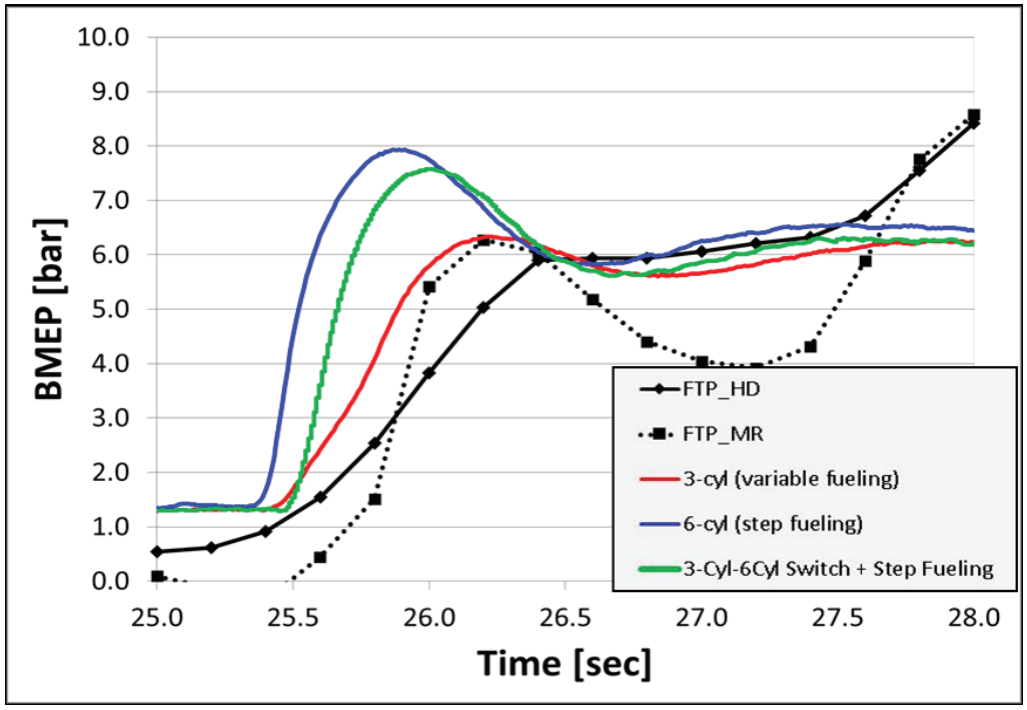

Figure 4.2. Load response comparison between various modes with reference to FTP-MR and FTP-HD at 1200 RPM.

From Figure 4.2, it is clear that the transition from *3-cylinder CDA* to *6-cylinder* mode during load increase can match the performance required by both the FTPs with respect to load response. In order to validate the test procedure, extra care was taken to make sure that the valve events and injector currents are in the right order.

The required order of events is exhaust-intake-injection. This is verified from Figure 4.3, which shows the events for cylinders 4,5,6 (initially deactivated) are reactivated during load increase.

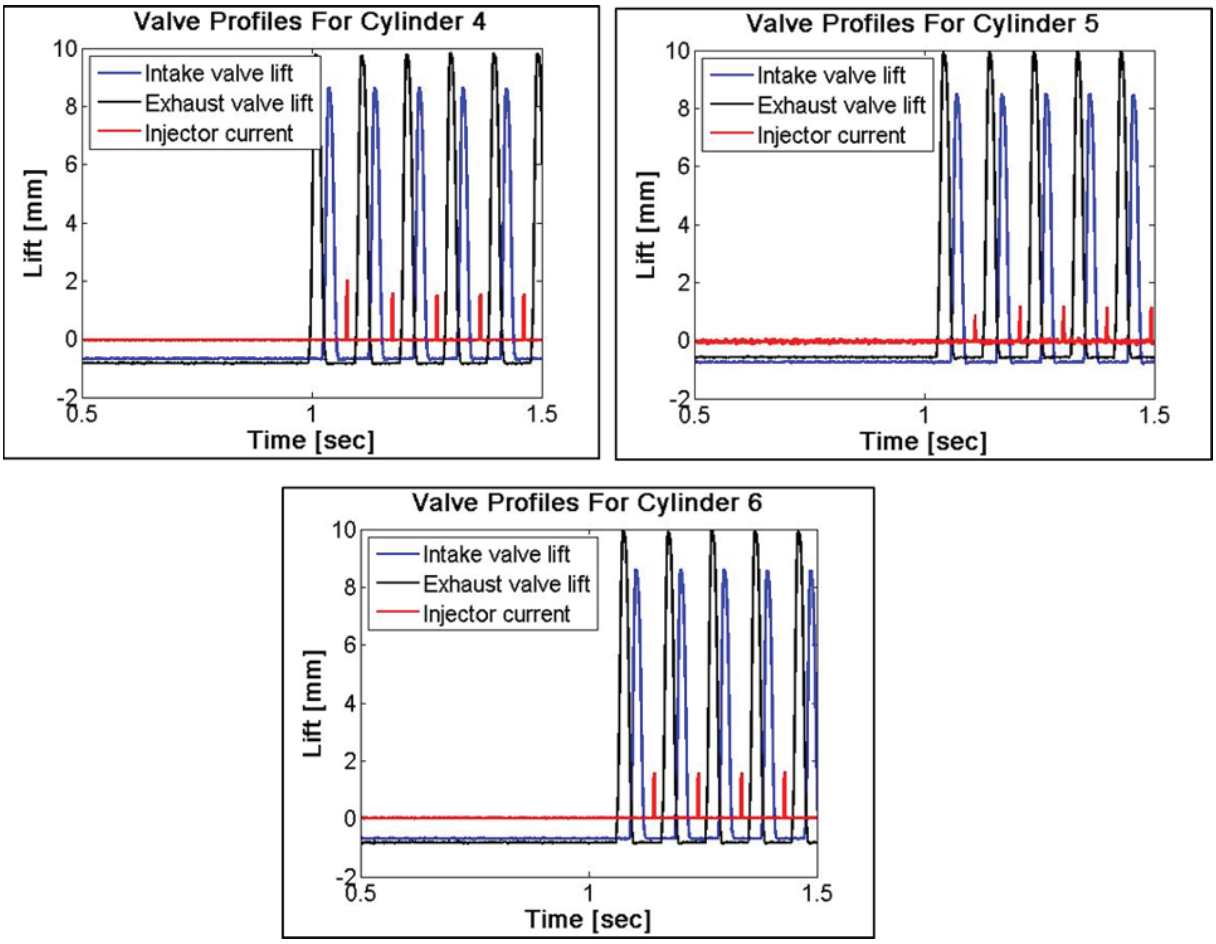

Figure 4.3. Valve profiles along with fuel injection events in the cylinders during the switch between *3-cylinder CDA* to *6-cylinder* operation.

The transient load response for *3-cylinder CDA* to *6-cylinder* operation is determined to be acceptable. The main criterion for this conclusion was the PM response. From prior work, the high PM response due to limited fresh air flow during the load transition in *3-cylinder* mode was the main drawback in increasing the performance in *3-cylinder* mode.

However during the *3-cylinder CDA* to *6-cylinder* switch, there is very minimal PM increase, as seen in Figure 4.4. This is because of the availability of increased fresh air flow during the transition. Since the load performance is matched without a large PM increase, this load response for *3-cylinder CDA* to *6-cylinder* operation is acceptable, and could serve as a viable solution to this transient air flow management in CDA.

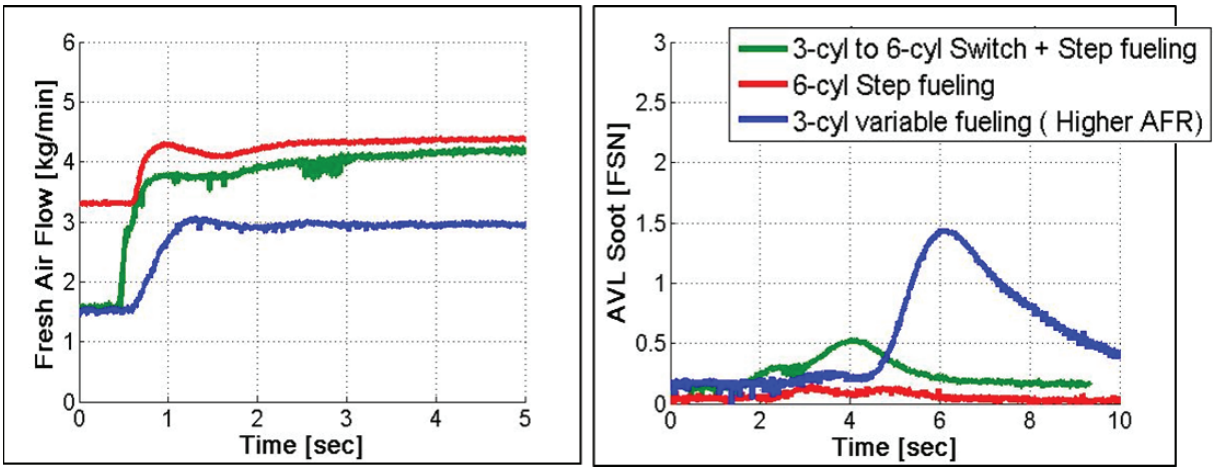

Figure 4.4. Fresh air flow and soot response during the load increase for various modes. Soot is reduced for the 3-cylinder to 6-cylinder switch due to immediate increase in air flow by reactivation of cylinders.

4.4 CDA transient summary

In this chapter one of the key challenges in meeting load transients with CDA is discussed and a potential solution of reactivation of cylinders during transients

is studied. Transients during *3-cylinder CDA* could be a potential issue due to the increase in PM because of limited airflow. However during the *3-cylinder CDA* to *6-cylinder* switch, there is very low PM increase as seen in the previous section. This is because of the immediate availability of fresh air flow during the transition after reactivation of cylinders. The absence of a sudden decrease in the IMP after all six cylinders are activated indicates that the engine air-path responds quickly enough to source enough fresh air to the intake manifold as to not "starve" the intake manifold of oxygen during cylinder reactivation. Since the load performance is matched without PM spikes, the load response for *3-cylinder CDA* to *6-cylinder* operation is acceptable. Hence this method of reactivation could serve a potential method of airflow management while operating in CDA mode. This finding served as crucial information for conducting several transient CDA experiments [26, 43, 53].

5. ALTERNATE BREATHING STRATEGIES

5.1 Motivation

Figure 5.1 shows the fuel consumption over a HDFTP mapped around 8 steady-state engine operating regions. The number displayed next to a bubble signifies the percentage of fuel consumed at these operating conditions. In a typical HDFTP, about 5.8 % of fuel consumed is consumed at idle operating conditions as shown in the figure.

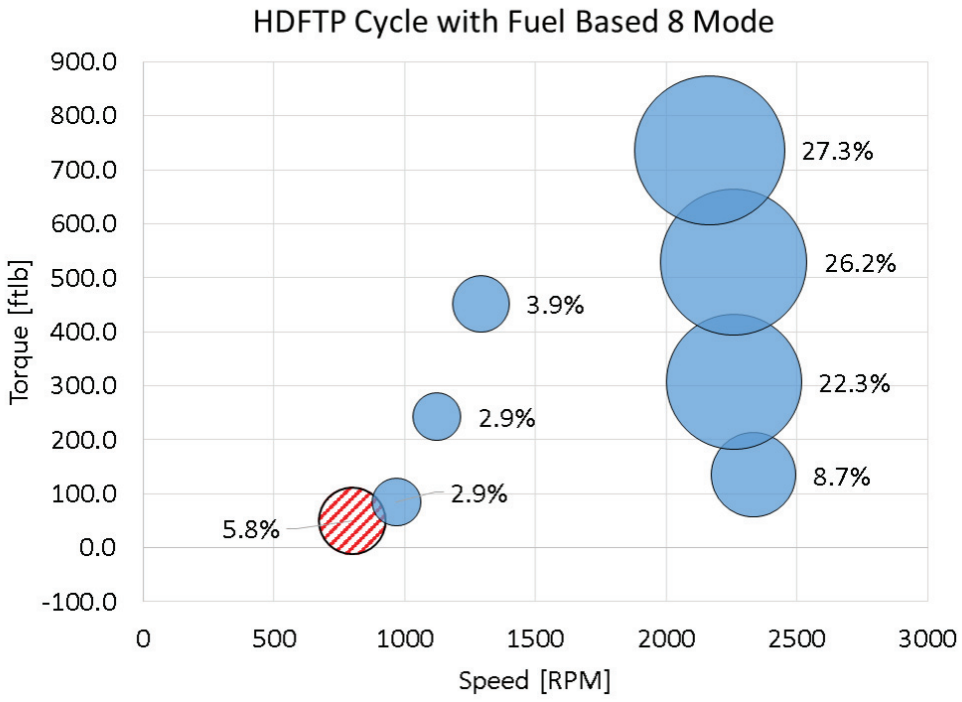

Figure 5.1. Bubble plot showing the fuel consumption percentage at idle for HDFTP. About 6% of the fuel being burnt over the while HDFTP is at Idle (800rpm / 50 ft-lbs), thus paving a need for optimizing the fuel efficiency without compromising the AFT thermal management characteristics at this condition.

Figure 5.2 shows the time spent at that operating condition over a HD-FTP mapped around 8 steady-state engine operating regions. The number displayed next to a bubble signifies the percentage of time spent at these operating conditions. In a typical HDFTP, about 43 % of time is spent at idle operating conditions which makes the thermal management a great challenge.

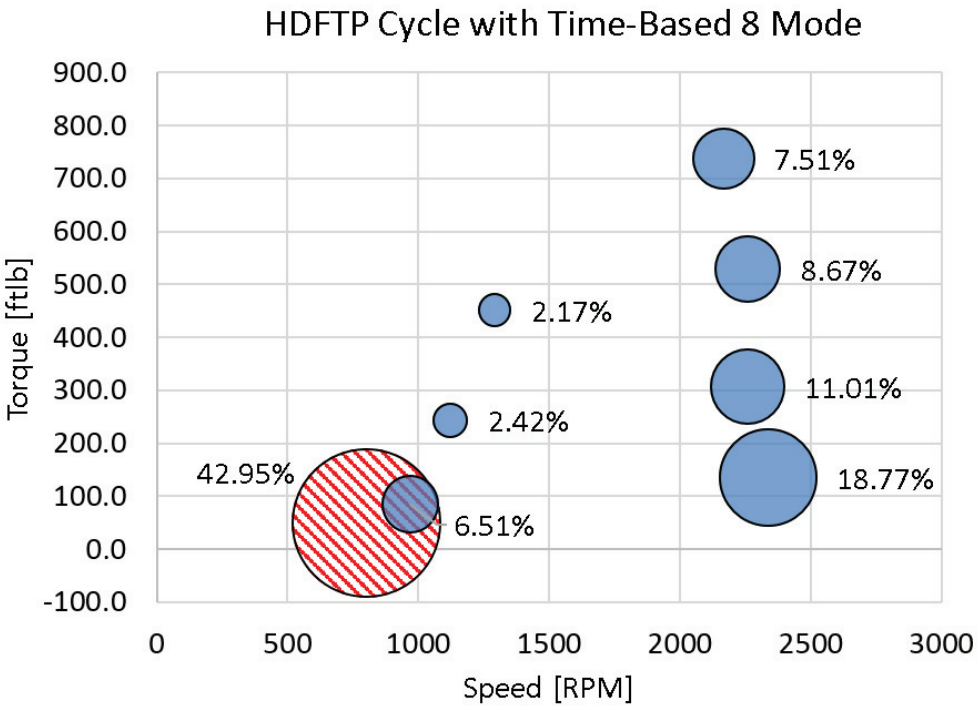

Figure 5.2. Bubble plot showing time spent at idle for HDFTP. A significant portion (around 43%) of the time during HDFTP is spent at Idle showing that there is major AFT thermal management challenge at Idle. Strategies like reverse breathing and ERB aim to improve the thermal management characteristics in a fuel efficient manner.

Traditional strategies, such as late injection, over-closing a variable geometry turbocharger or intake throttling, can increase exhaust temperatures, but lead to significant increase in fuel consumption.

This chapter introduces four novel engine breathing modes, namely fired reverse breathing (FRB), non-fired reverse breathing (NFRB), exhaust rebreathing (ERB),

intake rebreathing (IRB), that could be used to increase the TOT at low loads in a fuel efficient manner. The methodology section delves deeper into how each of these modes actually work. The experimental study emphasis is on the loaded idle conditions given the low engine exhaust temperatures and significant amount of time spent at these conditions in a HDFTP.

The effort described here will demonstrate how reverse breathing and ERB can be used to achieve thermal management in a more fuel efficient manner. This effort also will focus on the results taken with the stock turbocharger attached to the engine.

Initial screening work done at 750 rpm /11 ft-lbs for *ERB* and at 1200 RPM/50 ft-lbs for *FRB* with an turbocharger (consistent with heavy duty engine operation) attached to the engine. The results from that study serve as a motivation to study these novel breathing strategies at idle with the stock turbocharger attached to the engine. Figure 5.3 shows the BSFC vs TOT trade-off at unloaded idle for *ERB*. The TOT is increased by 30°C and the BSFC decreases by about 15% for *ERB*.

Figure 5.4 shows the BSFC vs TOT trade-off at 1200 rpm/50 ft-lbs for *FRB*. The TOT is increased by about 100°C and the BSFC decreases about 9% for two-cylinder *FRB*.

5.2 Methodology

This section focuses on how reverse and rebreathing strategies are implemented on the VVA testbed. The simulink code was modified and validated to allow cylinder independent transition between FRB/ERB modes and normal operation. The cylinder combination selection for these strategies should take into account the split exhaust manifold geometry of the engine. The following subsection discusses the viability of each strategy for the particular exhaust manifold design.

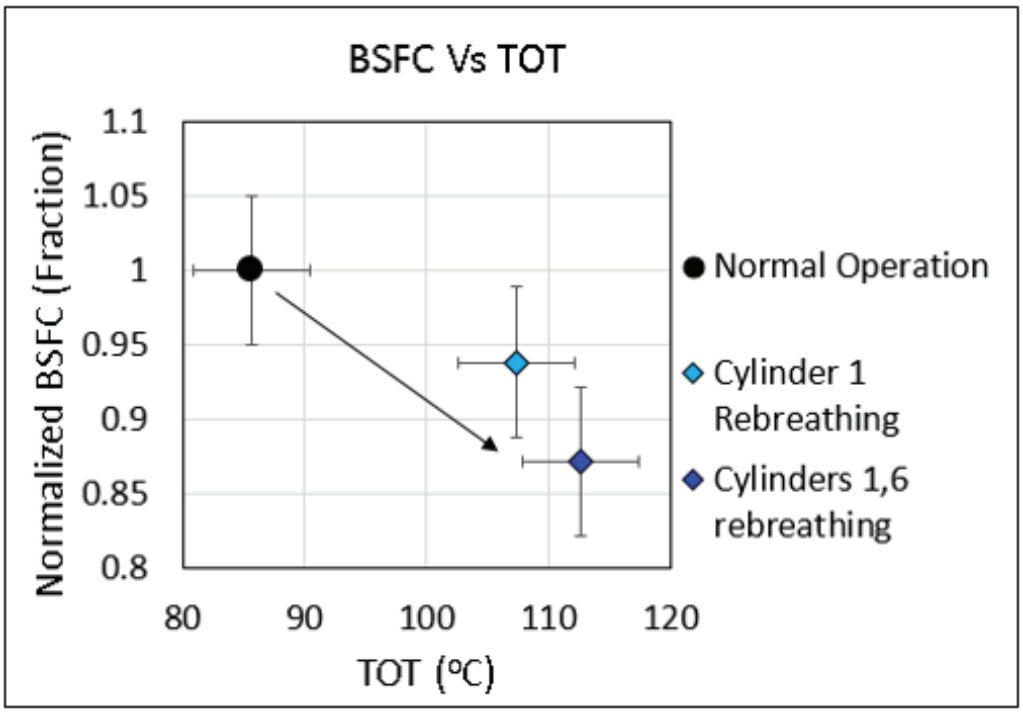

Figure 5.3. BSFC vs TOT trade-off at unloaded idle for *ERB*. [41]. *Exhaust rebreathing* is shown to give mild TOT and fuel economy benefits at 750 rpm /11 ft-lbs.

5.2.1 Cylinder Combination Selection

Exhaust manifold, as seen in Figure 5.5, is split into two halves containing cylinders (1, 2, 3) and (4, 5, 6) respectively. If two cylinders from the same split side are set to be reverse breathing, they will induct the exhaust only from the third cylinder, which will not contain enough oxygen to carry out complete combustion. To avoid starving the reverse breathing or rebreathing cylinders of oxygen, at the most, one cylinder from each split side was set to be reverse or exhaust rebreathing. For *IRB*, this will not be a limitation as the intake manifold is not a split manifold like the exhaust.

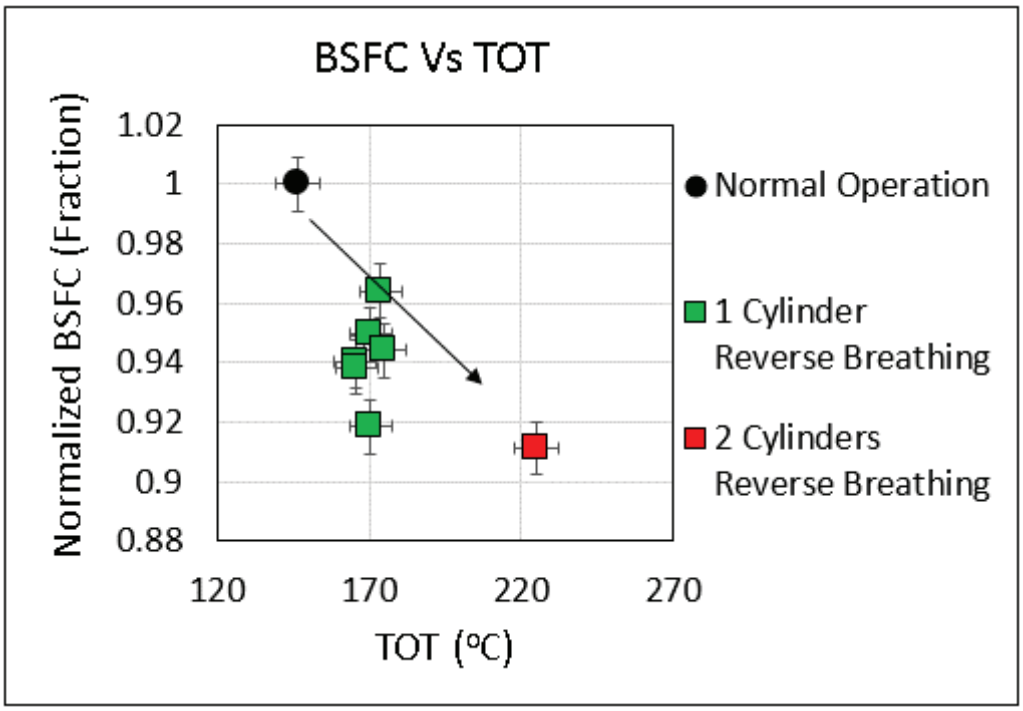

Figure 5.4. BSFC vs TOT trade-off at 1200 rpm/50 ft-lbs for *FRB*. [41]. *Fired reverse breathing* is shown as a way to increase the TOT while decreasing the fuel consumed at this particular operating condition.

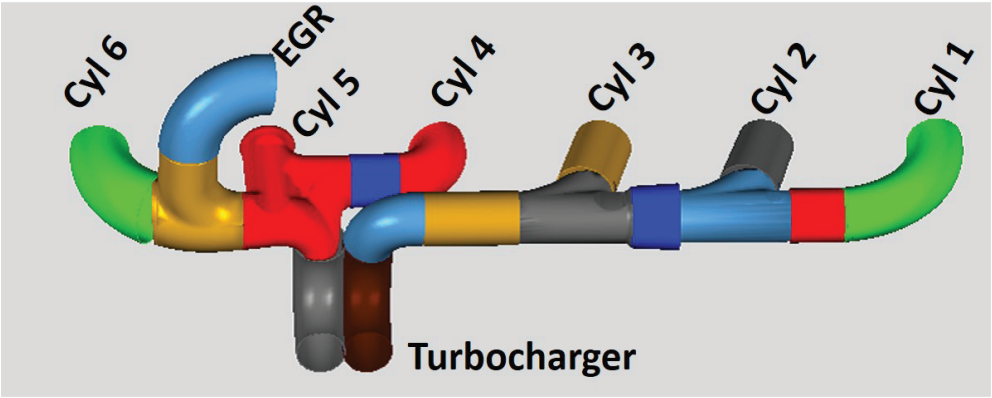

Figure 5.5. Schematic of the exhaust manifold of the diesel engine used for the study.

5.2.2 Breathing Modes

Figure 5.6 shows the normal operation of the engine with fresh air going into the engine and burnt gases coming out of the exhaust while certain fraction of burnt gases are recirculated into the intake manifold through EGR. This mode serves as a reference when alternate modes of breathing are explained in the following subsections.

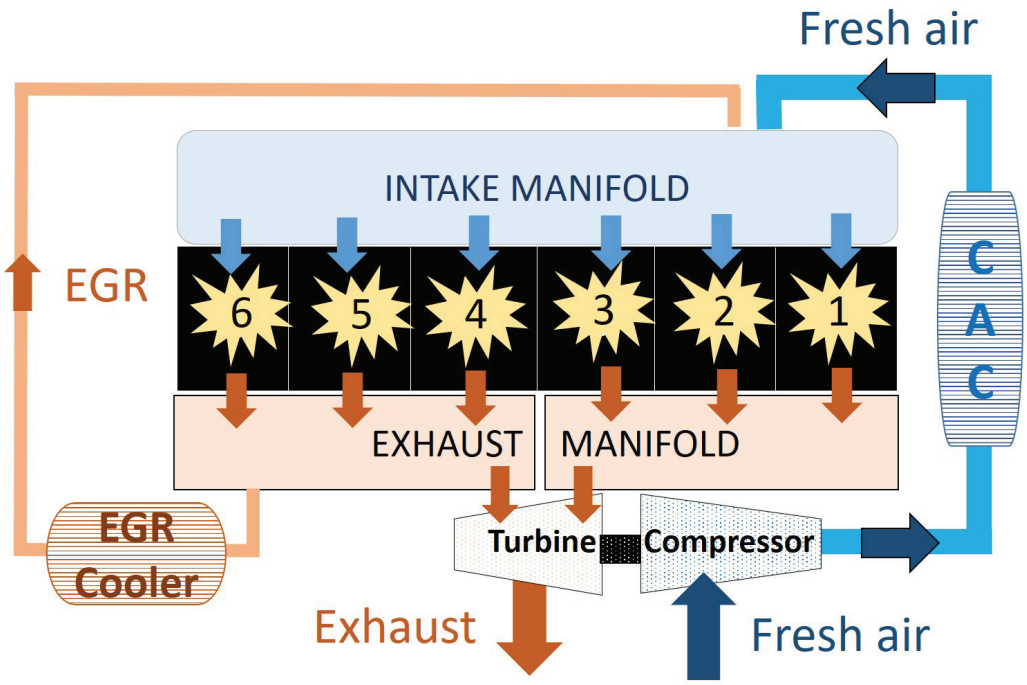

Figure 5.6. Normal mode of breathing where all six cylinders induct fresh air from the intake manifold and exhaust burnt gases into exhaust manifold.

Exhaust Rebreathing

Figure 5.7 illustrates the gas exchange occurring during single-cylinder ERB operation of the engine. Five of the six cylinders operate in a normal manner, whereas the rebreathing cylinder pulls in charge from the exhaust manifold, injects fuel for combustion and exhausts back into the exhaust manifold again. The EGR valve is

closed in this particular configuration in order to study the gas exchange process of this strategy. The effective amount of air flow to the engine is reduced to 5/6th of normal operation, as only five cylinders pull in charge from the intake manifold. The airflow can further be reduced by rebreathing in two cylinders as shown in Figure 5.8. The cylinder combination is based on the exhaust manifold as discussed in section 5.2.1.

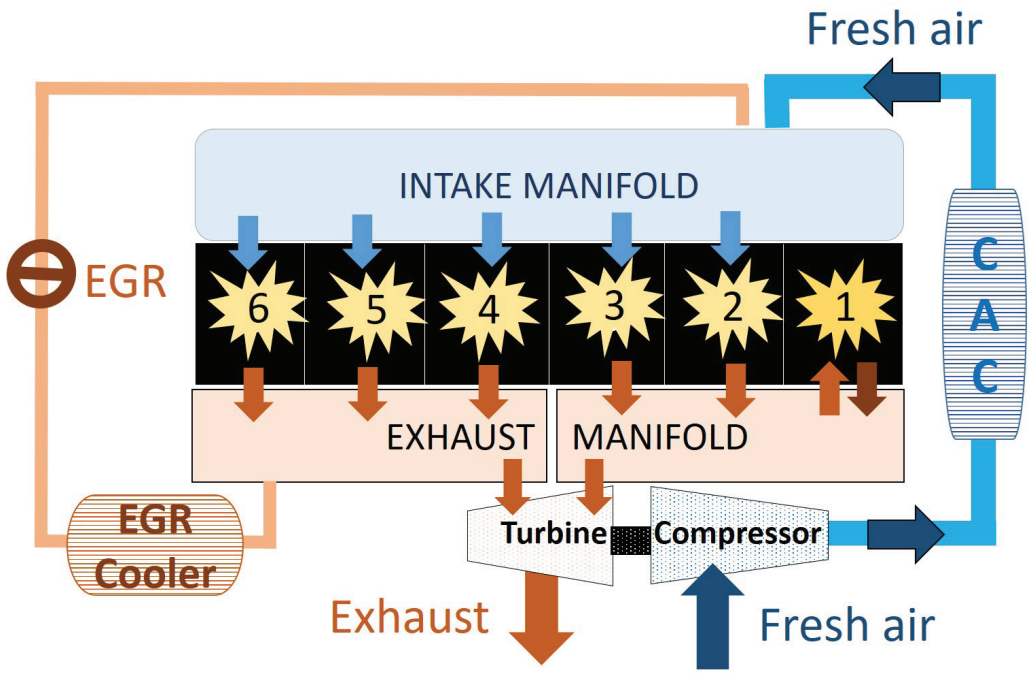

Figure 5.7. Single cylinder (cylinder 1) Exhaust rebreathing. Cylinder 1 inducts the burnt gases during intake stroke from the exhaust manifold and exhaust it back into the manifold during exhaust stroke.

Intake Rebreathing

Figure 5.9 illustrates the gas exchange occurring during single-cylinder IRB operation of the engine. Five of the six cylinders operate in a normal manner, whereas the intake rebreathing cylinder pulls in charge from the intake manifold, injects fuel

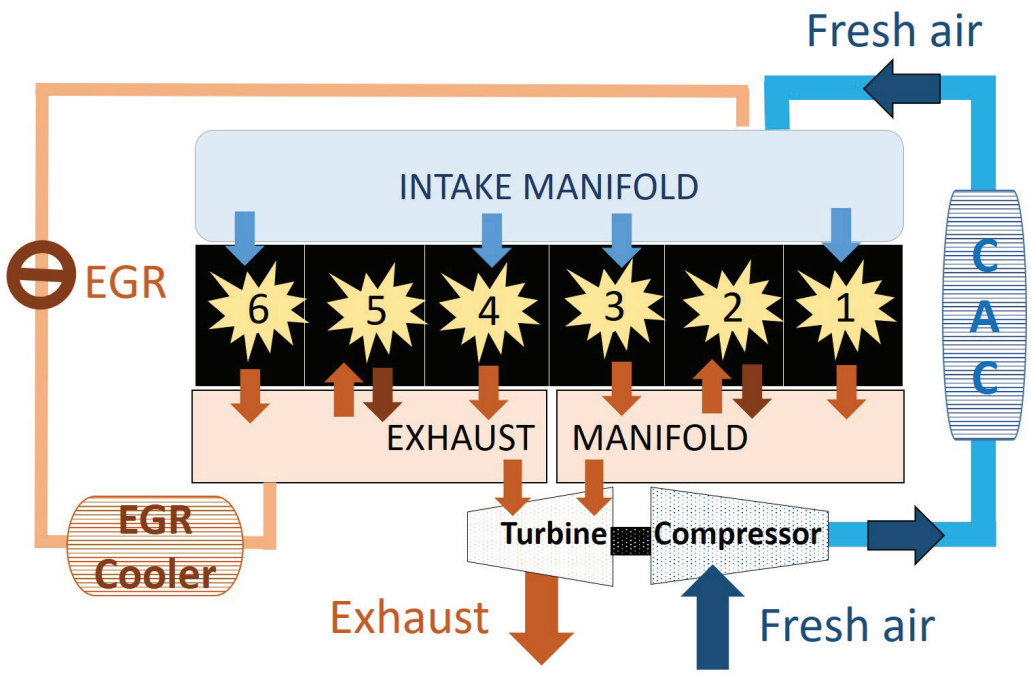

Figure 5.8. Two-cylinder (cylinders 2 and 5) exhaust rebreathing. Cylinders 2 and 5 induct the burnt gases during intake stroke from the exhaust manifold and exhaust it back into the exhaust manifold during exhaust stroke.

for combustion and exhausts back into the intake manifold. The EGR valve is closed in this particular configuration in order to study the gas exchange process of this strategy. The intake rebreathing cylinder acts similar to internal gas re-circulation system, which increases the burnt gases in the intake manifold as the intake valve is open throughout the intake and exhaust portions of the cycle as shown in Figure 5.10. The effective amount of air flow to the engine is reduced to about 2/3rd of normal operation, as only four cylinders effectively pull in charge from the intake manifold. The airflow can further be to about 1/3rd of normal operation by rebreathing in two cylinders, as shown in Figure 5.10. The cylinder combination is not restricted based on the exhaust manifold as discussed in section 5.2.1 as the charge intake is through the intake manifold.

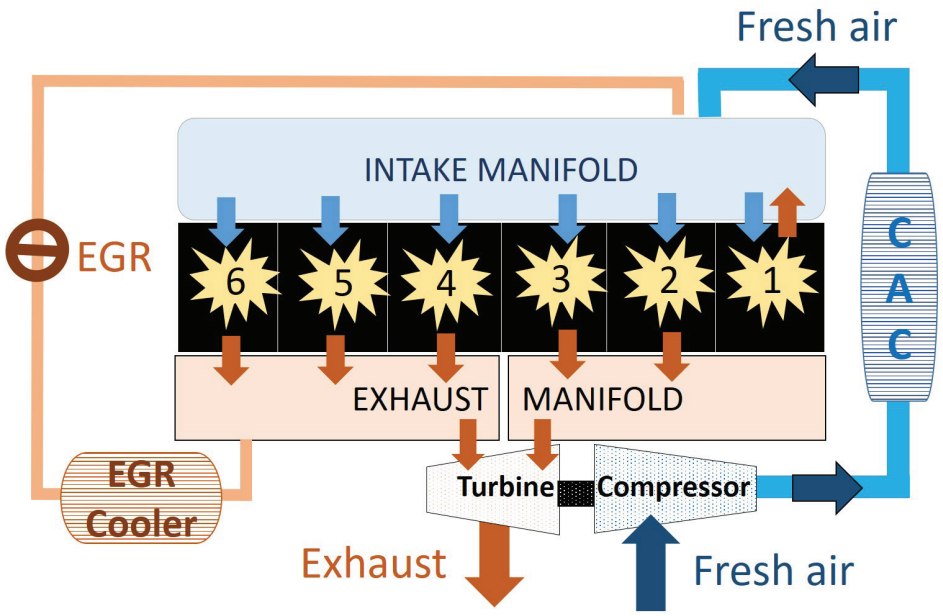

Figure 5.9. Single cylinder (cylinder 1) intake rebreathing. Cylinder 1 inducts the fresh air during intake stroke from the intake manifold and exhaust it back into the intake manifold during exhaust stroke.

Fired Reverse Breathing

Figure 5.11 illustrates the gas exchange occurring during single-cylinder FRB operation of the engine. Five of the six cylinders operate in conventional manner, whereas the reverse breathing cylinder (cylinder 1) inducts charge from the exhaust manifold, injects fuel for combustion and exhausts into the intake manifold. The EGR valve is closed in this particular configuration in order to study the gas exchange process of this strategy. The reverse breathing cylinder acts similar to internal gas re-circulation system, which increases the burnt gases in the intake manifold. The effective amount of air flow to the engine is reduced to 2/3rd of normal operation, as only four cylinders effectively pull in charge from the intake manifold. Since the airflow is decreasing, the TOT will increase which is essential for proper thermal management. The airflow can further be reduced by reverse breathing in two cylinders as shown in Figure 5.12.

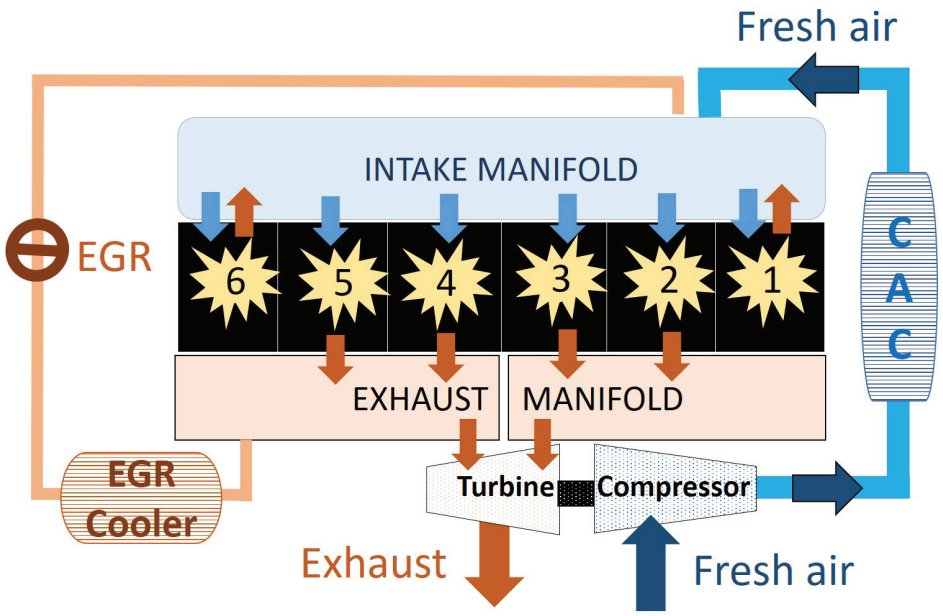

Figure 5.10. Two-cylinder (cylinders 1 and 6) intake rebreathing. Cylinder 1 and cylinder 6 induct the fresh air during intake stroke from the intake manifold and exhaust it back into the intake manifold during exhaust stroke.

The cylinder combination is limited based on the exhaust manifold as discussed in section 5.2.1.

Non-Fired Reverse Breathing

Figure 5.13 illustrates the two-cylinder NFRB of the engine. The fuel injection is deactivated in the reverse breathing cylinders, however the valves are still opening and closing similar to FRB during the strategy. NFRB combines characteristics of CDA and internal EGR as gases pass through the cylinder from exhaust manifold to the intake manifold. There could be a pumping penalty for the reverse breathing cylinders to push the gases from the exhaust manifold to the intake manifold. However if a net positive engine delta pressure is realized, it might be an optimum low-load operating mode.

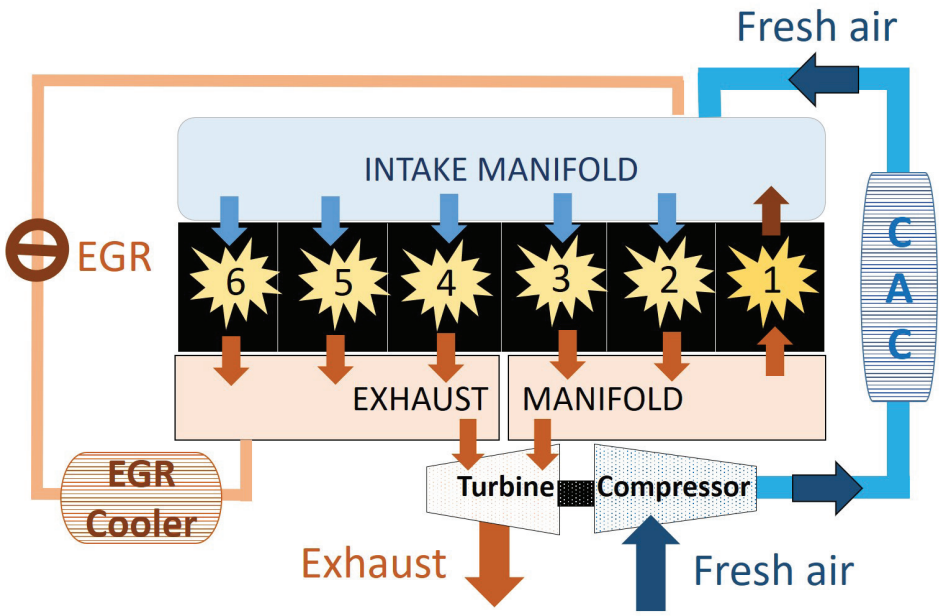

Figure 5.11. Single-cylinder (cylinder 1) fired reverse breathing. Cylinder 1 inducts burnt charge from exhaust manifold during intake stroke and exhaust it into the intake manifold during exhaust stroke acting like internal EGR.

5.2.3 Valve Profile Modifications

The valve profiles are modulated using the parameters: valve opening (IVO, EVO), valve closing (IVC, EVC), and valve lift (IVL, EVL). All valve open and close timings in this dissertation will be in terms of CAD. The nominal stock valve profile parameters are:

$$\begin{bmatrix} IVO = 340, & IVC = 565, & IVL = 8.5mm \\ EVO = 120, & EVC = 380, & EVL = 10mm \end{bmatrix}$$

Exhaust Rebreathing

The valve profile generator code in dspace controller was modified such that intake valves of rebreathing cylinders were shut at all times, and exhaust valves were

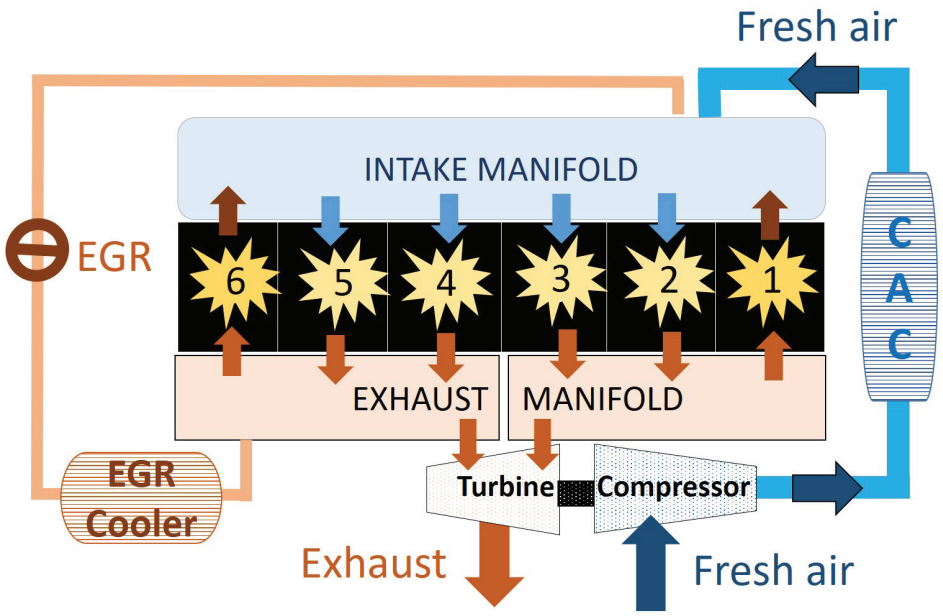

Figure 5.12. Two-cylinder (cylinders 1 and 6) reverse breathing. Cylinder 1 and 6 inducts burnt charge from exhaust manifold during intake stroke and exhaust it into the intake manifold during exhaust stroke.

actuated for both intake and exhaust events as shown in Figure 5.14 (b).

ERB valve profile parameters:

$$\begin{bmatrix} EVO^{ERB} = 340, & EVC^{ERB} = 565, & EVL^{ERB} = 8.5mm \\ EVO = 120, & EVC = 380, & EVL = 10mm \end{bmatrix}$$

A nominal valve profile, for $EVC > IVO$, leads to a positive overlap between intake and exhaust valves being open. Similarly during ERB, for $EVC > EVO^{ERB}$ leads to the exhaust valves being slightly open during the overlap ($340 - 380$ CAD).

Reverse Breathing

The valve profile generator code in simulink was modified such that timings of intake and exhaust valves were swapped. This causes the exhaust valve to open during

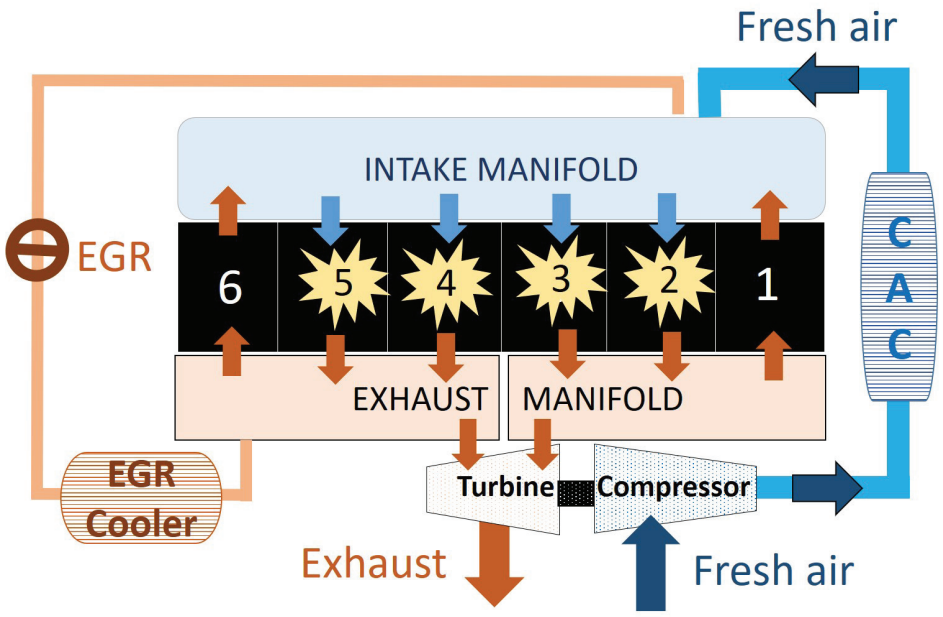

Figure 5.13. Two-cylinder (cylinders 1 and 6) non-fired reverse breathing. Cylinders 1 and 6 does not have a combustion event, thereby just recirculating the burnt gases from the exhaust manifold into the intake manifold.

the intake stroke as shown in Figure 5.14 (d), inducing charge from the exhaust manifold, and the intake valve opens during the exhaust stroke, letting the exhaust into intake manifold. This hot charge is then distributed into all the normally breathing cylinders.

Reverse breathing valve profile parameters:

$$\begin{bmatrix} EVO^{FRB} = 340, & EVC^{FRB} = 565, & EVL^{FRB} = 8.5mm \\ IVO^{FRB} = 120, & IVC^{FRB} = 380, & IVL^{FRB} = 10mm \end{bmatrix}$$

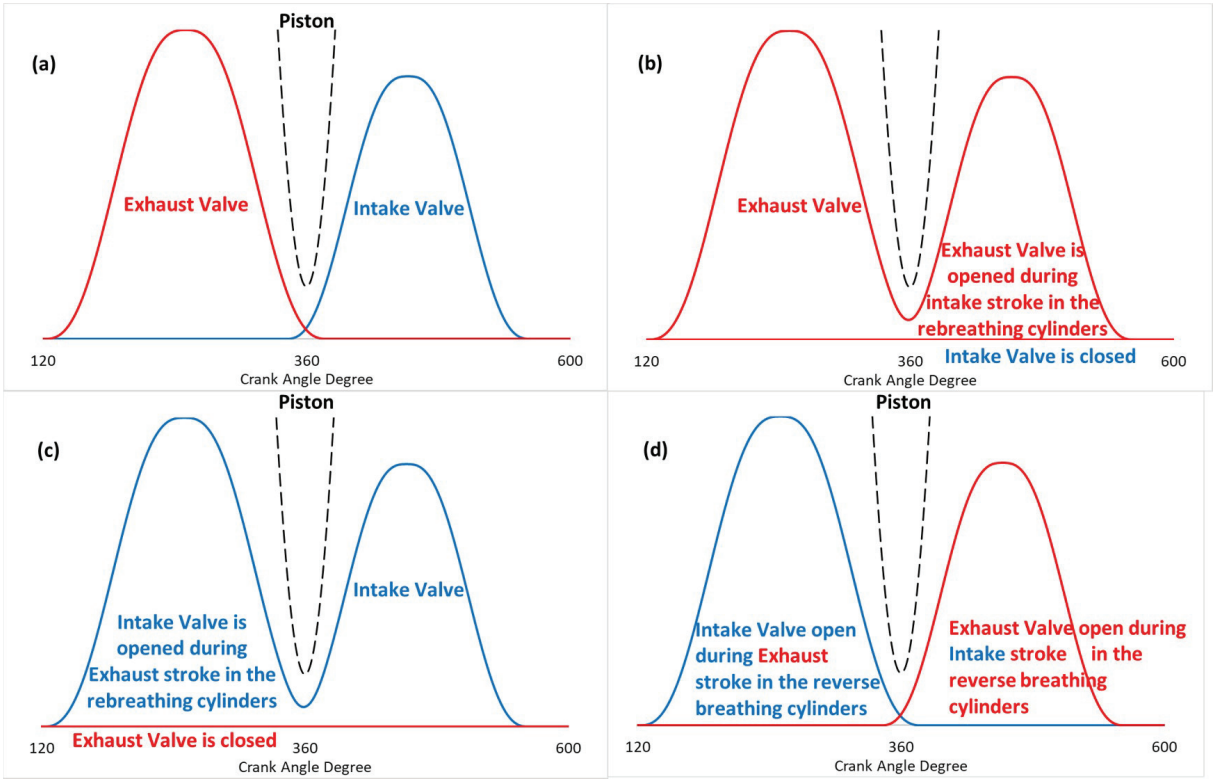

Figure 5.14. Valve profiles of the cylinders during (a) normal operation, (b) exhaust rebreathing, (c) intake rebreathing and (d) reverse breathing.

Intake Rebreathing

The valve profile generator code was modified such that intake valves of rebreathing cylinders were inactive at all times, and exhaust valves were actuated for both intake and exhaust event as shown in Figure 5.14 (c).

IRB valve profile parameters:

$$\begin{bmatrix} IVO^{IRB} = 340, & IVC^{IRB} = 565, & IVL^{IRB} = 8.5mm \\ IVO = 120, & IVC = 380, & IVL = 10mm \end{bmatrix}$$

During IRB, for $EVC > EVO^{IRB}$, the intake valves will be slightly open during the overlap ($340 - 380$ CAD).

5.3 GT Power Simulations at 800rpm/50 ft-lbs

The GT Power model was modified in order to implement and study FRB, NFRB, ERB and IRB strategies. These simulations using the model enable the study of the gas exchange processes for the strategies. GT power simulations were run for the single-cylinder (cylinder 1 through 6) ERB, IRB and FRB cases at 800 RPM/50 ft-lbs. The GT-Power initial conditions were taken from experimental engine data using an ECM-controlled operation with the EGR-position overridden to zero. The valve profiles were taken from the valve profiles observed on the engine. The model was modified to allow for separate control of each set of intake and exhaust valves in each cylinder. The model was run using both fixed heat release rate method as well as the Diesel Multi-Pulse Combustion model (DI pulse) method. One advantage of the DIPulse combustion model over the fixed heat release rate method, is that DIPulse has the ability to estimate exhaust emissions and hence only DIPulse model results are shown. However, the DIPulse model requires calibration/tuning to estimate the emission levels accurately. The model was just used as a tool to check the BSFC, BSNOx and TOT trends and to observe the gas exchange process during the re and reverse breathing operation.

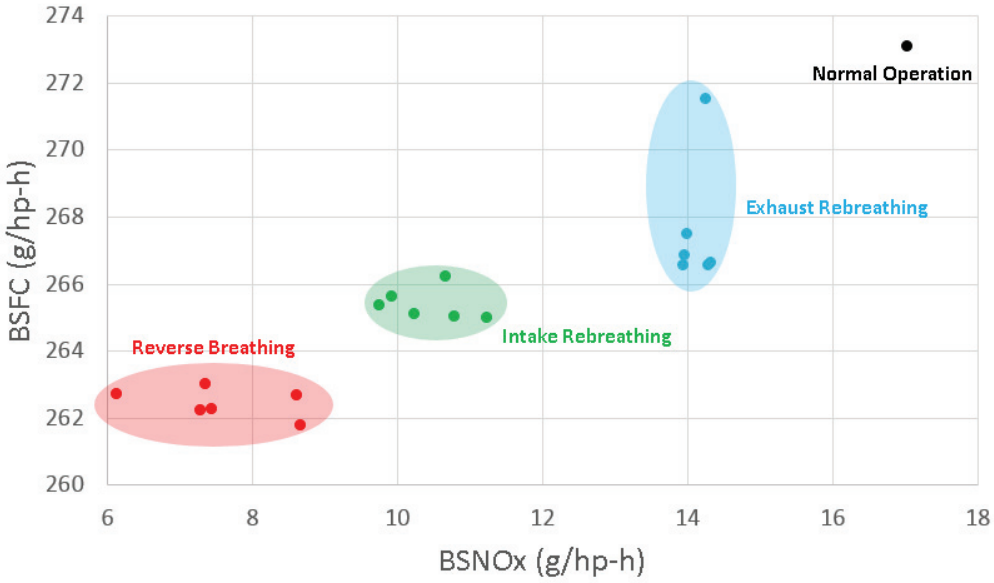

Figure 5.15. GT Power simulation results of BSFC vs BSNOx trade off for exhaust/intake rebreathing and fired reverse breathing. Simulations show a decrease in BSFC and BSNOx for these strategies.

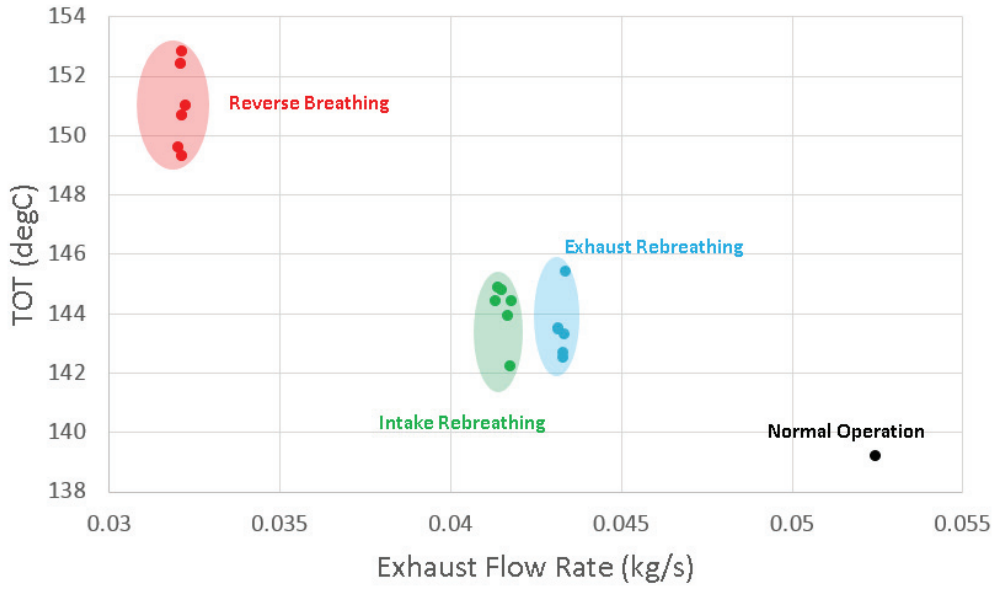

Figure 5.16. GT Power simulation results of TOT vs Exhaust Flow Rate trade off for for exhaust/intake rebreathing and fired reverse breathing. Simulations show a marginal improvement of TOT with a decrease in exhaust mass flow.

Figures 5.15 and 5.16 compare single-cylinder ERB, IRB and FRB to the normal operation (with zero EGR). All these three modes have lower NOx levels when compared to normal operation due to increased in-cylinder dilution. As shown, IRB appears to be preferable to ERB because of the lower NOx production levels with similar TOT. However, ERB was implemented first on the engine and after extensive code modifications, IRB was implemented on the engine. Experimental results for IRB are discussed in the next chapter where comparison of these strategies with other VVA strategies is made.

5.4 Experimental Results

This section shows the initial experimental screening results of FRB, NFRB and ERB strategies at Idle condition. This section is subdivided into the following three sections:

1. Screening with fixed input levers (SOI, rail pressure, VGT and EGR position) to understand the fuel efficiency and TOT impact of FRB, NFRB and ERB strategies,

2. Screening of different cylinder combinations of FRB and

3. PM reduction strategy for reverse breathing.

5.4.1 Screening with Fixed Input Levers

The focus of this study was to explore the fuel efficiency potential of these strategies. The EGR valve is completely closed and the VGT is fixed at 94% closed for the various strategies. This might not be optimal but it is chosen for preliminary examination of these strategies. The SOI and rail pressure is kept the same as stock operation (*6 cyl best BSFC*).

Figure 5.17 shows the normalized BSFC vs BSNOx trade-off for the initial screening of ERB, FRB and NFRB cylinders when compared with *6 cyl best BSFC* strategy.

Single-cylinder ERB (*ERB cyl 1*) and two-cylinder ERB (*ERB cyl 1,6*) have increased BSFC and BSNOx. The NOx levels are elevated for these two conditions as there is no burnt gases in the intake manifold because the EGR valve is closed. So only the ERB cylinders have burnt gases and the rest of the cylinders are effectively breathing in fresh air (no oxygen dilution), so the overall NOx levels are elevated.

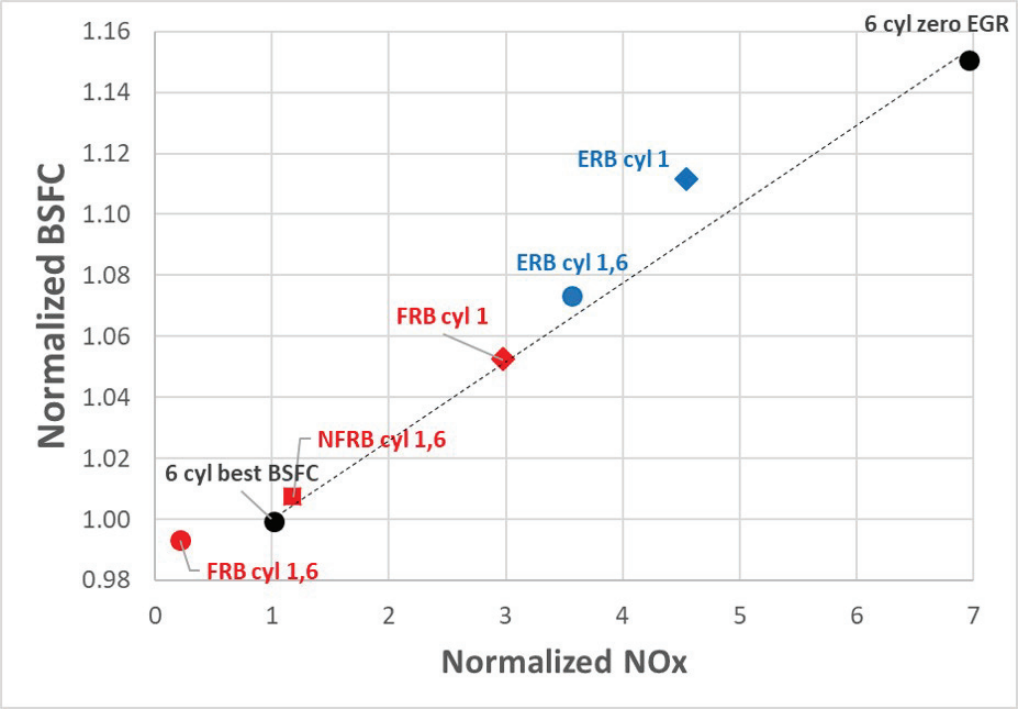

Figure 5.17. Normalized BSFC vs BSNOx trade off for exhaust re-breathing and reverse breathing.

Single-cylinder FRB (FRB cyl 1) has a better BSFC and BSNOx than the ERB cases as seen in Figure 5.17. This is because the FRB cylinder exhausts burnt gases into the intake manifold, which mixes with the incoming fresh air flow leading to oxygen dilution in the intake manifold, which is essential for lower NOx levels in all the cylinders. *Two-cylinder FRB* (FRB cyl 1,6) has better fuel consumption and almost a 5X reduction in NOx, due to higher oxygen dilution via burnt gases exhausted into the intake manifold by the FRB cylinders. This NOx reduction is enabled without

the use of external EGR loop, hence this strategy has potential in engines without external EGR. The AFR is reduced considerably as there are effectively only two cylinders worth of fresh air being breathed in by the engine at this condition which leads to increase in OCE as seen in Figure 5.18. Hence, the overall BTE is increased even though the CCE is slightly lower for *two-cylinder FRB* case when compared to the *6 cyl best BSFC* operation. The CCE decreases due to the elevated intake manifold temperature while in two-cylinder FRB mode.

For the *two-cylinder NFRB* (NFRB cyl 1,6) case, fueling was shut for the reverse breathing cylinders as shown in Figure 5.13. The NOx level increases when compared to *Two-cylinder FRB* because there is less charge dilution in the intake manifold, as there is no combustion happening in the reverse breathing cylinders. However, the NOx level is still comparable to the stock ECM original case. The OCE increases (per Figure 5.18) as there is less air being breathed in by the engine and the CCE increases as there is less heat loss given fewer fired cylinders. However, the mechanical efficiency decreases which leads to a similar BTE as the *6 cyl best BSFC* operation.

Figure 5.19 shows the TOT vs exhaust flow trade-off for the ERB, FRB and NFRB strategies compared with *6 cyl best BSFC* operation. ERB strategies enable about a 20°C increase in TOT while also increasing the exhaust flow. These are ideal during the warm-up mode for AFT thermal management. However, it is not a NOx constrained way to warm-up the AFT system. *FRB cyl 1* also has better TOT and exhaust flow but a higher NOx when compared to ECM original case. *Two-cylinder FRB* has a marginally better TOT but a lower exhaust flow when compared to ECM original case. However, it has a very low NOx value which might be a better during A/T management. *Two-cylinder NFRB* has about 40°C with similar exhaust flow and NOx levels. Hence this strategy would be a good stay-warm strategy for the AFT system.

Figure 5.20 shows the normalized PM vs BSNOx trade-off for the various strategies when compared with *6-cyl best BSFC* operation. The PM for ERB and FRB strategies are higher than *6-cyl best BSFC* operation. This is due to reduced oxygen

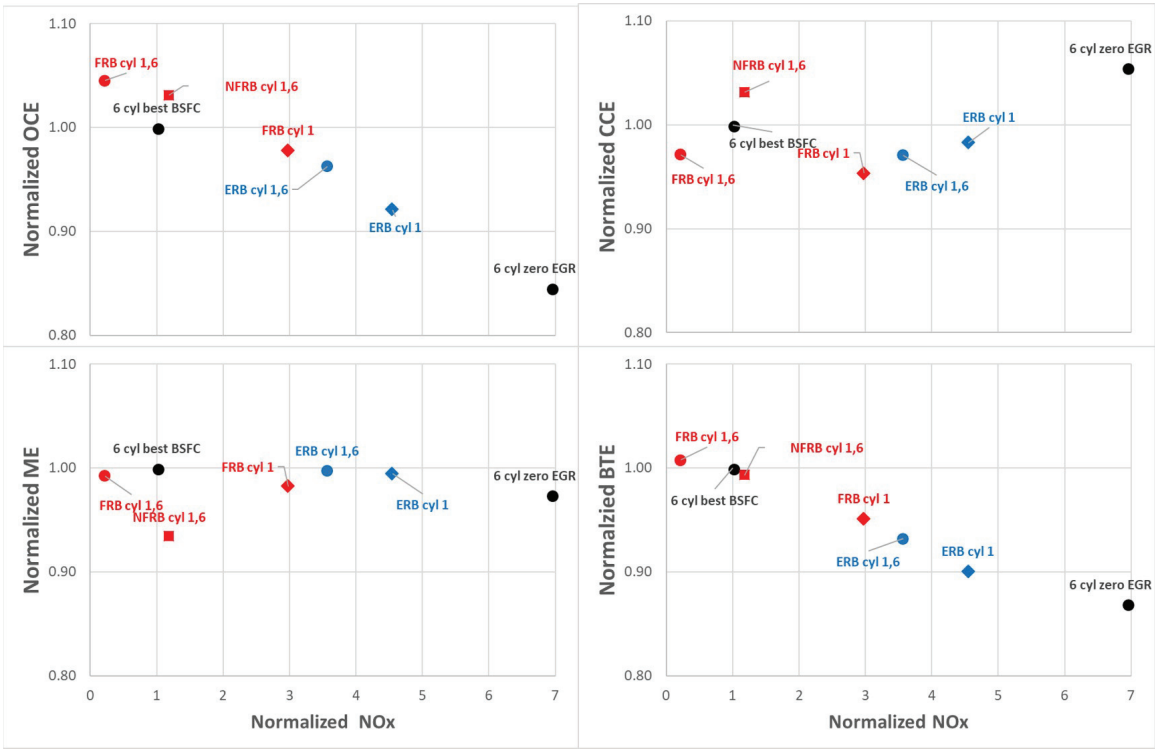

Figure 5.18. Normalized cycle efficiency breakdown for exhaust re-breathing and reverse breathing.

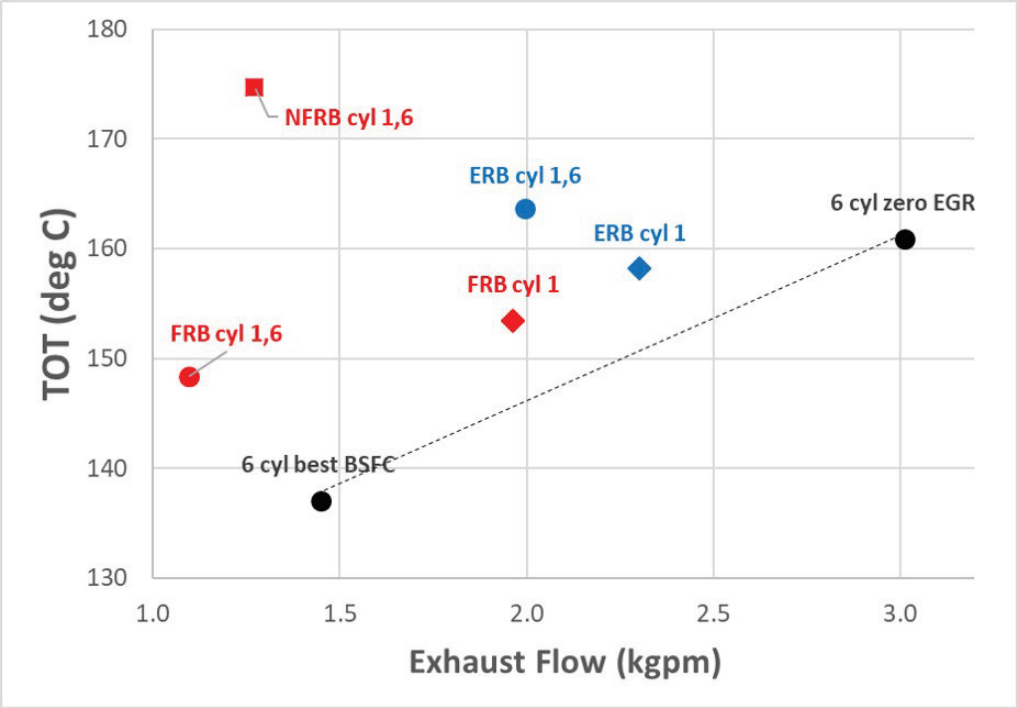

Figure 5.19. TOT vs Exhaust Flow trade off for exhaust rebreathing and reverse breathing.

availability in the cylinders for low PM combustion. The single-cylinder and two-cylinder ERB strategies have about 15X times PM as *6-cyl best BSFC* operation. Since there is less flexibility to control oxygen availability in the exhaust manifold there is less potential for reducing PM for ERB strategies. Without external EGR, there is even less potential for reducing NOx for ERB strategies and hence are not viable strategies for emission controlled engine operation. The PM for reverse breathing strategies, on the other hand, can be potentially lowered via intelligent selection of reverse breathing cylinders along with optimization with conventional levers such as EGR, VGT position, SOI timing and fuel rail pressure. This strategy will be explored in the following section.

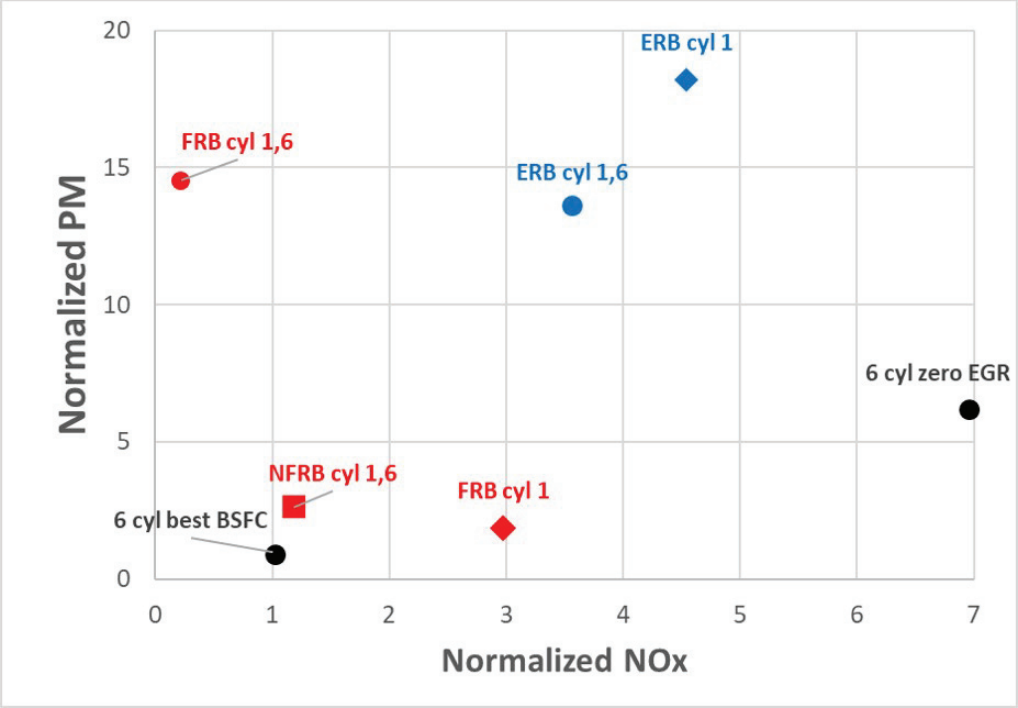

Figure 5.20. Normalized PM vs BSNOx trade off for exhaust re-breathing and reverse breathing.

5.4.2 Screening with Different Cylinder Combinations

This section compares the benefits of FRB with different combination of cylinders. Table 5.1 details the strategies that are compared in this subsection.

Table 5.1. Different combination of FRB modes compared with 6 cylinder operation.

Category	**Strategy**	**VGT Position**	**EGR Position**	**Figure**
-	-	% closed	% open	-
Normal 6-cylinder	6 cyl best BSFC	94	41	5.6
Normal 6-cylinder	63% EGR	94	100	5.6
Normal 6-cylinder	68% EGR	96	100	5.6
Normal 6-cylinder	74% EGR	98	100	5.6
Single-cylinder FRB	Cyl 1 FRB	94	33	5.21(a)
Single-cylinder FRB	Cyl 2 FRB	94	33	5.21(b)
Single-cylinder FRB	Cyl 3 FRB	94	33	5.21(c)
Single-cylinder FRB	Cyl 4 FRB	94	33	5.21(d)
Single-cylinder FRB	Cyl 5 FRB	94	33	5.21(e)
Single-cylinder FRB	Cyl 6 FRB	94	33	5.21(f)
Two-cylinder FRB	Cyl 3,4 FRB	94	0	5.22(a)
Two-cylinder FRB	Cyl 2,5 FRB	94	0	5.22(b)
Two-cylinder FRB	Cyl 1,6 FRB	94	0	5.22(c)

Figure 5.21 illustrates the various single-cylinder FRB strategies and Figure 5.22 illustrates the various two-cylinder FRB strategies compared in this subsection. The *6-cyl best BSFC* strategy has approximately 50% EGR. The EGR fraction was increased even further to explore the potential of external EGR and to give a fair

comparison with FRB. External EGR was enabled for single-cylinder FRB cases, to provide enough oxygen dilution to reduce NOx to *6-cyl best BSFC* levels. For the *two-cylinder FRB* cases, no external EGR was used. SOI and rail pressure was fixed the same as *6-cyl best BSFC* strategy.

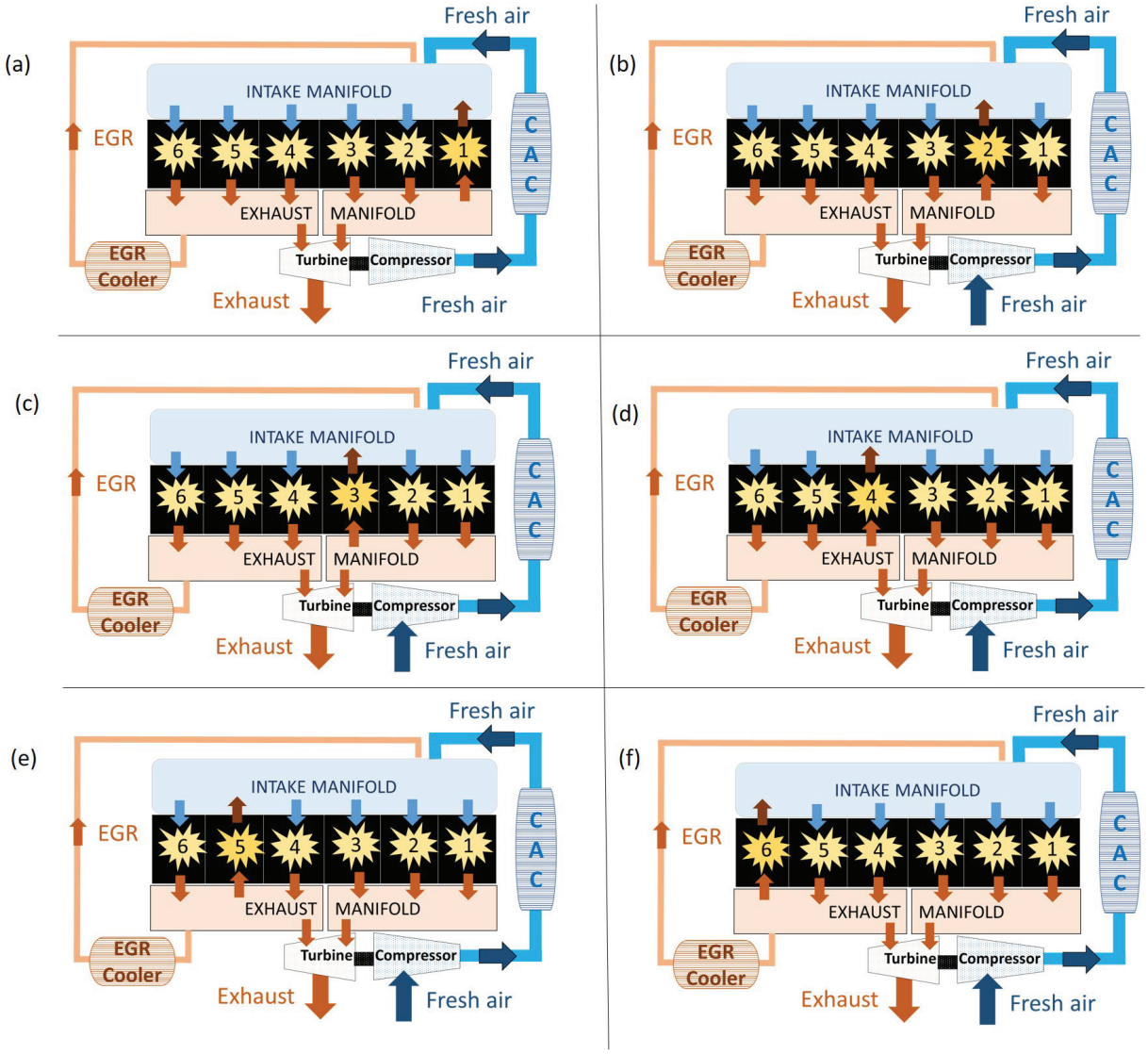

Figure 5.21. Schematic of single cylinder fired reverse breathing in (a) cylinder 1, (b) cylinder 2, (c) cylinder 3, (d) cylinder 4, (e) cylinder 5 and (f) cylinder 6.

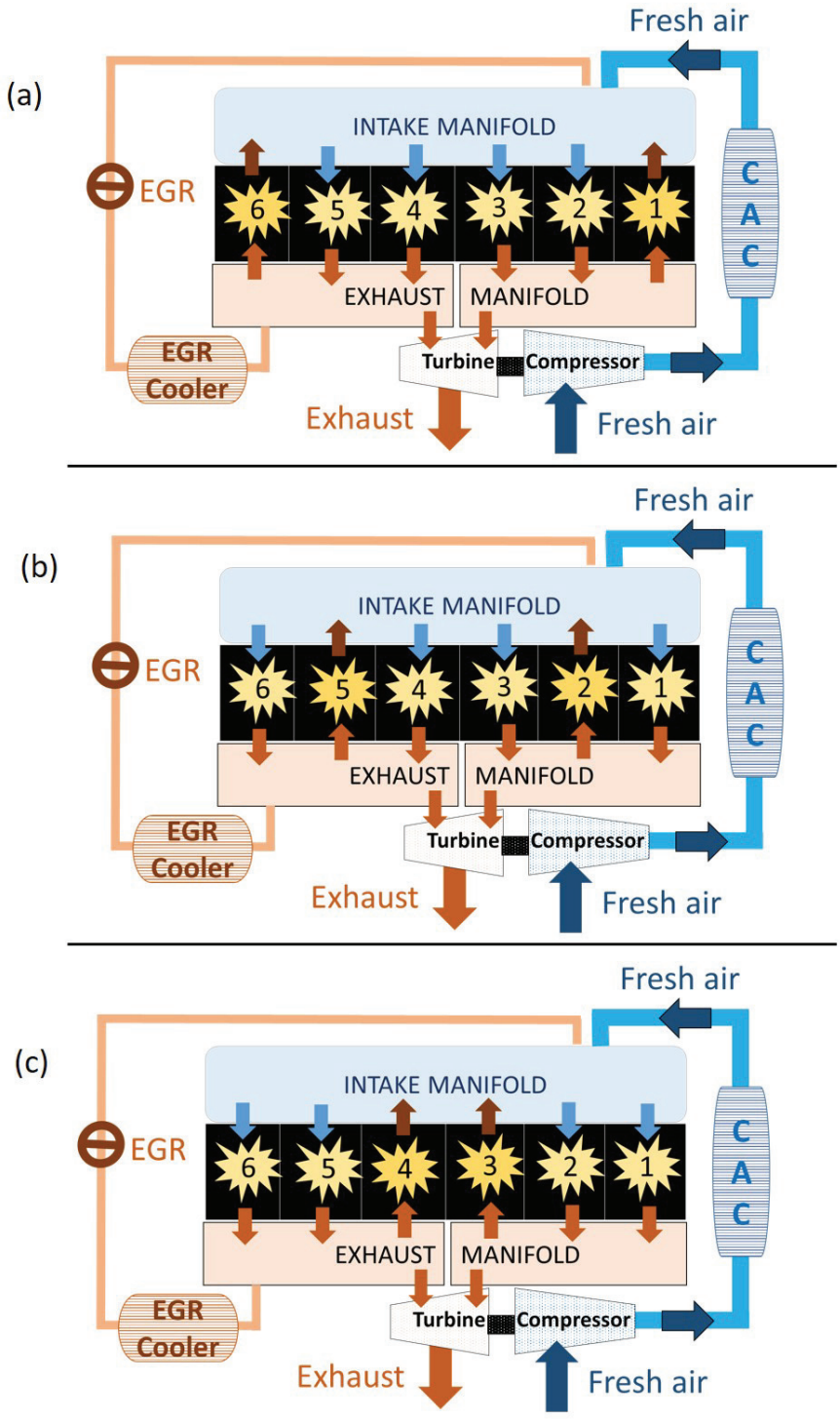

Figure 5.22. Schematic of two-cylinder fired reverse breathing in (a) cylinders 1 and 6, (b) cylinders 2 and 5, (c) cylinders 3 and 4.

Figure 5.23 shows the normalized BSFC vs BSNOx trade-off for the various cylinder combinations of FRB strategies. Single-cylinder FRB strategies use external EGR to enable enough oxygen dilution in intake manifold to reduce NOx levels below *63% EGR* operation. *Two-cylinder FRB* strategies have similar BSFC as compared to *6 cyl best BSFC* strategy. *Single-cylinder FRB* enable about 4-7% BSFC improvement over conventional 6-cylinder operation with external EGR.

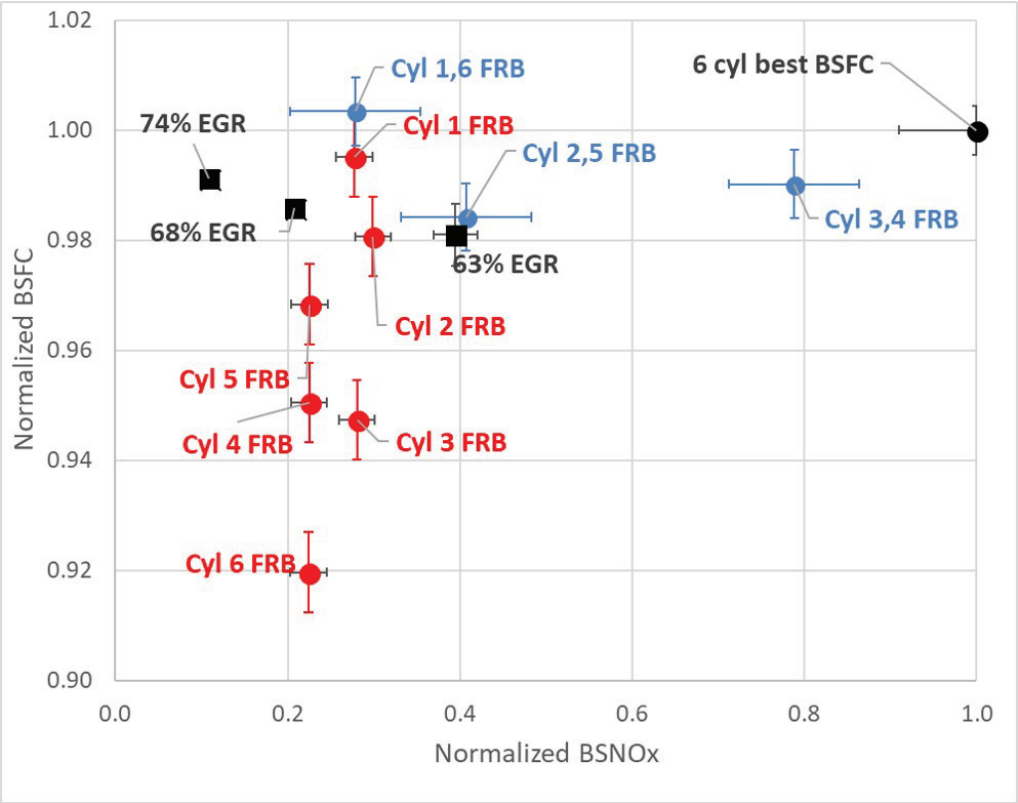

Figure 5.23. Normalized BSFC vs BSNOx trade off for the various cylinder combinations of fired reverse breathing strategies.

Figure 5.24 shows the normalized BSFC vs BSNOx trade-off for the various cylinder combinations of FRB strategies. Certain *two-cylinder FRB* strategies have about 20°C increase in TOT for similar exhaust flow indicating better AFT thermal management potential.

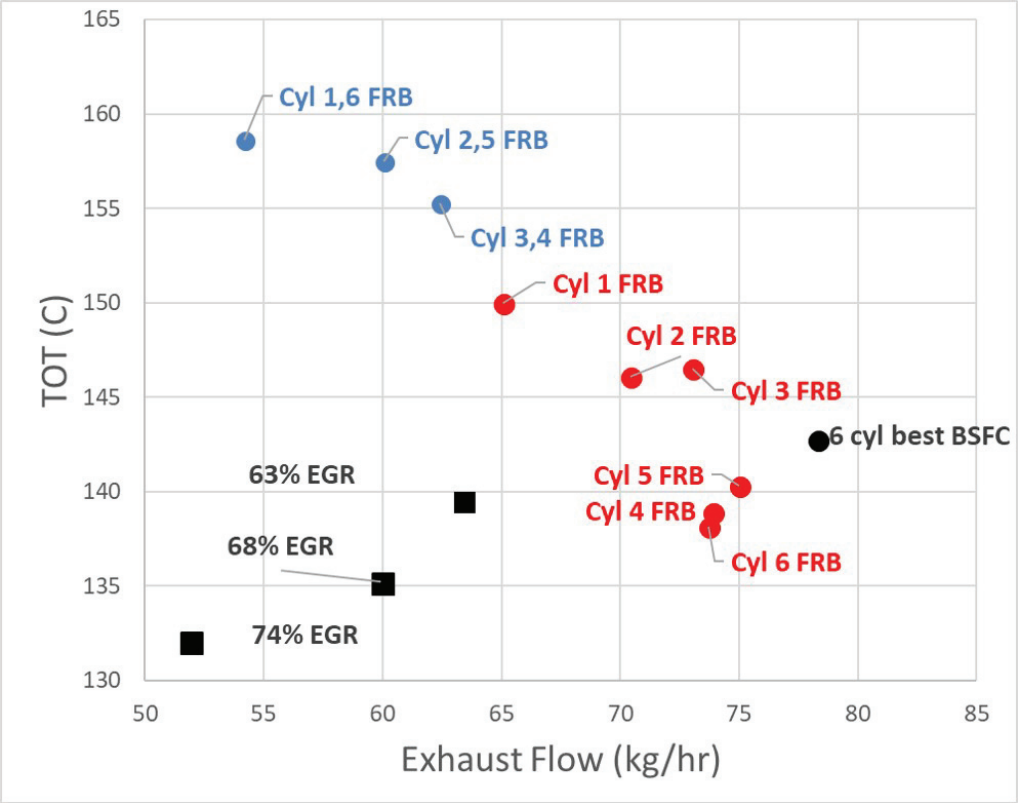

Figure 5.24. TOT vs Exhaust flow trade off for the various cylinder combinations of fired reverse breathing strategies.

Figure 5.25 shows the normalized BSPM vs BSNOx trade-off for the various cylinder combinations of FRB strategies. *Single-cylinder FRB* strategies have about 4-8 times the PM for a similar BSNOx level when compared to conventional operation with external EGR. *Two-cylinder FRB* strategies have about 8-24 times the PM, for a similar BSNOx level when compared to conventional operation with external EGR. However there is potential for reducing the PM by optimizing VGT, EGR, SOI and fuel rail pressure for each strategy. The next section explores this potential of PM reduction for *single-cylinder FRB* strategy.

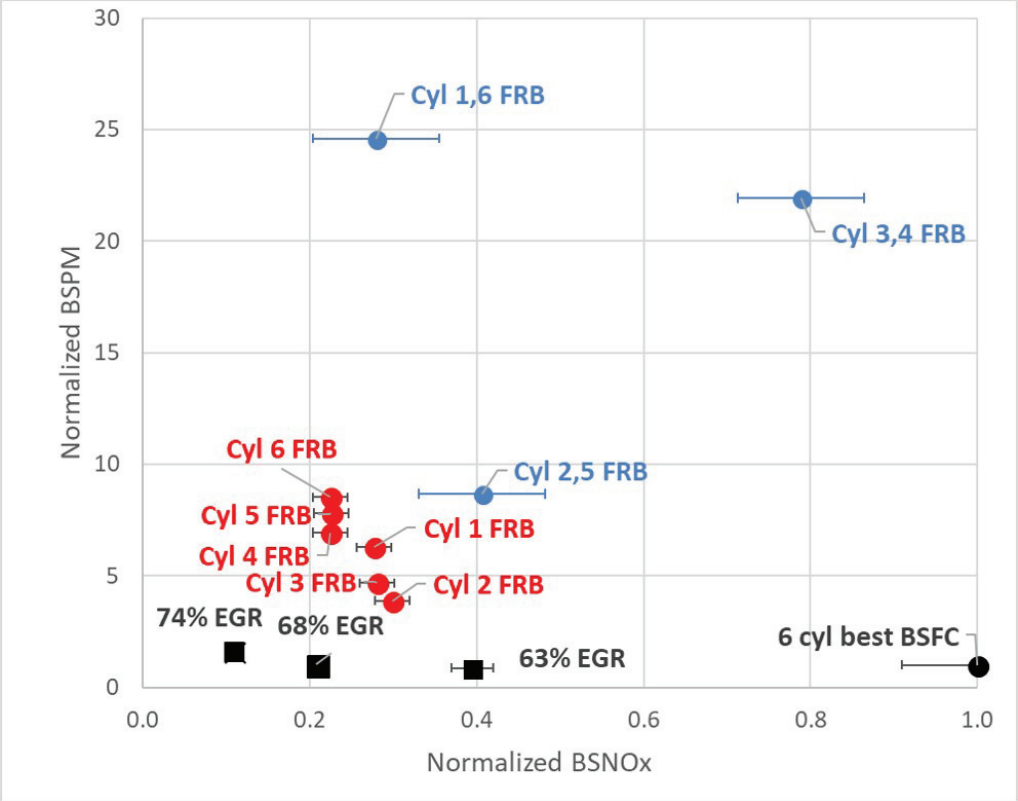

Figure 5.25. Normalized BSPM vs BSNOx trade off for the various cylinder combinations of fired reverse breathing strategies.

5.4.3 PM Reduction Strategy for Reverse Breathing

For this study, *cylinder 2 FRB* which has about 5 times the PM level for similar BSNOx level as compared to *6 cyl best BSFC* was chosen. The SOI, rail pressure, VGT and EGR position were modulated to reduce the PM level to conventional operation levels for this strategy as shown in Figure 5.26. The heat release rates for the *2 cyl FRB* strategy is delayed which is the primary reason for high PM level. By advancing the SOI for the FRB cylinder and increasing the fuel rail pressure the PM levels are decreased. This along with opening up the VGT enables an even lower PM level.

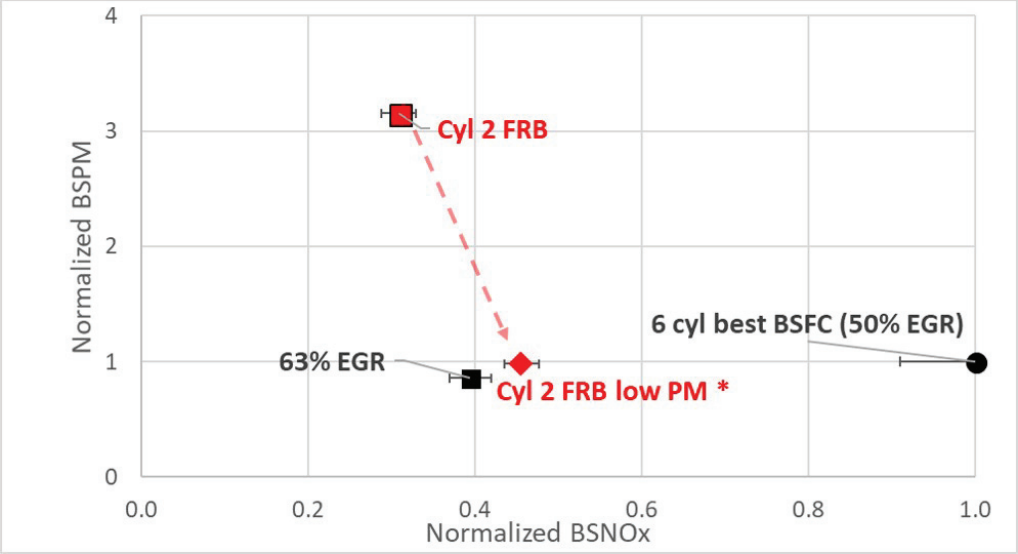

Figure 5.26. Normalized BSPM vs BSNOx trade off for cylinder 2 fired reverse breathing strategy.

Figure 5.27 shows the normalized BSFC vs BSNOx trade-off for the new strategy compared with the old *cyl 2 FRB* strategy. The new strategy yields lower BSFC for similar BSNOx levels.

The primary drivers for decrease in BSFC is via an increase in CCE and OCE as shown in Figure 5.28. CCE is increased as the SOI is advanced which leads to the

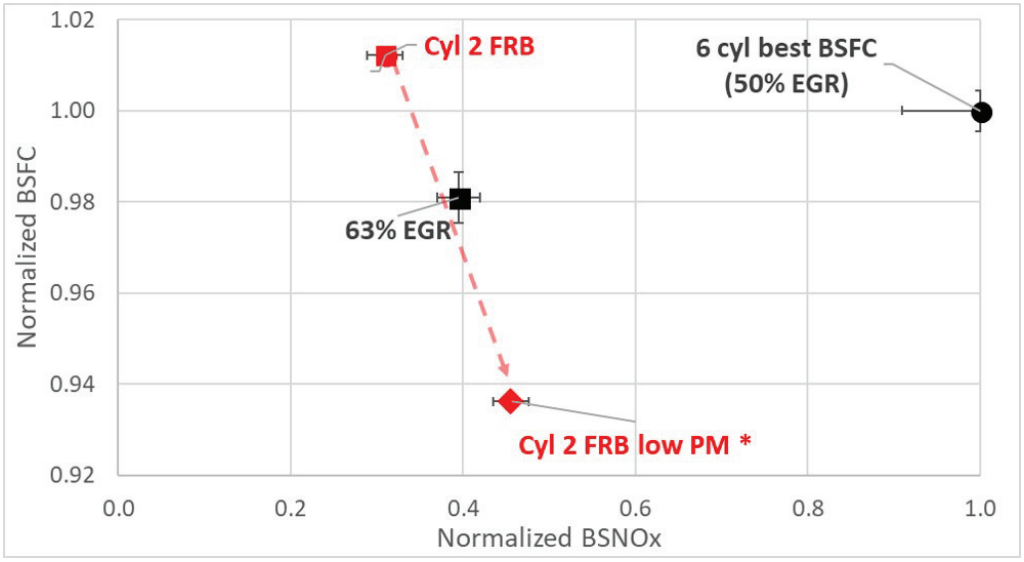

Figure 5.27. Normalized BSFC vs BSNOx trade off for cylinder 2 fired reverse breathing strategy.

centroid of heat release closer to TDC. OCE is increased as the VGT is more open, which leads to lowering of pumping work.

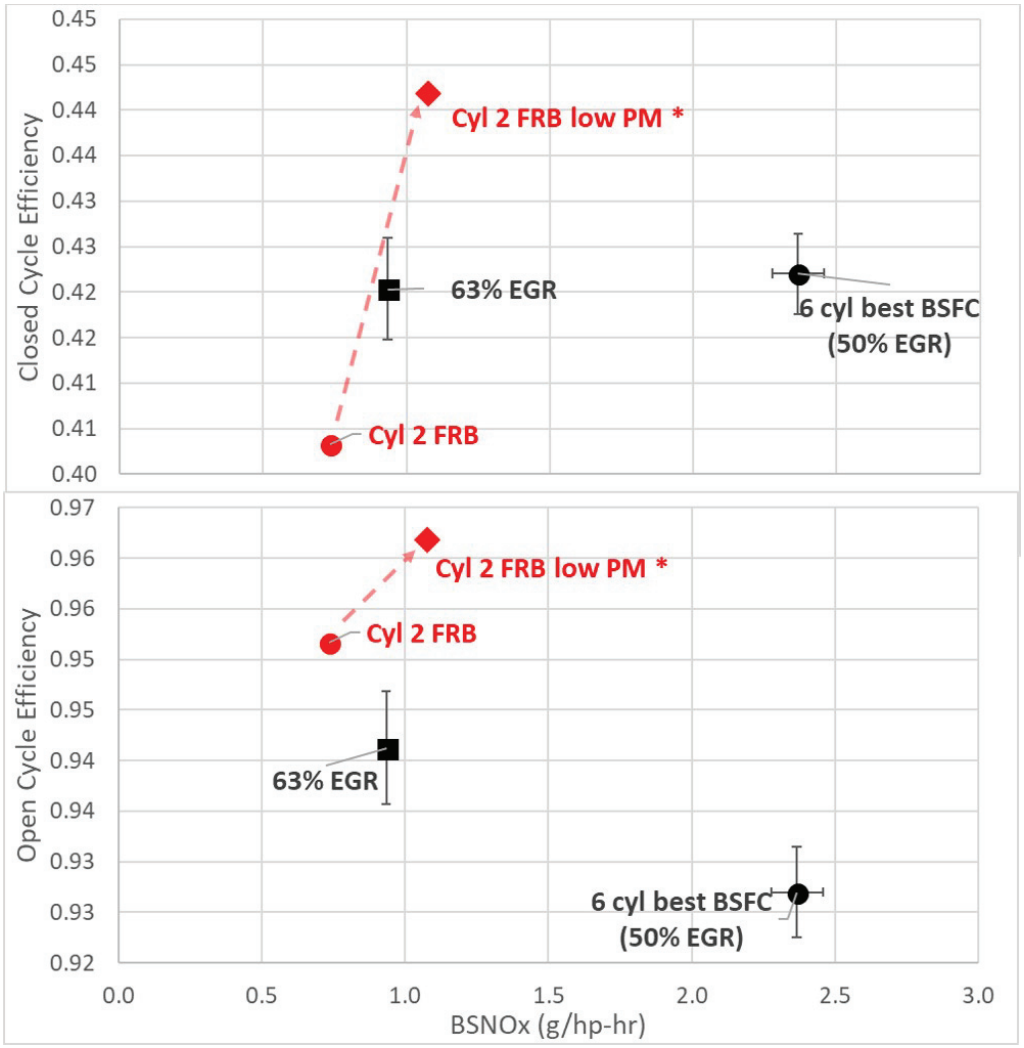

Figure 5.28. CCE and OCE vs BSNOx trade off for cylinder 2 fired reverse breathing strategy.

Figure 5.29 shows that the TOT and exhaust flow for both the new strategy and the old *cyl 2 FRB* strategy are similar.

This modulation recipe can be used for any reverse breathing strategy to lower PM levels without compromising TOT/fuel consumption. Hence this strategy is used

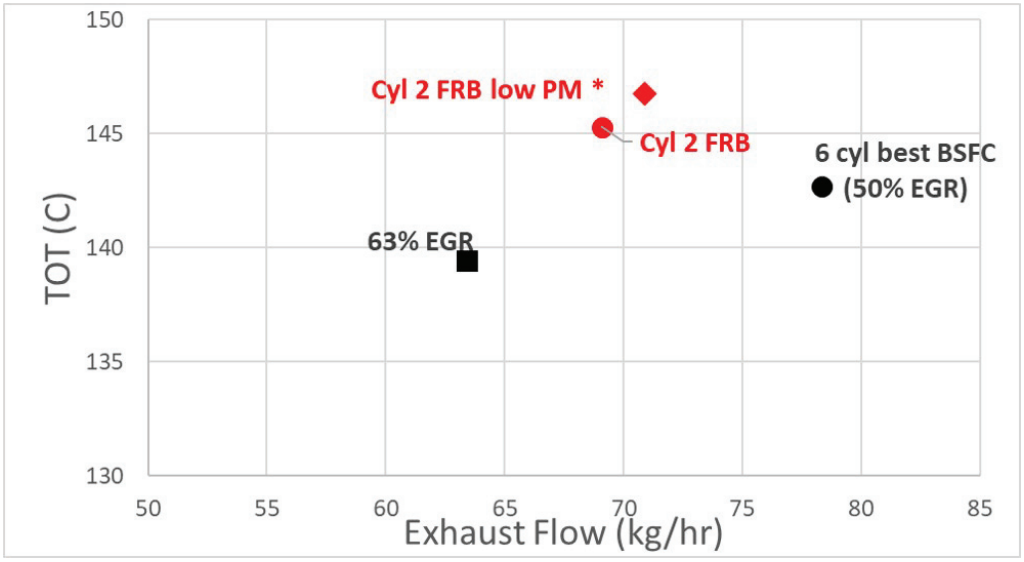

Figure 5.29. TOT vs Exhaust Flow trade off for cylinder 2 fired reverse breathing strategy.

for optimizing the various reverse breathing strategies while comparing against other VVA strategies in the following chapter.

5.5 Summary

This chapter introduces several novel strategies such as FRB, NFRB, IRB and ERB and discusses their potential for enabling better fuel economy and AFT thermal management at Idle. The chapter gives initial screening data from both GT power simulation and experimental testing. The EGR valve was closed and the VGT valve was fixed at 94 % closed for this initial study. This experimental data shows a potential for increasing TOT and lowering BSNOx in a fuel efficient way using these strategies as seen in Figures 5.17 and 5.19. *Two cylinder NFRB* was implemented for the first time on the experimental testbed and is demonstrated to give about 40°C improvement in TOT.

ERB strategies enable about a 20°C increase in TOT while also increasing the exhaust flow albeit with higher NOx levels. Since there is less flexibility to control oxygen availability in the exhaust manifold there is less potential for reducing PM for ERB strategies. Without external EGR, there is even less potential for reducing NOx for ERB strategies and hence are not viable strategies for emission controlled engine operation.

Two-cylinder NFRB showed a 5X reduction of BSNOx due to the high re-circulation of burnt gases from exhaust manifold into the intake manifold. However PM levels were higher for the screened reverse breathing cylinders. The PM for reverse breathing strategies can be potentially lowered via intelligent selection of reverse breathing cylinders along with optimization with conventional levers such as EGR, VGT position, SOI timing and fuel rail pressure. This PM reduction strategy is used for all the stay-warm reverse breathing strategies explored in the following chapter.

6. LOW LOAD STAY WARM STRATEGIES

6.1 Motivation

In the previous chapter, the potential for various types of reverse breathing modes at idle operation is established. This method of controlling the oxygen dilution in the intake manifold without using external EGR loop enables a fuel efficient way to reduce AFR as a means to increase TOT, decrease pumping work, and decrease exhaust flow - each of which is consistent with fuel efficient temperature maintenance of AFT system temperature. Other VVA methods for improving AFT thermal management by means of increased diesel engine exhaust temperatures also have been demonstrated [17–23, 26, 29]. The impact of advanced valve-train strategies on AFT thermal management can be assessed by evaluating strategies during operation in standardized test procedures, including the HDFTP. Figure 6.1 shows the speed and brake mean effective pressure (BMEP) profile through time for the HDFTP cycle for a modern diesel engine. The engine operates at the loaded idle operation for about 40% of the time during the HDFTP. TOT and exhaust flow rates during this condition therefore have a significant impact on the ability of the engine to warm-up, maintain, or cool the AF components. Figure 5.1 maps the HDFTP cycle to 8 steady-state operating conditions and the number displayed next to each bubble signifies the percentage of fuel consumed at these operating conditions. As shown, approximately 5.8% of the fuel is consumed near the loaded idle operating point.

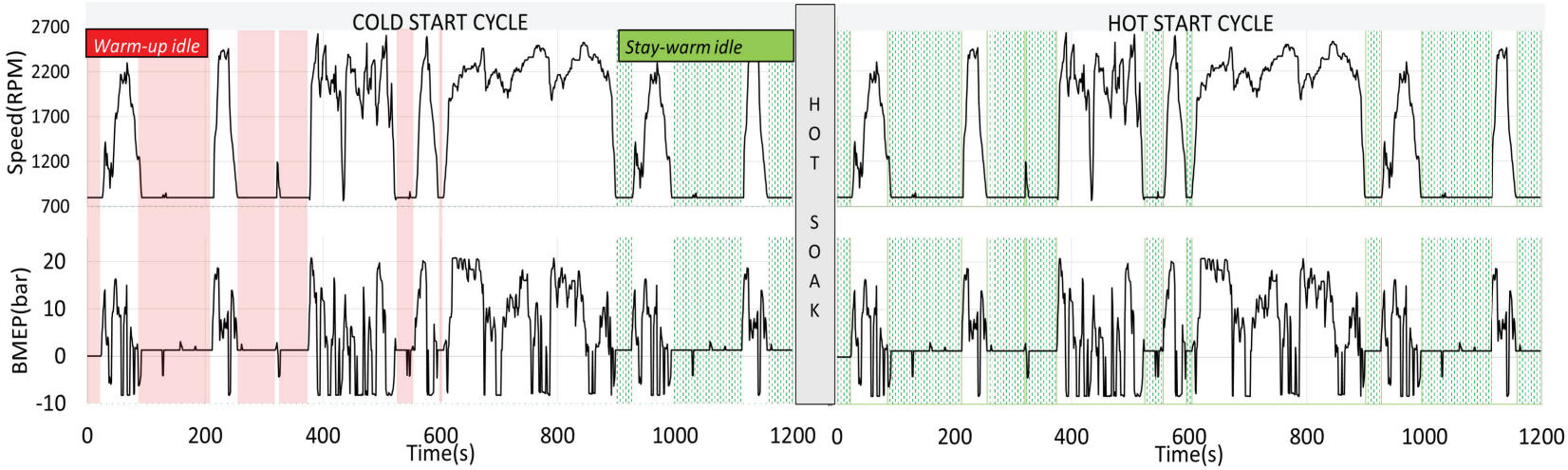

Figure 6.1. Speed and torque profiles for the HD-FTP show that about 40% of the HD-FTP operation occurs at idle conditions. Shaded areas highlight the idle (800 RPM/1.3 bar) sections.

Previous research has demonstrated that CDA is a fuel efficient method for maintaining elevated A/T component temperatures during idle operation [23,29]. Mrunal et al. [29] implemented CDA during idle over the HD-FTP to achieve a 3.4% fuel savings without sacrificing AFT system performance. IVC modulation has also been demonstrated as a fuel efficient method to increase TOT [22,26,51,52], also demonstrated in chapters 2 and 3. Negative valve overlap (NVO) as a way to provide internal EGR has also shown to improve the AFT warm up performance in diesel engines [23,54]. Internal EGR via exhaust re-induction has also been shown as way to increase the TOT of the engine at highway cruise operating condition [55]. Several studies have compared the benefits of NVO and exhaust reinduction strategies in gasoline engines at low-load operating conditions [56–58].

This chapter compares the stay-warm AFT thermal performance of FRB, NFRB and IRB, with conventional warm strategies and other VVA strategies, such as CDA, internal EGR and IVC modulation, at 800 RPM/ 1.3 bar BMEP. 3-cylinder IRB was implemented for the first time on the engine testbed, wherein gases are inducted from and exhausted into the intake in three of the six cylinders. This is achieved by opening the intake valve during the intake stroke and during the exhaust stroke while keeping the exhaust valve shut. The exhausted gases into the intake manifold enable a fuel efficient way without using any external EGR to control oxygen dilution, reduce AFR and increase TOT.

The methodology section describes each of the strategies and the results section illustrates the steady-state and transient HDFTP results for reverse breathing. Experimental results at 1200 RPM/ 1.3 and 2.6 bar BMEP are also discussed to study the impact of these strategies at higher speeds and loads.

6.2 Methodology

Steady-state experiments were performed at 800 RPM, 1.3 bar BMEP to study the fuel economy and AFT thermal management benefits of reverse breathing operation

at the loaded idle operation. Approximately 40% of the time and 5.8% of the fuel is consumed, during HDFTP, at the operating point. All experimental data shown and discussed in the following sections are subjected to strict mechanical constraints shown in Table 6.1.

Table 6.1. Mechanical constraints of CDA transient study.

Mechanical Parameter	**Unit**	**Limit**
Turbine Inlet Temperature	° C	760
Compressor Outlet Temperature	° C	230
Turbo Speed	kRPM	193
Peak Cylinder Pressure	bar	172
Exhaust Manifold Pressure	kPa	500
In-cylinder Pressure Rise Rate	bar/ms	100

6.2.1 Strategy Description

This section outlines the strategies compared for effective AFT stay-warm operation at idle operating conditions.

Conventional 6-Cylinder Operation

Figure 5.6 illustrates the gas exchange during conventional six-cylinder operation. Three six-cylinder strategies are used in this study as baseline comparisons as described below.

1. *6-Cyl Best BSFC* - Conventional six-cylinder engine operation targeting best BSFC via implementation of fuel-efficient injection profiles is characterized by low TOT and exhaust flow rate, both inconsistent with AFT warm-up or stay-warm operation. This mode is included here as a baseline to demonstrate the

fuel consumption increases typically required in conventional engine systems in order to increase and maintain desirable AFT temperatures for current tailpipe emissions compliance.

2. *6-Cyl Warm-up* - Conventional six-cylinder engine operation focusing on increasing AFT temperatures via implementation of a maximally closed VGT nozzle position and four late injections (which result in a fuel-inefficient delayed heat release) to increase TOT and exhaust flow rate for accelerated AFT warm-up, albeit at the expense of increased fuel consumption.

3. *6-Cyl Stay Warm* - Conventional six-cylinder engine operation with focus on maintaining elevated A/T temperatures while being as fuel efficient as possible. Similar to "6-cyl warm up" mode, this strategy implements the fuel-inefficient delayed heat release to maintain elevated TOT for A/T stay warm operation, and incorporates a less closed VGT nozzle position to improve fuel efficiency (relative to the *6-cyl warm up* mode).

   The valve profiles for the six-cylinder strategies described above are shown in Figure 6.4(a).

Internal EGR

Six-cylinder operation with internal EGR and with focus on maintaining elevated AFT temperatures while being as fuel efficient as possible is explored. Two types of Internal EGR strategies are compared with other strategies. The EGR valve is closed for both the internal EGR strategies. Figure 6.4(e) illustrates the valve profiles of Negative valve overlap strategy. The Negative valve overlap (NVO) enables exhaust gases to be trapped in the cylinders thereby providing in-cylinder dilution to reduce NOx and reduction of airflow to increase TOT. Figure 6.4(f) illustrates the valve profiles of exhaust reinduction wherein the exhaust valve is opened again during the

intake stroke. Reinducting exhaust gases into the cylinder is another way to increase in-cylinder dilution to reduce NOx and reduction of airflow to increase TOT.

IVC Modulation

Six-cylinder operation with IVC modulation and with focus on maintaining elevated AFT temperatures while being as fuel efficient as possible, is also explored. Late IVC and early IVC is studied and the valve profiles for these strategies are shown in Figure 6.4(b) and (d) respectively.

Cylinder Deactivation

CDA is a strategy where the valves and fuel are deactivated for a certain number of cylinders. Two versions of CDA are explored in this study. Three-cylinder engine operation with focus on fuel efficient AFT temperature maintenance and is referred as *3-Cyl stay warm* in this study. Figure 6.2 illustrates the gas exchange during three-cylinder operation wherein both valve motion and fuel injection are deactivated for cylinders 4, 5 and 6.

The valve profiles in the deactivated cylinders are illustrated in Figure 6.4 (c). Deactivation of cylinders decreases airflow which leads to increased TOT (via reduced air-to-fuel ratio) and lower exhaust flow in a fuel efficient manner (via lower pumping work), enabling fuel savings when compared to six cylinder operation.

The TOT can be increased by deactivating an additional cylinder. Two cylinder engine operation with focus on fuel efficient A/T temperature maintenance and is referred as *2-Cyl stay warm* in this study. Figure 6.3 illustrates the gas exchange during two cylinder operation wherein both valve motion and fuel injection is deactivated for cylinders 1,2,5 and 6. Cylinders 3 and 4 are chosen as active cylinders to reduce the heat loss to the cylinder wall.

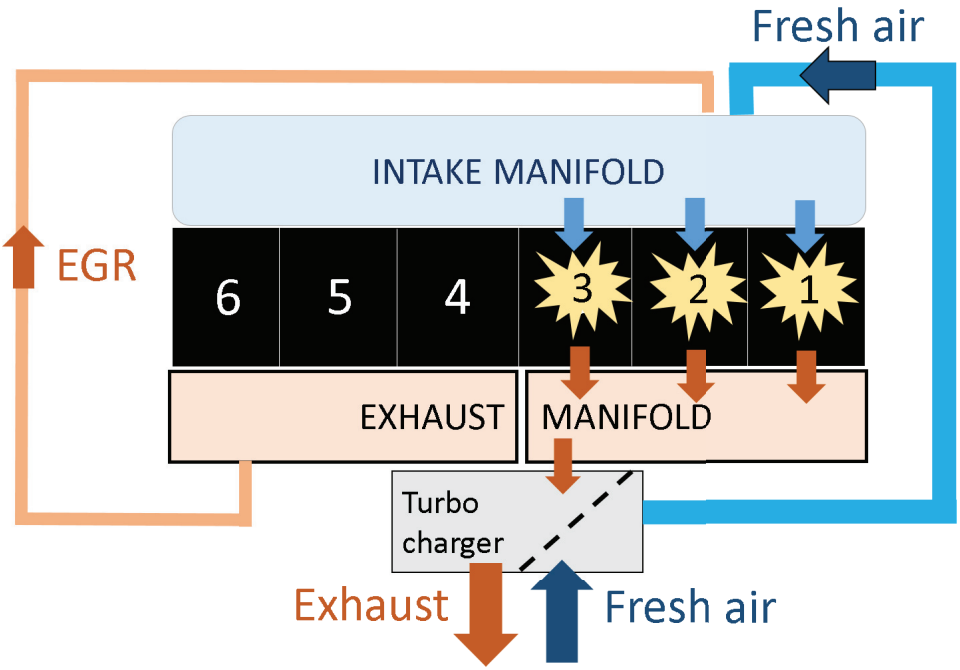

Figure 6.2. 3-cylinder CDA operation.

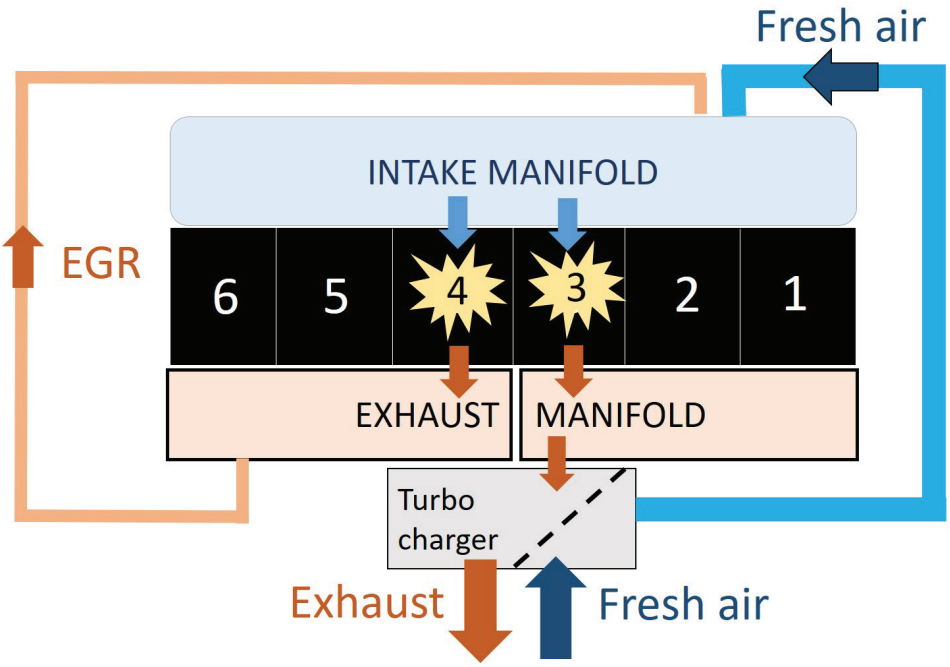

Figure 6.3. 2-cylinder CDA operation.

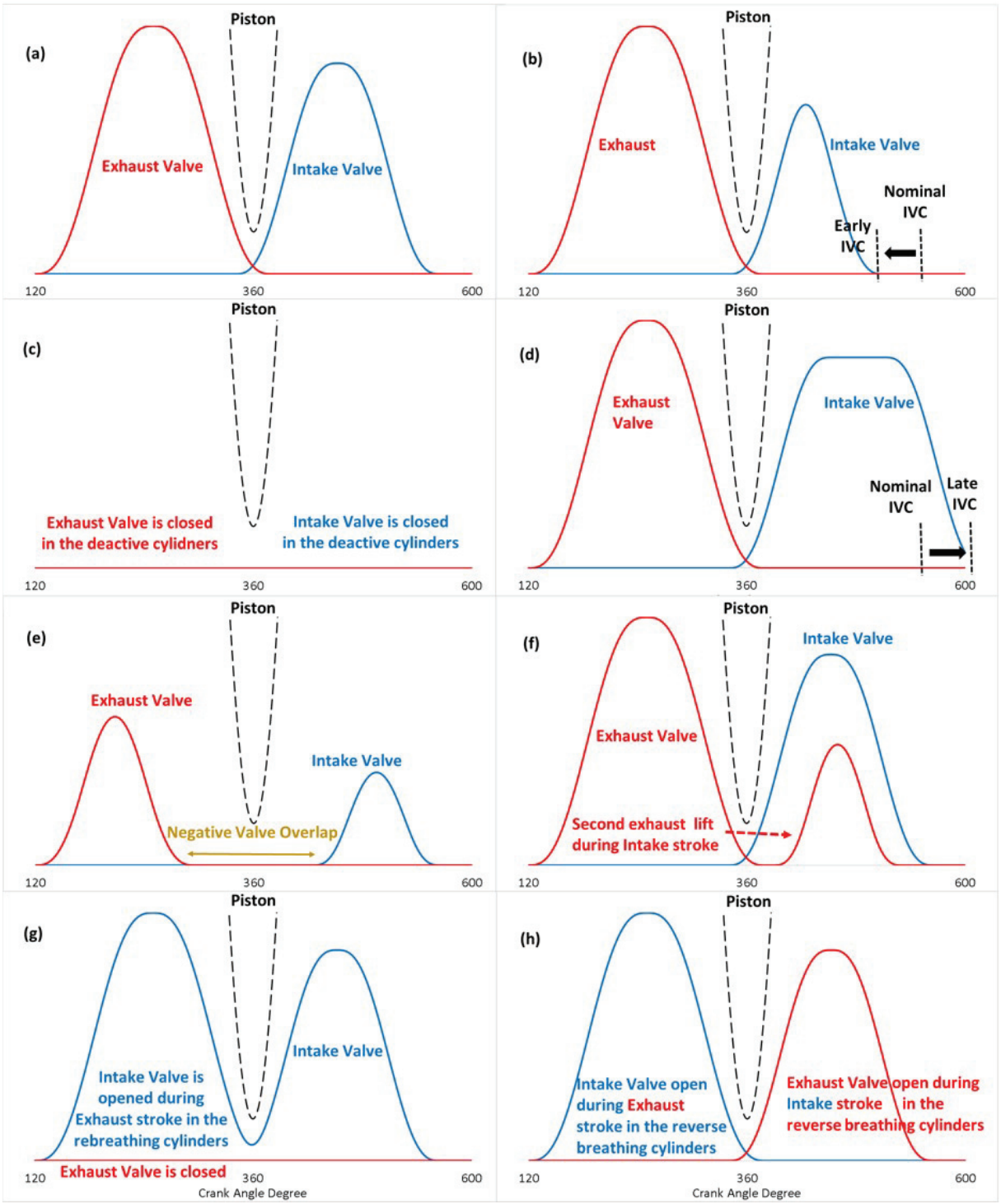

Figure 6.4. Valve profiles (a) conventional operation, (b) Early IVC Operation, (c) CDA, (d) Late IVC Operation , (e) Internal EGR via NVO, (f) Internal EGR via reinduction (g) Intake rebreathing and (f) Reverse breathing.

Fired Reverse Breathing (FRB)

Figure 5.11 illustrates single-cylinder fired reverse breathing engine operation (referred to as *1-cyl FRB*. Five of the six cylinders operate in conventional manner, whereas the reverse breathing cylinder (cylinder 1) inducts charge from the exhaust manifold, injects fuel for combustion and exhausts into the intake manifold. The external EGR valve is closed in this configuration. The valve profiles for the reverse breathing cylinder are shown in Figure 6.4(h). In order to flow enough burnt gases into the intake manifold, the VGT is squeezed more causing a higher delta pressure between the exhaust and intake manifold which leads to a higher mass flow between the manifolds via the cylinder.

The air flow and AFR can further be reduced and TOT increased by reverse breathing in two cylinders (referred to as *2-cyl FRB*) as shown in Figure 5.12, leading to higher levels of oxygen dilution in the intake manifold, resulting in lower NOx levels and exhaust flow. Additionally, the fuel injection timing for reverse breathing cylinders and fuel injection rail pressure for all cylinders was tuned to limit NOx, PM levels for reverse breathing strategies below the conventional 6-cylinder strategy levels.

Non-Fired Reverse Breathing (NFRB)

Figure 5.13 illustrates NFRB operation in two (cylinders 1 and 6) of the six cylinders in the engine (referred to as *2-cyl NFRB*). Fuel injection is deactivated in the NFRB cylinders while the exhaust valve opens during intake stroke and intake valve opens during exhaust stroke. The valve profiles for the reverse breathing cylinder is shown in Figure 6.4(h).

Additional AFR reductions are possible during reverse breathing in one, or more cylinders, by partially closing the VGT to increase exhaust manifold pressures which drive gas into the reverse breathing cylinders. Volumetric efficiency reduction via IVC

modulation is another means to decrease AFR [22] without the pumping penalties that result from partially closing the VGT. *2-cyl NFRB + LIVC* strategy uses LIVC breathing cylinders to further reduce the airflow to increase TOT.

The airflow can further be reduced by reverse breathing in three cylinders (referred to as *3-cyl NFRB*) as shown in Figure 6.5, wherein cylinders 4, 5 and 6 recirculate burnt exhaust gases into the intake manifold. Lower exhaust valve lifts are used during the intake stroke of the reverse breathing cylinders to control the oxygen dilution in the intake manifold, ensuring enough oxygen is present in the intake manifold for stable, low soot combustion in cylinders 1, 2 and 3.

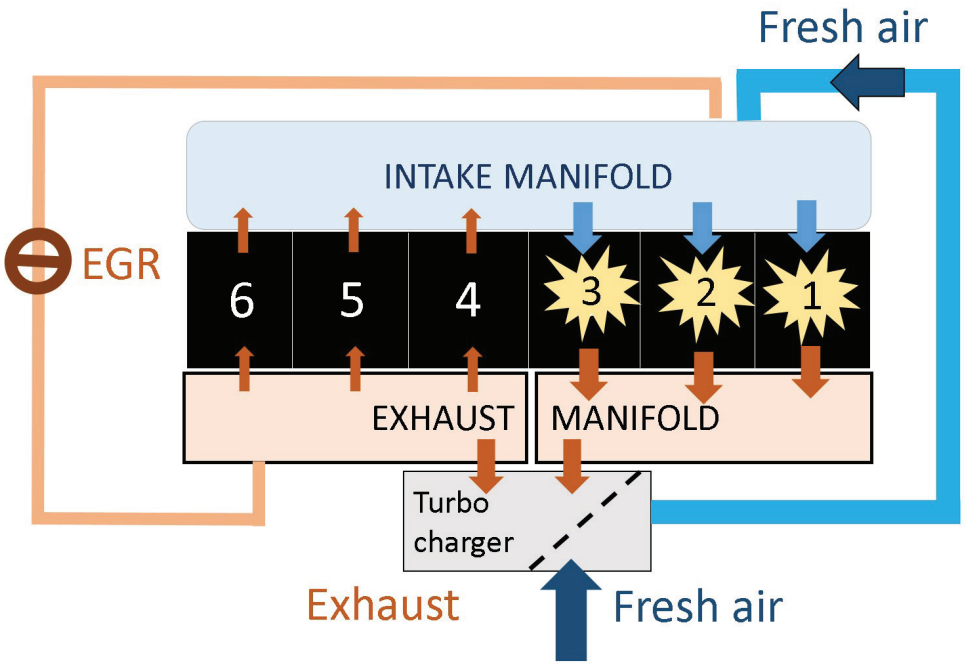

Figure 6.5. 3-cylinder (Cylinder 4,5 and 6) Non-fired reverse breathing. Cylinders 4, 5 and 6 do not have a combustion event, thereby flowing the burnt gases from the exhaust manifold into the intake manifold.

Intake Rebreathing (IRB)

Figure 6.6 illustrates IRB operation in three cylinders wherein cylinders 1,2 and 3 in the engine push the exhaust gases into the intake manifold after combustion. The burnt gases mix together with the fresh air in the intake manifold and are inducted back into the cylinders during the intake stroke. The strategy thus enables reduction of airflow via dilution of oxygen in the intake manifold. The EGR valve is shut during this operation. The valve profiles for the rebreathing cylinders are shown in Figure 6.4(g). Cylinders 1, 2 and 3 were chosen to enable better mixing of the burnt gases with the incoming fresh air flow in the intake manifold. Other combinations of cylinders (4, 5 and 6) had unstable heat release rates due to improper mixing.

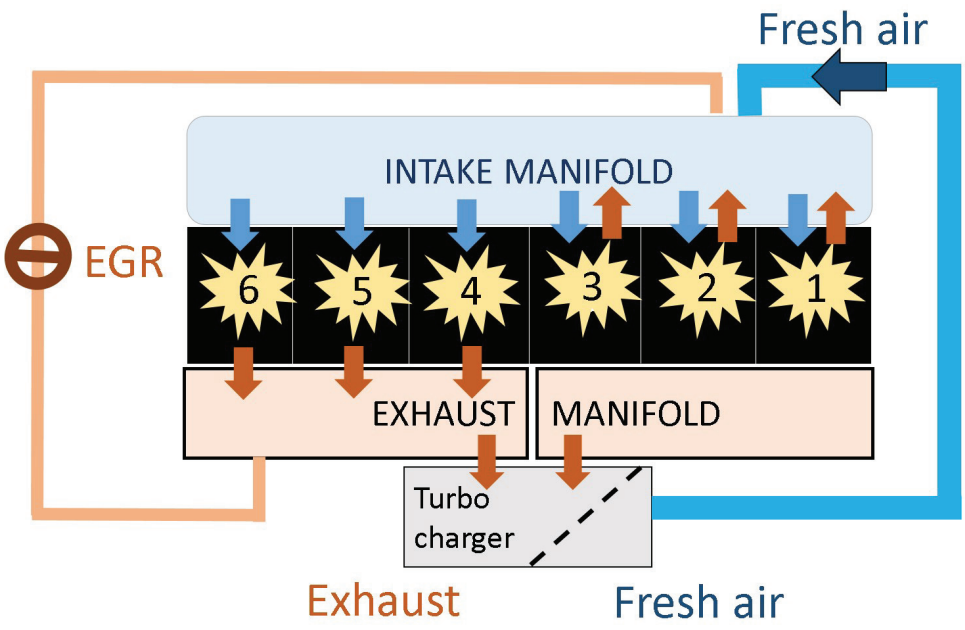

Figure 6.6. 3-cylinder (Cylinder 4,5 and 6) Intake Rebreathing operation. Cylinders 1,2 and 3 push exhaust gases into the intake manifold after combustion.

Table 6.2 gives the semi-optimized inputs for each strategy at 800 RPM/1.3 bar BMEP during stay-warm operation.

Table 6.2. Inputs for various stay-warm strategies (800 RPM/1.3 bar BMEP).

Strategy	**VGT Position**	**EGR Position**	**SOI**	**Rail Pressure**
-	% closed	% open	CAD BTDC	bar
6 cyl best BSFC	94	41	2.1	896
6 cyl warm-up	100	5	-11.4	583
6 cyl stay-warm	98	6	-11.4	600
1 cyl FRB + LIVC	98	0	-11.5	800
2 cyl FRB	72	0	-4.35/-11.5	1050
2 cyl NFRB	97	0	-11.4	600
2 cyl NFRB + LIVC	70	-8.7	-11.5	600
3 cyl NFRB	50	0	-4	1000
iEGR via NVO	66	0	-11.4	900
iEGR via reinduction	94	0	-11	1200
3 cyl IRB	100	0	-11	1600
3 cyl stay warm	79	100	-11.5	600
2 cyl stay warm	67	100	-11.5	600
6 cyl EIVC (510 CAD)	69	26	-10	600
6 cyl LIVC (635 CAD)	69	21	-10	600

The emission levels of conventional *6-cylinder warm-up* operation are set as constraints for the reverse breathing strategies. Engine cycle efficiency analysis is carried out in order to understand the fuel efficiency benefits. The BTE of the engine is the product of the CCE, OCE, and mechanical efficiency (as shown in Equation 6.1).

$$\text{BTE} = \eta_{\text{close cycle}} \times \eta_{\text{open cycle}} \times \eta_{\text{mechanical}} \tag{6.1}$$

6.3 Experimental Results at Idle

Each of the afore-described strategies were tested on the engine at the loaded idle (800 RPM, 1.3 bar BMEP) condition. The first part of the results section compares all reverse breathing with internal EGR strategies and 6-cylinder best BSFC and 6-cylinder warm-up operation. The second part of the results compare *2-cyl NFRB* strategy with CDA and 6-cylinder strategies. The third section compares the transient results when these strategies are run over the HDFTP drivecycle. The last section compares these strategies at 1200 RPM/ 1.3 and 2.6 bar BMEP, to evaluate the impact of these strategies at higher speeds and loads.

Figure 6.7 shows the experimental steady-state results at loaded idle (800 RPM, 1.3 bar BMEP) showing normalized (a) BSFC, (b) OCE, (c) CCE, (d) Mechanical efficiency, (e) exhaust flow and (f) AFR vs TOT for all reverse breathing and internal EGR strategies. The *6-cyl best BSFC* strategy is the baseline for evaluating the fuel efficiency comparisons for the different strategies. The *6-cyl warm up* which is the state of the art AFT thermal management strategy has higher TOT but is less fuel efficient than other strategies due to OCE penalty (as shown in Figure 6.7 (b)) as the *6-cyl warm up* strategy uses over-closed VGT to achieve the high TOT. The *2-cyl NFRB* strategy has a 60 °C higher TOT than *6-cyl best BSFC* strategy with similar fuel consumption as shown in Figure 6.7 (a). The increase in TOT is a result of an AFR reduction (Figure 6.7 (f)) through airflow reduction (via the amount of recirculation of gases through the reverse breathing cylinders). The reduction in airflow also results in reduction in exhaust flow, per Figure 6.7 (e) which is beneficial to keep the AFT warm.

There are two ways of reducing the airflow, one via over-closing the VGT and another via opening the VGT and using LIVC. Opening the VGT and using LIVC

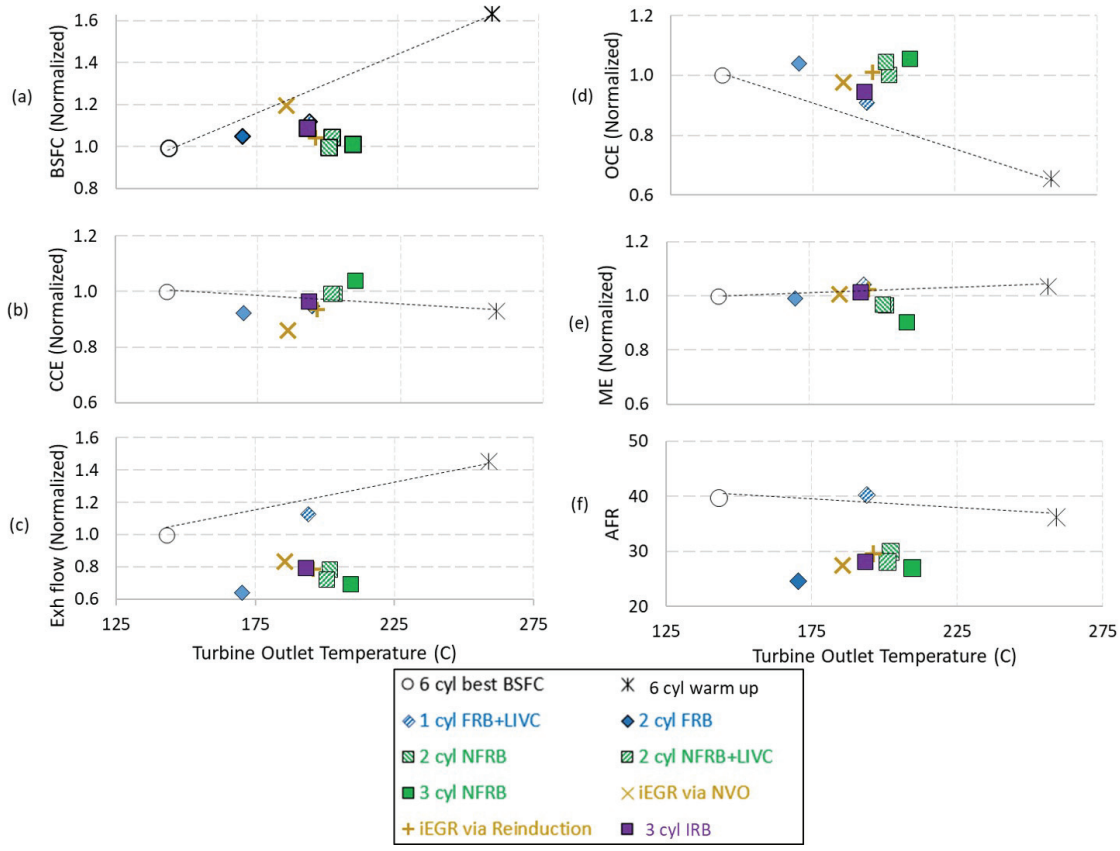

Figure 6.7. Experimental steady-state results at loaded idle (800 RPM, 1.3 bar BMEP) showing normalized (a) BSFC, (b) OCE, (c) CCE, (d) Mechanical efficiency, (e) exhaust flow and (f) AFR w.r.t TOT for all the strategies.

on the normal breathing cylinders is a more efficient process to reduce engine airflow while reverse breathing in one or more cylinders. Conventional *6-cylinder warm up* strategy, has a over-closed VGT configuration to reduce the airflow and achieve certain EGR fraction. Reverse breathing as a strategy can rely on airflow reduction via opening the VGT as no external EGR is used. Hence *2-cyl NFRB + LIVC* is more efficient than *2-cyl NFRB* as shown in Figure 6.7 (a) due to the OCE improvement (as shown in Figure 6.7 (b)) via opening the VGT and using LIVC.

3-cyl NFRB has the highest TOT (210 °C) among all the reverse breathing strategies studied and also has a similar BSFC when compared to *6-cyl best BSFC* strategy due to favorable gas exchange reflecting in the OCE improvement shown in Figure 6.7 (b).

1-cyl FRB + LIVC has a lower BSFC than the *6-cyl best BSFC* strategy primarily due to OCE penalty with this FRB strategy (as shown in Figure 6.7 (b)). The OCE is decreased as the VGT was slightly over closed for this strategy to ensure enough re-circulation of exhaust gases via reverse breathing cylinder to satisfy the emission constraints. TOT is 50 °C higher for *1-cyl FRB + LIVC* strategy when compared to *6-cyl best BSFC* primarily due to the difference in fuel injected in the cylinders. *2-cyl FRB* has about 30 °C increase in TOT with similar fuel consumption compared to *6-cyl best BSFC* as shown in Figure 6.7 (a). Since two cylinders are pushing hot exhaust gases into the intake manifold, the intake manifold temperatures are increased which leads to a decrease in CCE for *2-cyl FRB* compared to *6-cyl best BSFC* strategy. The VGT was completely opened for the *2-cyl FRB* to reduce the amount of recirculation exhaust gases in the intake manifold to maintain the emission constraints.

NFRB strategies have higher TOT, similar BSFC when compared to FRB strategies (as shown in Figure 6.7 (a)) primarily due to increased flexibility to reduce the airflow and manage the recirculation of exhaust gases in the intake manifold in a fuel efficient way at this operating condition.

NVO and *reinduction* are two conventional internal EGR strategies which can be used to reduce AFR via increased in-cylinder oxygen dilution. The external EGR

valve is shut for both these strategies. *NVO* and *reinduction* has similar TOT and exhaust flow as shown in Figure 6.7(e) and therefore similar stay-warm thermal performance. However *NVO* is less efficient than *reinduction* due to a lower OCE as shown in Figure 6.7(a) and (b). The lower OCE is due to a higher pumping work as shown in Figure 6.8. The CCE and ME are similar (as shown in Figure 6.7(b) and (c)) for both the strategies due to the same fuel injection timing.

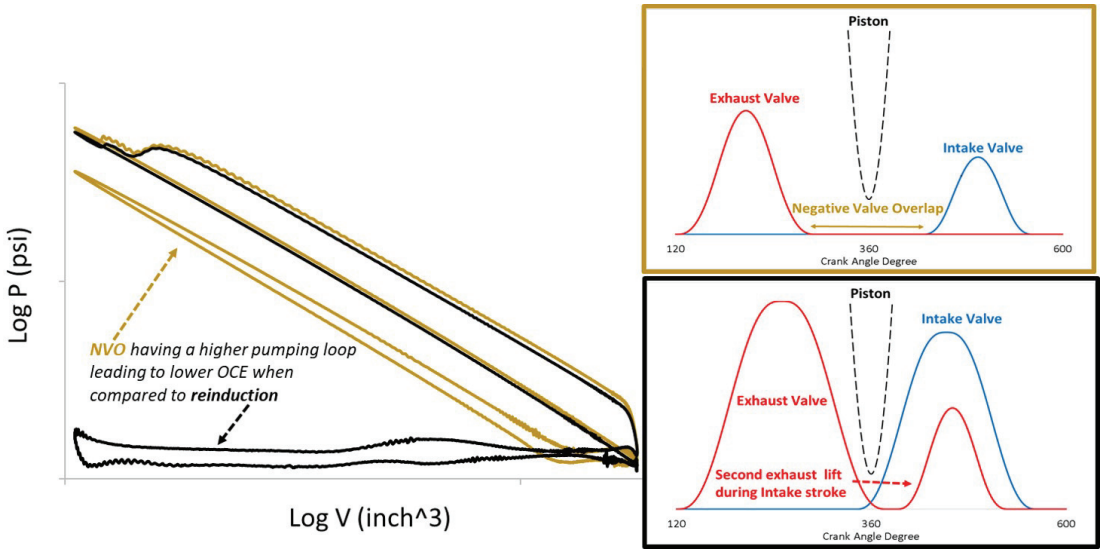

Figure 6.8. Comparison of PV diagram for iEGR via NVO and reinduction illustrating the larger pumping loop for NVO.

Reinduction has similar fuel consumption as *2-cyl NFRB* and similar TOT and exhaust flow as shown in Figure 6.7. From a valve-train perspective, *reinduction* or *NVO* needs to have valve train flexibility in all six cylinders to achieve the required stay-warm performance while *2-cyl NFRB* only requires valve-train flexibility in two of the six cylinders.

3-cyl IRB is a novel intake rebreathing strategy where the airflow can be reduced by rebreathing into the intake manifold, to increase TOT. *3-cyl IRB* has about 5% higher BSFC compared to *2-cyl NFRB* strategies with similar TOT and exhaust flow. Since all the cylinders are firing in the *3 cyl IRB* strategy, it is more balanced when compared to NFRB strategies.

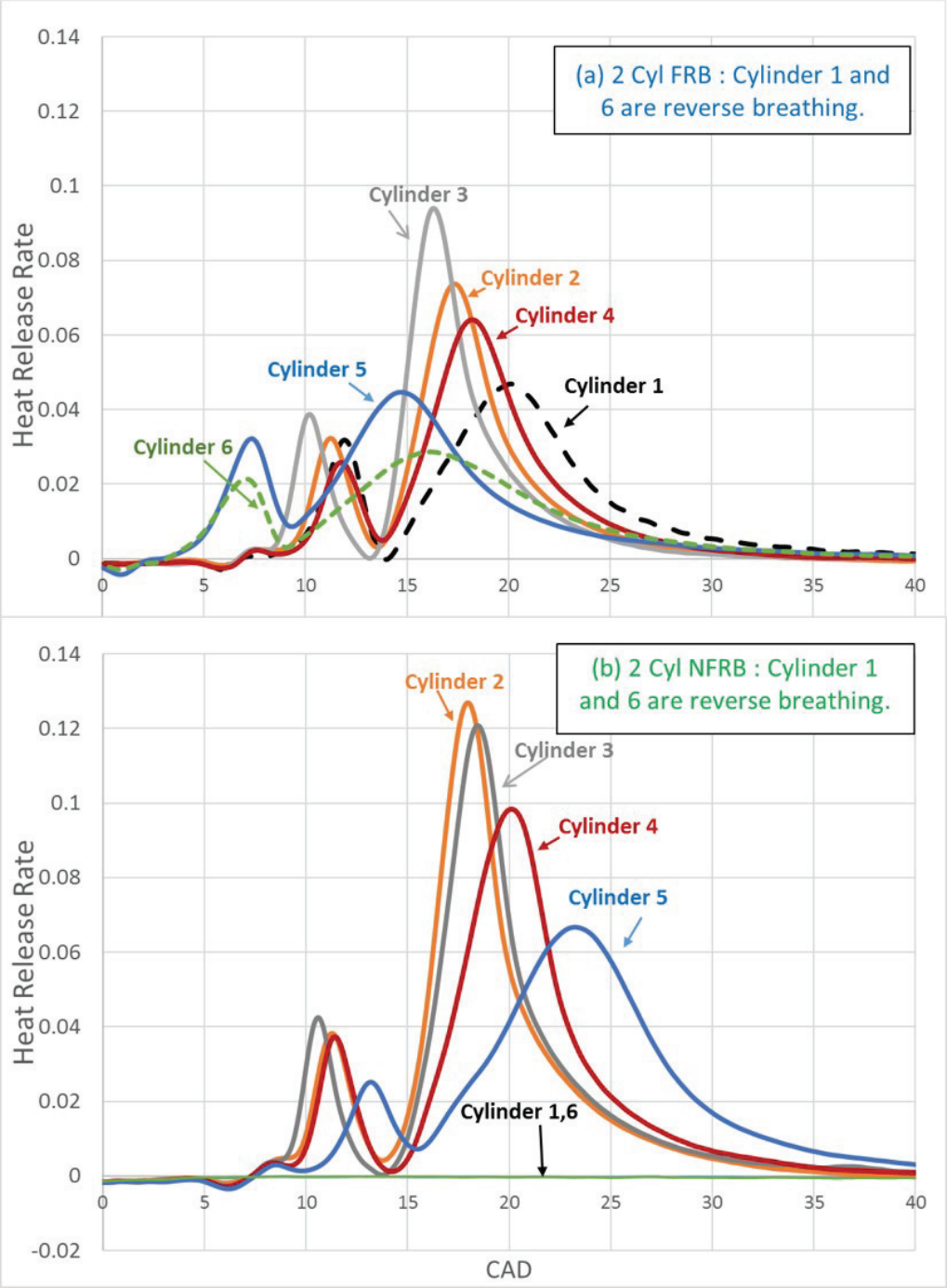

Figure 6.9. In-cylinder heat release rate comparison between (a) *2-cyl FRB* and (b) *2-cyl NFRB* showing the impact of advanced start of injection (SOI) used for *2-cyl FRB* compared to NFRB. For *2-cyl FRB* strategy, the SOI for cylinders 5 and 6 are even more advanced to maintain stable heat release rates in those cylinders. For *2-cyl NFRB*, cylinders 1 and 6 show a flat heat release due as there is no combustion in the respective cylinders.

Figure 6.9 shows the heat release comparison between *2-cyl FRB* and *2-cyl NFRB*. Cylinders 1 and 6 do not have any heat released as they are not firing for *2-cyl NFRB*. *1-Cyl FRB* also allows a 50 °C increase in TOT even though AFR is similar compared with *6-cyl best BSFC* due to delayed injection and no cooling losses in the external EGR path. *2-cyl FRB* leads to a 30 °C increase in TOT for a minor increase in fuel consumption when compared to the *6-cyl best BSFC* strategy and a lower fuel consumption when compared to the *6-cyl warm up* strategy.

Approximate steady-state heat transfer rates to the AFT components are compared for each strategy in order to evaluate the stay-warm capabilities of each of the strategies. The heat transfer rate between the exhaust gas and an AFT catalyst depends on the TOT, exhaust flow rate, and instantaneous catalyst bed temperature. The heat transfer rate between incoming gas into the A/T and the catalyst bed [23], is given by Equation 6.3.

$$\dot{q} = C \times \dot{m}^{4/5} \times (TOT - T_{Catalyst}) \tag{6.2}$$

$\dot{m}$ is the exhaust mass flow rate going through the catalyst, $T_{Catalyst}$ is the temperature of the catalyst, and C is a constant that depends on the geometry and material of the catalyst.

The model yields a predicted heat transfer rate from the exhaust gas to the catalyst for each $T_{Catalyst}$, by using the exhaust mass flow rate and the TOT. A positive heat transfer rate corresponds to catalyst warm-up as heat is transferred from the exhaust gas to the catalyst. Negative heat transfer rate corresponds to catalyst cooling down as the heat is transferred from the catalyst to the exhaust gas. When the AFT is already warm, lower cooling rates are favorable to keep the AFT warm.

The heat transfer rate to the catalyst at different catalyst bed temperatures is compared as shown in Figure 6.10 to evaluate the stay-warm potential for different strategies. The predicted heat transfer rates are normalized using the heat transfer rate of *6-cyl best BSFC* case at a catalyst bed temperature of 0°C. Lower exhaust

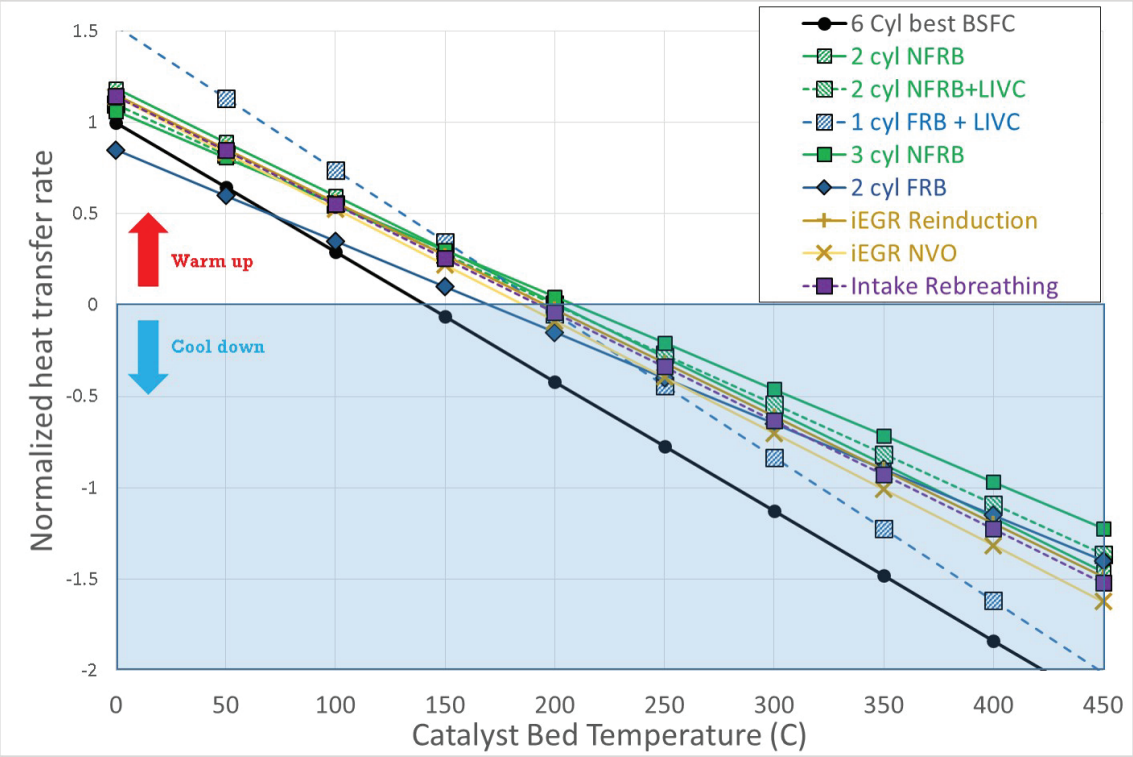

Figure 6.10. Catalyst warm up characteristics at 800 RPM , 1.3 bar BMEP for all reverse breathing strategies. The predicted heat transfer rates are normalized using the heat transfer rate of *6-cyl best BSFC* case at a catalyst bed temperature of 0°C. The *2-cyl NFRB* strategy is preferred given its lower exhaust flow rate, lower fuel consumption and elevated TOT as it cools down the AFT slower than six cylinder strategies. *2-cyl FRB* is preferred when compared to *1-cyl FRB* due to lower heat transfer rate at catalyst bed temperatures greater than 225°C.

flow and a higher TOT are preferred for efficient stay-warm performance. All of the reverse breathing strategies have better heat transfer rates when compared to the stock *6-cyl best BSFC* operation due to higher TOT and lower exhaust flow (Figure 6.7 (e)). *2-cyl NFRB with LIVC* is the preferred strategy due to its lower exhaust flow rate, lower fuel consumption and elevated TOT. *Reinduction* has similar heat transfer rate when compared to *2-cyl NFRB* strategy. *3-cyl IRB* also has similar heat transfer rates when compared to *2-cyl NFRB* and *reinduction* operation and better stay-warm potential than *6-cyl best BSFC* operation.

6.3.1 Comparison of NFRB with CDA

In this section, the best reverse breathing strategy (NFRB) is compared with CDA and IVC modulation strategies. Figure 6.11 shows the experimental steady-state results at loaded idle (800 RPM, 1.3 bar BMEP) showing normalized (a) BSFC, (b) OCE, (c) CCE, (d) Mechanical efficiency, (e) exhaust flow and (f) AFR vs TOT for *2-cyl NFRB*, CDA (*2-cyl stay warm*, *3-cyl stay warm*) and 6-cylinder (*best BSFC, stay warm, warm up, early IVC, late IVC*) strategies.

2-cyl NFRB has about 23 % lower BSFC and about 20°C lower TOT when compared to *6-cyl stay warm* due to an increased OCE as shown in Figures 6.11 (a) and (b). The *6-cyl stay warm* operation has a slightly more open VGT when compared to the *6-cyl warm up* operation and hence lower BSFC due to an increase in OCE as shown in Figure 6.11(a) and (b). 6-cylinder operation with early/late IVC and open VGT only increases the TOT by about 25°C w.r.t *6-cyl best BSFC* operation and hence is not a favorable stay warm strategy.

2-cyl NFRB has a comparable TOT and exhaust flow w.r.t *3-cyl stay warm*, however *3-cyl stay warm* operation is about 7% more fuel efficient than the NFRB strategies as shown in Figure 6.11(a) because of higher CCE for *3-cyl stay warm* operation (per Figure 6.11(d)) due to reduced in-cylinder heat losses in the deactivated cylinders. *2-cyl stay warm* has TOT comparable to *6-cyl warm up* operation with

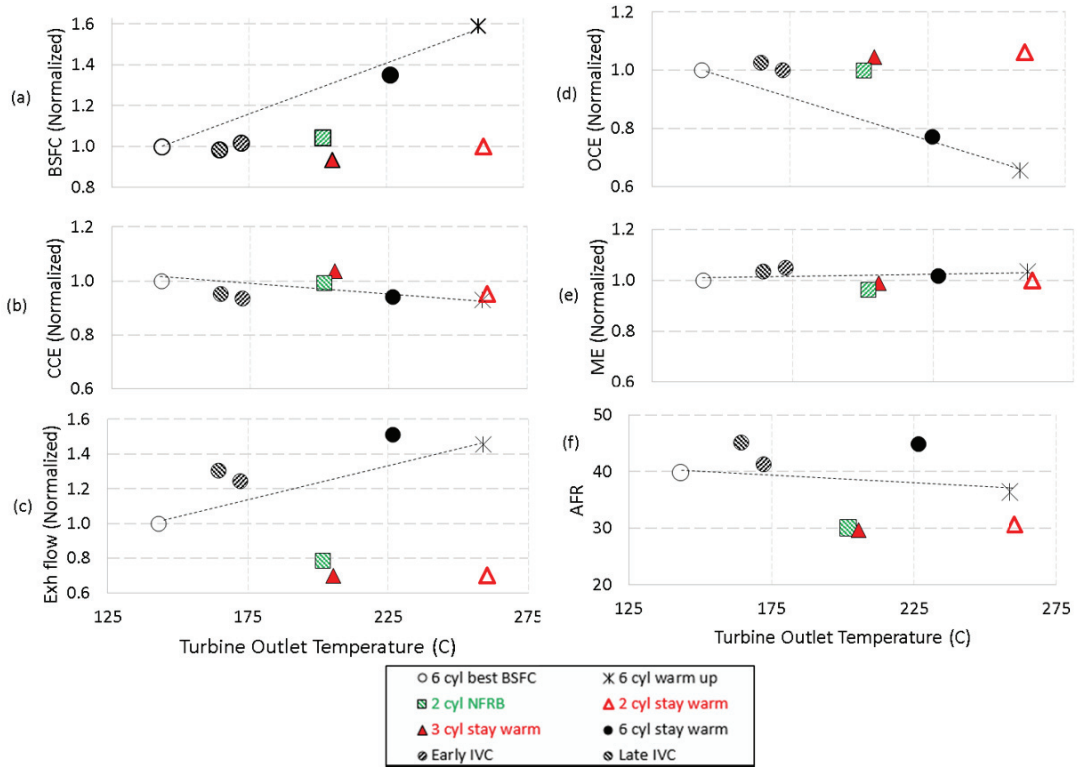

Figure 6.11. Experimental steady-state results at loaded idle (800 RPM, 1.3 bar BMEP) showing normalized (a) BSFC, (b) OCE, (c) CCE, (d) Mechanical efficiency, (e) exhaust flow and (f) AFR w.r.t TOT for all the strategies.

a fuel savings of about 40% due to a higher OCE as shown in Figure 6.11(a) and (b). The mechanical efficiencies and the CCE of all the strategies are very similar as shown in Figures 6.11(c) and (d). Exhaust flow plays a vital role in supplying heat and reducing the heat transferred to the AFT from the engine. When the AFT is at its efficient temperature zone, a lower exhaust flow is preferred to maintain the AFT system temperature [29]. *2-cyl NFRB*, *3-cyl stay warm* and *2-cyl stay warm* strategies have about 80% lower exhaust flow when compared to *6-cyl warm up* mode and about 30% lower exhaust flow when compared to *6-cylinder best BSFC* strategy as shown in Figure 6.11(e).

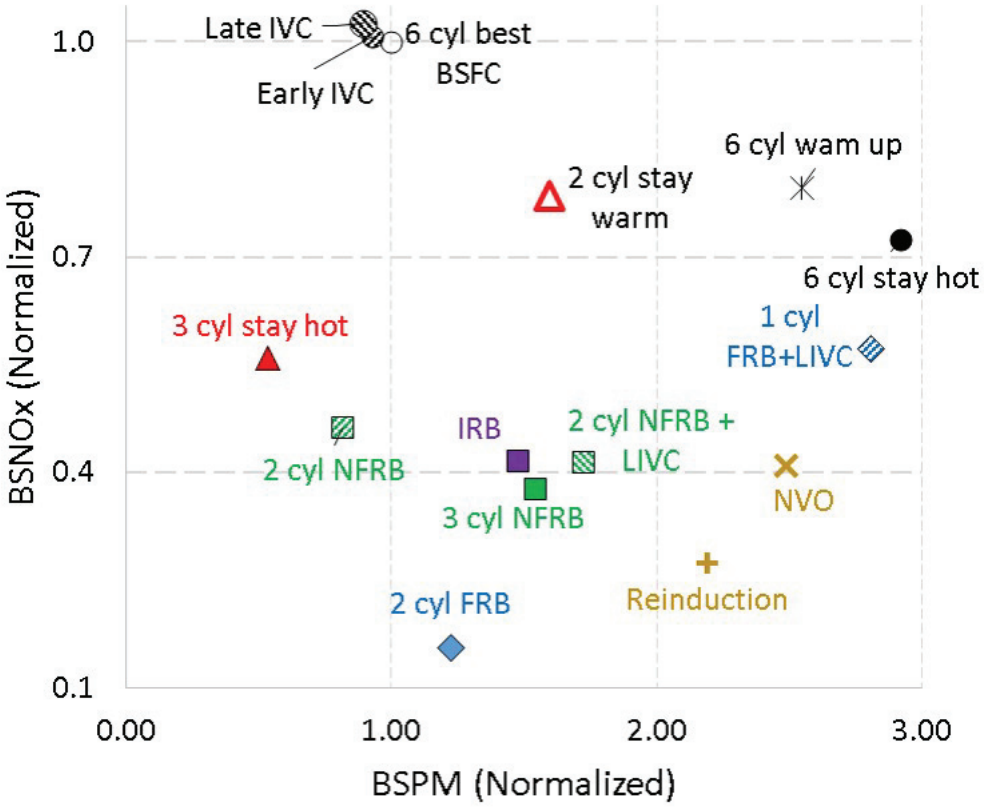

Figure 6.12. Experimental results at loaded idle showing the brake specific NOx and brake specific PM for all the strategies. All reverse breathing strategies have lower PM and NOx levels when compared to *6-cyl stay warm* strategy. *2-cyl FRB* has very low NOx with reasonable PM levels when compared to conventional strategies.

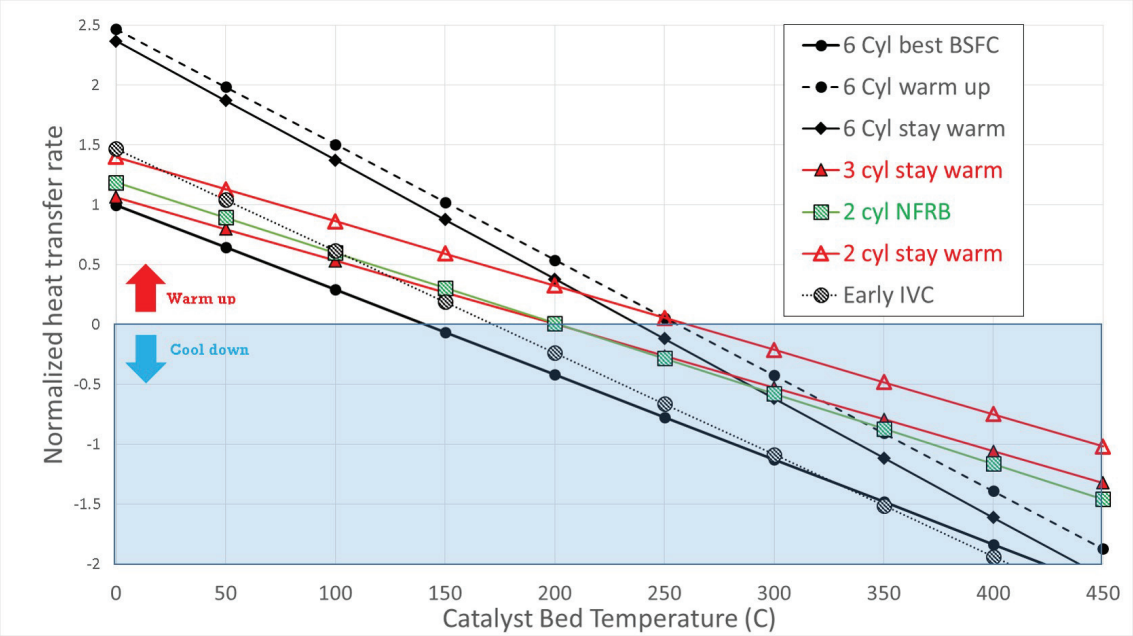

Figure 6.13. Catalyst warm-up characteristics comparison of *2-cyl NFRB* strategy and IVC modulation with 6-cylinder and CDA strategies at 800 RPM , 1.3 bar BMEP. The predicted heat transfer rates are normalized using the heat transfer rate of *6-cyl best BSFC* case at a catalyst bed temperature of 0°C.

The heat transfer rates of *2-cyl NFRB* strategy are compared with CDA and 6-cylinder (best BSFC, stay warm, warm up, early IVC) strategies in Figure 6.13. The predicted heat transfer rates are normalized using the heat transfer rate of *6-cyl best BSFC* case at a catalyst bed temperature of 0°C. Catalyst warm-up is fastest during the *6-cyl warm up* strategy due to its higher TOT and exhaust flow. Once catalyst temperatures reach desirable temperature (e.g., 300 °C), the *2-cyl NFRB* strategy is preferred given its lower exhaust flow rate, and elevated TOT as it cools down the AFT slower than 6-cylinder strategies. The heat transfer rates for the *2-cyl NFRB* strategy are very similar to *3-cyl stay warm* strategy. *2-cyl NFRB* also has a higher heat transfer rate when compared to *6-cyl stay warm* strategy at temperatures above 270 C. *2-cyl stay warm* strategy has better heat transfer rate characteristics when compared to *3-cyl stay warm* and *2-cyl NFRB* operation.

Figure 6.12 shows the normalized brake specific NOx and PM for all the strategies. All reverse breathing strategies have lower, or comparable PM and NOx levels compared to conventional *6-cyl warm up* operation. This was achieved by tuning the combustion system through adjustment of rail pressure and injection timing. *2-cyl FRB* has about 5 times lower BSNOx when compared to the *6-cyl best BSFC* strategy due to high charge dilution in the intake manifold. When compared with NFRB, FRB has lower NOx (as shown in Figure 6.12) as the gases that pass through the reverse breathing cylinders experience a combustion event, which leads to lower oxygen levels in the intake manifold. PM reductions are achieved by a combination of optimal rail pressure and delayed injection events during these reverse breathing stay warm operation. *3-cyl stay warm* has comparable PM and generally slightly higher NOx with the reverse breathing strategies.

In summary, the reverse breathing strategies studied in this study have elevated TOTs, low exhaust flows and improved fuel efficiency that combined outperform the conventional *6-cyl stay warm* strategy. Thus, reverse breathing is a prime candidate for AFT stay-warm operation at idle without utilizing an external EGR loop. The "stay warm" thermal management benefits of reverse breathing are similar to *3-cylinder CDA* albeit with higher fuel consumption. The "stay warm" benefits of reverse breathing in comparison to conventional 6-cylinder, *3-cylinder CDA* and *2-cylinder CDA* operation, respectively, continues in next section where HDFTP drive-cycle results are analyzed and compared.

6.4 Transient Drive-Cycle Results

This subsection compares the fuel consumption and tailpipe NOx reduction of reverse breathing enabled A/T thermal management strategies during the HD-FTP. The *2-cyl NFRB* strategy was run during stay-warm idle portions of the HD-FTP to evaluate its impact in comparison to conventional 6 and 3-cylinder operation. Figure 6.14 illustrates the process by which the tailpipe NOx is predicted in this study. The

AFT system is connected passively to the engine exhaust and gas temperatures at the inlet and outlet of DOC, DPF and SCR are measured using thermocouples. Measured SCR temperature is used to predict the SCR efficiency from which tailpipe NOx is predicted. The SCR efficiency curve shows that efficiency reaches its maximum value for catalyst temperatures between 250°C and 450°C.

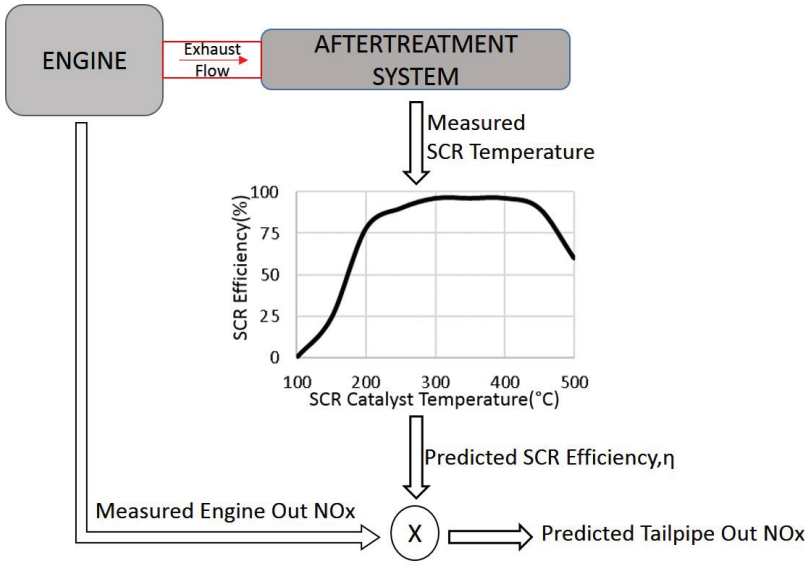

Figure 6.14. Measured SCR temperature from the A/T hardware is used to predict SCR efficiency. The SCR efficiency curve shows that efficiency reaches its maximum value for catalyst temperatures between 250°C and 450°C (Eaton 2015). Tailpipe out NOx is estimated using this predicted SCR efficiency.

Four cycles were run and compared:

1. *6-cyl best BSFC cycle* - the result of running the engine across the HD-FTP using an engine calibration developed for best engine fuel economy. This strategy incorporates the *6-cyl best BSFC* strategy described in the previous section during idle, and provides a baseline for tailpipe emissions and fuel consumption using conventional operation.

2. *6-cyl AFT stay-warm cycle* - the results of running the engine across the HD-FTP using an engine calibration that meets current on-highway emissions limits.

This strategy incorporates delayed fuel injections at all possible operating conditions (including non-idle conditions), and maximally closed VGT positions at idle, in order to increase TOT and flow rates. The approach uses the previously described *6-cyl warm up* and *6-cyl stay-warm* strategies during idle portions of the cycle where SCR outlet temperatures are below 200°C (shaded red "warm-up" idle sections in Figure 6.1), and above 200°C (shaded green "stay-warm" idle sections in Figure 6.1), respectively. At non-idle conditions the late injections also reduce engine-outlet NOx, which together with faster AFT system warm-up, reduce tailpipe NOx to acceptable levels. This operating mode is included to demonstrate the fuel consumption increases typically required during conventional six-cylinder engine operation in order to thermally manage the AFT in a way consistent with meeting current emissions limits.

3. *3-cyl A/T stay-warm idle cycle* - similar to *6-cyl stay-warm* cycle with one modification: using the *3-cyl stay-warm* mode instead of the *6-cyl stay-warm* mode once the SCR outlet temperature is above 200°C (shaded green sections in Figure 6.1). This strategy demonstrates the fuel savings possible through use of CDA during idle for AFT component temperature maintenance.

4. *2-cyl AFT stay-warm idle cycle* - similar to *3-cyl stay-warm* cycle with one modification: using the *2-cyl stay-warm* mode instead of the "3-cyl stay-warm" mode once the SCR outlet temperature is above 200°C (shaded green sections in Figure 6.1). This strategy demonstrates the fuel savings possible through use of CDA during idle for A/T component temperature maintenance.

5. *2-cyl NFRB AFT stay-warm idle cycle* - similar to *3-cyl stay-warm* cycle with one modification: using the *2-cyl NFRB* strategy at idle instead of *3-cyl stay-warm* strategy once the SCR outlet temperature is above 200°C (shaded green sections in Figure 6.1). This strategy demonstrates the fuel savings possible through use of *2-cylinder NFRB* during idle for AFT system temperature maintenance.

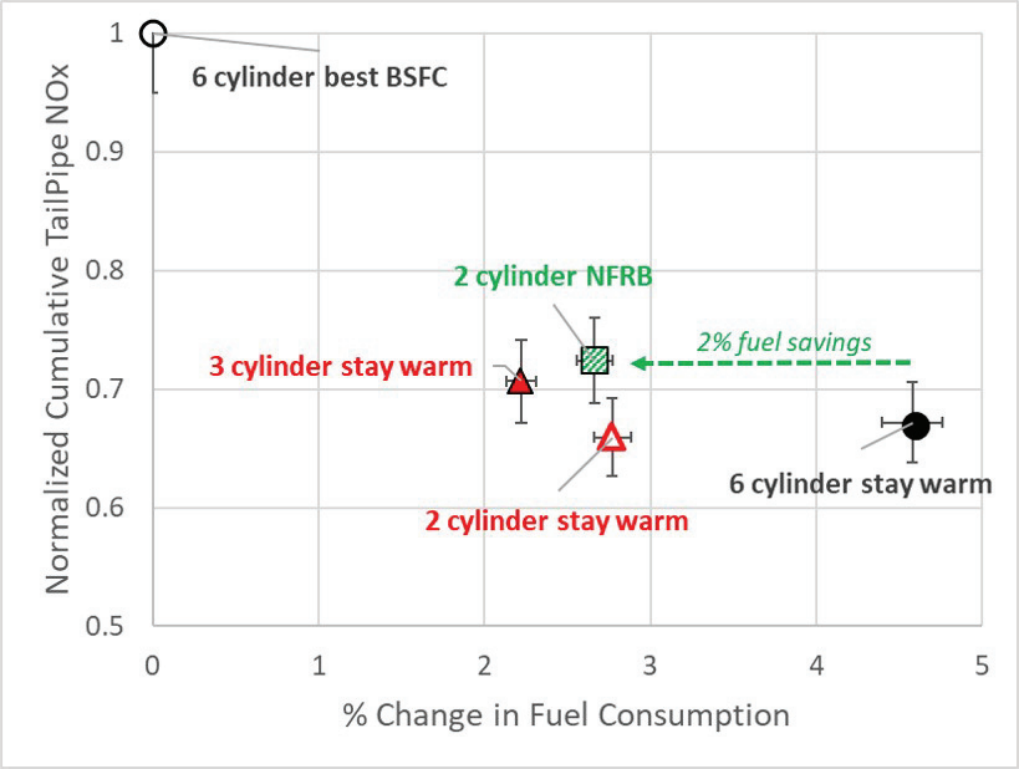

Figure 6.15. HDFTP drive-cycle results showing the NOx vs Fuel consumption trade-offs, comparing reverse breathing strategy with 6-cylinder and CDA strategies. *NFRB* strategy at stay-warm idle operation enables about 2% fuel consumption benefit with similar tailpipe out reduction when compared to *6-cylinder stay-warm* operation.

Figure 6.15 summarizes the main HD-FTP cycle results for all the described strategies. As shown, a 35% reduction in tailpipe NOx was possible via the *6-cyl stay-warm* strategy, albeit at the expense of an approximate 4.5% increase in fuel consumption over the HD-FTP. The implementation of the *2-cyl NFRB* strategy during idle conditions, when the SCR system temperature was at least 200°C, results in very similar tailpipe NOx levels, and enables a 2% fuel consumption reduction compared to the *6-cyl stay-warm* cycle. As described in detail in *Joshi et al* [29], the implementation of *3-cylinder CDA* during stay-warm operation allows about 2.3% reduction in fuel consumption. The implementation of *2-cylinder CDA* during stay-warm idle conditions yields similar fuel savings as *2-cyl NFRB* but about 6% lower tail pipe NOx due to better stay-warm performance. The fuel consumption results shown in Figure 6.15 were determined via experimental fuel consumption measurements on the test engine. Measured SCR-outlet temperatures were used as inputs to an assumed SCR NOx conversion efficiency map (per Figure 6.14) to estimate the instantaneous tailpipe NOx emissions. These were then integrated to generate the results shown in Figure 6.15. Figure 6.16 shows the TOT, SCR inlet temperature, SCR NOx conversion efficiency, predicted tailpipe out NOx, Measured engine-out PM for each of the strategies. The TOT plot shows that using *2-cyl NFRB* at idle is almost as effective in maintaining elevated A/T temps as the *6-cyl stay-warm*, *3-cyl stay warm* and *2-cyl stay warm* strategies. Combined with the lower engine-out NOx levels for *2-cyl NFRB* (per Figure 6.12), a comparable cumulative tailpipe NOx level results during the HD-FTP (per Figure 6.15). The NFRB strategy at idle is more fuel efficient when compared to the *6-cyl stay warm* strategy, hence the fuel consumed is about 2% less over the entire HD-FTP. The engine-out PM is also the lowest for the *2-cyl NFRB* strategy indicating there is potential for less frequent active DPF regenerations during engine operation.

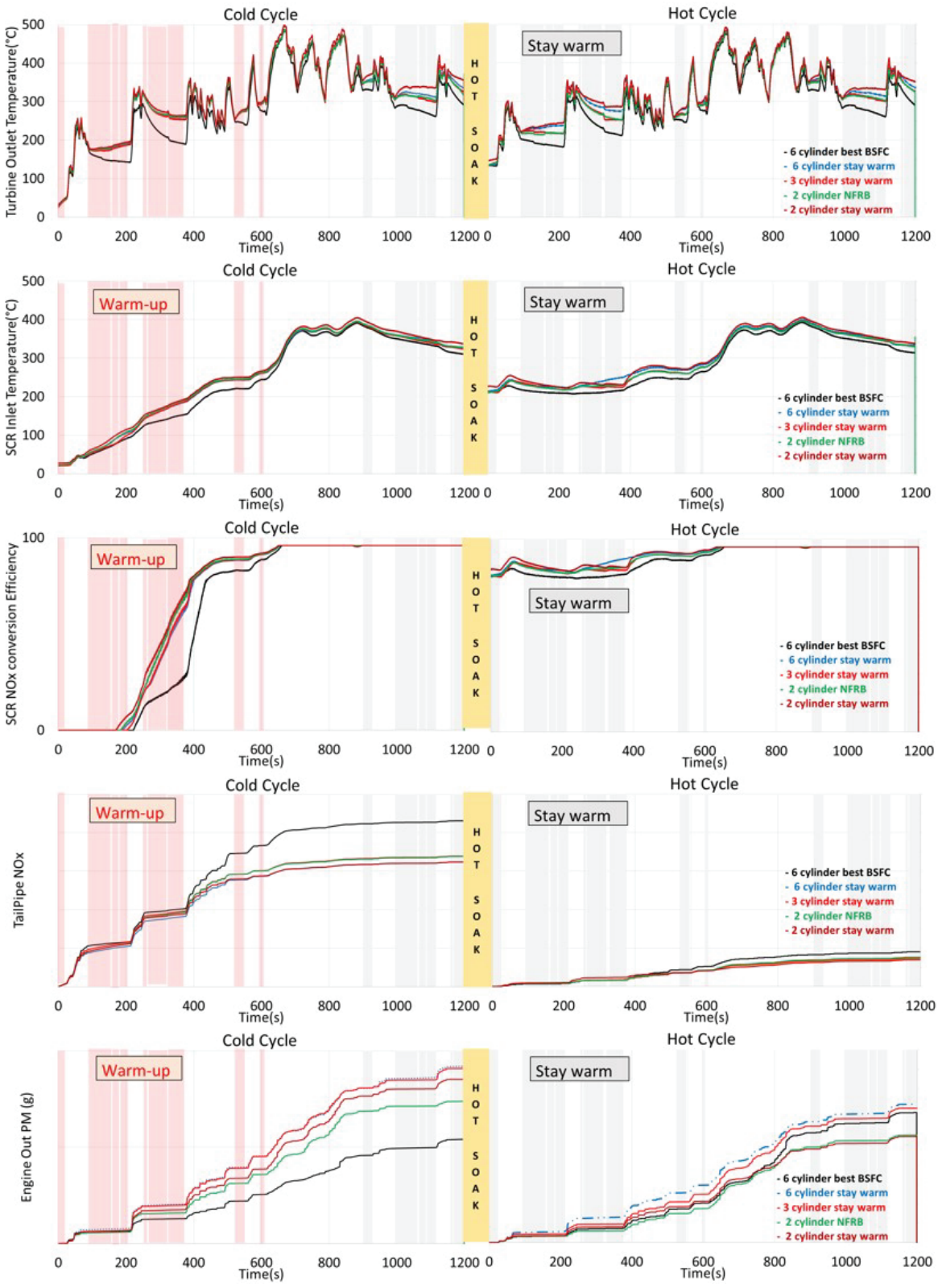

Figure 6.16. Transient HD-FTP (cold and hot start) data.

6.5 Experimental Results at 1200 RPM

The benefit of reverse breathing is established in the previous sections. This section explores the benefits of reverse breathing strategies when compared to other VVA strategies at higher speeds and loads. Specifically, experimental testing was carried out at 1200 RPM at two operating conditions:

1. 1.3 bar BMEP
2. 2.6 bar BMEP

6.5.1 1200 RPM 1.3 bar BMEP

Figure 6.17 shows the experimental steady-state results at loaded idle (1200 RPM, 1.3 bar BMEP) showing normalized (a) BSFC, (b) OCE, (c) CCE, and (d) ME, w.r.t TOT for all the strategies. *6-cyl warm up* strategy has the highest TOT but also the highest fuel consumption as shown in Figure 6.17(a). The VGT is over-closed for *6-cyl warm up* resulting in a higher engine delta pressure which lowers the OCE and results in a higher fuel consumption. All the other strategies have a relatively open VGT position. The *3-cyl stay warm* and *2-cyl NFRB* strategy have about 25°C lower TOT however has 40% lower fuel consumption. The lower fuel consumption is primarily due to the higher OCE. ME and CCE is similar for all the strategies as seen in Figures 6.17(c) and (d).

NVO has similar TOT compared to *2-cyl NFRB* strategy but has a higher fuel consumption due to a relatively lower OCE. *6-cyl best BSFC* is the fuel efficient 6-cylinder strategy which has a relatively open VGT and earlier SOI. However since the TOT is about 100°C lower than other strategies, it is not a viable thermal management strategy. *FRB* in cylinder 1 results in about 25°C higher than *6-cyl best BSFC* with similar BSFC. *Reinduction* strategy yields TOT above 200°C with 10% lower BSFC when compared to *6-cyl best BSFC* strategy.

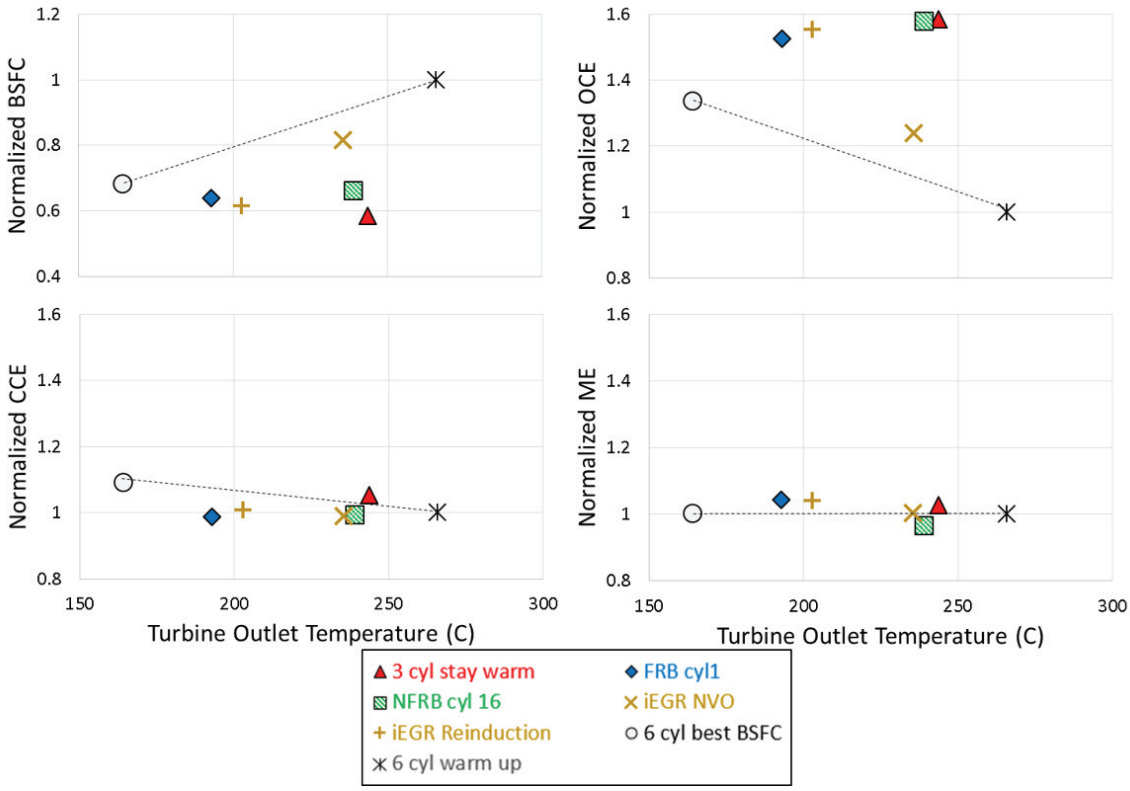

Figure 6.17. Experimental steady-state results at loaded idle (1200 RPM, 1.3 bar BMEP) showing normalized (a) BSFC, (b) OCE (c) CCE, and (d) CCE, w.r.t TOT for all the strategies.

In order to evaluate the warm-up and stay-warm characteristics of these strategies, the heat transfer from the exhaust to the catalyst is to be considered. The heat transfer rate between the exhaust gas and an AFT catalyst depends on the TOT, exhaust flow rate, and instantaneous catalyst bed temperature. Figure 6.18 shows the normalized exhaust flow vs TOT for all the strategies. *6-cyl warm up* strategy is state of the art thermal management strategy. This strategy has TOT of 265°C and high exhaust flow. *3-cyl stay warm* and *2-cyl NFRB* strategy have similar TOT and 60% lower exhaust flow when compared to *6-cyl warm up* strategy.

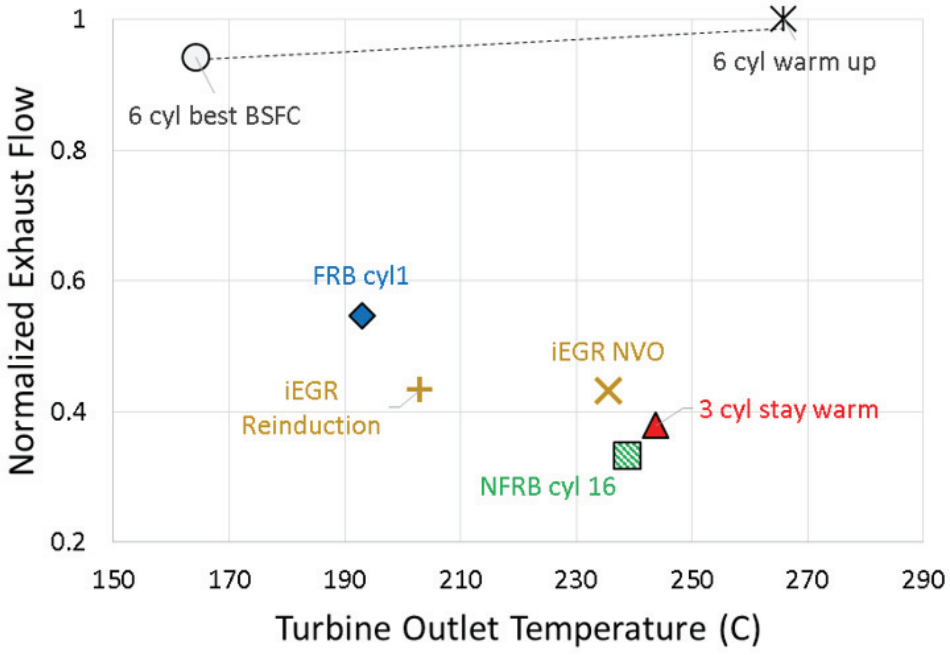

Figure 6.18. Experimental steady-state results at 1200 RPM, 1.3 bar BMEP showing normalized exhaust flow vs TOT for all the strategies. For stay warm operation of the engine, higher TOT and lower exhaust flow is preferred.

The heat transfer rate between incoming gas into the A/T and the catalyst bed [23], is given by Equation 6.3:

$$\dot{q} = C \times \dot{m}^{4/5} \times (TOT - T_{Catalyst}) \tag{6.3}$$

Figure 6.19 shows the catalyst warm-up characteristics comparison of *2-cyl NFRB* strategy with *6-cylinder* and *CDA* strategies at 1200 RPM , 1.3 bar BMEP. At temperatures above 280°C, *2-cyl NFRB* strategy cools down the catalyst slower than *6-cyl warm up* strategy while saving 34% fuel. *2-cyl NFRB* and *3-cyl stay warm* have very similar heat transfer characteristics and fuel consumption as seen in Figures 6.17(a) and 6.19. When the flexibility of an over-closed VGT is not available, all the strategies perform better than the *6-cyl best BSFC* strategy at catalyst bed temperatures above 100°C.

All the strategies were screened to keep emissions within *6-cyl warm up* strategy limits as shown in Figure 6.20.

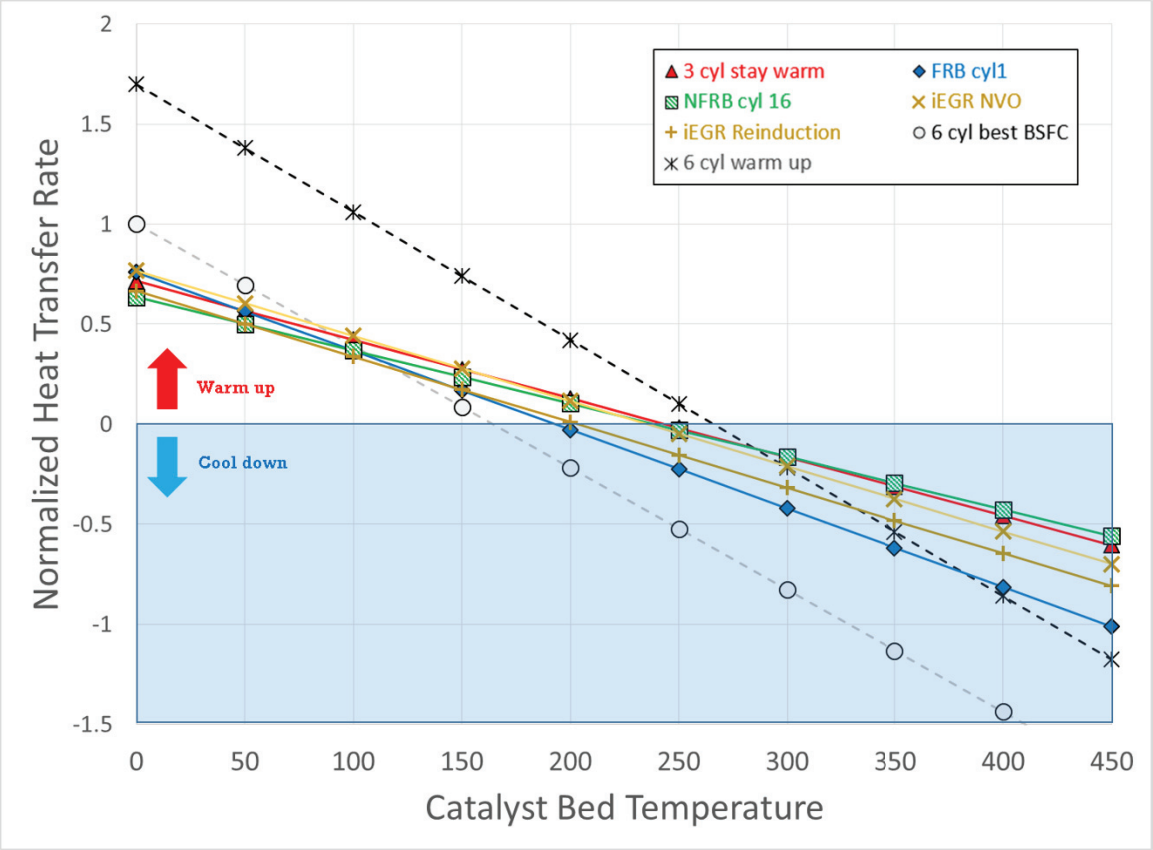

Figure 6.19. Catalyst warm-up characteristics comparison of *2-cyl NFRB* strategy with 6-cylinder and CDA strategies at 1200 RPM, 1.3 bar BMEP. The predicted heat transfer rates are normalized using the heat transfer rate of *6-cyl best BSFC* case at a catalyst bed temperature of 0°C. Negative heat transfer represents cooling of the catalyst and positive heat transfer represents heating of the catalyst.

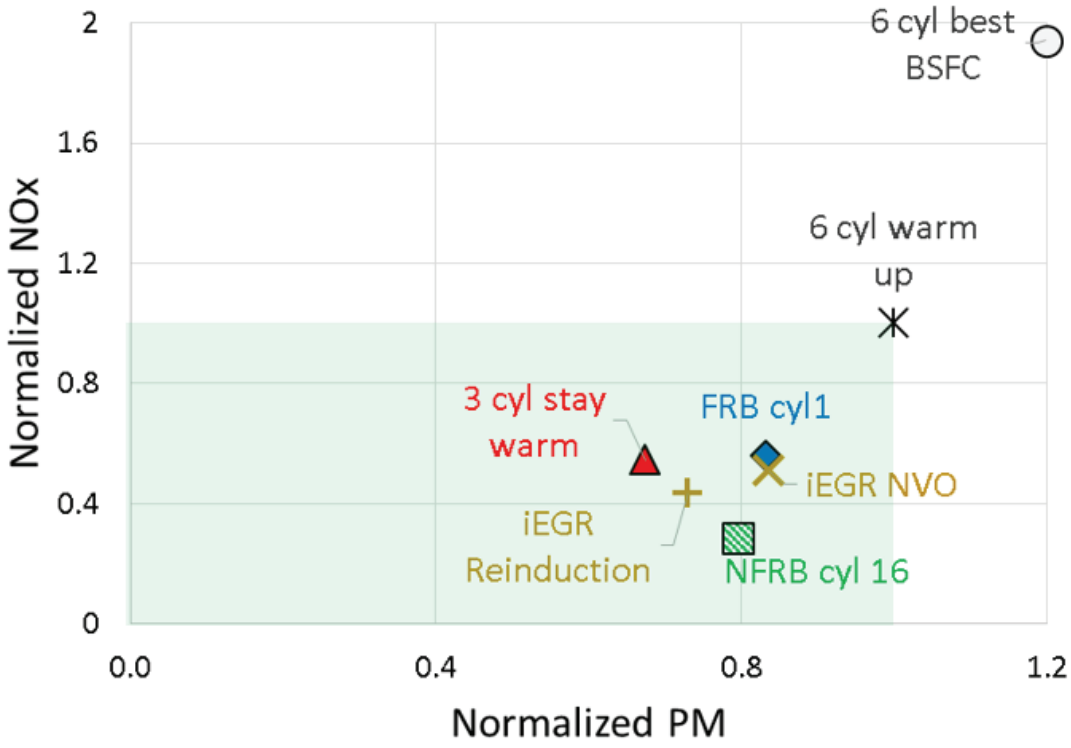

Figure 6.20. Experimental steady-state results at loaded idle (1200 RPM, 1.3 bar BMEP) showing normalized PM vs normalized NOx for all the strategies.

6.5.2 1200 RPM/ 2.6 bar BMEP

Figure 6.21 shows the experimental steady-state results at loaded idle (1200 RPM, 2.6 bar BMEP) showing normalized (a) BSFC, (b) OCE, (c) CCE, and (d) ME, w.r.t TOT for all the strategies. *2-cyl NFRB* and *3-cyl stay warm* have about 7°C and 35°C higher TOT than *6-cyl warm up* strategy as shown in Figure 6.21(a), while saving 27% and 30% fuel respectively. The primary driver for lower fuel consumption is lower OCE due to reduced pumping work, as the airflow is reduced. The over-closed VGT for *6 cyl warm up* resulting in a higher engine delta pressure which lowers the OCE and results in a higher fuel consumption. All the other strategies have a relatively open VGT position. ME and CCE are similar for all the strategies as seen in Figures 6.21(c) and (d). *NVO* has similar TOT compared to *2-cyl NFRB* strategy but has 10% higher fuel consumption due to lower OCE. *FRB in cylinder 1* results in about 50°C higher than *6-cyl best BSFC* with similar BSFC. *Reinduction* strategy yields TOT above 260°C with 10% lower BSFC when compared to *6-cyl best BSFC* strategy.

In order to evaluate the warm-up and stay-warm characteristics of these strategies, the heat transfer from the exhaust to the catalyst is to be considered. Figure 6.22 shows the normalized exhaust flow vs TOT for all the strategies. *3-cyl stay warm* and *2-cyl NFRB* strategies have higher TOT and 50% lower exhaust flow when compared to *6-cyl warm up* strategy and hence would serve as better stay-warm strategies.

Figure 6.23 shows the catalyst warm-up characteristics comparison of *2-cyl NFRB* strategy with *6-cylinder* and *CDA* strategies at 1200 RPM , 2.6 bar BMEP. At temperatures above 300°C, *2-cyl NFRB* strategy cools down the catalyst slower than *6-cyl warm up* strategy while saving 27% fuel. At temperatures above 275°C, *3-cyl stay warm* strategy has higher heat transfer rates than *6-cyl warm up* strategy while saving 30% fuel. *3-cyl stay warm* have very similar heat transfer characteristics and fuel consumption as seen in Figures 6.21(a) and 6.23. When the flexibility of an over-closed VGT is not available, all the strategies perform better than the *6-cyl best BSFC* strategy at catalyst bed temperatures above 100°C.

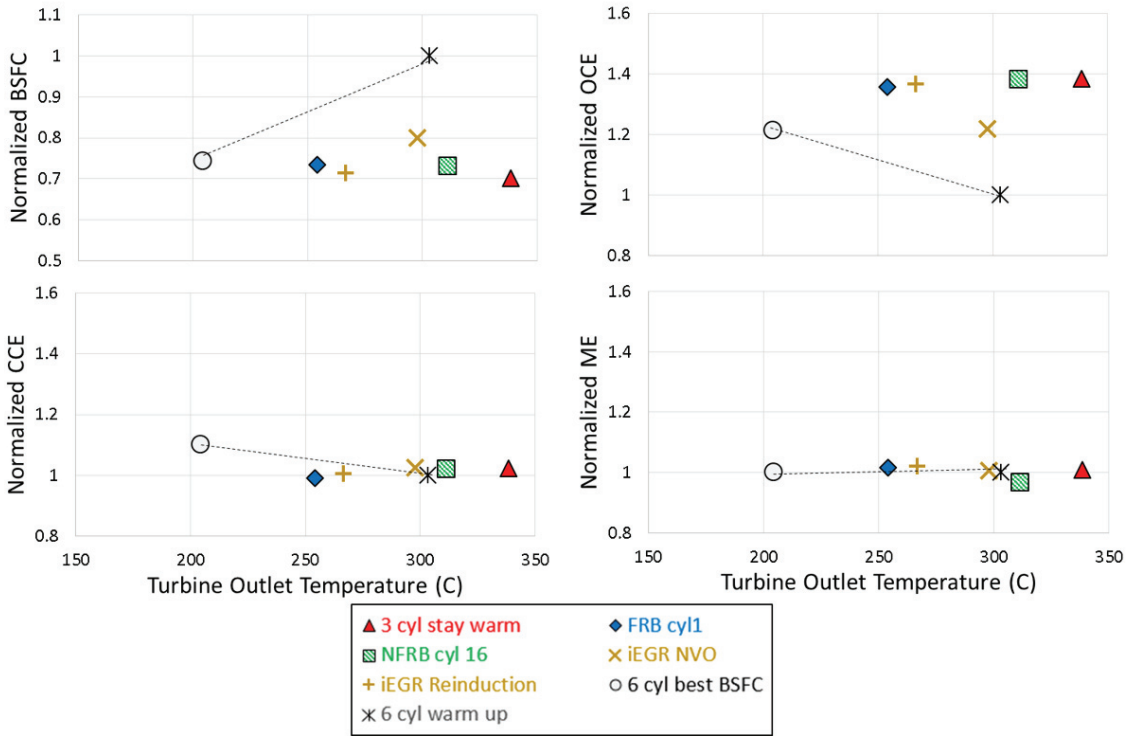

Figure 6.21. Experimental steady-state results at loaded idle (1200 RPM, 2.6 bar BMEP) showing normalized (a) BSFC, (b) BTE, (c) OCE, and (d) CCE, w.r.t TOT for all the strategies.

All the strategies were screened to keep emissions within *6-cyl warm up* strategy limits as shown in Figure 6.24. However for the *FRB* strategy, it was not possible to reduce PM below *6-cyl warm up* strategy due to not enough oxygen being present in the intake manifold.

6.6 Summary

This chapter compares the stay-warm AFT thermal performance of FRB, NFRB and IRB, with conventional strategies as well as VVA strategies, such as CDA, internal EGR and IVC modulation at 800 RPM/1.3 bar BMEP and 1200 RPM/1.3 & 2.6 bar BMEP. This chapter also introduces two novel strategies, that were implemented

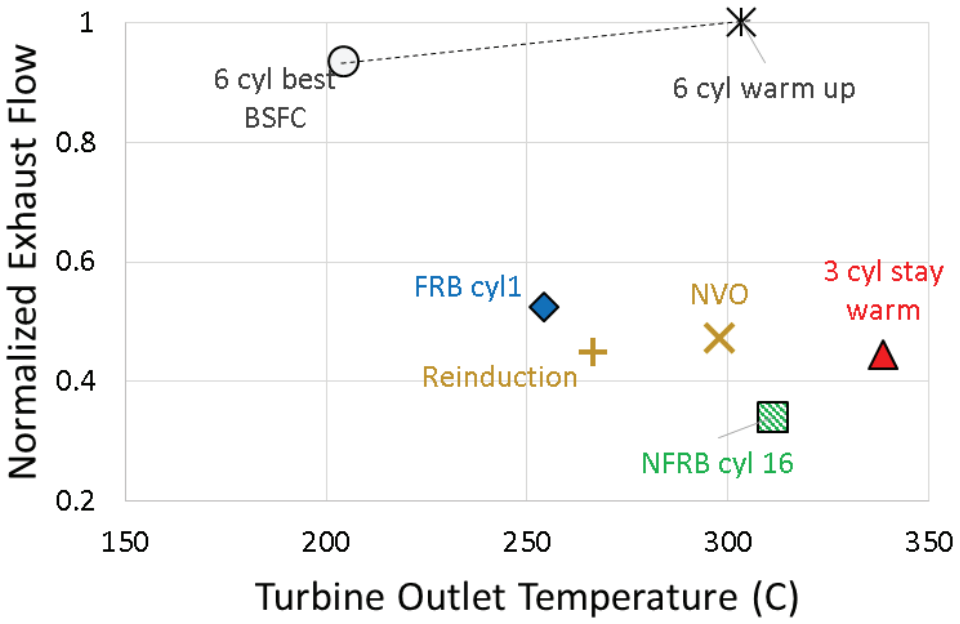

Figure 6.22. Experimental steady-state results at loaded idle (1200 RPM, 2.6 bar BMEP) showing normalized exhaust flow vs TOT for all the strategies.

for the first time on the engine: *3-cyl IRB* and *3-cyl NFRB*. NFRB was also implemented over the HDFTP drive-cycle. The results demonstrate that *2-cyl NFRB* can maintain AFT temperatures in a more fuel efficient manner than conventional strategies through reductions in airflow pumping work and exhaust flow. Specifically, the incorporation of *2-cyl NFRB* to maintain desired AFT temperatures during the idle conditions of the HD-FTP was experimentally demonstrated to result in fuel savings of 2% over the HD-FTP drive-cycle. Additional findings include:

1. At loaded-idle steady-state operation *2-cyl NFRB* enables 60°C increase in TOT without any fuel or emission penalty and 28% reduction in exhaust flow compared to conventional 6-cylinder operation optimized for fuel consumption reduction. *2-cyl NFRB* also enables about 26% fuel savings with comparable stay-warm performance when compared to *6-cylinder stay-warm* operation.

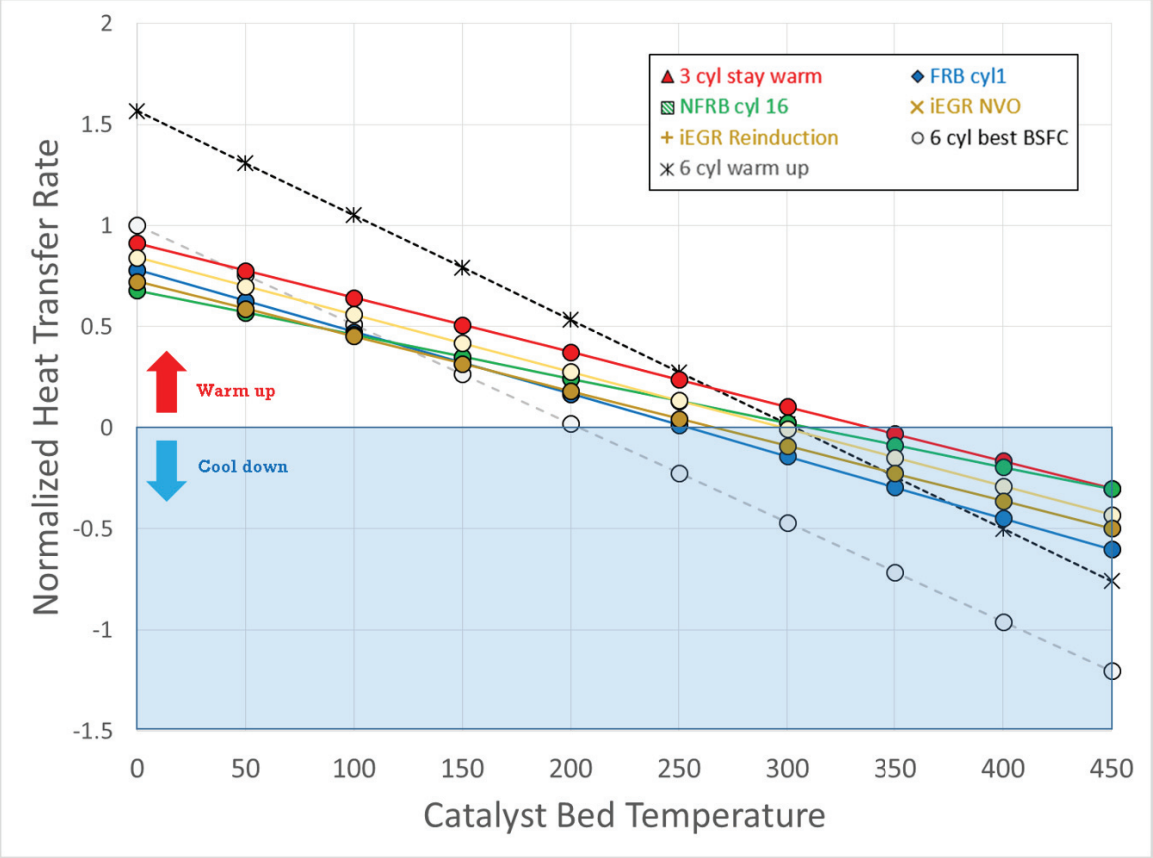

Figure 6.23. Catalyst warm-up characteristics comparison of *2-cyl NFRB* strategy with 6-cylinder and CDA strategies at 1200 RPM, 2.6 bar BMEP. The predicted heat transfer rates are normalized using the heat transfer rate of *6-cyl best BSFC* case at a catalyst bed temperature of 0°C.

2. Using LIVC to reduce airflow while reverse breathing is more fuel efficient than using conventional levers such as over-closing the VGT due to reduced airflow pumping work.

3. *2-cyl NFRB* strategy at idle yields about 2% fuel consumption reduction compared to conventional 6-cylinder operation over the HDFTP cycle. Further benefits could be realized if reverse breathing is enabled at other operating conditions.

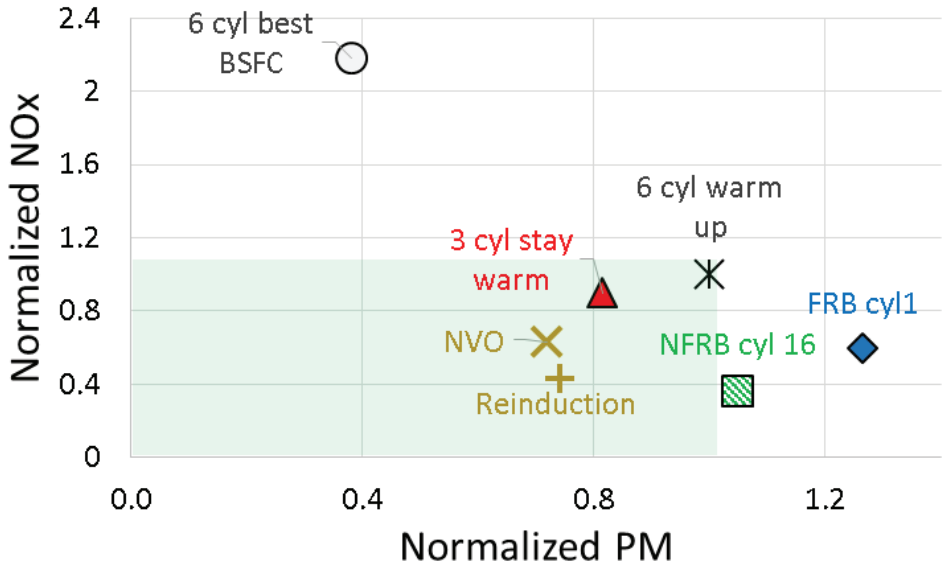

Figure 6.24. Experimental steady-state results at loaded idle (1200 RPM, 2.6 bar BMEP) showing normalized PM vs normalized NOx for all the strategies.

4. *3-cyl NFRB*, although having higher OCE and CCE, has a lower BTE due to its lower mechanical efficiency because of higher heat losses in the reverse breathing cylinders.

5. NFRB strategy enables higher TOT when compared to FRB due to a combination of lower AFR and late injections. Injection timing is advanced for FRB strategy in order to maintain stability in the heat release in the cylinder, which in turn decreases the TOT.

6. All reverse breathing strategies are within the NOx and PM levels of the 6-cylinder strategy without using external EGR. This is achieved by tuning the combustion system by using rail pressure, injection timing and intake manifold dilution.

7. *2-cyl NFRB* strategy is comparable to *3-cyl stay warm* strategy with respect to TOT, exhaust flow and fuel efficiency. The better strategy from a manufacturer standpoint likely comes down to durability, cost, and ease of implementation.

8. *2-cyl stay warm* strategy enables similar TOT with 80% lower exhaust flow while being 40% fuel efficient when compared to *6-cylinder warm up* strategy and fares better than other stay-warm strategies studied in this study.

9. 6-cylinder operation with IVC modulation only enables about 25°C increase in TOT and hence is not a favorable stay-warm strategy when compared to reverse breathing and CDA strategies.

10. Internal EGR via reinduction of exhaust gases gives similar TOT, exhaust flows and BSFC (and hence similar stay-warm performance) when compared to *3-cyl stay warm* and *2-cyl NFRB* strategies.

11. At 1200 RPM/ 1.3 bar BMEP, *3-cyl stay warm* and *2-cyl NFRB* strategies have about 25°C lower TOT, but have about 40% lower fuel consumption, compared to *6-cyl warm up* strategy. The lower fuel consumption is primarily due to the higher OCE.

12. At 1200 RPM/ 2.6 bar BMEP, *2-cyl NFRB* and *3-cyl stay warm* have about 7°C and 35°C higher TOT than *6 cyl warm up* strategy, while saving 27% and 30% fuel, respectively.

7. SUMMARY AND FUTURE WORK

7.0.1 Summary

VVA strategies serve a great potential for fuel efficient AFT thermal management for modern multi-cylinder diesel engine. Certain VVA strategies such as CDA and IVC modulation have high potential to improve the AFT thermal management in a fuel efficient manner. Novel strategies such as reverse breathing and intake rebreathing have good potential for fuel efficient NOx reduction without using any external EGR. Hence it could be a potential technology for non-EGR engines equipped with a fixed geometry turbine turbocharger. Chapter 2 shows that at high speeds, low air flow strategies such as CDA and IVC modulation can be used to reduce the fuel consumption by 5 to 30% depending on the load, increase the rate of warm-up of AFT, maintain higher AFT temperatures, or achieve active diesel particulate filter regenerations without requiring HC dosing of the diesel oxidation catalyst. Implementation of CDA at all loads below 3 bar BMEP yields fuel savings of 3.4% over the HDFTP drive-cycle when compared to conventional thermal management strategies. Chapter 3 shows that at cruise operating condition, IVC modulation increases the TOT by about 200°C, however it does not give any fuel efficiency benefits, as the engine is already optimized for best BSFC at this condition.

In order to capture the steady-state benefits of CDA, transient operation of CDA is studied. The performance of CDA during transient operation is limited by the low airflow which causes an increase in soot emissions. Chapter 4 concludes that the transient CDA performance problem could be solved by reactivation of the deactive cylinders when limited airflow condition is detected. Chapter 5 introduces three novel engine breathing modes, namely, fired/non-fired reverse breathing, exhaust rebreathing and intake rebreathing. These strategies were implemented for the first

time on a multi-cylinder diesel engine. At idle (800 rpm /50 ft-lbs), these strategies show good potential to increase the TOT in a fuel efficient manner at low-load operation where excess oxygen is available in the exhaust manifold. PM control was a challenge, however, with careful tuning of input parameters PM, can be reduced to baseline levels while improving TOT and fuel economy. Chapter 6 compares these novel breathing modes with other VVA strategies such as CDA, IVC modulation and internal EGR. The results demonstrate that NFRB can maintain AFT temperatures in a more fuel efficient manner than conventional strategies through reductions in airflow pumping work and exhaust flow. Specifically, the incorporation of NFRB to maintain desired AFT temperatures during the idle conditions of the HDFTP was experimentally demonstrated to result in fuel savings of 2% over the drive-cycle.

7.0.2 Recommendations

Future work will include exploring the benefits of reverse breathing at other operating conditions over the torque-speed space. Future work also includes implementing reverse breathing at higher speeds and loads over the HD-FTP cycle and combining CDA and reverse breathing to further improve thermal performance. These strategies can be also studied at other transient applications such as port drayage drive-cycle and extended idle. Potential future work includes studying the impact of reverse breathing on NVH and studying the benefits of using reverse breathing with fixed geometry turbocharger without external EGR.

The VVA strategies discussed in this dissertation can also be studied for spark ignited and natural gas engines to improve fuel efficiency.

REFERENCES

REFERENCES

[1] D Stanton. Systematic development of highly efficient and clean engines to meet future commercial vehicle greenhouse gas regulations. *Diesel Engine*, 2013:05–16, 2013.

[2] R. Pichs-Madruga Y. Sokona E. Farahani S. Kadner K. Seyboth A. Adler I. Baum S. Brunner P. Eickemeier B. Kriemann J. Savolainen S. Schlmer C. von Stechow T. Zwickel Edenhofer, O. and J.C. Minx (eds.). Contribution of working group iii to the fifth assessment report of the intergovernmental panel on climate change. 2014.

[3] Department of environmental food and UK rural affairs. Clean air strategy 2018. 2018.

[4] D Stanton, S Charlton, and P Vajapeyazula. Diesel engine technologies enabling powertrain optimization to meet US greenhouse gas emissions. *SAE International Journal of Engines*, 6(3):1757–1770, 2013.

[5] Office of Transportation and EPA Air Quality. Heavy-duty highway compression-ignition engines and urban buses: Exhaust emission standards. 2016.

[6] T Johnson. Vehicular emissions in review. *SAE International Journal of Engines*, 5(2):216–234, 2012.

[7] M.J. Lzaro, Maria Galvez, Alicia Boyano, Sonia Ascaso, Isabel Suelves, Rafael Moliner, Izabela Pieta, Concepcion Herrera, M.A. Larrubia, and L.J. Alemany. Catalytic technologies for diesel engines exhausts gas cleaning. 01 2011.

[8] M Koebel, M Elsener, and M Kleemann. Urea-SCR: a promising technique to reduce NOx emissions from automotive diesel engines. *Catalysis Today*, 59(3):335–345, 2000.

[9] J Girard, G Cavataio, R Snow, and C Lambert. Combined fe-cu SCR systems with optimized ammonia to NOx ratio for diesel NOx control. *SAE International Journal of Fuels and Lubricants*, 1(1):603–610, 2009.

[10] Christine Lambert, Robert Hammerle, Ralph McGill, Maadi Khair, and Christopher Sharp. Technical advantages of urea SCR for light-duty and heavy-duty diesel vehicle applications. *SAE transactions*, 113(4):580–589, 2004.

[11] S Charlton, T Dollmeyer, and T Grana. Meeting the US heavy-duty EPA 2010 standards and providing increased value for the customer. *SAE International Journal of Commercial Vehicles*, 3(1):101–110, 2010.

[12] AP Walker. Controlling particulate emissions from diesel vehicles. *Topics in catalysis*, 28(1-4):165–170, 2004.

[13] R Allanson, P Blakeman, B Cooper, H Hess, P Silcock, and A Walker. Optimising the low temperature performance and regeneration efficiency of the continuously regenerating diesel particulate filter (CR-DPF) system. *Development*, 2012:05–10, 2002.

[14] S Stadlbauer, H Waschl, A Schilling, and L del Re. DOC temperature control for low temperature operating ranges with post and main injection actuation. Technical report, SAE Technical Paper, 2013.

[15] X Song, H Surenahalli, J Naber, G Parker, et al. Experimental and modeling study of a diesel oxidation catalyst (DOC) under transient and CPF active regeneration conditions. *Diesel Engine*, 2007:10–01, 2007.

[16] M Naseri, R Conway, H Hess, and C Aydin. Development of emission control systems to enable high NOx conversion on heavy duty diesel engines. 2014.

[17] J Parks, S Huff, M Kass, and J Storey. Characterization of in-cylinder techniques for thermal management of diesel aftertreatment. *studies*, 10:11, 2007.

[18] P Singh, A Thalagavara, J Naber, J Johnson, and S Bagley. *An experimental study of active regeneration of an advanced catalyzed particulate filter by diesel fuel injection upstream of an oxidation catalyst*. PhD thesis, Michigan Technological University, 2006.

[19] J Schwoerer, K Kumar, B Ruggiero, and B Swanbon. Lost-motion VVA systems for enabling next generation diesel engine efficiency and after-treatment optimization. *Training*, 2013:10–14, 2010.

[20] M Magee. *Exhaust Thermal Management Using Cylinder Deactivation*. Master's thesis, Purdue University, Purdue University, West Lafayette, Indiana, 2013.

[21] X Lu, C Ding, A Ramesh, G Shaver, E Holloway, J McCarthy, M Ruth, E Koeberlein, and D Nielsen. Impact of cylinder deactivation on active diesel particulate filter regeneration at highway cruise conditions. *Frontiers in Mechanical Engineering*, 1(9), 2015.

[22] A Garg, M Magee, C Ding, L Roberts, and G Shaver. Exhaust thermal management using cylinder throttling via intake valve closing timing modulation. Manuscript submitted for publication, 2013.

[23] C Ding, L Roberts, D Fain, A Ramesh, G Shaver, J McCarthy, M Ruth, E Koeberlein, E Holloway, and D Nielsen. Fuel efficient exhaust thermal management for compression ignition engines during idle via cylinder deactivation and flexible valve actuation. *International Journal of Engine Research*, page 1468087415597413, 2015.

[24] K Dean Edwards, R Wagner, and T Briggs. Investigating potential light-duty efficiency improvements through simulation of turbo-compounding and waste-heat recovery systems. Technical report, Oak Ridge National Laboratory (ORNL); National Transportation Research Center, 2010.

[25] KJ Douglas, N Milovanovic, JWG Turner, and D Blundell. Fuel economy improvement using combined cai and cylinder deactivation (cda)-an initial study. *Training*, 2013:11–06, 2005.

[26] A Ramesh, G Shaver, C Allen, S Nayyar, D Gosala, D Parra, E Koeberlein, J McCarthy Jr., and D Nielsen. Utilizing low airflow strategies, including cylinder deactivation, to improve fuel efficiency and aftertreatment thermal management. *International Journal of Engine Research*, 0(0):1468087417695897, 0.

[27] A Ramesh, D Gosala, C Allen, M Joshi, J McCarthy Jr, L Farrell, E Koeberlein, and G Shaver. Cylinder deactivation for increased engine efficiency and aftertreatment thermal management in diesel engines. In *WCX World Congress Experience*. SAE International, apr 2018.

[28] M Foster, M Foster, and K Price. Engine cylinder deactivation to improve the performance of exhaust emission control systems, June 14 2005. US Patent 6,904,752.

[29] M Joshi, D Gosala, C Allen, K Vos, M Van Voorhis, A Taylor, G Shaver, J McCarthy Jr., D Stretch, E Koeberlein, and L Farrell. Reducing diesel engine drive-cycle fuel consumption through use of cylinder deactivation for aftertreatment component temperature maintenance during idle operating conditions. *IJER*, 2017.

[30] J McCarthy. *Cylinder deactivation improves Diesel aftertreatment and fuel economy for commercial vehicles*, pages 1013–1039. Springer Fachmedien Wiesbaden, Wiesbaden, 2017.

[31] J Deng and R Stobart. Bsfc investigation using variable valve timing in a heavy duty diesel engine. *SAE Technical Paper 2009-01-1525*, 2009.

[32] B. Yang and P. Keller. Analysis of diesel engine emissions reduction by late intake valve close and vtg turbocharger using 1-d simulation. *SAE Technical Paper 2008-01-2444*, 2008.

[33] M Fessler, Hand Genova. An electro-hydraulic lost motion VVA system for a 3.0 liter diesel engine. *SAE transactions*, 113(3):1639–1649, 2004.

[34] J Mitcalf. M Warth. S Schneider. D, Gurney. Integrated simulation, analysis and testing of a variable valve train for passenger car diesel engines. *SAE Technical Paper 2012-01-0829*, 2012.

[35] S Gehrke, D Kovács, P Eilts, A Rempel, and P Eckert. Investigation of VVA-based exhaust management strategies by means of a HD single cylinder research engine and rapid prototyping systems. *SAE International Journal of Commercial Vehicles*, 6(1):47–61, 2013.

[36] Y Murata, J Kusaka, M Odaka, Y Daisho, D Kawano, H Suzuki, H Ishii, and Y Goto. Emissions suppression mechanism of premixed diesel combustion with variable valve timing. *International Journal of Engine Research*, 8(5):415–428, 2007.

[37] W De Ojeda. Effect of variable valve timing on diesel combustion characteristics. *SAE paper*, pages 01–1124, 2010.

[38] R Constantine and G Evangelos. *Diesel engine transient operation: principles of operation and simulation analysis*. Springer, 2009.

[39] R Kitabatake, A Minato, N Inukai, and N Shimazaki. Simultaneous improvement of fuel consumption and exhaust emissions on a multi-cylinder camless engine. *SAE International Journal of Engines*, 4(1):1225–1234, 2011.

[40] L Roberts. *Analysis of the Impact of Early Exhaust Opening and Cylinder Deactivation on aftertreatment Thermal Management and efficiency for Compression Ignition engines.* Master's thesis, Purdue University, Purdue University, West Lafayette, Indiana, 2014.

[41] S Nayyar. *Implementation and Analysis of Reverse Breathing and Cylinder Deactivation for Aftertreatment Thermal Management and overall Efficiency on Diesel Engines.* Master's thesis, Purdue University, Purdue University, West Lafayette, Indiana, 2015.

[42] A Ramesh, G Shaver, C Allen, D Gosala, S Nayyar, D Parra, E Koeberlein, J McCarthy Jr, and D Neilson. Cylinder deactivation during dynamic diesel engine operating conditions. *International Journal of Engine Research*, 2016.

[43] D Gosala, C Allen, A Ramesh, G Shaver, J McCarthy Jr, S Dale, E Koeberlein, and L Farrel. Cylinder deactivation during dynamic diesel engine operating conditions. *International Journal of Engine Research*, 2016.

[44] M Halbe, B Pietrzak, D Fain, A Ramesh, G Shaver, J McCarthy, M Ruth, and E Koeberlein. Oil accumulation and first fire readiness analysis of cylinder deactivation. *Frontiers in Mechanical Engineering*, 3:1, 2017.

[45] W Lee, E Schubert, Y Li, S Li, D. Bobba, and B. Sarlioglu. Electrification of turbocharger and supercharger for downsized internal combustion engines and hybrid electric vehicles-benefits and challenges. In *2016 IEEE Transportation Electrification Conference and Expo (ITEC)*, pages 1–6, June 2016.

[46] O. Grondin, L. Thibault, and C. Qurel. 3rd ifac workshop on engine and powertrain control, simulation and modeling transient torque control of a diesel hybrid powertrain for nox limitation. *IFAC Proceedings Volumes*, 45(30):286 – 295, 2012.

[47] N Ishikawa. A study on emissions improvement of a diesel engine equipped with a mechanical supercharger. *International Journal of Engine Research*, page 1468087411434885, 2012.

[48] Y Wang, H Zhang, and Z Sun. Optimal control of the transient emissions and the fuel efficiency of a diesel hybrid electric vehicle. *Proceedings of the Institution of Mechanical Engineers, Part D: Journal of Automobile Engineering*, 227(11):1546–1561, 2013.

[49] M Sivertsson and L Eriksson. An optimal control benchmark: Transient optimization of a diesel-electric powertrain. In *Proceedings of the 55th Conference on Simulation and Modelling (SIMS 55), Modelling, Simulation and Optimization, 21-22 October 2014, Aalborg, Denmark*, number 108, pages 59–63. Linköping University Electronic Press, 2014.

[50] C Florell. Utilizing look-ahead information to minimize fuel consumption and nox emissions in heavy duty vehicles. 2015.

[51] W De Ojeda. Effect of variable valve timing on diesel combustion characteristics. Technical report, SAE Technical Paper, 2010.

[52] B. Lombard and R. L. Forestier. A high power wide torque range efficient engine with a newly developed variable valve lift and timing mechanism, 2006.

[53] M Joshi, D Gosala, C Allen, S Srinivasan, A Ramesh, M VanVoorhis, A Taylor, K Vos, G Shaver, J McCarthy Jr, L. Farrell, and E Koeberlein. Diesel engine cylinder deactivation for improved system performance over transient real-world drive cycles. In *WCX World Congress Experience*. SAE International, apr 2018.

[54] D Gosala, A Ramesh, C Allen, M Joshi, A Taylor, M Voorhis, G Shaver, L Farrell, E Koeberlein, Jr J McCarthy, and D Stretch. Diesel engine aftertreatment warm-up through early exhaust valve opening and internal exhaust gas recirculation during idle operation. *International Journal of Engine Research*, 0(0):1468087417730240, 0.

[55] C Ding. *Thermal efficiency and emission analysis of advanced thermodynamic strategies in a multi-cylinder diesel engine utilizing valve-train flexibility.*

[56] P Borgqvist, P Tunestal, and B Johansson. Comparison of negative valve overlap (nvo) and rebreathing valve strategies on a gasoline ppc engine at low load and idle operating conditions. *SAE International Journal of Engines*, 6(1):366–378, apr 2013.

[57] X Zhang, H Wang, Z Zheng, R Reitz, and M Yao. Experimental investigations of gasoline partially premixed combustion with an exhaust rebreathing valve strategy at low loads. *Applied Thermal Engineering*, 103:832 – 841, 2016.

[58] P Borgqvist, P Tunestal, and B Johansson. Investigation and comparison of residual gas enhanced hcci using trapping (nvo hcci) or rebreathing of residual gases. In *SAE International Powertrains, Fuels and Lubricants Meeting*. SAE International, aug 2011.

VITA

VITA

EDUCATION:

Purdue University, West Lafayette, IN:

Ph.D. in Mechanical Engineering, August 2018

Indian Institute of Technology Hyderabad, India:

B.Tech in Mechanical Engineering, May 2013

EMPLOYMENT EXPERIENCE:

Purdue University, Herrick Laboratories: Graduate Research Assistant, August 2013-August 2018.

Cummins, Inc.: Intern, May-August 2017.

Purdue University, Engineering Education: Graduate Teaching Assistant, August 2014-December 2014.

ACADEMIC FELLOWSHIPS:

Ward A. Lambert Graduate Teaching Fellowship 2017

Dr. Helen and Marvin Adelberg Fellowship for Graduate Studies August 2017-2018

JOURNAL PUBLICATIONS:

Aswin K Ramesh, Gregory M Shaver, Cody M Allen, Soumya Nayyar, Dheeraj B Gosala, Dina Caicedo Parra, Edward Koeberlein, James McCarthy, Jr and Doug Nielsen *Utilizing Low Airflow Strategies, Including Cylinder Deactivation, to Improve Fuel Efficiency and Aftertreatment Thermal Management*, International Journal of Engine Research (IJER), March 14, 2017.

Aswin K Ramesh, Troy E Odstrcil, Dheeraj B Gosala, Gregory M Shaver, Soumya Nayyar, Edward Koeberlein and James McCarthy Jr *Reverse Breathing in Diesel Engines for Aftertreatment Thermal Management*, IJER, June 14, 2018.

Aswin K Ramesh, Dheeraj B Gosala, Cody M Allen, Gregory M Shaver, Mrunal Joshi, Lisa Farrell, Edward Koeberlein and James McCarthy Jr *Cylinder Deactivation for Increased Engine Efficiency and Aftertreatment Thermal Management in Diesel Engines*, SAE International, April 2018.

Dheeraj B Gosala, **Aswin K Ramesh**, Cody M Allen, Mrunal C Joshi, Alexander H Taylor, Matthew Van Voorhis, Gregory M Shaver, Lisa Farrell, Edward Koeberlein, James McCarthy, Jr, Dale Stretch *Diesel engine aftertreatment warm-up through early exhaust valve opening and internal exhaust gas recirculation during idle operation*, IJER, September 20, 2017.

Dheeraj B Gosala, Cody M Allen, **Aswin K Ramesh**, Gregory M Shaver, James McCarthy, Jr, Dale Stretch, Edward Koeberlein, Lisa Farrell *Cylinder deactivation during dynamic diesel engine operation*, IJER, March 14, 2017.

Xueting Lu, Chuan Ding, **Aswin K. Ramesh**, Gregory M. Shaver, Eric Holloway, James McCarthy Jr., Michael Ruth, Edward Koeberlein and Douglas Nielsen *Impact of cylinder deactivation on active diesel particulate filter regeneration at highway cruise conditions*, IJER, August 24, 2015.

Alexander H Taylor, Troy E Odstrcil, **Aswin K Ramesh**, Gregory M Shaver, Edward Koeberlein *Model-Based Compressor Surge Avoidance Algorithm for IC Engines Utilizing Cylinder Deactivation During Motoring Conditions*, IJER, in progress - 2018.

Kalen R. Vos, Gregory M. Shaver, **Aswin K. Ramesh**, James McCarthy Jr. and Lisa Farrell *Impact of Cylinder Deactivation and Cylinder Cutout via Flexible Valve Actuation on Fuel Efficient Aftertreatment Thermal Management at Curb Idle*, International Journal of Engine Research, in progress - 2018.

Chuan Ding, Leighton Roberts, David J Fain, **Aswin K Ramesh**, Gregory M Shaver, James McCarthy Jr., Michael Ruth, Edward Koeberlein, Eric A Holloway and Douglas Nielsen *Fuel efficient exhaust thermal management for compression ignition engines during idle via cylinder deactivation and flexible valve actuation*, International Journal of Engine Research, August 12, 2015.

Mayura Halbe, Brad Pietrzak, David Fain, **Aswin Ramesh**, Greg Shaver, James E. McCarthy Jr., Mike Ruth and Edward Koeberlein *Oil Accumulation and First Fire Readiness Analysis of Cylinder Deactivation*, International Journal of Engine Research, August 12, 2015.

Mrunal Joshi, Dheeraj B Gosala, Cody M Allen, **Aswin K Ramesh**, Matthew VanVoorhis, Alexander Taylor, Kalen Vos, Gregory Shaver, Lisa Farrell, Edward Koeberlein and James McCarthy Jr *Diesel Engine Cylinder Deactivation for Improved System Performance over Transient Real-World Drive Cycles*, SAE International, April 2018.